THE RESPONSE OF MARINE BENTHIC MICROBIAL POPULATIONS TO THE DEEPWATER HORIZON OIL SPILL

A Dissertation
Presented to
The Academic Faculty

By

Will A. Overholt

In Partial Fulfillment
Of the Requirements for the Degree
Doctor of Philosophy in Bioinformatics in the
School of Biological Sciences

Georgia Institute of Technology

May 2018

THE RESPONSE OF MARINE BENTHIC MICROBIAL POPULATIONS TO THE DEEPWATER HORIZON OIL SPILL

Approved by:

Dr. Joel E. Kostka, Advisor
Schools of Biological Sciences and Earth & Atmospheric Sciences
Georgia Institute of Technology

Dr. Brian K. Hammer
School of Biological Sciences
Georgia Institute of Technology

Dr. Markus Huettel
Department of Earth, Ocean, and Atmospheric Sciences
Florida State University

Dr. David J. Hollander
College of Marine Science
University of South Florida

Dr. Konstantinos T. Konstantinidis
School of Civil and Environmental Engineering
Georgia Institute of Technology

Dr. Stefan J. Green
School of Biological Sciences and Director of DNA Services
University of Illinois at Chicago

Date Approved: 14 March 2018

To my parents, who have always been there for me. Thank you for all the love, support, and encouragement.

ACKNOWLEDGEMENTS

Over the past six years I have received support and encouragement from a great many fantastic individuals. My advisor, Dr. Joel E. Kostka, has been a mentor, a colleague, and a friend. His guidance and advice for my scientific research as well as such diverse topics as health, happiness, personal and professional fulfillment, and handling stress have been invaluable and cannot be overstated. Indeed, I have felt a part of the Kostka family and for that I am extremely thankful. Dr. Stefan J. Green has played a similar role and his thoughtful and frank discussions early in my career emboldened me to continue in research. I would also like to thank Dr. Markus Huettel, Dr. Kostas Konstantinidis, and Dr. David Hollander for providing astute guidance, general collegiality, as well as challenging me throughout my graduate student tenure. In addition, I would like to Dr. King Jordan for his unwavering and exceptional support at the last minute, I am forever grateful for this.

I would like to thank the members of the Cabbagetown Running Club for excellent stress relief as we slowly wore through the rubber on our shoes. Their willingness to listen and in some (many) cases laugh at me has helped me keep my perspective and my sanity. The graduate students, post docs, and faculty at Georgia Tech also need to be mentioned for enabling a culture of support, collaboration, and friendship. There are too many additional amazing people who have played a large role in my life over these years to acknowledge individually, but I offer a sincere “Thank you!”. Finally, I would like to thank my brother Luc for his humor, support, and friendly banter.

TABLE OF CONTENTS

LIST OF TABLES

LIST OF FIGURES

LIST OF SYMBOLS AND ABBREVIATIONS

PHC	Petroleum hydrocarbon contamination
DWH	Deepwater Horizon Disaster / oil spill
GOM	Gulf of Mexico
NGoM	Northern Gulf of Mexico
SGoM	Southern Gulf of Mexico
MC252	Mississippi Canyon Block – Lease Number 252
BP	British Petroleum
TPH	Total petroleum hydrocarbons
PAH	Polyaromatic hydrocarbons
BTEX	Monoaromatic hydrocarbons (benzene, toluene, ethylbenzene, xylene)
WAF	Water accommodate fraction, portion of oil that is entrained in the water column
CEWAF	Chemically enhanced water accommodated fraction, portion of oil entrained in water following chemical dispersal
EPA	Environmental Protection Agency
NCP	National Oil and Hazardous Substance Pollution Contingency Plan
NGDC	National Geophysical Data Center
OSAT	Operational Science Advisory Team
ODC	Operation Deep Clean, BP driven beach cleaning using large excavation equipment
GRIIDC	The Gulf of Mexico Research Initiative Information and Data Cooperative
PEMEX	Mexican state-owned petroleum company
SOM	Submerged oil mats
SRB	Surficial residual balls

PB	Pensacola Beach, FL
SGI	St. George Island, FL
CO_2	Carbon dioxide
O_2	Molecular oxygen
N	Nitrogen
P	Phosphorous
S	Sulfur
DOM	Dissolved organic matter
POM	Particulate organic matter
GC	Gas chromatography
GC-FID	Gas chromatography with a flame ionization detector
GC-MS	Gas chromatography mass spectroscopy
AlkB	Alkane-1-monooxygenase
pMMO	Particulate methane monooxygenase
BMM	Bacterial multicomponent monooxygenase protein family
CYP153	One of the cytochrome protein families
AlmA	Flavin binding monooxygenase, long chain alkane monooxygenase
LadA	Long chain alkane monooxygenase, originally isolated from *Geobacillus thermodenitrificans*
Bcr	class I benzoyl-CoA reductase
Bam	class II benzoyl-CoA reducatse
ASS	Family of alkylsuccinate synthase proteins
BSS	benzylsuccinate synthase
MAS	1-methyl alkylsuccinate synthase
CoA	Coenzyme A

TCA	The citric acid cycle, krebs cycle
LC50	Lethal concentration of toxin that kills 50% of the test animals
SSU rRNA	Small submit ribosomal RNA gene
IS	Internal standard method for GC-MS quantification
SDS	Sodium dodecyl sulfate
DOSS	Dioctyl Sodium Sulfosuccinate
EPS	Extracellular polymeric substances
OTU	Operational taxonomic unit (operationally defined microbial species)
CFU	Colony forming unit
CPE	Chloroplastic pigment equivalents, proxy for phytoplankton detritus
ANI	Average nucleotide identity
PCoA	Principal coordinates analysis (ordination method)
NMDS	Non-metric multidimensional scaling (ordination method)
SD	Standard Deviation
SE	Standard Error
ANOVA	Analysis of variance
RMSE	Root mean squared error

SUMMARY

The Deepwater Horizon (DWH) disaster in the Gulf of Mexico represents the largest accidental, marine oil spill in history, the first large spill that occurred in the deepsea, and is unique in the unparalleled volumes of chemical dispersant that were applied during emergency response efforts. Microbial biodegradation ultimately removes most of the hydrocarbons discharged during oil spills, which allows ecosystems to recover. However, the environmental controls that regulate this process are poorly understood. Furthermore, benthic environments are understudied relative to their pelagic counterparts, and were contaminated with approximately 20 % of the released oil after the DWH blowout. Aside from the emergence of hydrocarbon-degrading bacterial populations, oil contamination may impact sensitive, benthic microbial groups and disrupt critical biogeochemical cycles, causing far-reaching and largely unknown ecosystem level consequences.

The work presented in this dissertation addresses knowledge gaps associated with the environmental controls of the structure and function of benthic microbial communities across the Gulf of Mexico as well as their response to major perturbations such as oil contamination. Specifically, the overall goal was to advance our understanding of the fate and consequences of deposited DWH crude oil to benthic ecosystems and the *in situ* microbial community in the Gulf of Mexico. Objectives were to: (1) determine the impacts of chemical dispersant on individual oil-degrading microbial populations and the consequences to oil ecotoxicity, (2) interrogate the natural or baseline state of benthic microbial communities and construct a model to predict their distribution throughout

oligotrophic sediments in the Gulf, and (3) quantify the environmental controls of biodegradation and impacts to microbially-mediated ecosystem services, specifically nitrogen cycling, in sandy coastal ecosystems. The objectives were achieved in part through the generation of novel bioinformatic analysis pipelines and integrative data analysis frameworks that leveraged the Georgia Tech PACE HPC environment.

One of the unique aspects of the DWH oil spill was the unprecedented amount of chemical dispersant that was applied at depth or on surface slicks. The results presented here contribute to the growing understanding that chemical dispersants can have unintended consequences for the microbially-mediated biodegradation of petroleum hydrocarbons. Microbial populations were shown to have disparate responses in growth rate and biodegradation efficiency to dispersed oil or crude oil. These differences in physiological response have the potential to directly impact the ecotoxicity of dissolved or dispersed oil constituents as well as intermediate degradation products.

Over 1000 km of Gulf of Mexico shoreline was impacted by weathered crude oil from the DWH disaster. Research presented here quantified the *in situ* decomposition of buried DWH oil on Florida beaches along with the biogeochemical mechanisms controlling its degradation. Further, the abundance, composition, and succession of beach sand microbial communities were characterized in parallel with changes in the evolution of petroleum hydrocarbon (PHC) chemistry in a 2-year time series. Rapid rates of PHC degradation were observed that could be attributed to tidal pumping that transported oxygen into the buried oil layers while removing carbon dioxide. Amazingly, within one-year after oil came ashore, microbial communities had recovered to baseline conditions and hydrocarbon concentrations had returned to background levels.

A substantial portion of discharged DWH oil blanketed deepsea sediments through oiled-marine snow deposition or via deep subsurface plumes that impinged upon bottom contours of the seafloor. However, prior to these events, the indigenous microbial communities and their distribution on the oligotrophic Gulf of Mexico deep seafloor were virtually unknown. Therefore, in order to characterize the baseline condition for deep ocean sedimentary microbial communities at the ocean-basin-wide scale, over 800 samples were analyzed (29 distinct sites, across four years) and the largest marine sediment microbial community composition dataset ever compiled was generated. A new bioinformatic analysis pipeline had to be constructed and verified in order to accommodate this unprecedented dataset. Microbial distributions were mapped across gradients in environmental parameters including sedimentary oxygen content, water depth, sediment depth, latitude, and longitude in the Gulf of Mexico. Based on these well resolved microbial distributions, a predictive model was developed using a machine learning approach. The sole inputs to the model were environmental parameters that could be derived from freely available maps. All sensitivity and specificity tests as well as predictions were performed on Georgia Tech's high-performance cluster environment. The applicability of the model was verified by using previously published datasets on Gulf microbial communities acutely impacted by the Deepwater Horizon oil spill. Model results showed that highly contaminated sites deviate strongly from the model predictions, while unimpacted samples are consistent with our predictions of baseline microbial community composition at the seafloor.

Finally, knowledge gaps in understanding the fate of oil sequestered in nearshore, subtidal sediments were addressed. Mesocosms were constructed using advective-flow

chambers to reproduce in situ physical-chemical conditions at the sediment-water interface of permeable sands sampled from Florida beaches, and the underlying ecological principles governing the response of microbial populations to an oil disturbance were robustly tested. The most significant findings from the mesocosm study demonstrate the occurrence of large-scale disruptions to the marine nitrogen cycle in subtidal sands in response to oil contamination through the inhibition of nitrification. This disruption can be linked to the microbial populations that mediate nitrification along with other nitrogen cycling processes, offering direction for environmental monitoring programs to assess ecosystem health and recovery.

Overall, this dissertation advances understanding of the fate and consequences of deposited DWH crude oil in benthic ecosystems, focusing on impacts to the structure and function of *in situ* microbial communities. The results elucidate constraints on the rates and pathways of oil biodegradation, and can be directly incorporated into predictive models to forecast recovery pathways for future spills as well as hindcast the fate of remaining DWH oil in the Gulf of Mexico.

CHAPTER 1. INTRODUCTION

1.1 The Deepwater Horizon Oil Spill

On April 20th, 2010, the Deepwater Horizon Mobile Offshore Drilling Unit suffered from a catastrophic blowout while drilling an exploratory well in the Macondo Prospect, in Mississippi Canyon Block 252 (MC252) (Lubchenco *et al.*, 2012). Due to a complex interconnected set of 8 established critical failures, an uncontained release of gaseous hydrocarbons vented onto the rig and violently ignited (BP Accidental Report, 2010). The rig burned out of control for 36 hours before ultimately sinking to the seafloor. Eleven crewmen lost their lives and an additional 17 were injured during the explosion (BP Accidental Report, 2010). Hydrocarbons continued to escape from the damaged wellhead for 87 days until it was successfully capped on July 15th, 2010, and ultimately closed through the creation of relief wells and was declared completely sealed on September 19th, 2010 (Lubchenco *et al.*, 2012).

Over a three-month period, approximately 4.1 – 4.9 million barrels of crude oil was discharged into the deep ocean at 1,544 m water depth along with 250,000 metric tons of gaseous hydrocarbons which represented ~30-50 % of the mass of liquid hyrocarbons, primarily as methane (McNutt *et al.*, 2012; Joye, 2015). Approximately 50 % of all

discharged hydrocarbons remained entrained in the deep ocean in several intrusion layers from 900-1200 m water depth due to kinetic fractionation (Valentine *et al.*, 2012). These deep subsurface plumes contained all the soluble gaseous hydrocarbons, monoaromatic hydrocarbons (BTEX), as well as larger molecular weight insoluble compounds that were sequestered in small neutrally buoyant droplets (Valentine *et al.*, 2012). Furthermore, 2.1 million gallons of chemical dispersant was injected at the wellhead into the rising hydrocarbon plume (discussed below). Of the oil discharged from MC252, 17 % was recovered by drill or skimming ships, 29 % was naturally or chemically dispersed, 23 % evaporated or dissolved, and the remaining 23 % was left in the environment sequestered in both deep benthic or shallow coastal sediments (Lehr *et al.*, 2010; Lubchenco *et al.*, 2010; McNutt *et al.*, 2012). Within the water column, dissolved and dispersed hydrocarbons induced rapid changes in microbial communities (Kleindienst et al. 2015a). The microbial response to DWH oil in planktonic ecosystems has been extensively covered in a series of three review articles and the reader is referred to these as the primary focus for this dissertation is on benthic environments (Kimes *et al.*, 2014; King *et al.*, 2014; Joye *et al.*, 2016).

1.2 Oil Contamination in Shelf and Slope Sediments

Oil was transported to the deep seafloor via two main mechanisms, through subsurface intrusions impinging on bottom sediments (Romero *et al.*, 2015; Daly *et al.*, 2016), or through the sedimentation of oiled marine snow across large areas of the northern Gulf of Mexico (Passow, Ziervogel, Asper, and A. Diercks, 2012; Hollander *et al.*, 2013; Brooks *et al.*, 2015; Romero *et al.*, 2017). Estimates for the amount of DWH oil sequestered in deep ocean sediments range from 2 to 31% (Chanton et al., 2012; Valentine et al., 2014;

Bagby et al., 2016; Romero et al., 2017,) and vary in footprint size, dependent on oil concentration, from 3,200 km^2 to 32,000 km^2 (Valentine *et al.*, 2014; Romero *et al.*, 2017). The chemistry of deposited oil in sediments indicates that biodegradation rates were dependent on the degree of oiling, and consistent with previous findings, the smallest molecular weight compounds exhibited the fastest decay rates (Bagby *et al.*, 2016). Surprisingly, the previously established recalcitrant biomarker 17α(H),21β(H)-hopane used to determine the extent of oiling showed a relatively high susceptibility for degradation in low to moderately contaminated sediments (Bagby *et al.*, 2016).

In areas immediately surrounding the DWH wellhead that were heavily contaminated to above EPA limits, microbial communities responded quickly, adjusting to a different state dominated by a *Colwellia* population as well as a single uncultured Gammaproteobacterium that comprised up to 18 % of the total community (Mason *et al.*, 2014). Total metabolic potential was enriched in both aliphatic and PAH degradation pathways as well in anaerobic respiratory metabolism (Mason *et al.*, 2014) . Subsequently, Yang et al., used a clone library approach to follow the succession in deep benthic communities, including a pulse in sulfate-reducing bacterial populations followed by a longer persistence of the PAH-degrading genus *Cycloclasticus*, and evidence of recovery after one year (Yang *et al.*, 2016). The rates of recovery suggested by these studies exceed estimates of decay rates in contaminating hydrocarbons. This is potentially due to a dilution effect from sedimented natural organic matter, whereby few contaminated oil particles settling to the seafloor result in low to moderately contaminated sediments (Bagby *et al.*, 2016).

1.3 Oil Contamination in Nearshore Environments

A substantial portion of the DWH oil that reached the surface ocean was transported to coastal ecosystems. A large swath of shoreline, nearly 2200 km, from east Texas to west Florida was impacted by oiling, including beaches (50.8 %), marshes (44.9 %), and other (4.3 %) coastal ecosystems (Michel *et al.*, 2013; Nixon *et al.*, 2016). Surfaced oil that was transported to the near shore was either entrained in sediments and transported and buried in nearshore environments or washed ashore (Operational Science Advisory Team, 2013; Nixon *et al.*, 2016). Oil was transported high onto the supratidal zone of beaches by waves and tides associated with storms (Michel *et al.*, 2013), and a portion of the oil was deposited in the intertidal and subtidal zones near the beach. Because of the dynamic nature of coastal sediments, storms often resulted in the rapid burial of oil in the sediments.

Total petroleum hydrocarbons, aliphatic and aromatic compounds, were shown to be highly weathered and depleted within the first few months to years after oil from the DWH spill came ashore in beaches (Hayworth *et al.*, 2015; Yin, John, *et al.*, 2015) and wetlands (Mahmoudi *et al.*, 2013; R E Turner *et al.*, 2014; R Eugene Turner *et al.*, 2014; Atlas *et al.*, 2015) since 2010. Whereas the alkanes and lower molecular weight PAHs were largely depleted in coastal sediments, higher molecular weight PAHs (e.g. chrysene) persist and are projected to remain in the ecosystems for many years. Oil is degraded at much reduced rates when buried (Yin, John, *et al.*, 2015). Thus, submerged oil mats, tens to hundreds of meters long and up to 20 cm thick, have been reported at the inner shelf of the northern Gulf (Operational Science Advisory Team (OSAT), 2010; Dalyander *et al.*, 2014), and tar balls, typically 0.5–5 cm in diameter and containing 5% to 16% hydrocarbons by weight (Urbano *et al.*, 2013; Elango *et al.*, 2014) continue to wash up on northeastern Gulf of Mexico shores (Yin, John, *et al.*, 2015).

Oil contamination from the DWH spill had a profound impact on the abundance, structure, and metabolic potential of sedimentary microbial communities at beaches (Kostka *et al.*, 2011; Bik *et al.*, 2012; Newton *et al.*, 2013; Engel and Gupta, 2014) and marshes (Mahmoudi *et al.*, 2013; Atlas *et al.*, 2015) of the northern Gulf coast. Specifically, a time series study conducted at municipal Pensacola Beach (PB), Florida, where total petroleum hydrocarbons reached 11,000 mg kg^{-1}, revealed a bloom of bacteria during the first 4 months after oil came ashore, with microbial abundance in oiled sands exceeding that of clean sands by 1 to 4 orders of magnitude (Kostka *et al.*, 2011). Geochemical evidence confirmed the role of microorganisms in the degradation of weathered oil (Ruddy *et al.*, 2014), and the succession of indigenous microbial populations was shown to parallel the chemical evolution of the petroleum hydrocarbons (Rodriguez-R *et al.*, 2015). The most extensive metagenomic time series describing microbial hydrocarbon degradation to date was collected from these Pensacola Beach sands (Rodriguez-R *et al.*, 2015). The dataset showed a similar progression of microbial populations linked to hydrocarbon degradation that has been observed in other coastal sediments with some surprises. Oil deposition led to a decrease in taxonomic diversity, in corroboration of previous studies. The bloom was dominated by members of the Gamma- and Alphaproteobacteria, and the abundance of genes for hydrocarbon degradation pathways closely paralleled microbial population dynamics. A clear succession pattern was observed, whereby early responders to oil contamination (*Alcanivorax*), likely degrading aliphatic hydrocarbons, were replaced after 3 months by populations capable of aromatic hydrocarbon decomposition (*Hyphomonas*, *Parvibaculum*, *Marinobacter*). However, an increase in functional diversity of the community was observed in response to oil contamination, and a functional

transition occurred from generalist populations within 4 months after oil came ashore to specialists a year later, when oil was undetectable (Rodriguez-R *et al.*, 2015). After one year, a typical beach community had reestablished that showed little to no evidence of oil hydrocarbon degradation potential, but differed significantly from the community before the oil spill (Rodriguez-R *et al.*, 2015). The results indicate that benthic microbial communities respond to crude oil perturbation according to the specialization disturbance hypothesis. Beach ecosystems in the Gulf are characterized by nutrient poor conditions. Following a pulsed disturbance from oil input, specialist populations adapted to oligotrophic conditions such as chemolithoautotrophic archaea (*Nitrosopumilus*) were replaced by generalists capable of hydrocarbon degradation (Rodriguez-R *et al.*, 2015).

In intertidal wetlands, fine-grained sediments accumulate under relatively quiescent tidal and current conditions. Dominated by halophyte plants, the sediments of these ecosystems are heterogeneous, organic-rich, and anoxic close to the sediment surface. Although less information is available in comparison to beaches, hydrocarbons were shown to accumulate in the surface sediments and were largely degraded within the first few years after oil came ashore (Mahmoudi *et al.*, 2013; Atlas *et al.*, 2015). Results indicated not surprisingly that oxygen supply dictated the extent of hydrocarbon degradation and anaerobic microbial populations such as sulfate-reducing members of the Deltaproteobacteria and methanogens increased in relative abundance in sediments where hydrocarbons were degraded (Atlas *et al.*, 2015). Oil degradation genes associated with anaerobic pathways increased dramatically at oiled sites, and even the higher molecular weight PAHs were substantially biodegraded.

1.4 Consequences of the Use of Chemical Dispersants

Chemical dispersants are one of the main tools used during emergency response to oil spills and this strategy is aimed at minimizing coastal impacts, diluting oil constituents to reduce or remove oil-associated toxicity, and stimulating biodegradation by increasing the surface area to volume ratio of oil droplets while alleviating nutrient stresses (Chapman *et al.*, 2007; Prince, 2010; Kleindienst *et al.*, 2015). Molecular components of dispersants were detected in nearshore coastal waters until at least October 2010, although due to a lack of benchmarks prior to the spill, it is not possible to unequivocally attribute these components to response efforts (Operational Science Advisory Team (OSAT), 2010). For example, Hayworth and Clement argue that detection of many compounds from COREXIT 9500A in the coastal waters surrounding Orange Beach, AL, likely originated from point and non-point sources of the Perdido Bay watershed and not from DWH dispersant applications (Hayworth and Clement, 2012). It should be noted that one of the main considerations in the use of chemical dispersants in oil spill response efforts is proximity to shorelines, and in US coastal waters, responders have pre-authorization for dispersant use in water at least 10 meters deep and 3 miles from shore (FOSC Dispersant Pre-Approval Guidelines, 2001). Regardless, the unintended consequences of COREXIT 9500A to sensitive coastal ecosystems must be considered to inform future response efforts.

A review by Lessard and DeMarco in 2000 summarized the feasibility of near-shore dispersant applications from research dating back to 1981 (Lessard and DeMarco, 2000). In the majority of studies, chemical dispersion of spilled oil was a recommended response that limited ecosystem damages from oil spills, with the exception of a single study that showed large damages to a coral reef ecosystem (Ballou *et al.*, 1989; Lessard and DeMarco,

2000; Fuller *et al.*, 2004). The authors concluded that dispersant use in near-shore environments may be appropriate or even preferable under certain conditions, and damages to ecosystems from chemically dispersed oil were less extensive or as extensive as from crude oil alone. Furthermore, certain ecosystems were observed to recover faster from chemically dispersed oil in comparison to crude oil (Page *et al.*, 2000).

However, the microbial community response to chemical dispersants remains controversial due to inconsistent results obtained for studies of biodegradation in laboratory experiments (Lee *et al.*, 2013; Kleindienst *et al.*, 2015). In beaches and marshes, the impacts of chemically dispersed oil to microbial communities is a vastly understudied subject and more research must be done to constrain the impacts and predict changes in microbial mediated ecosystem functions in order to better inform future response efforts. In addition to microbial response, the physical impacts of dispersed oil must be considered, and in one such study by Zuijdgeest and Huettel, the authors' showed that COREXIT 9500A facilitates the transport of PAHs deep into sandy sediments. This transport mechanism has the potential to sequester petroleum hydrocarbons in anaerobic zones where biodegradation rates will be slowed (Zuijdgeest and Huettel, 2012).

In one of the few studies on microbial responses to dispersed oil in beach sands, Hamdan and Fulmer showed differential responses in microbial communities to chemically dispersed as compared to crude oil treatments at various COREXIT concentrations (Hamdan and Fulmer, 2011). The authors then isolated several bacterial strains identified as *Marinobacter*, *Acinetobacter*, and *Vibrio*. All isolates showed near total mortality to COREXIT at concentrations of 10 mg ml^{-1} (10000 ppm), and both *Marinobacter* and *Acinetobacter* isolates showed strong inhibition at < 1 mg ml^{-1} and detectable inhibition at

< 0.1 mg (100 ppm) using a method that assessed cell viability (Hamdan and Fulmer, 2011). At concentrations of 0.2 mg ml^{-1}, COREXIT 9500A is considered nontoxic to the standard EPA test organism *Menidia beryllina*, and while the ratios used by Hamdan and Fulmer are in line with EPA recommendations, the absolute concentrations greatly exceed *in situ* observations immediately following dispersant application (Prince *et al.*, 2013). These concentrations are also likely higher than what beach environments were exposed to, although this is not known and the authors' suggest their results represent the maximum concentrations that would be encountered (Hamdan and Fulmer, 2011). The effect of different microbial communities evolving in chemically dispersed oil on biodegradation extent or rate was not constrained in this study and to the best of our knowledge has not been shown in beach environments.

A study by Bookstaver et al., concluded that the well-studied model hydrocarbonclastic strain, *Alcanivorax borkumensis* is negatively impacted by COREXIT 9500A, as well as all anionic dispersants tested (Bookstaver *et al.*, 2015). It seems clear that chemical dispersants result in a wide variation of bacterial responses through a range of mechanisms including: physically changing the oil-water interface (altering oil droplet sizes, lowering tension between oil and water phases, physically repelling bacteria in the case of anionic surfactants), impacting bacterial membranes causing toxicity, increasing entrained-oil concentrations, and likely changing metabolic responses (Foght *et al.*, 1989; Cameotra and Singh, 2009; Bookstaver *et al.*, 2015; Kleindienst *et al.*, 2015).

Pietroski et al., examined the potential impacts of chemical dispersants on microbial nitrogen cycling processes including ammonification and denitrification. These critical ecosystem processes regulate primary productivity, organic matter mineralization

(including petroleum hydrocarbons), and improve water quality by removing excess inorganic nitrogen (Pietroski *et al.*, 2015). While dispersed oil was not tested, the authors show that COREXIT 9500A significantly and negatively impacts both ammonification and denitrification processes at ratios of Corexit to sediment wet weight > 1:1000 (>1 mg g^{-1} sediment) (Pietroski *et al.*, 2015). Shi and Yu also investigated potential disruptions to denitrification using crude oil, COREXIT 9500A, and chemically dispersed crude oil (Shi and Yu, 2014). As Pietroski et al. show, Shi and Yu observed significant decreases in denitrification in COREXIT treated mesocosms, as well as in COREXIT dispersed oil treatments and this inhibitory effect was more pronounced with higher nitrate concentrations. Crude oil alone had no significant impact on denitrification potential. Surprisingly, both COREXIT alone and dispersed oil treatments stimulated CO_2 production, largely to the same degree, and generated more reducing conditions than crude oil alone. These results suggest that other respiration processes or fermentation were stimulated by COREXIT, and that COREXIT potentially increases the lability of autochthonous organic matter (nearly the same increase in CO_2 production as seen in the dispersed oil treatment with even greater reducing conditions generated) (Shi and Yu, 2014).

1.5 Pathways of Hydrocarbon Degradation

Crude oil is one of the most complex chemical mixtures observed in nature composed of tens of thousands of individual constituents. These compounds are generally classified into four main operational groups, the saturated hydrocarbons, mainly of alkanes, the aromatics, and the polar asphaltenes and resins (Head *et al.*, 2006). Marine environments have been exposure to petroleum hydrocarbons for millions of years, and it

is estimated 600 million tons of petroleum hydrocarbons enter the marine environment per year from natural sources alone (ranging between 200 and 2000 million tons) (on Oil in the Sea and Fates, 2003). Over this time frame, an astonishing diversity of metabolic pathways have arisen to consume many of these compounds for growth or transform them to minimize toxic effects, under both aerobic and anaerobic conditions. Particular emphasis has been placed on elucidating the microbial pathways involved in the degradation and/or transformation of the aliphatic and aromatic portions of crude oils as these are GC amendable and therefore easier to study, as well as the dominant fraction in most crude oils. Hydrocarbon degradation pathways have been extensively reviewed and here we briefly summarize some of the major pathways (Foght, 2008; Rojo, 2009; Fuchs *et al.*, 2011; Abbasian *et al.*, 2015; Ladino-Orjuela *et al.*, 2016).

Alkane biodegradation pathways are probably the best understood, particularly n-alkane degradation pathways, and these were recently reviewed (Rojo, 2009; Wang and Shao, 2013). Alkanes are detected ubiquitously across all environments and there are many known analogous systems that initiate alkane activation by breaking strong C-H bonds, considered one of the most energetically demanding processes catalyzed by microbes (Borovik, 2011). Alkane degradation pathways are often classified operationally based on the length of the alkane oxidized, short chain (C1 – C4, gaseous n-alkanes), mid chain (C5 – C16), and long chain (C17+). The initial step in aerobic alkane degradation typically, but not always, occurs at a terminal carbon generating a primary alcohol, which is subsequently oxidized to the corresponding aldehyde via an alcohol dehydrogenase, followed by oxidation to a fatty acid by an aldehyde dehydrogenase (Watkinson and Morgan, 1990). Fatty acids can then be processed via beta-oxidation or converted to phospholipids and

incorporated into the cellular membrane. Most alkane hydroxylases are metalloenzymes that use a metal species in the active site to activate oxygen and attack the C-H bond.

Short chain alkanes are oxidized by two known groups of metalloenzymes, particulate methane monooxygenase (pMMO) and soluble methane monooxygenases and their homologs (propane monooxygenase and butane monooxygenase). Particulate methane monooxygenases use a di-copper active site and can oxidize up to C_5 n-alkanes (Ng *et al.*, 2008; Culpepper and Rosenzweig, 2012). Soluble methane monooxygenases are part of the large bacterial multicomponent monooxygenase family (BMM), which have a non-heme diiron active site, and can oxidize up to C_8 alkanes including branched alkanes, cycloalkanes, and even small aromatics (Froland *et al.*, 1992). Mid length alkane hydroxylases fall into two main classes, membrane associated non-heme diiron monoxygenases (AlkB) that share no homology to bacterial multicomponent monooxygenase, and heme based cytochrome P450 (family CYP153) enzymes. Both classes are highly diverse, often found together in hydrocarbon degrading bacteria and have extensive overlapping substrate ranges that appear redundant. Both classes also perform terminal alkane oxidation resulting in a primary alcohol. The majority of AlkB alkane hydroxylases preferentially act upon $C_{10} – C_{18}$ alkanes, although the best studied AlkB from *Pseudomonas putida* GPo1 preferentially uses $C_5 – C_{13}$ n-alkanes (van Beilen and Funhoff, 2007; Koch *et al.*, 2009; Bertrand *et al.*, 2013). Many model alkane degrading microorganisms contain multiple AlkB homologs (van Beilen and Funhoff, 2007). Cytochrome P450s have a heme prosthetic group and are highly diverse found in all domains of life. All bacterial alkane hydroxylase cytochrome P450s belong to the CYP153 family, are soluble, and primarily act upon n-alkanes between C_6 and C_{15} (van Beilen and

Funhoff, 2007; Austin and Groves, 2011). Long chain alkane oxidation enzymes are not as well characterized and only a few pathways have been determined. The best described are two enzymes that share no apparent homology, both using a flavin cofactor. AlmA, a flavin-binding monooxygenase is thought to act upon C_{20} to $>C_{32+}$ n-alkanes and was first identified in *Acinetobacter sp.* DMS17874. Homologs have since been identified in many other oil degrading bacteria (Throne-Holst *et al.*, 2007; Wang and Shao, 2013). LadA is a member of the SsuD bacterial luciferase sub-family that oxidizes C15 – C36 alkanes that has only been found in thermophilic bacteria belonging to the *Geobacillus* genus. (Feng *et al.*, 2007; Boonmak *et al.*, 2014).

Under anaerobic conditions, there are two known systems for alkane activation that involve fumarate addition to a subterminal or terminal carbon (in a case of propane activation) producing a substituted succinate compound (Grundmann *et al.*, 2008; Gittel *et al.*, 2015). Enzymes involved are known as alkylsuccinate synthases (ASS) or 1-methylalkyl succinate synthases (MAS), and most likely function through the generation of a glycyl radical (Widdel and Rabus, 2001). These enzymes share homology and similar suggested mechanisms as the better understood benzylsuccinate synthase seen in toluene degradadtion (see below). After fumarate addition, CoA is thought to be added via a CoA transferase and then carbon skeletal rearrangements via a mutase followed by decarboxylation, analogous to carbon rearrangements seen with methylmalonyl-CoA mutase (Wilkes *et al.*, 2002).

Microbial pathways involved in aromatic degradation have recently reviewed and discussed in detail (Fuchs *et al.*, 2011; Ladino-Orjuela *et al.*, 2016). Simplifying greatly, a very diverse set of pathways, termed peripheral pathways, transform an aromatic

containing compound into one of a few key central intermediates. Under aerobic conditions these are typically monooxygenases or dioxygenases that hydroxylate the aromatic compound, mainly producing catechol, protocatechuate, gentistate, or homogentistate (Fuchs *et al.*, 2011). The aromatic ring component of these central intermediates can be cleaved by two oxygen dependent strategies (anaerobic mechanisms are discussed below). The best studied involve dioxygenases that cleave the hydroxyl-substituted aromatic ring, of which the β-ketoadipate pathway is a well-known example (Ornston and Stanier, 1966; Harwood and Parales, 1996). Alternately, the hydroxylated aromatic ring can be further substituted with CoA followed by ring cleavage using expoxidases that belong to the bacterial multicomponent monooxygenase family, examples include benzoate and phenylacetate epoxidation (Rather *et al.*, 2010; Teufel *et al.*, 2010; Fuchs *et al.*, 2011). The resulting compounds are often incorporated into central metabolism as acetyl-CoA, succinyl-CoA, and pyruvate and fed into the TCA cycle. The reader is encouraged to read the chapter by Ladino-Orjuela et al for more details on aerobic aromatic hydrocarbon degradation (Ladino-Orjuela *et al.*, 2016).

Anaerobic aromatic hydrocarbon degradation has also been extensively reviewed (Harwood *et al.*, 1998; Foght, 2008; Fuchs *et al.*, 2011). Similar to aerobic peripheral pathways, anaerobic pathways are widely diverse and represent many different mechanisms that generate a few key central intermediates, of which benzoyl-CoA is the most well-known. One well understood peripheral anaerobic pathway involves the degradation of toluene that is initiated by fumarate addition through benzylsuccinate synthase (BSS) via a gylcyl radical, homologous to anaerobic alkane degradation through fumarate addition mentioned above. Unsubstituted aromatics may be methylated, directly

carboxylated, or hydroxylated before being converted to benzoyl-CoA (Foght, 2008). Following the generation of benzoyl-CoA, the aromatic ring is susceptible to reduction reactions outlined in Harwood et al (Harwood *et al.*, 1998). The first step is catalyzed by a class I benzoyl-CoA reductase (BcrABCD), which requires 2 ATP. An ATP-independent mechanism is also known using a non-homologous class II benzoyl-CoA reducatse (BamBCDEFGHI) potentially driven by electron bifurcation (Fuchs *et al.*, 2011).

Even less is known about the metabolic pathways involved in asphaltene and resin degradation, although work is being conducted as a viable method for reducing heavy crude oil viscosity and improving oil well extraction efficiency (Lavania *et al.*, 2012). It is known that these very high molecular weight, heteroatom containing, polar structures are resistant to biodegradation and accumulate when crude oil is biodegraded as lower molecular weight compounds are preferentially targeted (Head *et al.*, 2006). A few isolates, *Garciaella petrolearia* TERIG02 (bacterial) and *Neosartorya fischeri* (fungal) among very few others, have been characterized that can degrade asphaltenes in heavy crude oils. *G. petrolearia* was able to preferentially degrade asphalt under anaerobic conditions, in part producing CO_2, H_2, as well as organic acids, smaller aromatics, and n-alkanes (Lavania *et al.*, 2012). The underlying mechanism and genetic pathways involved are not known. The fungus *N. fischeri* was also shown to grow on asphaltenes as a sole carbon source (Hernández-López *et al.*, 2016). *N. fischeri* is thought to use cytochrome P450 monooxygenases due to the observed metabolic intermediates. Other fungal isolates have also been shown to degrade high molecular weight PAHs using cytochrome P450s (Syed *et al.*, 2011). Interestingly, the resistance of asphaltenes and resins may be due to their solubility and not due to their high molecular weight nature and complexity (Marin-Spiotta *et al.*, 2014).

1.6 Environmental Regulation of Hydrocarbon Degradation

Similar to the breakdown of natural organic matter, biodegradation mediated by indigenous microbial communities is the ultimate fate of the majority of petroleum hydrocarbons (oil and gas) that enter the marine environment. All of the same environmental pressures that impact microbial food webs are in play during oil discharge including: temperature, pressure, oxygen and nutrient availability, and physical or chemical form of the oil (Ronald M Atlas, 1981; Leahy and Colwell, 1990; Head *et al.*, 2006). A large body of literature, including laboratory and field studies, is devoted to the effects of the marine environment on hydrocarbon degradation (Prince, 2010; Hazen and Prince, 2015).

We posit that local environmental conditions of temperature and the availability of oxygen and nutrients, which have been shown to limit the rate and extent of hydrocarbon degradation or weathering, are determined by physical processes and the exchange of water masses in the oceans. Although less data is available, pressure is also thought to limit degradation rates through effects on chemical solubility and/or the physiology of hydrocarbon-degrading bacteria. The majority of laboratory studies of hydrocarbon biodegradation have been performed with pure cultures or enrichment cultures under conditions that resemble the surface ocean, and relatively few studies have been conducted under high pressure and low temperature conditions that mimic deep-water conditions. This fundamental gap in the understanding of microbial hydrocarbon degradation is in contrast to the petroleum industry trend of increasing oil and gas production from ultradeep (>1500 m) wells and the risk of another deepsea oil well blowout. Application of chemical dispersants and their influence on biodegradation or weathering has yet to be interrogated

across the full range of oceanographic conditions observed in areas of oil exploration/ production. In addition, more information is available on the environmental controls of hydrocarbon degradation under conditions relevant to marine water columns in comparison to the seafloor or sediments. This lack of knowledge of the impacts of oceanographic controls, especially in the deepsea, acts as a critical obstacle to the effective parameterization of oil plume models.

Results from the Deepwater Horizon discharge indicate that oxygen is rarely depleted in the oil-contaminated water column (Hazen and Prince, 2015). The focus of research has thus been on temperature and nutrient limitation. The capacity and efficiency of petroleum hydrocarbon degradation in seawater has long been shown to be strongly limited by temperature in laboratory-based studies (Zobell, 1946; Atlas, 1975; Bagi *et al.*, 2013, 2014), although relatively rapid rates equivalent to half-lives of 1-8 days for C13-C26 alkanes were observed in the permanently cold deep ocean (Hazen *et al.*, 2010). These quick rates were reproduced by (Brakstad *et al.*, 2015) using 5 °C seawater incubations amended with Macondo crude oil. Although these data indicate that temperature was not the overriding factor limiting degradation, in many cases, the temperature response was quantified under high nutrient conditions.

Oil is an unusual carbon substrate for microbial growth. Not only is it largely insoluble, it is also low in major nutrients (N, P). A large body of research has shown that nutrient availability determines the rate of microbial oil degradation in marine systems (Ronald M Atlas, 1981; Leahy and Colwell, 1990; Prince, 2010). These observations serve as the basis for bioremediation strategies, such as that employed in response to the Exxon Valdez spill (Prince, 2010). However, more than two decades after the Exxon Valdez

disaster, evidence remains equivocal regarding nutrient limitation of hydrocarbon degradation in studies surrounding the DWH discharge. (Hazen *et al.*, 2010) reported evidence of enhanced respiration and growth of hydrocarbon-degrading bacteria in oil plumes resulting from the DWH discharge, suggesting that sufficient nutrients were available for degradation. In a study conducted in mesocosms of surface seawater from the Gulf, nutrients also appeared to limit hydrocarbon degradation as respiration rates as well as biomass did not change in response to Macondo oil addition (Ortmann and Lu, 2015). In contrast, under severely nutrient limited conditions near the DWH wellhead, (Edwards *et al.*, 2011) observed enhanced respiration rates and a half-life of 26 days for oil degradation in the surface mixed layer. Because bacterial biomass levels did not appear to differ in the surface slick relative to surrounding waters, it was suggested that top-down processes such as grazing or viral lysis suppressed the elevation of biomass. Based on evidence from ultra-high resolution mass spectrometry, recent work demonstrates that oil-derived dissolved organic matter could serve as a nutrient (N, S, P) source for oil degradation in deep waters collected near an active hydrocarbon seep in the Gulf (Kleindienst *et al.*, 2015; Seidel *et al.*, 2015). Finally, a metagenomic time series from coastal sediments exposed to oil from the DWH discharge showed that the abundance of genes associated with nutrient scavenging (nitrogen fixation, iron chelation) was positively correlated with the abundance of genes for hydrocarbon catabolism (Rodriguez-R *et al.*, 2015).

Together these data indicate that the ocean environment dictates the efficiency and capacity of microbial communities to perform hydrocarbon degradation. However, we have yet to discern how multiple environmental pressures interact to determine final

catabolic outcomes. Thus, despite an extensive knowledge base on hydrocarbon degradation, quantitative understanding is lacking and the incorporation of microbial biodegradation into numerical models of oil fate and transport remains poorly defined, despite its importance to accurate construction of hydrocarbon budgets (Vilcáez *et al.*, 2013; Bagi *et al.*, 2014).

1.7 Research Scope and Objectives

Microbial biodegradation or combustion are the only two mechanisms that completely eliminate petroleum hydrocarbons from the environment by converting them to carbon dioxide and water (Prince, 2010). Therefore, the entirety of oil entrained in Gulf of Mexico benthic sediments is regulated by microbial populations capable of degrading oil constituents, or through burial processes. In addition, oil contamination can have far reaching and negative impacts on ecosystems through competitive exclusion, direct inhibition / toxicity, altered nutrient availability, and disruption of biogeochemical cycles. Thus, the overall objective of this document is to advance our understanding of the fate and consequences of deposited Deepwater Horizon crude oil to benthic ecosystems and the *in situ* microbial community. A key guiding concept that links the subsequent four chapters involves improving our mechanistic and therefore predictive understanding on the environmental controls that regulate microbial biodegradation. The results presented herein are intended to guide future response efforts to marine oil spills as well as to improve hindcasts towards the long-term consequences of the Deepwater Horizon disaster.

The second chapter from this dissertation investigates the unintended consequences of chemical dispersant on individual populations of hydrocarbon-degrading bacteria

isolated from contaminated beach sands. *Alcanivorax* is a well-studied obligate hydrocarbonoclastic genus that has a limited carbon substrate range, a cosmopolitan distribution, and rapidly responds to oil in the environment. *Acinetobacter* sp. are less studied generalists with a broad carbon substrate range and a well-known capacity to degrade hydrocarbons in terrestrial and marine ecosystems. This was the first study conducted to investigate the effects of bacterial-mediated biodegradation of oil and dispersant constituents on overall oil toxicity. It was found that each strain responded uniquely to dispersed oil as compared to crude oil. Considering our results, it is not appropriate to generalize that hydrocarbon-degrading bacterial populations uniformly respond positively to dispersed oil. Instead, specific microbial groups interact with oil and dispersed oil through varying mechanisms, likely involving biosurfactant/bioemulsifier production and modification of cellular membrane composition. The outcome of this interaction will determine the efficiency of biodegradation as well as overall ecosystem impacts.

In chapter 3, the decomposition of buried oil in supratidal beach sands is determined along with the mechanisms that control its degradation. Hydrocarbon decay rates were determined in the field by quantifying changes in the concentrations of aliphatic and aromatic compounds over time. Furthermore, the abundance, composition, and succession in microbial communities is characterized at high resolution and demonstrated to parallel changes in hydrocarbon chemistry. Finally, the high rates of degradation observed were attributed to tidal pumping that transported oxygen into the buried oil layers while removing carbon dioxide, as well as regulating temperature and moisture gradients within

the beach. Within one-year, hydrocarbon concentrations had returned to background levels and microbial communities had recovered to near baseline conditions.

The fourth dissertation chapter interrogates the environmental factors that determine the distribution of benthic microbial populations across the northern and southern regions of the Gulf of Mexico. In order to determine the microbial response to oiling, the natural state of fine-grained sediments must first be understood. However, prior to the Deepwater Horizon disaster, the microorganisms present at the oligotrophic Gulf of Mexico deep seafloor were virtually unknown. Therefore, deep ocean sedimentary microbial communities were characterized across the region to establish baseline conditions over large spatial scales. Elucidated distributions were used to map the biogeographical patterns in microbial community structure across the Gulf of Mexico. Due to strong gradients in community structure induced by geospatial factors, a model to predict the abundance of dominant microbial populations across the Gulf of Mexico was generated. Finally, this model was used in a meta-study to robustly determine if impacted regions had returned to baseline conditions.

The final research chapter seeks to address knowledge gaps in our understanding the fate of oil sequestered in nearshore, subtidal sediments. Advective-flow chambers were employed to reproduce the dominant solute transport pathways in permeable sands under rigorously controlled and well-replicated conditions. As a result, the underlying ecological principles governing the response of microbial populations to oil disturbance could be robustly tested. Unlike in the supratidal sands studied in the field in chapter 3, oxygen and solute transport are controlled by pore-water exchange rates. The objectives were to (1) determine oil-induced disruptions to carbon and nitrogen biogeochemical cycling

processes, (2) quantify rates of oil degradation and the transformation of specific compound classes, (3) determine the acute impacts of weathered crude oil to sensitive microbial populations, and (4) examine the controls of biodegradation activity.

This dissertation concludes with a synthesis of the results and highlights of the most important findings to guide future response efforts. Common findings between the chapters are discussed and are linked to overarching ecological themes. In addition, unanswered questions, current knowledge gaps, and important future research efforts are emphasized.

CHAPTER 2. HYDROCARBON DEGRADING BACTERIA EXHIBIT A SPECIES SPECIFIC RESPONSE TO DISPERSED OIL WHILE MODERATING ECOTOXICITY

2.1 Abstract

The Deepwater Horizon blowout in April 2010, represented the largest accidental marine oil spill and the largest release of chemical dispersants into the environment. While dispersant application may provide numerous benefits to oil spill response efforts, the impacts of dispersants and potential synergistic effects with crude oil on individual hydrocarbon degrading bacteria are poorly understood. In this study, two environmentally relevant species of hydrocarbon degrading bacteria were utilized to quantify the response to Macondo crude oil and COREXIT® 9500A dispersed oil in terms of bacterial growth and oil degradation potential. Furthermore, specific hydrocarbon compounds were quantified in the dissolved phase of the medium and linked to ecotoxicity using an EPA-approved rotifer assay. Bacterial treatment drastically reduced the toxicity associated with dispersed oil (increasing the LC_{50} by 215%). Growth and crude oil degradation potential of *Acinetobacter* were inhibited by COREXIT 34% and 40%, respectively; conversely, COREXIT enhanced the growth of *Alcanivorax* by 10% relative to un-dispersed oil.

Furthermore, both bacterial strains were shown to grow with COREXIT as the sole carbon and energy source. Hydrocarbon-degrading bacterial species demonstrate a unique response to dispersed oil as compared to crude oil, with potentially opposing impacts on toxicity. While some species have the potential to enhance the toxicity of crude oil by producing biosurfactants, these same bacteria may reduce the toxicity associated with dispersed oil through degradation or sequestration.

2.2 Introduction

The Deepwater Horizon (DWH) oil spill discharged approximately 4.9 million barrels of light crude oil into the ocean at a depth of 1500 meters below the sea surface (Operational Science Advisory Team (OSAT), 2010). In an attempt to enhance biodegradation and to prevent oil from reaching sensitive shorelines, approximately 1.84 million gallons of the chemical dispersants COREXIT® 9500A and COREXIT® 9527A were applied at both the surface (1.06 million gallons) and directly to the wellhead in the deep sea (0.78 million gallons) (Operational Science Advisory Team (OSAT), 2010). Although dispersant was used in response strategies prior to the DWH oil spill, the DWH oil spill marks the first large-scale subsea application of dispersants. Therefore, understanding the impacts of dispersants on Gulf of Mexico ecosystems is crucial.

Biodegradation is the ultimate fate of the majority of hydrocarbons that enter the marine environment (Leahy and Colwell, 1990; Prince, 2010). Based on calculations of remaining and dispersed oil in the Gulf of Mexico, it was estimated that hydrocarbon-degrading bacteria removed up to 50% of the hydrocarbons released during the DWH oil spill (Ramseur, 2010). Analysis of *in situ* microbial community composition, gene

expression, and hydrocarbon degradation rates in oil-contaminated seawater samples support these claims (King *et al.*, 2014). Amplicon sequencing of SSU rRNA genes revealed that taxa with high sequence identity to known oil-degrading bacteria were enriched in oil-contaminated seawater samples compared to uncontaminated samples (Camilli *et al.*, 2010; Hazen *et al.*, 2010; Mason *et al.*, 2012, 2014). Additionally, genes involved in hydrocarbon degradation were significantly enriched and enhanced rates of biodegradation were reported in deep-sea plumes exposed to Macondo oil from the DWH blowout (Valentine *et al.*, 2010; Lu *et al.*, 2012; Rivers *et al.*, 2013).

Dispersants, which are composed of a surfactant dissolved in a hydrocarbon-based solvent, function by reducing the interfacial surface tension between water and oil that results in the formation of tiny oil droplets that rapidly disperse (Lessard and DeMarco, 2000). Although dispersant formulations have been continuously improved to reduce toxicity since the 1960s, the possible synergistic effects of oil and dispersant mixtures on toxicity to organisms still requires further research (Rico-Martínez *et al.*, 2013). Based on criteria set forth by the EPA, the majority of dispersants range from slightly toxic to practically non-toxic (George-Ares and Clark, 2000). Dispersant-oil mixtures, however, have been shown in numerous studies to be significantly more toxic than dispersants alone. Rico-Martinez et al. demonstrated that the synergistic effect of COREXIT® 9500A with Macondo crude oil increased toxicity to the marine rotifer *Brachionus manjavacas* 47-52 fold relative to the water accommodated fraction (WAF) generated from Macondo crude, and 66 fold relative to COREXIT® 9500A alone (Rico-Martínez *et al.*, 2013). *B. manjavacas* is a member of the *B. plicatilis* species complex that has routinely been used in assessments of marine ecotoxicity since the organism grows rapidly, is easy to cultivate,

genetically homozygous, and plays a central role in coastal food webs (Snell and Janssen, 1995; Dahms *et al.*, 2011). Furthermore, the EPA required BP to assess the toxicity of dispersed oils using the *Brachionus* rotifers test following the Deepwater Horizon oil spill (U.S. Coast Guard and Agency, 2010). In another study, Hemmer et al. showed that dispersant-crude oil mixtures were more toxic than dispersants alone to mysid shrimp (*Americamysis bahia*) and inland silverside fish (*Menidia beryllina*) (Hemmer *et al.*, 2011). Other studies observed that dispersed oil and dispersant constituents showed higher toxicity to coral species than crude oil alone (Ballou *et al.*, 1989; Shafir *et al.*, 2007). Components of the dispersant also potentially inhibit or delay microbial oil degradation. For example, in one study comparing different dispersant-oil mixtures, lags in biodegradation were attributed to preferential degradation of the dispersant (Mulkins-Phillips and Stewart, 1974).

In addition to synthetic dispersants, biosurfactants and bioemulsifiers are produced by a diversity of hydrocarbon degrading microorganisms from all domains of life (Banat *et al.*, 2010). These compounds impact the physical-chemical properties of oil in a similar, and often more effective, manner to synthetic chemical dispersants (Ron and Rosenberg, 2002; Banat *et al.*, 2010; Rosenberg and Ron, 2013). Microbially synthesized surfactants are primarily classified based on their molecular weights. Low molecular weight biosurfactants are generally lipopeptides and glycolipids that function to lower surface and interfacial tensions, increasing the solubility of hydrocarbons (Ron and Rosenberg, 2002). High molecular weight compounds include polysaccharides, proteins, lipopolysaccharides, lipoproteins, as well as complex mixtures of these biopolymers (Rosenberg and Ron,

2013). Biosurfactants likely play a role in hydrocarbon resource partitioning between microbial populations responding to crude oil released into the environment.

Since biodegradation represents an important fate for hydrocarbons in the environment, it is important to understand how components of COREXIT® 9500A ultimately impact bacterial degradation and biosurfactant production, and how degradation of the synthetic dispersant and oil affects toxicity to marine life. To our knowledge, no study has investigated the effects of bacteria-mediated biodegradation of oil and dispersant constituents on overall toxicity. The two primary objectives of this study were (i) to quantify the hydrocarbon-degradation potential of two bacterial strains isolated from oil-contaminated sands, *Alcanivorax sp.* P2S70 and *Acinetobacter sp.* COS-3, with crude oil alone, with COREXIT® 9500A dispersed oil, and with COREXIT® 9500A alone and (ii) to link bacterial growth and activity to observed changes in overall toxicity and the solubility of specific hydrocarbon compounds. We demonstrate that the effects of COREXIT® 9500A on the biodegradation of crude oil are species specific with opposite responses in biodegradation observed. Similarly, results indicate that some populations of hydrocarbon degrading bacteria may enhance the toxicity of light crude oil, likely through the production of biosurfactants that increase the solubility of several classes of hydrocarbon compounds. Conversely, the activity of both strains significantly reduced overall toxicity of dispersed oil to *Brachionus manjavacas* in comparison to un-inoculated controls. In order to achieve a predictive understanding of biodegradation, the potential synergistic effects that crude oil and dispersants have on microbial processes require further research.

2.3 Materials and Methods

2.3.1 Bacterial Strains

In previous work, 24 bacterial strains were isolated using Macondo oil as a sole carbon source from beach sands exposed to oil deposited from the Deepwater Horizon (DWH) discharge at Pensacola Beach (Kostka *et al.*, 2011; Overholt *et al.*, 2013). Of these, two strains were chosen to represent contrasting functional roles in hydrocarbon degradation. *Alcanivorax* spp. are obligate hydrocarbon degrading bacteria, specializing in aliphatic hydrocarbon degradation (Head *et al.*, 2006; Yakimov *et al.*, 2007). *Alcanivorax* strain P2S70 is representative of a dominant population detected *in situ* in contaminated beach sands (Overholt *et al.*, 2013). This environmentally abundant strain had a ca. 25 % reduced genome size compared to another *Alcanivorax* strain (PN-3) isolated from these same beach sands. It also encodes ~40 % fewer genes known to be associated with hydrocarbon degradation, indicating a higher degree of specialization (Overholt *et al.*, 2013). In contrast, *Acinetobacter* spp. are considered generalists with a broad carbon substrate range including PAHs and aliphatic hydrocarbons (Di Cello *et al.*, 1997; Gao *et al.*, 2006; Kang *et al.*, 2011). Along with *Alcanivorax* strains, *Acinetobacter* sp. showed the highest potential for oil degradation in pure culture (Kostka *et al.*, 2011).

2.3.2 Culture Conditions

All bacterial cultures were grown in an artificial seawater medium at 25 °C in the dark to prevent hydrocarbon photo-oxidation (F. Widdel, 2010). The cultures were shaken in Erlenmeyer flasks with at least a 70 % headspace at 150 rpm to promote sufficient aeration. Three carbon source treatments were tested throughout this study, (1) 0.5% (v/v) crude oil, (2) 0.01% COREXIT® 9500A, or (3) a 1:50 COREXIT® 9500A:oil mixture

(hereafter referred to as crude oil, COREXIT, and dispersed oil treatments, respectively). The concentration of oil (5g/L) used in this study was based upon previous studies investigating the toxicity of the water accommodated fraction of crude oil as well as microbial degradation of crude oils [Shafir et al. at 5g/L (Shafir *et al.*, 2007), Gardiner et al. at 10g/L (Gardiner *et al.*, 2013), Hemmer et al., at 25g/L (Hemmer *et al.*, 2011), Anderson et al. at 25g/L (Anderson *et al.*, 2014), Campo et al. at 5g/L (Campo *et al.*, 2013), Swannell et al. at 0.3 g/L (Swannell and Daniel, 1999)]. The crude oil used in this study is surrogate MC252 oil collected from the Marlin Platform in the Dorado Field and provided by British Petroleum (BP) (Pelz *et al.*, 2011). The crude oil and dispersant mixture was adjusted to a 1:50 ratio, which is at the lower end of the range of EPA recommended ratios for dispersing oil (US Environmental Protection Agency, 2014). All experiments were performed with triplicate cultures, with the exception of the specific hydrocarbon class analysis where only one sample was used per treatment. For hydrocarbon analysis, cultures were sacrificed after 7 and 14 days of incubation. Only the cultures from 7 days of incubation were used for compound specific analysis (see below).

2.3.3 Hydrocarbon Analyses

Extraction and analysis of hydrocarbon compounds was performed according to a modified version of EPA method 3510C with accompanying QA/QC protocols. Briefly, bacterial and control treatments were extracted for quantification of total petroleum hydrocarbons (TPHs) as well as the specific hydrocarbon compound classes, aliphatics (*n*-alkanes C_{12}-C_{40}, and isoprenoids pristine and phytane) and polycyclic aromatic hydrocarbons (PAHs). Extracts were concentrated under a gentle stream of nitrogen using

a TurboVap and reconstituted in hexane (100%) for chromatographic analysis (see supporting information for more details).

TPHs in the samples was quantified using GC-FID. A one mL of EPH Surrogate Spiking Solution (ISM-581X, Lot CL-1009, Ultra, Kingstown, RI, USA) containing *o*-terphenyl and 1-chlorooctadecane was added directly to the separatory funnel before extraction. TPH concentrations were corrected for extraction efficiency based on recovery of the EPH spiking solution and mass of oil added.

Aliphatics and PAHs entrained in the culture media (WAF, the water accommodated fraction; and CEWAF, the chemically enhanced water accommodated fraction) were quantified in a gas chromatograph/mass spectrometric detector (GC/MS) in full scan mode (*m/z* 50-550). Splitless injections of 1μL of the sample were conducted, and a RXi®5sil column (30 m x 0.25 mm x 0.25 μm) was used. Quantitative analysis of aliphatics and PAHs were conducted using the IS (internal standard) method (see supporting information for more details). Concentrations are expressed as volume sample (L), and all recoveries were generally within QA/QC criteria of 90-120% for aliphatics and 70-120% for aromatics.

2.3.4 Quantification of Bacterial Growth

Bacterial growth was quantified as total cellular protein. Cultures were grown in 15 mL of artificial seawater medium (F. Widdel, 2010) and were supplemented with crude oil, dispersed oil, or COREXIT alone as detailed above. Additional controls included an un-inoculated treatment (non-bacterial control) for each substrate and an inoculated control

with no added carbon source but containing bacterial inoculum in the same volume as the carbon treatments (non-carbon control). All treatments were performed in triplicate.

Treatments (3 replicates each) were sacrificed at each time point. The entire volume of culture medium was added to a 15 mL falcon tube that was centrifuged at 3200x g for 20 minutes. The supernatant was removed without disturbing the cell pellet and the samples were stored at -20 °C until further analysis. Total cellular protein was extracted using 1 ml of 2% SDS lysis buffer (50 mM Tris-HCl buffer with 2% (w/v) SDS) followed by a room temperature incubation for 20 minutes. Samples were sonicated (Fisher Scientific Sonic Dismembrator model 550, amplitude of 4) for 15 seconds total (half a second on, half a second off). The samples were then centrifuged at 3200 g for another 20 minutes. Total cellular protein quantified following the Pierce Bicinchoninic Acid protein assay protocol according to the manufacturer instructions (Life Technologies, Grand Island, NY, USA).

2.3.5 Ecotoxicity Assays

Static acute toxicity tests were conducted using the marine rotifer, *Brachionus manjavacas*. The water-accommodated fraction (WAF, from the crude oil treatment) and chemically-enhanced water accommodated fractions (CEWAF, from dispersed oil treatment) were prepared following methods outlined in Singer et al. and modified to permit bacterial growth (Singer *et al.*, 2000). Specifically, cultures were shaken at 150 rpm instead of mixed with a stir bar and air exchange was permitted to prevent the headspace from going anaerobic. Furthermore, the mixing time suggested by Singer et al. was insufficient for bacterial growth (Singer *et al.*, 2000). Thus, for our purposes, the WAF and CEWAF were prepared following the same conditions throughout all of the experiments.

A preliminary experiment was conducted using un-inoculated controls to compare the Singer et al., method and our modified method (Singer *et al.*, 2000). Our modified method did not significantly alter toxicity results to *B. manjavacas* (Figure A.1).

After seven days of incubation, based on bacterial growth curves and TPH analysis, the samples were poured into separatory funnels and allowed to settle for four hours. Approximately 10 ml of the WAF or CEWAF were collected in autoclaved Hungate tubes for use in the toxicity tests. The toxicity tests were conducted in 24-well plates, and samples of the WAF and CEWAF were diluted with 15 ppt artificial sea water in aliquots of 20% from 0 to 100% in order to determine the concentration killing 50% of test animals (LC_{50}) (Rico-Martínez *et al.*, 2013). In each well, 10 rotifers were added and their viability was scored after 24- and 48-hours (we present only the 48 hour results). The plates were incubated at 25 °C in the dark. The trimmed Spearman-Karber method (Hamilton et al. 1977) was used to calculate the 48 h LC_{50} values as implemented in the R package 'tsk' (Stone, 2012). Data was trimmed using parameters generated by the package and data was smoothed when mortality was observed in the controls (total rate of 1.8% across all controls).

2.4 Results

2.4.1 Bacterial Growth on Crude Oil and Dispersant.

Bacterial growth assays for *Acinetobacter sp.* COS-3 and *Alcanivorax sp.* P2S70, hereafter referred to as *Acinetobacter* and *Alcanivorax* respectively, were conducted using the five treatments detailed above, (1) crude oil (0.5% v/v), (2) COREXIT® 9500A dispersed crude oil (1:50 Corexit: oil), (3) COREXIT® 9500A, (4) a non-bacterial control,

and (5) a non-carbon control. In all treatments studied, *Acinetobacter* showed faster growth rates and a higher maximum biomass accumulation (Figure 2.1, Figure A.2).

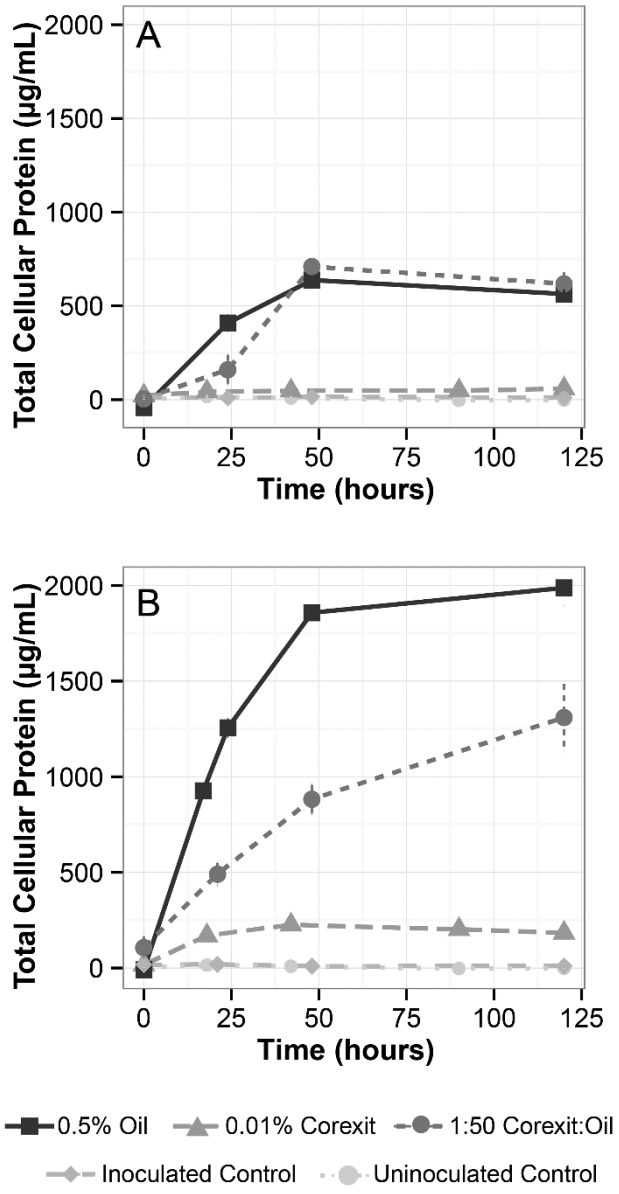

Figure 2.1 Bacterial growth curves determined using a Pierce Bicinchoninic Acid protein assay. Carbon sources are indicated by line type and point shape. (A) Growth of Alcanivorax sp. P2S70. (B) Growth of Acinetobacter sp. COS-3. See Figure S2 for an expanded view

Alcanivorax showed similar maximum growth yields (50 hour time point, two sample t-test: t = -1.41, p = 0.23) when grown on dispersed oil (709.7±56.3 µg/ml total protein) and on crude oil alone (637.8±29.9 µg/ml total protein), although a lag was observed in the dispersed oil treatment (Figure 2.1 A). Significant growth of *Alcanivorax* was observed with COREXIT as the sole carbon and energy source (58.3±22.2 µg/ml; t = 4.05, p = 0.015, Figure A.2) in comparison to the inoculated no-carbon control (11.0±3.6 µg/ml), comprising approximately 10 times less growth in comparison to that on crude oil as the carbon source. Little to no cell protein accumulated with time in either of the control treatments (Figure 2.1 A).

Acinetobacter demonstrated maximum growth rates and maximum protein produced when grown on crude oil alone (1988.0±160.4465 µg/ml, Figure 2.1 B). The dispersed oil treatment (1309.9±175.5 µg/ml) produced 34% less protein in comparison to crude oil alone, and resulted in a slower growth rate. Similar to *Alcanivorax*, *Acinetobacter* was capable of growth on COREXIT alone (183.6±7.8 µg/ml, although the growth yield comprised 11 % of the protein compared to growth on crude oil alone (Figure A.2). Except for the two controls (t = -1.41, p = 0.23), all treatments yielded significantly different maximum protein concentrations compared to the controls (Table A.1).

2.4.2 Quantification of Oil Degradation

Total petroleum hydrocarbons (TPHs) were extracted from the oil-amended treatments. Oil degradation potential was determined in parallel through comparison of bacterial treatments to the un-inoculated control. Volatile hydrocarbons are lost during extraction analysis using this method, and thus only n-alkanes > C11 were detected in the

control and bacterial treatments, not unlike weathered oil washed ashore at Pensacola Beach (Gros *et al.*, 2014).

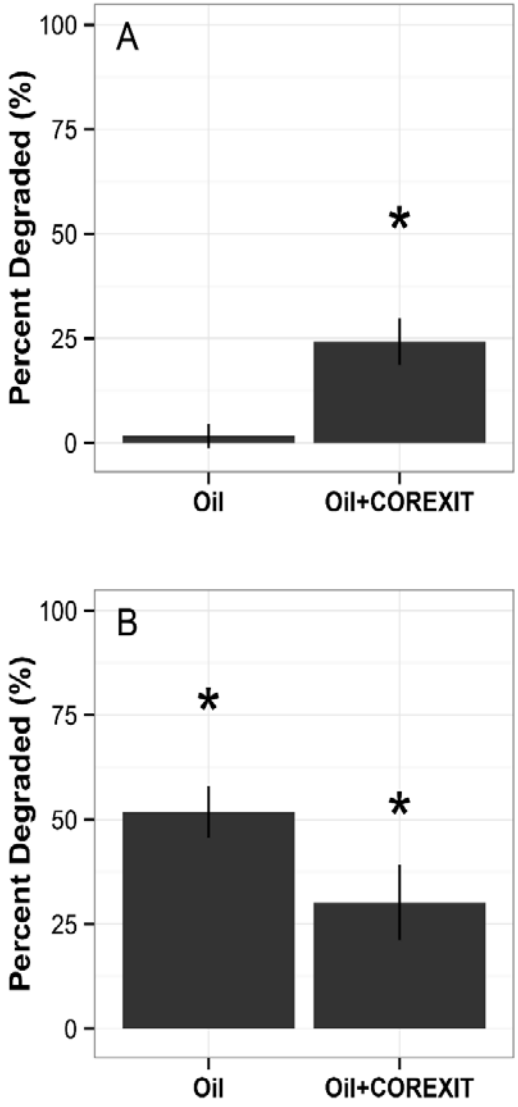

Figure 2.2 Potential of bacterial strains to degrade or transform petroleum hydrocarbons. Values are relative to the un-inoculated control and are corrected for extraction efficiency and mass of oil added. TPHs were used by summing areas under each peak as determined by GC-FID. (A) Oil degradation potential for Alcanivorax sp. P2S70; (B) oil degradation potential for Acinetobacter sp. COS-3. An outlier from Acinetobacter was removed; see Fig. S3 for a version of this figure that includes the outlier. Asterisks indicate samples that are significantly different from the control samples. Data shown were collected after 7 days of incubation.

Alcanivorax and *Acinetobacter* showed contrasting patterns in oil degradation capacity in pure culture. Concomitant with bacterial growth, *Alcanivorax* degraded or transformed 25% of the TPHs in dispersed oil relative to the un-inoculated control (Figure 2.2 A, $t = -4.45$, $p = 0.011$). In the absence of COREXIT (crude oil treatment), no detectable transformation or removal of TPHs was observed in *Alcanivorax* cultures after 7 days of incubation ($t = -0.75$, $p = 0.49$). In contrast, 52% of the TPHs present in the crude oil treatment relative to the un-inoculated control were degraded or transformed in *Acinetobacter* cultures ($t = -7.35$, $p = 0.0019$), while only 30% oil removal or transformation was observed in the dispersed oil treatment ($n=2$, $t = -4.44$, $p = 0.021$ *[$p = 0.07136$ if unequal variances are assumed]*, Figure 2.2 B). See the Appendix A for a discussion of an outlier removal; Figure A.3 interprets these data with the outlier included. When incubations were extended to 14 days, *Acinetobacter* transformed or removed 54% and 44% of TPHs in the oil only and dispersed oil treatments, respectively (Figure A.3; $t=-7.0$, $p = 0.0075$; $t = -11.8$, $p = 0.0024$; respectively). No change was observed in the *Alcanivorax* cultures between 7 and 14 days of incubation ($t = -1.0$, $p = 0.32$).

2.4.3 Quantifying the Effect of Bacterial Treatments on Rotifer Toxicity

Three sets of acute toxicity tests were conducted to quantify the impacts of bacterial degradation on the toxicity crude oil, dispersed oil, and COREXIT alone within the water accommodated fraction. All *B. manjavacas* toxicity tests met the requirement of >90% control survival to accept them as valid estimates of toxicity. All toxicity tests consisted of an un-inoculated control, and treatments of media inoculated with *Acinetobacter*, or media

inoculated with *Alcanivorax*. All COREXIT only treatments resulted in similar toxicity and statistically indistinguishable LC_{50} values with a mean of 80.56 µg COREXIT / ml after 48 hours (ANOVA, F = 2.43, p = 0.17, Figure 2.3 A, Table 1). According to EPA standards, these treatments are classified as "slightly toxic". The crude oil un-inoculated

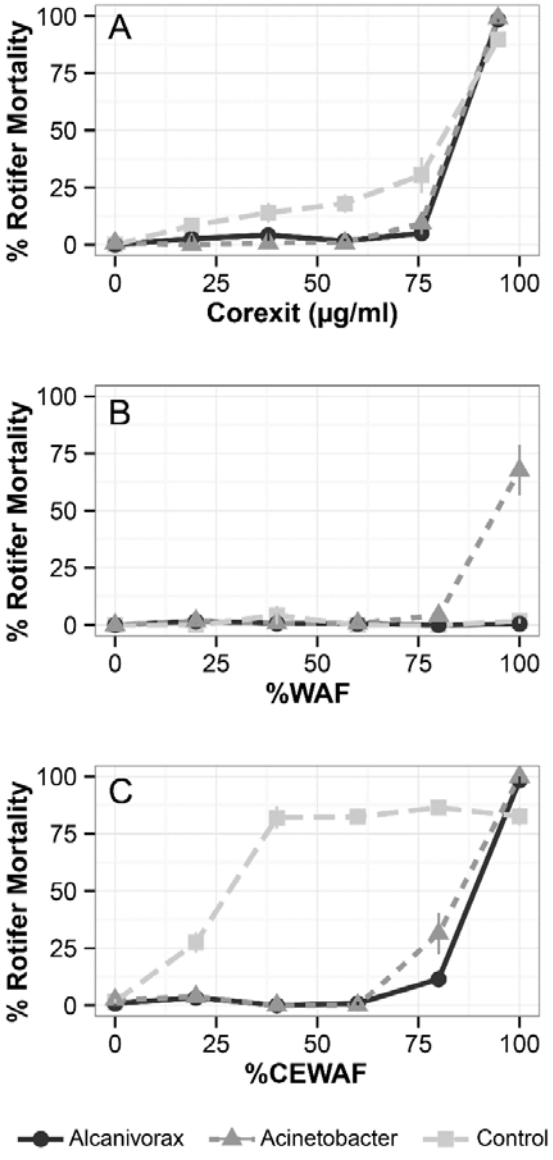

Figure 2.3 Ecotoxicity of bacterial treated crude oil and dispered crude oil, and COREXIT only. All toxicity measurements were determined using the marine rotifer Brachionus plicatilis. All controls met the minimum requirement for survival (>90%). (A) Toxicity associated with COREXIT 9500A alone. (B) Toxicity associated with 0.5% (v/v) Macondo surrogate crude oil alone. (C) Toxicity associated with 1:50 COREXIT 9500A dispersed Macondo crude oil.

control (WAF) and crude oil *Alcanivorax* treatments (WAF) were not acutely toxic to *B. manjavacas* with 0% mortality observed in all replicates at the tested concentrations (Figure 2.3 B, Table 2.1). However, when *Acinetobacter* was grown on crude oil, acute toxicity was observed with an LC_{50} of 94.0 % WAF (see Figure A.4 for conversion to µg/L). The dispersed oil un-inoculated control (CEWAF) was significantly more toxic than either COREXIT alone or crude oil alone (WAF) when compared as percent dilutions (Figure 2.3 C, Table 2.1). Bacterial degradation greatly reduced acute toxicity associated with dispersed oil (CEWAF), independent of the strain used ($t = -1.53$, $p = 0.23$). No mortality of *B. manjavacas* was observed in the bacterial treated dispersed oil when CEWAF was diluted to 40 % or greater.

Table 2.1 LC50 values for all treatments tested in this study.

Treatment	48-h LC_{50}	LC_{50} 95% confidence limits[a]	p-value	Percent LC_{50} change[b]
0.01% Corexit® 9500A (ug/mL)				
Uninoculated Control	75.06	71.33-80.05	--	
Alcanivorax	83.8	81.08-84.70	0.191	--
Acinetobacter	82.85	81.93-84.16	0.251	--
1:50 Corexit® 9500A:Oil (% CEWAF)				
Uninoculated Control	27.74	24.90-28.71	--	--
Alcanivorax	87.51	85.79-88.53	**7.3×10^{-6}**	**215%**
Acinetobacter	83.02	81.00-84.60	**4.5×10^{-6}**	**199%**
0.5% Oil (%WAF)				
Uninoculated Control	N/A	n.d.t	--	--
Alcanivorax	N/A	n.d.t	--	--
Acinetobacter	94.03	92.03-96.08	--	

P-values were determined with pairwise two sample t-tests comparing bacterial treatments to the corresponding un-inoculated control. [a] n.d.t = no detectable toxicity. [b] Percent change in LC_{50} relative to the control. This was only calculated if significant change was observed.

2.4.4 Compound Specific Analysis

To better understand the observed changes in toxicity between crude oil (WAF), dispersed oil (CEWAF), and the impact of bacterial transformations on both, analyses of specific hydrocarbon compounds present in the water accommodated fractions were performed after 7 days of growth.

In the non-bacterial control for crude oil treatments, low levels of aliphatic compounds were present in the WAF (Figure 2.4 A, Figure A.5, sum total = 116 µg/L, compound max = 9.1 µg/L). As expected, the aromatic fraction was slightly more soluble, particularly the C1-C4 naphthalenes with C2-napthalene reaching a max concentration of 58.1 µg/L and total aromatics reaching a concentration of 127.2 µg/L in the WAF (Figure 2.4 B, Figure A.5). In all inoculated treatments (crude oil and dispersed oil), total aliphatic and aromatic fractions were approximately 3-fold enriched relative to the un-inoculated crude oil treatment (Figure A.5, TPHs: *Alcanivorax* = 468.2 µg/L, *Acinetobacter* = 428.1 µg/L). In the aliphatic fraction, *Alcanivorax* greatly increased the solubility of all n-alkanes and removed or transformed the branched alkanes (pristane, phytane) into non-GC amendable forms. In contrast, *Acinetobacter* solubilized branched alkanes as well as *n*-alkanes > C17 (Figure 2.4 A). In the aromatic fraction, the *Alcanivorax* treatment increased total PAH concentrations by 2-fold to 216.3 µg/L and the *Acinetobacter* treatment increased the concentration of aromatic hydrocarbons present in the WAF by 5-fold to 563.5 µg/L (Figure 2.4 B). Unlike *Alcanivorax*, *Acinetobacter* substantially increased the solubility of PAHs including the phenanthrenes, fluoranthenes, and benz[a]anthracenes which were undetectable in all other treatments.

In the non-bacterial control for dispersed oil treatments (CEWAF), total aliphatic concentrations were 52 times higher than in the corresponding non-bacterial control for

crude oil treatments (WAF) (6128 µg/L and 116.6 µg/L, respectively; Figure 2.4 C, Figure A.4). Relative to the dispersed oil control treatment, *Alcanivorax* reduced aliphatic concentrations in the CEWAF 3-fold, down to 2197 µg /L. While *Acinetobacter* greatly decreased the detected aliphatic concentrations, we suspect this may be due to biomass sequestration during the oil extraction due to extremely high amounts of EPS in the media and do not show the data. *Alcanivorax* slightly decreased total aromatic hydrocarbons from 1076 µg/L to 924 µg/L, evenly across all aromatic hydrocarbons analyzed. An expanded version of Figure 2.4 is available in Appendix A.

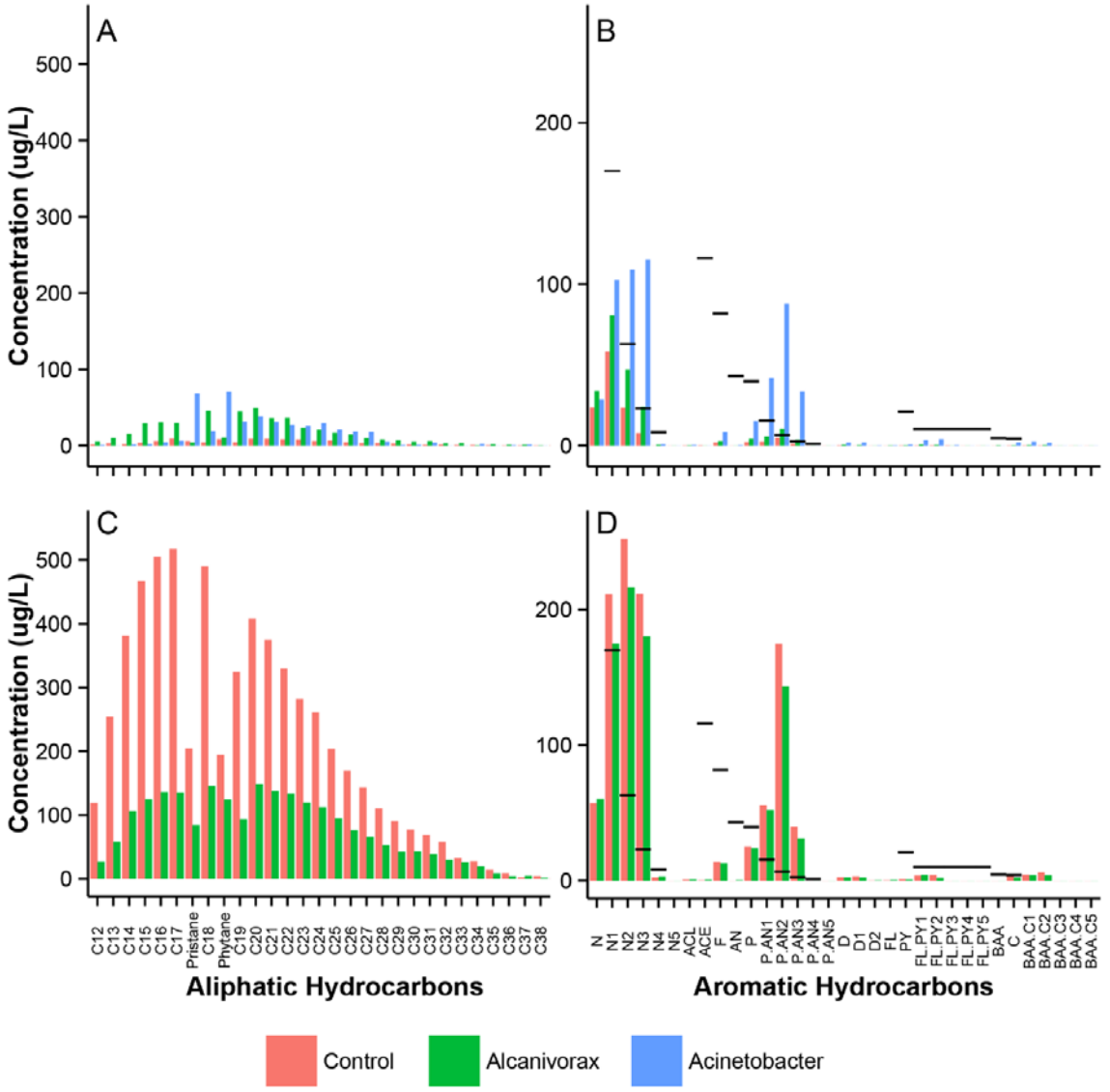

Figure 2.4 Detailed analysis of aliphatic (A, C) and aromatic (B, D) hydrocarbons present in the water accommodated fraction from the crude oil treatment (A, B) or the chemically enhanced water accommodated fraction from the dispersed oil treatment (C, D). Controls are indicated by red bars, Alcanivorax treated samples by green bars, and Acinetobacter treated samples by blue bars. EPA acute potency divisor values for aromatic hydrocarbons are indicated on plots B, D by black bars. Target PAHs are: Naphthalene (N) and alkylated homologues (NC1-C4), Acenaphthylene (ACL), Acenaphthene (ACE), Fluorene (F), Dibenzothiophene (D) and alkylated homologues (DC1-C2), Phenanthrene (P), Anthracene (AN), and their alkylated homologues (P/ANC1-C4), Fluoranthene (FL), Pyrene (PY), and their alkylated homologues (FL/PYC1-C4), Benz[a]anthracene (BAA), Chrysene (C), and their alkylated homologues (BAA/CC1-C4), Benzo[b]fluoranthene (BBF), Benzo[k]fluoranthene (BKF), Benzo[a]pyrene (BAP), Dibenz[a,h]anthracene (DA), and alkylated homologues (BP/PERC1-C4), Indeno[1,2,3-cd]pyrene (ID), and Benzo[ghi]perylene (BGP).

2.5 Discussion

The use of chemical dispersants is considered one of the main oil spill response tools as outlined in the National Oil and Hazardous Substance Pollution Contingency Plan (NCP) Subpart D §300.310. Dispersants are globally used to mitigate the damages caused by an oil spill, especially in minimizing the impact to near shore habitats by removing surface oil, diluting oil constituents to below toxic levels, and improving hydrocarbon accessibilities to oil degrading bacteria (Lessard and DeMarco, 2000; Chapman *et al.*, 2007). Furthermore, degradation of dispersed oil constituents in the ppm range will not be limited by background nutrient concentrations (National Research Council, 2005). In order to prevent crude oil released by the Deepwater Horizon oil blowout from reaching sensitive coastal ecosystems, the Unified Area Command (EPA and the National Incident Commander) approved the use of chemical dispersants following protocols outlined in the NCP and ultimately 1.84 million gallons of COREXIT® 9500A and COREXIT® 9527A were applied to the surface and at depth next to the wellhead (Allen, 2010; Operational Science Advisory Team (OSAT), 2010).

One of the primary aims in applying dispersants is to stimulate microbial biodegradation leading to the removal of petroleum hydrocarbons (Lessard and DeMarco, 2000; Chapman *et al.*, 2007; Lubchenco *et al.*, 2012). Past studies have typically focused on quantifying changes to biodegradation based on dispersant application, and maximizing microbial community biodegradation activity (see review by Prince, 2010 and references within). Unlike prior studies, we investigated how specific bacterial populations interact with crude oil and dispersed oil to elucidate impacts on bacterial growth, biodegradation potential, and ecotoxicity. Here we tested two strains based on their relevance to the

Deepwater Horizon oil spill and different metabolic strategies (Kostka *et al.*, 2011). *Alcanivorax* is a well-studied obligate hydrocarbonoclastic genus that has a limited carbon substrate range, a cosmopolitan distribution, and rapidly responds to oil in the environment (Head *et al.*, 2006; Yakimov *et al.*, 2007; King *et al.*, 2014). *Acinetobacter* sp. are less studied generalists with a broad carbon substrate range and a well-known capacity to degrade hydrocarbons in terrestrial and marine ecosystems (Vaneechoutte *et al.*, 1999; Kang *et al.*, 2011; Kostka *et al.*, 2011; Overholt *et al.*, 2013).

2.5.1 Species specific response to dispersant application.

In this study, we found that each strain responded uniquely to dispersed oil as compared to crude oil. We further demonstrated that both strains are capable of growth on COREXIT® 9500A alone, although *Acinetobacter* appeared to grow far better than *Alcanivorax* on COREXIT® alone (Figure 2.5). These results are corroborated by previous microcosm studies that showed microbial consortia were capable of rapidly degrading both the hydrocarbon fraction and the dioctyl sodium sulfosuccinate (DOSS) fraction of COREXIT® 9500A (Baelum *et al.*, 2012; Chakraborty *et al.*, 2012; Campo *et al.*, 2013). To our knowledge, this is the first report of cultivated strains exhibiting growth using COREXIT® 9500A as the sole carbon and energy source. Considering our results, it is not

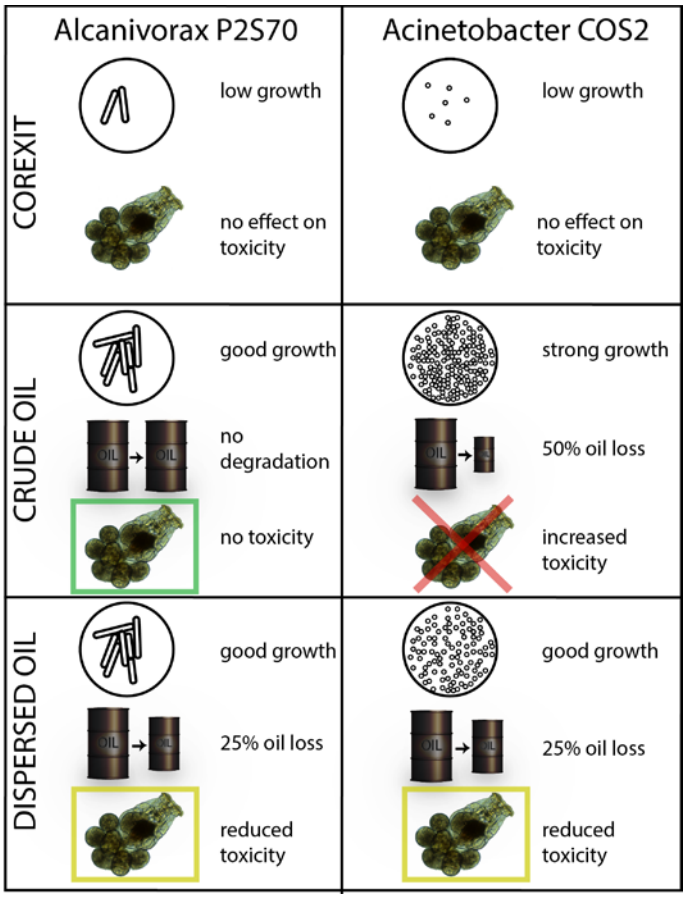

Figure 2.5 Strain-specific responses of growth, biodegradation potential, and toxicity as determined by an EPA-approved rotifer assay. Both bacterial strains tested were shown to grow with Corexit as the sole carbon and energy source, and no effect of bacterial transformation was observed on the toxicity of Corexit. Crude oil supported the growth of both bacterial strains, but the extents of biodegradation and their linkage to toxicity showed large variation between the strains. Although both strains showed similar rates of growth, degradation potentials, and linkages to toxicity, each strain responded uniquely to dispersed oil versus crude oil.

appropriate to generalize that hydrocarbon degrading bacterial populations uniformly respond positively to dispersed oil.

While *Alcanivorax* exhibited similar growth rates on dispersed oil and on crude oil, the potential for oil degradation or transformation was significantly higher in the dispersed oil treatment. It may be that this *Alcanivorax* strain targets only the short chain *n*-alkanes when grown on crude oil (which are not analyzed by this method and would show no

evidence of degradation potential), and can access or target a wider range of hydrocarbons when grown on dispersed oil. In crude oil treatments, *Alcanivorax* was capable of solubilizing many of the aliphatic constituents, which are thought to represent the primary carbon source for this microbial group. Furthermore, two branched alkane species (pristine and phytane) were present in much lower concentrations in the crude oil WAF compared to the *n*-alkane compounds. This observation is significant since it is thought that *Alcanivorax* strains specialize in the utilization of branched alkanes (Yakimov *et al.*, 1998, 2007). *Alcanivorax* weakly solubilized the PAH fraction in the crude oil treatment, primarily the (methyl-) naphthalenes, which were also evident in the control sample. As in the crude oil control, we did not detect a toxicity effect associated with the *Alcanivorax* WAF (crude oil) that may in part be explained by the low PAH concentrations observed in both, as discussed in more detail below. However, a toxicity effect on *B. manjavacas* was observed in the dispersed oil treatment where concentrations of PAHs and aliphatics were higher compared to the crude oil treatment (Figure 2.4).

In contrast to observations with *Alcanivorax*, the growth of *Acinetobacter* was inhibited by 37% in the COREXIT 9500A dispersed oil treatment in comparison to crude oil alone. This growth inhibition corresponded to a 69% reduction in oil degradation potential after 7 days, and a 19% reduction after 14 days. Hamdan and Fulmer also reported that *Acinetobacter* strains isolated from contaminated beach sands were negatively impacted by COREXIT (Hamdan and Fulmer, 2011). Compared to *Alcanivorax*, *Acinetobacter* more effectively solubilized PAHs and *n*-alkanes in the crude oil treatment. Large increases in naphthalene, phenanthrene, fluoranthrene, and benz[a]anthracene concentrations were observed. This potentially explains the toxicity observed in the crude

oil *Acinetobacter* treatment. For the aliphatic fraction, long chain *n*-alkanes (>C19) were found at similar concentrations to the *Alcanivorax* WAF (crude oil treatment), branched alkanes were substantially enriched, and shorter chain alkanes were depleted (Figure 2.4 A).

Previous field and laboratory evidence on the impacts of synthetic dispersants to hydrocarbon degrading microorganisms is contradictory. While the majority of prior studies showed that dispersants dramatically increased the growth and activity of indigenous hydrocarbon degrading bacteria relative to oil that was physically dispersed, a few showed an adverse effect of dispersant on biodegradation (Mulkins-Phillips and Stewart, 1974; Varadaraj *et al.*, 1995; Swannell and Daniel, 1999; Prince, 2010). Prince et al. concluded that most laboratory studies do not effectively represent how dispersants behave in the environment, where dispersed oil is expected to rapidly diffuse to concentrations below 100 ppm (Prince *et al.*, 2013). Studies conducted under close to *in situ* dispersed oil conditions (2.5 ppm oil by volume) revealed rapid oil degradation, little effect of dispersant addition, and no dispersant inhibitory effect to biodegradation. However, these studies should be extended to include response of the microbial populations, and biodegradation capacity, along with ecotoxicity (Prince *et al.*, 2013; Prince and Butler, 2014).

2.5.2 Impacts of Bacterial Degradation and Transformation on Ecotoxicity

Following the Deepwater Horizon spill, the EPA developed benchmarks for the toxicity of PAHs to marine life (EPA, 2015). Results are reported as an acute potency divisor, which is derived from the 5th percentile of a distribution of acute LC50 values

divided by 2. The most solubilized PAHs detected in the WAF or CEWAF of our study were naphthalene (acute potency divisor = 402 µg/L), C1-C3 methyl-napthalenes (170, 63, 23 µg/L), and C1–C3 methyl-phenanthrenes (15.5, 6.65, 2.62 µg/L). Aromatic constituents in the WAF from the crude oil control and *Alcanivorax* treated crude oil samples fell below these benchmarks for the most part and were not associated with rotifer toxicity, while in the *Acinetobacter* crude oil treatment the undiluted WAF was acutely toxic to rotifers. In this treatment we observed C2-C3 napthalenes and C1-C3 phenanthrenes in concentrations up to 13 times higher than EPA limits.

Alcanivorax and un-inoculated controls from dispersed oil treatments had concentrations of substituted napthalenes and phenanthrenes in the CEWAF up to 21 and 26 times higher than EPA limits, respectively. Both treatments were associated with rotifer mortality. However, we observed a much lower toxicity in the CEWAF of *Alcanivorax* treated dispersed oil samples than the un-inoculated dispersed oil control. This may be due to much lower levels of aliphatics, and slightly lower levels of PAHs in the *Alcanivorax* treatment. Alternately, the bacterial biomass may sequester some of the toxic constituents, limiting rotifer exposure. Unfortunately, CEWAF hydrocarbon specific extractions from *Acinetobacter* were not successful due to very high levels of extracellular polymeric substance (EPS), although CEWAF from *Acinetobacter* treated dispersed oil showed similar toxicity as CEWAF from *Alcanivorax* treated dispersed oil.

It is likely that the observed different responses to dispersed oil exhibited by these two strains can be attributed to the production of different biosurfactants or bioemulsifiers. *Acinetobacter* species are some of the best studied high molecular weight surfactant producers (Rosenberg and Ron, 2013). These compounds are thought to be substrate

specific, and *Acinetobacter radioresistens* is known to produce alasan, a bioemulsifier known to solublize PAHs (Barkay *et al.*, 1999). If our strain of *Acinetobacter* produces a similar compound, it would explain the toxicity and greater entrainment of PAHs seen in the crude oil WAF treated with *Acinetobacter* relative to the control and to *Alcanivorax* WAF. In contrast, *Alcanivorax* strains are better known for producing low molecular weight surfactants that lower surface and interfacial tensions and increase hydrocarbon solubility (Rosenberg and Ron, 2013). *Alcanivorax borkumensis* produced 10 different derivatives of glucose lipids (a type of glycolipid) when grown on *n*-alkanes and these compounds reduced the surface tension of water from 72 to 29 mN/m (Abraham *et al.*, 1998). *Alcanivorax dieselolei* produces a lipoprotein (proline lipids) when grown on hexadecane, and this strain reduces the surface tension of water to 29.6 – 32.8 mN/m. This strain did not produce detectable glycolipids (Qiao and Shao, 2010). The *Alcanivorax* strain used in this study (P2S70) is not closely related to either *A. dieselolei* or *A. borkumensis* (average nucleotide identity (ANI) of 80.2 % and 81.6 % respectively) and at this time we cannot speculate on the biosurfactant produced by this strain. However, our results suggest that *Alcanivorax* P2S70 does produce a biosurfactant that increases the entrainment of the aliphatic fraction of crude oil into the culture media.

The observed increase in toxicity associated with the un-inoculated dispersed oil is consistent with the literature, and numerous studies have shown dispersant-oil mixtures to be significantly more toxic than dispersants alone (Ballou *et al.*, 1989; Shafir *et al.*, 2007; Hemmer *et al.*, 2011; Goodbody-Gringley *et al.*, 2013; Rico-Martínez *et al.*, 2013). Similarly to Rico-Martinez et al. we see a synergistic effect of COREXIT® 9500A with Macondo crude oil increasing the toxicity to the marine rotifer *Brachionus manjavacas*

relative to COREXIT alone or physically dispersed crude oil (Rico-Martínez *et al.*, 2013). Our results support the conclusion that dispersants increase the toxicity of oil by introducing a larger percentage of oil components into the soluble phase as much higher concentrations of PAHs and aliphatics are detected when dispersants are present (George-Ares and Clark, 2000).

2.6 Conclusions

Here we demonstrate that dispersants do not enhance biodegradation to the same degree or perhaps by the same mechanism for each strain of hydrocarbon degrading bacteria (Figure 2.5). This suggests that specific microbial groups interact with oil and dispersed oil through varying mechanisms, likely involving biosurfactant/bioemulsifier production and modification of cellular membrane composition, and the outcome of this interaction will determine the efficiency of biodegradation as well as overall ecosystem impacts. Both positive and negative effects of dispersants on biodegradation can be expected. While we show that individual populations demonstrate a unique response to the application of dispersant to crude oil, more research is needed to uncover the mechanisms of interaction at the strain or population level. The transformation of specific compounds must be related to the activities of specific organismal groups, both in the laboratory and in the field. We foresee the ultimate goal of such studies directed towards the implementation of a predictive model incorporating how specific microbial populations respond to dispersant applications in the environment.

2.7 Acknowledgements

This work was made possible in part by a grant from BP/The Gulf of Mexico Research Initiative to the C-IMAGE consortium and in part by a National Science Foundation Graduate Research Fellowship (WAO) under grant no. 2013172310. The authors would like to thank N. Zenzola and Q. Miller for their help during the laboratory work. Any opinions, findings, and conclusions or recommendations expressed in this material are those of the authors and do not necessarily reflect the views of the National Science Foundation.

CHAPTER 3. DEGRADATION OF DEEPWATER HORIZON OIL BURIED IN A BREATHING FLORIDA BEACH

Reproduced with permission from Huettel, M., W.A. Overholt, J.E. Kostka, C. Hagan, J. Kaba, W.B. Wells, S. Dudley. Degradation of Deepwater Horizon oil buried in a breathing Florida beach. Mar. Pollut. Bull. Vol 126, 488-500.
https://doi.org/10.1016/j.marpolbul.2017.10.061

3.1 Abstract

After Deepwater Horizon oil reached the Florida coast, oil was buried in Pensacola Beach (PB) sands to ~70 cm sediment depth, resulting in Total Petroleum Hydrocarbon (TPH) concentrations up to ~2 kg per meter of beach. This study followed the decomposition of the buried oil and the factors influencing the degradation. The abundance of bacteria increased by 2 orders of magnitude within one week after oil burial, while diversity decreased by ~ 50 %. Half-lives of aliphatic and aromatic hydrocarbons reached 25 and 22 days, respectively. Rapid aerobic oil decomposition promoted by tidal pumping, and human cleaning activities effectively removed buried oil from the beach. After one year, concentrations of GC-amenable hydrocarbons in PB beach were similar to those in the uncontaminated control beach at St. George Island/FL, and microbial populations that disappeared after the oil contamination had reestablished in the beach. Oxyhydrocarbons can be found to the present day.

3.2 Introduction

The oil slick produced by the 2010 Deepwater Horizon (DWH) accident in the Gulf of Mexico covered an average area of 11200 km^2 (Garcia-Pineda *et al.*, 2013; MacDonald *et al.*, 2015) that moved mainly in a northeast direction toward the US-shoreline (Mezić *et al.*, 2010). Exposure to O_2, seawater and light weathered the floating oil and decreased its volatile components (C9-C16 n-alkanes and BTEX/C3-benzenes) (Liu *et al.*, 2012). Model estimates suggest that 22000 t of this weathered oil reached the coast (Boufadel *et al.*, 2014).

By 11th of May 2010, oil began washing onto the shores of Louisiana, and later the coasts of Mississippi, Alabama, Florida and Texas, eventually polluting 965 km of sandy beaches (OSAT, 2011; Michel *et al.*, 2013; Mulabagal *et al.*, 2013; Hayworth *et al.*, 2015; Yin, Hayworth, *et al.*, 2015; Nixon *et al.*, 2016). Immediate initiation of massive clean up activities removed a large fraction of the surface oil, but sand moved by wind, waves, and human activities buried oil sheets and oiled sands (Wang and Roberts, 2013). Shielded from photooxidation and mechanical dispersion (Prince *et al.*, 2003; King *et al.*, 2014), buried oil can persist in beach sediments for years to decades as found after the Prestige and Exxon oil spills (Bernabeu *et al.*, 2009; Boufadel *et al.*, 2010).

The oil degradation within the sediment is mainly mediated by bacteria and fungi (Leahy and Colwell, 1990; Bik *et al.*, 2012; Simister *et al.*, 2015). Kostka et al. (2011) identified 24 oil-degrading bacterial strains in DWH-oiled Gulf of Mexico beach sands, and the increase of the relative abundance and expression of functional genes involved in oil decomposition confirmed the microbial degradation process in the sand (Kappell *et al.*, 2014; Kimes *et al.*, 2014; Lamendella *et al.*, 2014; King *et al.*, 2015; Rodriguez-R *et al.*, 2015). The microbial degradation rates are mainly controlled by the quality of the oil,

temperature, availability of nutrients, and access to O_2 (Head *et al.*, 2006; Prince, 2010; Hazen and Prince, 2015; Joye *et al.*, 2016). Oil degradation increases with temperature up to ~ 37°C; at higher temperatures, rates become limited due to protein denaturation and membrane toxicity of the hydrocarbons (Sikkema *et al.*, 1995; Rowland *et al.*, 2000; Vyas and Dave, 2007). Because crude oil contains low concentrations of major nutrients (nitrogen, phosphorus), application of fertilizer and the presence of natural organic matter can accelerate microbial oil decomposition (Atlas and Hazen, 2011; Mortazavi *et al.*, 2013; Horel *et al.*, 2014). Oil degradation typically progresses at much faster rates in aerobic environments (Leahy and Colwell, 1990), and can be negligible under anoxic conditions (Reddy *et al.*, 2002; Prince, 2010). One major difference between water column and sedimentary oil degradation is that the growth of heterotrophic microorganisms in oiled sediments often results in the local depletion of O_2 (Fernández-Álvarez *et al.*, 2006), which leads to the preservation of buried hydrocarbons. For example, hydrocarbons contained in submerged DWH oil mats (SOM) buried along Gulf shores showed little evidence of biodegradation in contrast to the oil in surficial residual balls (SRB) that accumulated on exposed beach surfaces (Elango *et al.*, 2014). In sandy beaches, O_2 is supplied to buried oil by diffusion and airflow through sediment pores, or by O_2-rich groundwater (Turner and Nielsen, 1997; Heiss and Michael, 2014; Geng *et al.*, 2015). In the lower beach, tidal groundwater water level changes within the sand (tidal pumping) can affect O_2 concentrations by enhancing water and air circulation (Li *et al.*, 2005; Charbonnier *et al.*, 2013). Nonetheless, oil buried in sandy shores can be a source for harmful polycyclic aromatic hydrocarbons (PAHs) for decades as found after the Gulf war (Bejarano and Michel, 2010).

The subsurface contamination of Gulf beaches thus raised concerns regarding the potential impact of toxic oil components on environmental and human health (Dickey and Huettel, 2016). To address problems that could arise from buried oil, BP conducted "Operation Deep Clean" designed to mechanically extract larger oil-sand aggregates from Louisiana, Alabama and Florida beaches (Hayworth *et al.*, 2011). ODC removed the contaminated beach sand with a specifically designed oil cleaning/sifting machine dubbed the "Sand Shark" that removed sand to a depth of ~45 cm and separated particles >2 mm from the sand. Some deeper oil was removed by excavators that put the contaminated sand onto a separate sifter. The sifted sand was re-deposited onto the beaches. Despite these activities and substantial monitoring efforts, it was not possible to assign categorical oiling descriptors to the numerous subsurface oiling observations (Michel *et al.*, 2013; Nixon *et al.*, 2016) and the processes controlling buried oil decomposition and decay rates remained largely unquantified.

We therefore initiated a project that studied the degradation of the buried oil and the mechanisms controlling its decomposition. Research was guided by the working hypotheses that the burial of the oil triggered blooms of aerobic microbial communities in the sand that degraded oil particles and oil adhering to sand. We further hypothesized that these blooms of bacteria could rapidly degrade petroleum hydrocarbons because tidal pumping kept the oiled sediment layer aerobic. To investigate these hypotheses, the project addressed the following main goals:

1. Quantify the concentration changes of aliphatic and aromatic oil components buried in the beach over time.

2. Assess the abundance, composition and succession in the sedimentary microbial communities, and
3. Determine the transport of O_2 and CO_2 across the surface of the beach, and the gradients of O_2, temperature and moisture within the beach.

These research goals were addressed through a one-year time series study at Pensacola Beach/Florida, in-situ flux chamber experiments, and laboratory tide simulator experiments.

3.3 Materials and Methods

3.3.1 Study sites

The field work was conducted from June 2010 to July 2011 at Pensacola Beach (PB), Florida (30°19'32.08"N, 87°10'30.55"W) (Figure 3.1), where the municipal beach was heavily polluted by oil after the DWH accident (Michel *et al.*, 2013). The sediments at PB are composed of well-sorted medium quartz sand with low carbon and nitrogen content (Table 3.1). The tides at PB are diurnal, with a range of 12 cm (neap tide) to 61 cm (spring tide). The reference site was a sandy beach at St. George Island (SGI, 29°41'8.63"N, 84°47'17.10"W), which is situated approximately 350 km east of PB and was not impacted by the DWH spill. Except a slightly lower median grain size, the sands at SGI were similar in their characteristics to those at PB (Table 3.1).

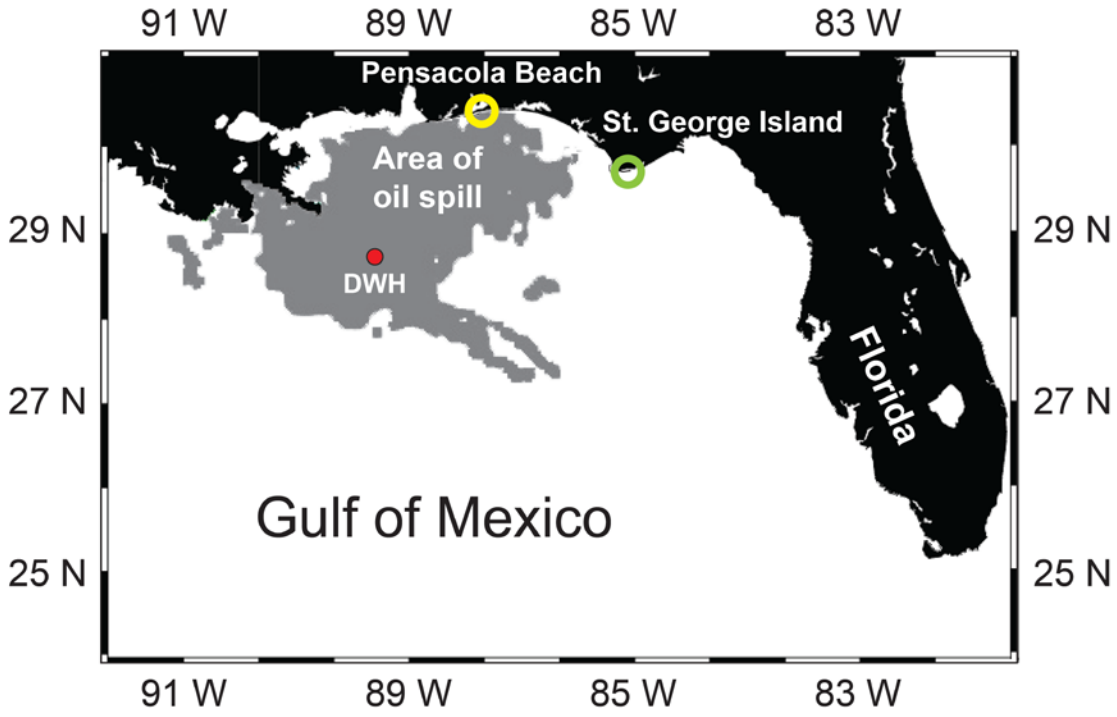

Figure 3.1 Map of the study area. Yellow circle: location of the study site on Santa Rosa Island at the public beach of Pensacola Beach/Florida. Green circle: Reference site at St. George Island. Red solid circle: Location of the Deepwater Horizon accident. Grey area shows the area reached by the surface oil slick as detected by satellite pictures (modified after Garcia et al. 2013).

Table 3.1 Beach sand characteristics at Pensacola Beach and St. George Island. Q1: Quartile 1 of the grain size distribution, Q3: Quartile 3 of the grain size distribution, C%: carbon content in % sediment dry weight, N%: nitrogen content in % sediment dry weight, C:N : Carbon/Nitrogen ratio.

Site	Latitude	Longitude	Grain size median (µm)	Q1 (µm)	Q3 (µm)	Porosity (%)	Permeability (m^2)	C % (dw/dw)	N % (dw/dw)	C:N
Pensacola Beach	30°19'32 .08"N	87°10'30. 55"W	449	363	550	40 (1SD = 2.0)	6.0×10^{-11}, (1SD = 3.3×10^{-12})	0.08 (1SD = 0.006)	0.003 (1SD = 0.0002)	26.5 (1SD = 3.4)
St. George Island	29°41'11 .86"N	84°47'20. 33"W	360	253	526	37 (1SD = 3.8)	2.4×10^{-11} (1SD = 1.1×10^{-12})	0.10 (1SD = 0.02)	0.004 (1SD = 0.0004)	23.6 (1SD = 3.8)

3.3.2 Assessment of the distribution of oil, microbes and key environmental parameters in the beach

Measurements and sampling at the study site took place in 2010 on June 30, July 25 and 30, September 1, October 20, and December 2, and in 2011 on January 19, March 2, April 21, and June 16. To assess the distribution of the oil, microbes, O_2, temperature and moisture in the beach, we excavated trenches perpendicular to the water line (approximately 10-13 m long, 1-1.4 m deep and 1 m wide), reaching from the beach face to the landward edge of the beach oil contamination. Immediately after the excavation of one trench segment, O_2 optode sensors (Presens fiberoptodes encased in hypodermic syringe needles with fiber tip protectors) were pushed approximately 10 cm horizontally into the sand at 5 cm depth intervals for the determination of O_2 in the pore space. Temperature profiles were measured by pushing a 2 mm thin PT100 temperature probe horizontally approximately 10 cm into the vertical trench wall at the same depths intervals. For the assessment of sediment moisture, 250 cm^3 sand samples were collected at 5 cm depth intervals using clean glass jars with gastight lids. The moisture in these samples was determined by subtracting the dry weight of the sample from the weight of the moist sample. During each site visit, 6 sediment cores were sampled using transparent polycarbonate core liners (75 to 100 cm long, 5.5 cm inner diameter) for the quantitative assessment of the distribution of oil and microbes in the beach. The cores were collected vertically parallel to the excavated trenches, with 2 cores collected in the center, 2 cores near the seaward edge, and 2 cores near the landward edge of the contaminated beach area. Ten reference cores of the same dimensions were collected at similar distance from the

water line at the reference beach at SGI/Florida on June 8, 2010. The cores were transported in a cooler to the lab where they were photographed and frozen until analysis.

3.3.3 Oil analyses

The frozen sediment cores were sliced at 5 cm depth intervals. Petroleum hydrocarbons were extracted from 10 g subsamples of the homogenized sand sections using automated Soxhlet extraction according to EPA method 3541. After mixing a subsample with anhydrous sodium sulfate for moisture removal, it was extracted with 50 mL of 1:1 (v/v) acetone/hexane followed by a rinsing step with the same solvent mixture. The extract was concentrated using a Turbovap-II rapid solvent evaporator (55ºC) to less than 5 mL, and then transferred to 20 mL cyclohexane for further concentration to a volume of 2 ml. This concentrated extract was cleaned according to the EPA 3630C method and first analyzed on an Agilent 7890A Series gas chromatograph (GC column: Agilent HP-5MS, 30 m × 250 μm × 0.25 μm) connected to an Agilent 7890A flame ionization detector. For the determination of polycyclic aromatic hydrocarbons (PAHs), samples were injected into an Agilent 7890A Series GC (Column: Agilent DB-EUPAH, 20 m × 180 μm × 0.14 μm) coupled to an Agilent 7000 triple quadrupole MS system with electron ionization source according to an Agilent PAH-specific multiple reaction monitoring method. As calibration standard, we used the ULTRA SCIENTIFIC PM-610 Polynuclear Aromatic Hydrocarbons Mixture with 16 common PAHs (Acenaphthene, Acenaphthylene, Anthracene, Benz[a]anthracene, Benzo[b]fluoranthene, Benzo[k]fluoranthene, Benzo[ghi]perylene, Benzo[a]pyrene, Chrysene, Dibenz[a,h]anthracene, Fluoranthene, Fluorene, Indeno[1,2,3-cd]pyrene, Naphthalene, Phenanthrene, and Pyrene). Hydrocarbon concentrations measured in the beach sands were normalized using C30-17α,21β (H)-

hopane, a polycyclic saturated petroleum hydrocarbon that is highly resistant to biodegradation (Venosa et al., 1997). The concentrations of n-alkanes, aromatic hydrocarbons and Total Petroleum Hydrocarbons (TPH, C10 - C32) are presented in mg kg^{-1} dry weight sediment.

3.3.4 Hydrocarbon decay rates

Decay rates were calculated using first order kinetics:

$$C_t = C_0 e^{-kt} \quad (1)$$

where C_t denotes the residual concentration of hydrocarbons (mg kg^{-1}) at time t, C_0 is the initial concentration of hydrocarbons (mg kg^{-1}), k is the rate constant of the hydrocarbon concentration decrease in the sediment (d^{-1}) and t is the time since burial (d (days)). Studies have found that the decay of petroleum hydrocarbons in aerobic environments can be described reasonably well with first order kinetics (Mohajeri *et al.*, 2010; Zahed *et al.*, 2010, 2011; Agarry *et al.*, 2013).

3.3.5 Microbial community analyses

Microbial community abundance and composition were characterized through the extraction and analysis of total genomic DNA and sequencing of SSU rRNA genes (Bacteria and Archaea) from the beach sediment sections. The DNA was extracted from sand with a MoBio Powersoil DNA extraction kit (Mo Bio Laboratories, Carlsbad, CA). Microbial abundance was determined by qPCR using primers targeted to amplify bacterial SSU rRNA genes (Kostka et al., 2011). The V4 hypervariable region of the SSU rRNA

gene for Bacteria and Archaea was PCR amplified and sequenced using the primer set 515F (5'-GTGCCAGCMGCCGCGGTAA-3') and 806R (5'-GGACTACHVGGGTWTCTAAT-3') on an Illumina MiSeq platform. Sequencing was conducted using v2 chemistry (paired-end 250 bp reads) according to standard protocols. Paired-end reads were merged using PEAR v0.9.0 (Zhang *et al.*, 2013). Operational taxonomic units (OUT) were defined at 97% similarity using the 'pick_open_ref_otus' script in QIIME v1.8 using UCLUST and UCLUST REF clustering algorithms (Caporaso et al., 2010b; Edgar, 2010). Sequence libraries were normalized to a common scale with the cumulative-sum scaling method with the R package 'metagenomeSeq' and the default quantile estimate (0.5) (Paulson *et al.*, 2013). Representative sequences of each OTU were classified using RDP classifier that had been trained on the Greengenes database v13_8 at 50% confidence (DeSantis *et al.*, 2006; Wang *et al.*, 2007). OTUs associated with early oiling and those associated with more weathered oil were identified by testing oiled samples from July 2, 2010 and July 25, 2010 against oiled samples from Sept 1 and October 20, 2010. Multiple differential abundance tests on dominant OTU (>100 total counts and present in at least 10 samples, ~ 500 total OTU) were conducted using the fitZig function in 'metagenomeseq' with default parameters between groups of samples. All sequences were grouped according to the degree of oiling and sampling date, and centroids for each group were calculated with their 95% confidence ellipses. Shannon diversity, shown as true diversity of order one or the exponential of Shannon ($e^{H'}$), was calculated using the R package 'vegan' and averaged across all beach samples collected on the same date (Oksanen *et al.*, 2015). When the order is one, all species are weighed by their frequency without favoring either common or rare species (Jost, 2006). Populations that declined in

relative abundances following the oil exposure were determined by comparing groups of uncontaminated samples (June 8, 2010; June 14, 2011; and July 26, 2011) and groups of oil-contaminated samples. Sequence data were uploaded to NCBI under BioProject ID PRJNA294056.

3.3.6 In situ flux chamber measurements

The effect of sedimentary oil degradation on the composition of air exchanged between the beach and overlying atmosphere was tested with flux chamber measurements conducted at the Pensacola Beach study in June 2014. In preparation for these measurements, homogenized beach sand from the study site (layer 10-40 cm, hydrocarbon concentration < 2 mg kg^{-1}) was filled into three core liners (40 cm long, 10 cm inner diameter). A second set of 3 core liners of the same size was filled with the same sand mixed with Deepwater Horizon weathered crude oil (0.4 g kg^{-1}, 190 g TPH m^{-2}, oil weathered through exposure to day light and evaporation for 6 months). All cores then were connected to a peristaltic pump that pumped moisturized air at 50 ml h^{-1} through the cores for a period of three weeks to allow sand microbial communities to respond to the oil addition. After this incubation period, 6 long sediment cores (120 cm long, 10 cm diameter) were taken with polycarbonate core tubes in the center of the previously polluted beach area at the study site. The upper 40 cm of sand from these cores was replaced by one of the 30 cm long sand cores that had been incubated in the lab, covered by a 10 cm thick layer of non-oiled beach surface sand. The three tubes with control sand and three tubes with oil-amended sand were closed at the upper end with an opaque gas-tight lid with gas vent, and at the lower end with a gauze cover (250 μm mesh). The 6 cores then were embedded vertically in the beach during low tide at the same location where they were removed, with

the gauze-covered ends of the cores reaching about 10 cm deep into the groundwater-saturated layer of the beach. The gas vents were connected via gastight tubing to a LICOR® LI-840A CO_2 Gas Analyzer and a Hach® rigid O_2 optode sensor that measured CO_2 and O_2 concentration in the air released from the sediment cores. The gas concentrations were recorded on a DataQ710 data logger at 5 min intervals, starting at low tide (9:00) and ending at the following low tide (15:00). The groundwater level was measured in 15 min intervals in a separate well installed in the beach next to the sediment-filled tubes.

3.3.7 Laboratory flux chamber measurements

After the in-situ flux measurements, the six sediment cores were removed from the beach and incubated in a laboratory tide simulator to determine the effect of the tidal pumping on the decay rates of the buried oil. This tide simulator consisted of a trough (90 (l) x 50 (h) x 40 (w) cm), in which the water level was adjusted by a computer-controlled pump such that the water table change in the simulator mimicked the natural tidal groundwater table oscillations in timing and magnitude (25 cm diurnal tidal water table oscillation). CO_2 and O_2 concentrations in the air exchanged by the cores were measured with a LICOR® LI-840A CO_2 Gas Analyzer and Hach® rigid O_2 optodes at 15 min time intervals and recorded by a DataQ710 logger. In the first run of this incubation, one control sediment and one oil-contaminated sediment were excluded from the tidal water oscillations by placing the sediment cores in containers that maintained a constant groundwater level of 25 cm within the incubated sediments. In the second and third runs of this experiment, one control and two oil-contaminated cores were excluded from tidal pumping. Each experiment ran with 6 cores for 6 months. To assess the influence of the tidal pumping on the O_2 concentrations in the subsurface layers of uncontaminated and oil

contaminated beach sands, one of the uncontaminated sediment cores and one of the oil-contaminated sediment cores were incubated in the tide simulator. Hach® O_2 optodes were inserted through ports in the flux chamber walls to monitor O_2 concentrations at 20 cm sediment depth. O_2 data were recorded at 15-minute intervals. After one month, the pump was stopped to assess the long-term effect of the tidal pumping on the O_2 concentration in the sediment. Four months later, the tidal pumping was resumed to assess how long it takes for the sediment to reach the previous O_2 concentration at 20 cm depth.

3.4 Results

3.4.1 Deposition of oil in the beach

Weathered DWH oil reached Pensacola Beach on the night of June 22-23, 2010 (Figure 3.2 A). High flood water levels associated with the lunar cycle and a shallow beach profile supported the deposition of petroleum hydrocarbons on the dry beach. Waves carried water with oil inshore into a ~13 m wide shallow depression of the beach plateau that retained the polluted water. Here oil was separated from the water and adsorbed to the sand grains when the oiled water filtered into the permeable sand. Sunny weather with daytime temperatures exceeding 37°C melted the oil deposited on the sand, producing large cohesive oil sheets up to 10 m (Figure 3.2 A). Cleanup crews removed a large fraction of this surface oil, yet by June 30th, the upper 30 cm of the Pensacola Beach sand were contaminated by oil within a 7-13 m wide zone paralleling the high tide water line. The distal passage of Hurricane Alex (June 25 – July 2), Tropical Depression Two (July 8-9) and Tropical storm Bonnie (July 24-25) interrupted cleanup activities and pushed more oiled water onto the shore. Substantial lateral sand transport associated with the storms and

the depositional cycles between them moved offshore sands mixed with oil particles onto the beach. This sand filled the beach depression and built a higher beach profile that prevented further overwash and deposition of oil on the beach plateau (Figure 3.2 B, C, D).

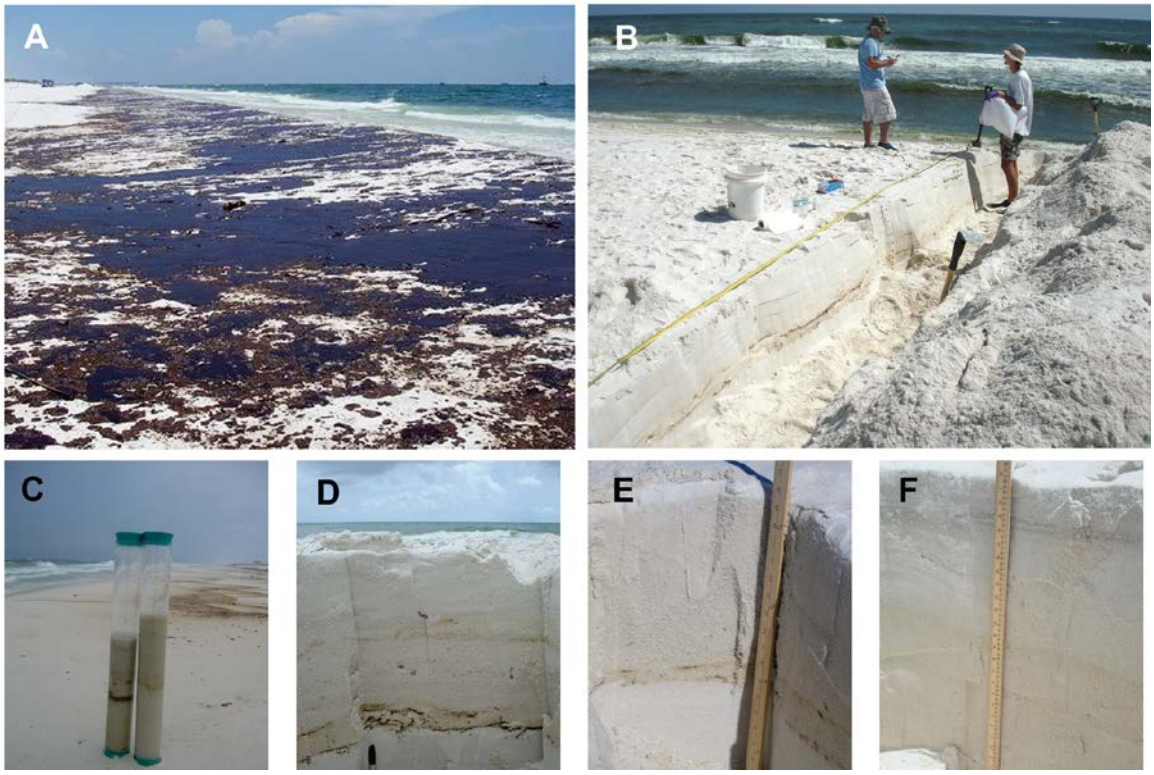

Figure 3.2 DWH oil contamination at our study site at Pensacola Beach/Florida. (A) Oil deposited in the depression of the beach plateau on June 24, 2010 (image Florida DEP, public domain) (B) Trench excavated on September 1st, 2010 with a ~10 m long dark vein of buried oil showing in the cross section of the sediment (C) Sediment cores collected on June 30th, 2010, with one core showing a thick embedded oil layer at ~20 cm sand depth. Note oil deposits on depressed beach plateau in the background. (D) Beach cross section on July 25th, 2010 with a dark double layer produced by oil deposited during the nights of June 22 and June 23 at 45-50 cm depth. (E) Cross section on December 2nd, 2010, with a homogeneously brown stained sand layer of re-deposited sand after ODC. Some remains of the deep dark oil layers depicted in (C) were still present. (F) Beach cross section on April 21st, 2011. No visible oil stains were left in the sediment at the study site. Grey layers near the surface are detrital material, not oil. Images by M. Huettel except A.

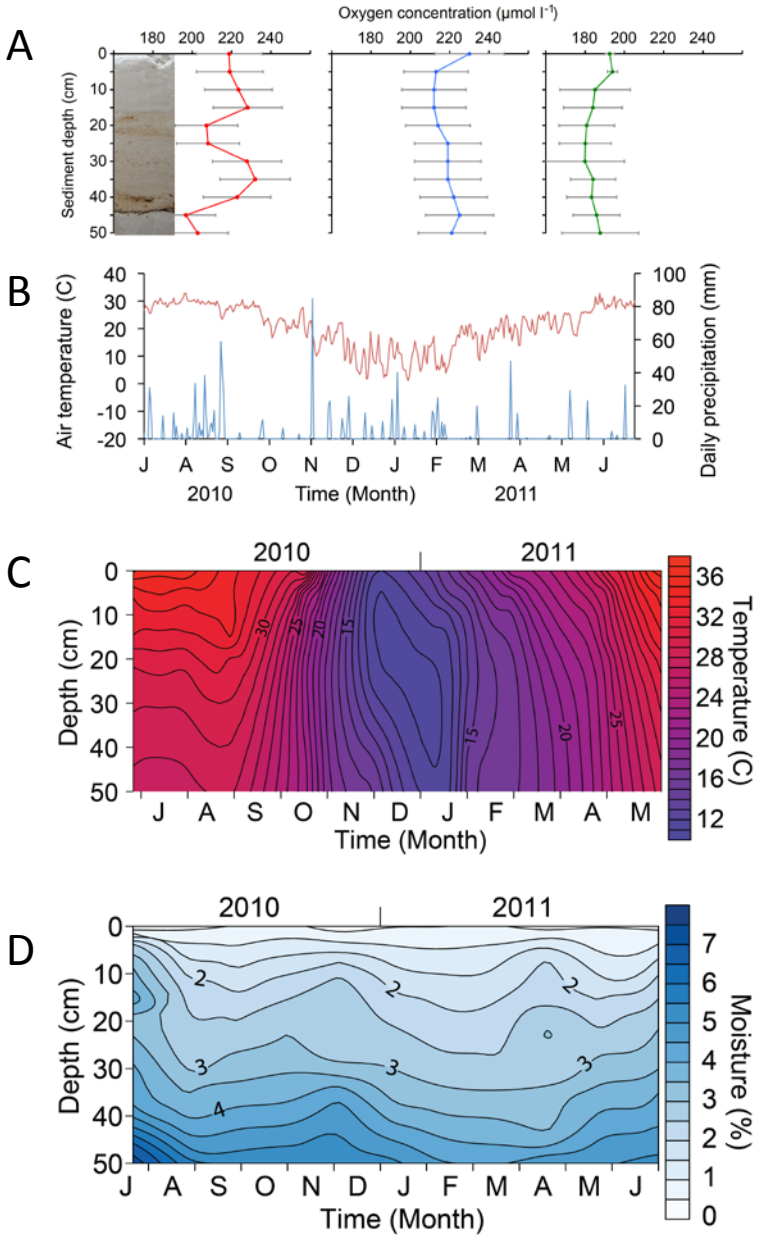

Figure 3.3 O2, temperature and moisture distribution in the beach. (A) O2 profiles measured in the Pensacola beach sand in September 2010 (red), December 2010 (blue) and June 2014 (green). Minima in September 2010 profiles coincided with heavily oiled sediment layers (insert). Error bars represent 1 SD. (B) Air temperature (red) and precipitation (blue) at Pensacola Beach during the study period. Source: National Weather Service, http://www.weather.gov (C) Isoline diagram of the temperature changes in the beach sand. (D) Isoline diagram of the moisture changes in the beach sand throughout the study period.

3.4.2 Environmental settings for oil degradation

Oxygen, temperature and moisture in the beach produced favorable conditions for microbial oil decomposition (Figure 3.3). In the upper 50 cm of the beach, temperatures remained above 28^{o}C until September 2010, and moisture levels ranged from 2 to 7% except in the uppermost 10-15 cm of the sand. Aerobic conditions, with O_2 levels > 50% air O_2 saturation, persisted throughout the contaminated sediment column at all times. Vertical O_2 profiles revealed O_2 minima in sand layers with increased oil concentration and increasing concentrations below ~25 cm sediment depth.

3.4.3 Buried oil characteristics and concentrations.

The buried oil (Figure 3.4 A, B, Table B.1) contained a clear signature of the DWH oil (Ruddy et al., 2014) and was characterized by a loss of shorter-chain hydrocarbons (Fig. 4B insert). TPH concentrations in the contaminated layer reached 11000 mg kg^{-1} (dw/dw, June 30th), with saturated hydrocarbons contributing on average 54% (1SD=31%) of the TPH (Figure 3.4 A). Based on the thickness and width of the oiled sand layer and its average TPH concentration (421.5 mg kg^{-1}, 1SD=421.4 mg kg^{-1}) the areal contamination was 202 g TPH m^{-2} (1SD=201 g TPH m^{-2}), or approximately 2 kg per meter of beach.

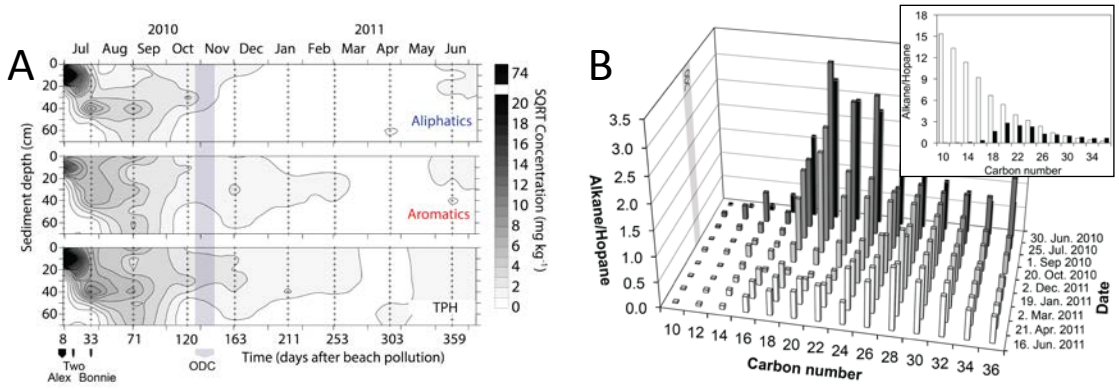

Figure 3.4 Petroleum hydrocarbon concentrations in PB sand. (A) Spatial and temporal distribution of buried oil concentrations. Note that the concentrations were square root transformed to accommodate their full ranges. Small "+" symbols indicate sampling dates and depth intervals. Black arrows at the lower left (below numbered X-axis) indicate dates and durations of the tropical storms that affected Pensacola Beach. (B) Temporal development of the alkane/hopane ratios in the buried oil. Insert: White and black bars depict alkane/hopane ratios in the source oil and buried oil (June 30th, 2010), respectively.

By July 25, 2010, the upper ~45 cm of the beach were oil stained, with a darker layer near the surface (5-15 cm) and the initially deposited oil layers now at 45-50 cm depth (Figure 3.2 D). The average TPH concentration in the contaminated sand layer had decreased to 39.7 mg kg^{-1} (1SD=11.2 mg kg^{-1}). By October 20th, the oil-stained sand layer had grown to 70 cm thickness with an average TPH concentration of 6.7 mg kg^{-1} (1SD=2.9 mg kg^{-1}). Aliphatics and aromatics with carbon numbers smaller than 16 had decomposed to near background levels except for C8-C10 aromatics. The areal contamination had decreased to 7.5 g TPH m^{-2} (1SD=3.3 g TPH m^{-2}), equivalent to 5% of the initial contamination recorded in June.

Operation Deep Clean reached our study site on October 27, 2010. ODC removed the upper 45-65 cm of the beach sand and re-deposited a 25-45 cm thick layer of sifted, homogenously oil-stained sand with an average TPH concentration of 12.9 mg kg^{-1} (1 SD=7.8 mg kg^{-1}, Dec. 2, 2010) that overlaid remains of the heavily oiled base layers (Figure

3.2 E). The oil inventory at the study site increased from 75 g m^{-1} prior to ODC to 144 g m^{-1} after ODC, implying that sand from more heavily oiled adjacent areas was mixed into the re-deposited sand layer. In the re-deposited layer, the average concentration of aliphatics had decreased (0.7 mg kg^{-1}, 1SD=0.3 mg kg^{-1}), while aromatic hydrocarbons had increased (12.3 mg kg^{-1}, 1SD=7.8 mg kg^{-1}). By March 2, 2011, nine months after the initial beach contamination, TPH concentrations (2.2 mg kg^{-1}, 1SD=0.3 mg kg^{-1}, 1.8 g m^{-2}, 1SD=0.2 g m^{-2}), had dropped by two orders of magnitude compared to the initial concentrations, and were statistically not different from the background level measured at our SGI reference site (3.7 mg kg^{-1}, 1SD=0.5 mg kg^{-1}). The sand at PB now appeared uniformly white down to 1 m depth (Figure 3.2 F), and its total solvent-extractable hydrocarbon carbon content 0.002% dw/dw (1SD=0.015) was less than that at the SGI reference site (0.005% dw/dw (1SD=0.002).

3.4.4 Hydrocarbon decay rates.

Within the first year after beach pollution, hydrocarbon decay rates k in the contaminated sediment layer averaged 0.013 d^{-1} (SE=0.001 d^{-1}) for aliphatics, 0.010 d^{-1} (SE=0.003 d^{-1}) for aromatics, and 0.012 d^{-1} (SE=0.002 d^{-1}) for TPH (Figure 3.5 A), corresponding to half-lives $t_{1/2}$ of 53, 69, and 58 d, respectively. Within the sediment column, the decay rates scaled with oil concentration. Prior to ODC, decay rates peaked at 5-15 cm and 45-50 cm below the surface, with rate maxima reaching 0.028 d^{-1}(SE=0.013 d^{-1}, $t_{1/2}$ = 25 d) for aliphatics, and 0.031 d^{-1} ($t_{1/2}$ = 22 d) for aromatics (SE=0.029 d^{-1}) and TPH (SE=0.024 d^{-1}) (Figure 3.5 B, Table B.2). At 25-35 cm depth, rates dropped to a

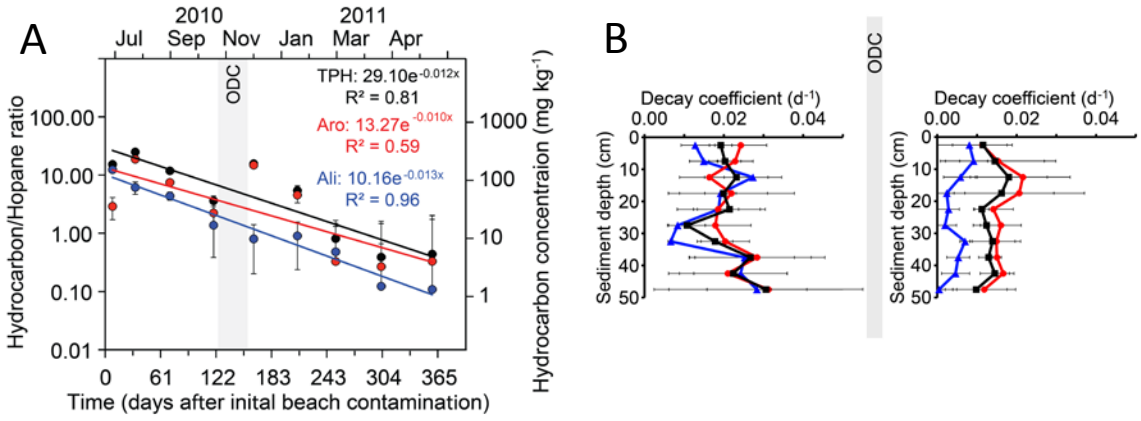

Figure 3.5 Decay of buried oil at Pensacola Beach. (A) Hopane-normalized aliphatics (blue symbols and line), aromatics (red) and TPH (black). Error bars depict one standard deviation. Second Y-axis indicates hopane-normalized average hydrocarbon concentration (B) Hydrocarbon decay rate coefficients in the contaminated sediment layers before (June 30 to October 20, 2010) and after (December 2, 2010 to June 16, 2011) ODC. Error bars depict one standard deviation. Color code as listed for (A).

minimum. ODC resulted in a lowering of the peak decay rates at 5-15 cm, and eliminated the peaks at 45-50 cm depth and the distinct minimum, thereby smoothing the vertical decay rate profiles.

3.4.5 Response of the microbial community

The decomposition of the buried oil was mediated by oil-degrading microbes. Microorganisms in the sand responded to the petroleum hydrocarbon input with rapid growth and changes in community composition (Figure 3.6). Bacterial abundance, as determined by qPCR of SSU rRNA genes, increased by two orders of magnitude in heavily oiled (i.e. oil layers present) compared to lightly-oiled sands (i.e. no oil layers present). In parallel with the burial of the oil, the depth of increased bacterial abundance moved deeper into the beach sand, with the total abundance increasing steadily over time from June to October. Oil acted as a strong selective pressure, resulting in a more than 50% decrease in Shannon diversity caused by blooms of hydrocarbon-degrading bacterial populations in

parallel with suppression of other microbial groups (Figure 3.6 A). A succession of bacterial populations progressed with the chemical evolution of petroleum hydrocarbon compounds. One week after the beach was contaminated, sedimentary blooms were dominated by Gammaproteobacteria (*Marinobacter, Alcanivorax,*), Flavobacteria (*Muricauda*) and Alphaproteobacteria (*Oceanicaulis*). A high resolution depth profile (Figure 3.6 B) illustrates the pronounced change in the abundance and community composition, with the relative abundance of *Marinobacter* (Alteromonadales), a known hydrocarbonoclastic group, exceeding 50% in the heavily oiled sand layers. The abundance of these early colonists decreased during the following months (Figure 3.6 C), while other hydrocarbon-degrading populations (Gammaproteobacteria OTU within the order *Chromatiales*, *Alcanivorax-OTU2,* and *Alcanivorax-OTU3,* and Alphaproteobacteria *Hyphomonas*) increased (Figure 3.6 D), reaching peak abundances late October 2010, just before ODC.

The increase in oil-degrading taxa (e.g. *Alcanivorax, Marinobacter*) was accompanied by a concurrent decline in other microbial groups, most notably Archaea affiliated with *Nitrosopumilus* (Thaumarchaeota) and two bacterial groups within the Gemmatimonadetes (*Gemm-1, Gemm-2*) (Figure 3.6 E). ODC resulted in an abrupt decrease in the overall abundance of bacteria that bloomed during the months prior to the cleaning.

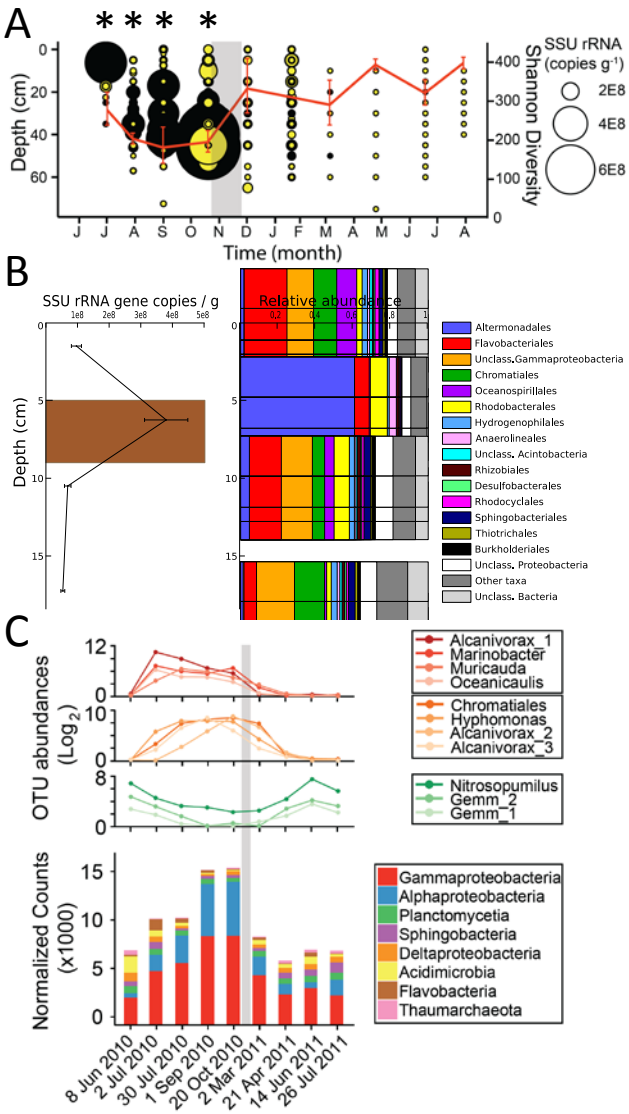

Figure 3.6 Development of microbial communities in Pensacola Beach sands. (A) Abundances of bacterial small-subunit (SSU) rRNA genes in heavily-contaminated sand layers (solid black circles) and in lightly contaminated layers (yellow circles). The red line depicts the average Shannon diversity (eH', secondary y-axis) with error bars representing standard error. Asterisks above graph indicate significant differences between heavily and lightly oiled sand (Welch's t-test, $p < 0.05$) (B) Vertical profile of the microbial community collected on 30 June, 2010. Left: Abundance of bacterial SSU rRNA genes. Right: Relative abundances of microbial groups in the four sediment layers. Marinobacter represented >50% of the total community in the heavily oiled sand layer at 5 to 10 cm depth. (C) Time series of the abundances of oil degrading bacteria that peaked in the first week after beach contamination. Marinobacter, which dominated in June (B), had already decreased by July 2nd (D) Oil degraders that increased one week after beach contamination, (E) Microbial groups that declined after oiling

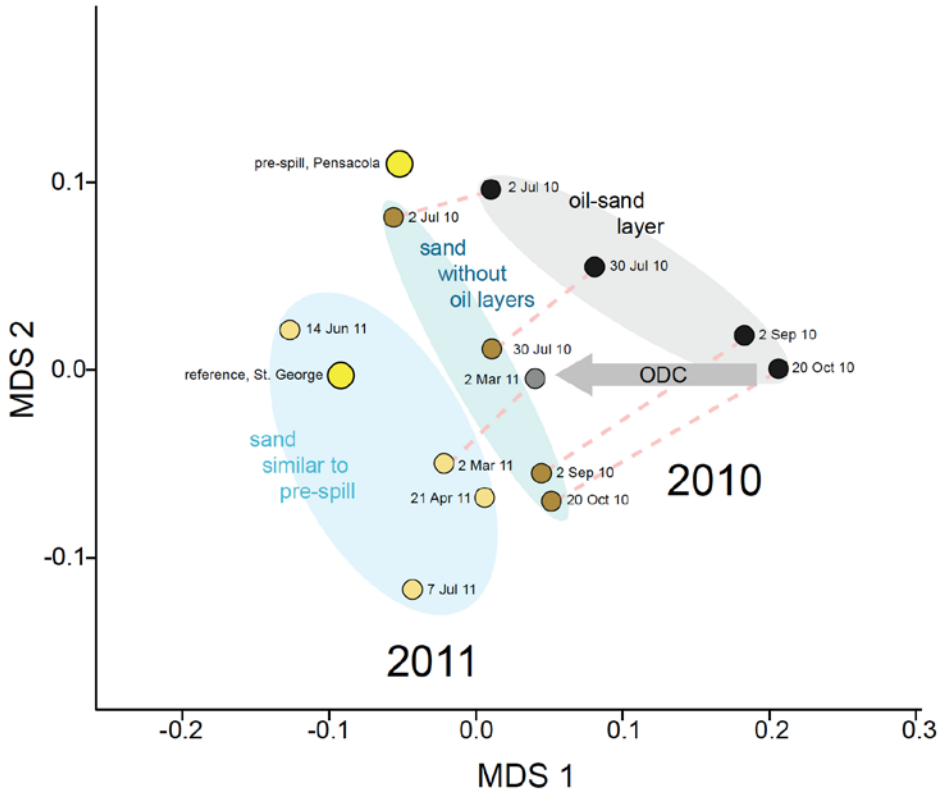

Figure 3.7 Non-metric multidimensional scaling (MDS) plot generated from weighted UniFrac distances between normalized sequence libraries. Large yellow circles represent microbial communities in samples not affected by DWH oil,, black circles communities in heavily oiled-sand layers, brown circles communities in lightly oiled-sand layers,,and tan circles microbial communities in sand with hydrocarbon concentrations similar to the background concentration prior to the spill. Pink dashed lines indicate samples collected at PB on the same day from heavily oiled sand and sand without visible oil layers. The grey arrow depicts the shift in the microbial community composition in oiled sand between 20 Oct 2010, before ODC and 2 Mar 2011 after ODC.

After October 2010, the microbial communities rebounded with an increase in diversity, including a resurgence in members of the *Thaumarchaeota* and *Gemmatimonadetes*. By March 2011, the abundance and diversity of beach microbial communities resembled pre-spill conditions (Figure 3.6 F). The weighted UniFrac distances between normalized sequence libraries graphed in a non-metric multidimensional scaling plot revealed separate clusters of heavily-oiled, lightly-oiled and clean sediment

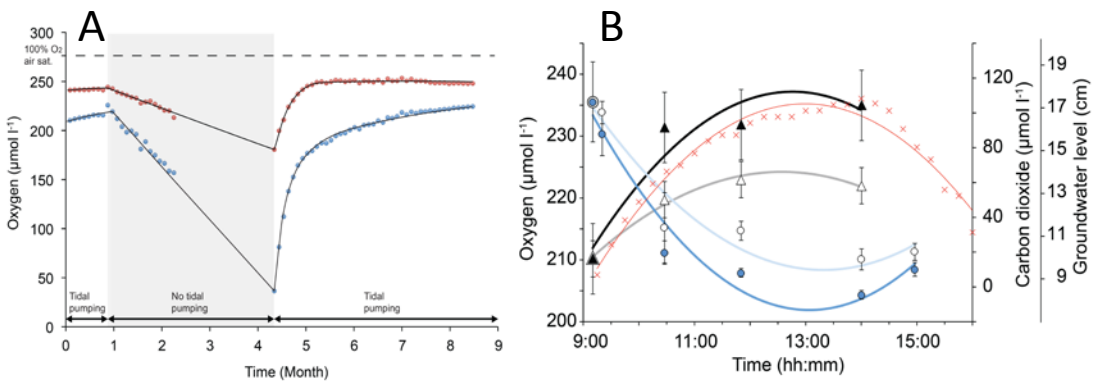

Figure 3.8 The effect of tidal pumping on gas exchange and O_2 in the beach sand. (A) Results from the in-situ flux chamber experiment at PB. Circles depict O_2 and triangles CO_2 concentrations in the air released from the flux chambers during rising and falling tidal groundwater table (red crosses and line). Open symbols and lighter curves represent concentrations in air released from beach sands with natural organic matter content, solid symbols and darker curves concentrations in air released from oil-contaminated sands. Larger circle and triangle shown at time 9:15 depict O_2 and CO_2 concentrations in the ambient air. Error bars represent 1 SD. All curves are polynomial fits of second order. (B) Results from the tide simulator experiment, which show the decrease of O_2 at 20 cm sediment depth of a control and an oil-amended sediment caused by the interruption of tidal pumping.

microbial communities reflecting the impact of the presence of oil and the effect of ODC (Figure 3.7).

3.4.6 O_2 and CO_2 transport in the beach.

The aerobic microbial oil decomposition produced O_2 concentration minima at the depths of heavily contaminated sand layers (~20 and ~45 cm) (Figure 3.3 A). The distinct minima disappeared after ODC but O_2 profiles maintained a profile with increasing O_2 concentrations below ~25 cm depth, implying a transport mechanism other than molecular diffusion supplying O_2 to the deeper sediment layers. The groundwater table, at ~1.2 m below the surface of the contaminated beach plateau, rose and fell with the tides by 6 to 30 cm (neap-spring tide range) and functioned as piston pump that moved air into and out of

the beach in tidal rhythm, a process known as “tidal pumping” (Santos *et al.*, 2009) (Figure 3.8 A). The results of the in-situ flux chamber incubations revealed that the rising groundwater pushed air upward and out of the beach at rates reaching 26 L m^{-2} h^{-1} during an intermediate flood tide (tidal range: 36 cm). The following faster groundwater drop during ebb tide drew air into the beach at up to 31 L m^{-2} h^{-1}. Air pumped out of uncontaminated beach sand contained 11% (1SD=0.8%) less O_2 and 351% (1SD=37%) more CO_2 than the ambient air (Figure 3.8 A). In the flux chambers enclosing sediment amended with weathered oil (470 g TPH m^{-2}), these percentages significantly increased to 13% (1SD=0.3%, p=0.03, α=0.05, df=10, Mann-Whitney U Test) and 597%, (1SD=43%, p=0.01, α=0.05, df=16, Mann-Whitney U Test).

3.4.7 Effect of tidal pumping on O_2 concentration in the sediment and buried oil decay

The laboratory tide simulator experiments confirmed the in-situ flux chamber results and indicated that the tidal pumping maintains high O_2 concentrations in the beach sediment. Shutting-off of the tidal pumping led to a steady decrease of the O_2 concentration in the control and oil-contaminated beach sands (Figure 3.8 B). O_2 sensors inserted at 20 cm sediment depth recorded an O_2 decrease to 72% (1SD=4%) air saturation in uncontaminated sands and 37% (1SD=4%) in oil-contaminated sand within the first 3 months of incubation.

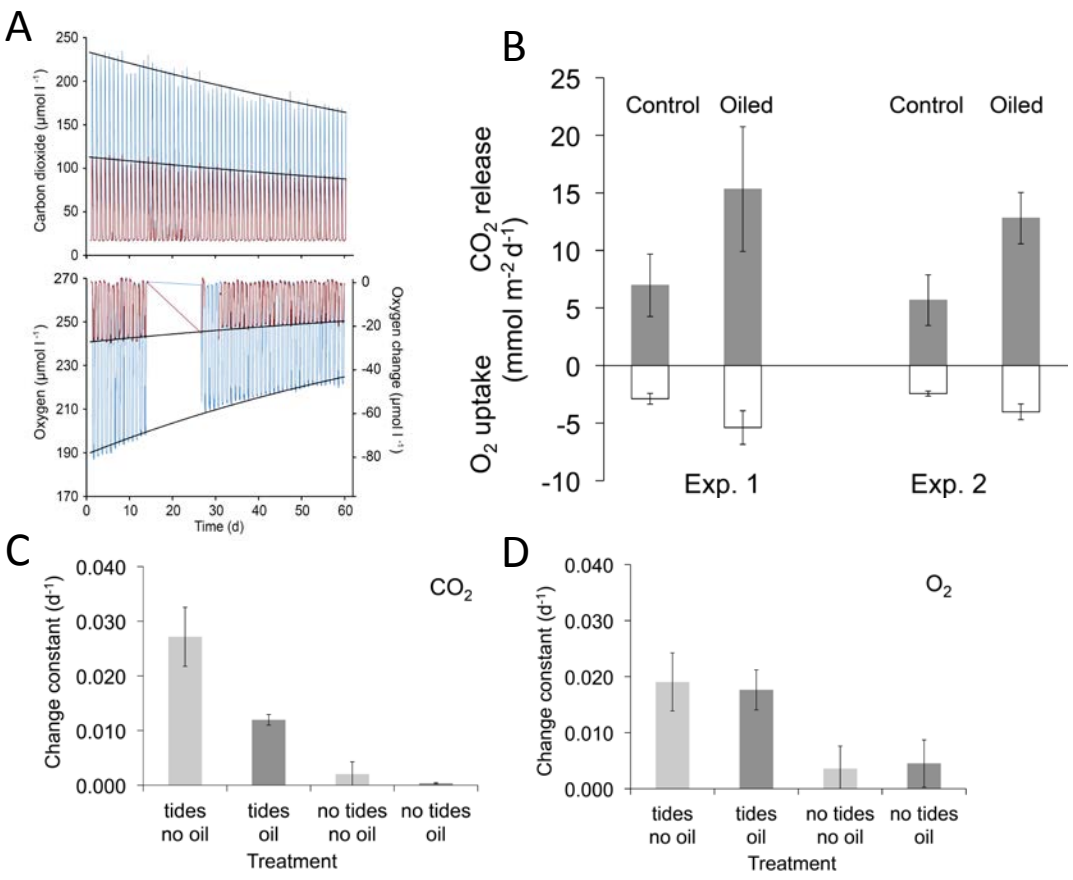

Figure 3.9 Results from the laboratory tide simulator experiment. (A) Gas concentrations in air released from incubated sediments exposed to tidal pumping. Red lines represent control sediments without oil, blue lines oil contaminated sand. At the beginning of each simulated flood groundwater table rise, CO_2 and O_2 concentrations in the air released from the incubated sediment were close to the respective concentrations in the ambient air. As the water level rose, the concentrations of CO_2 pushed out of the sediment increased, while the concentrations of O_2 decreased. With initiation of the ebb tide, the concentration changes reversed and rapidly resumed ambient air concentrations. The gap in the O_2 data between days 14 and 28 was caused by a sensor failure. (B) Initial CO_2 and O_2 fluxes averaged over the first month of experiment 1 and 2 for uncontaminated control sediment and oil-contaminated sand. White columns represent O_2 fluxes, grey columns CO_2 fluxes. (C) Change constants of CO_2 production and (D) O_2 consumption in control and oil-amended sediments with and without tidal pumping. Error bars represents one standard deviation.

Reinitiating tidal pumping reestablished fully oxic conditions within one month. In sediment exposed to tidal pumping, the CO_2 concentrations in the air released from the cores were higher and O_2 concentrations lower compared to the respective concentrations in the air released from control sediment without oil (Figure 3.9 A). The initial (first month, tide simulator exps. 1 and 2) CO_2 release fluxes from the oiled sediment cores were 2.2-fold higher (1SD=0.1) and their O_2 uptake fluxes 1.8-fold higher (1SD=0.2) than those of the control sediment (Figure 3.9 B). The CO_2 concentrations in the air released from the cores containing oiled sand decreased with an exponential decay that had an average change constant of 0.012 d^{-1} (1SD=0.001 d^{-1}, $t_{1/2}$ = 58 d) when ventilated by tidal pumping (Figure 3.9 C). Without tidal pumping, CO_2 change constants were more than 30-fold smaller 0.0004 d^{-1} (1SD=0.0001 d^{-1}, $t_{1/2}$ = 1733 d, p=0.002, α=0.05, t-test), revealing a slower decomposition process. Similarly, the change constants of CO_2 decrease in the air released from sands without oil but containing natural organic matter decreased by an order of magnitude in the non-ventilated sands (0.027d^{-1}, 1SD=0.005, $t_{1/2}$ = 26 d, vs. 0.002, 1SD=0.003, $t_{1/2}$ = 347 d, p=0.001, α=0.05, t-test). The time course of the O_2 concentration loss in the air released from the cores supported the results from the CO_2 measurements, indicating a faster decay in the tide-ventilated compared to the non-ventilated sediments (Figure 3.9 D). The differences of the O_2 change constants between ventilated and non-ventilated cores were smaller (ratio: 3.9) than observed for the respective CO_2 constants, and in contrast to the latter, the O_2 change constants did not differ between sediment with or without oil.

3.5 Discussion

Clean up crews removed about 100000 t of oiled material with an estimated oil

content of <15% from the coast (BP press release, 15 April 2014), suggesting that about half of the 22000 t of DWH oil that reached the shore (Boufadel *et al.*, 2014) was removed**.** Retention, burial and degradation of the oil washed onto the beaches were influenced by the characteristics of the DWH oil and a combination of uncommon environmental settings. The DWH oil is a light sweet crude oil (Reddy *et al.*, 2012; Ryerson *et al.*, 2012), with a relatively high degradability owing to its high concentrations of low molecular weight and saturated compounds (Atlas and Hazen, 2011; Edwards *et al.*, 2011; Hazen and Prince, 2015; King *et al.*, 2015). Because of the close proximity of the spill site to the coast, oil reaching the shore still contained relatively high concentrations of compounds that could be rapidly decomposed by microbes (Figure 3.4 B) despite the weathering during transport in the ocean (Liu *et al.*, 2012).

Beach morphology dynamics and sediment characteristics enhanced retention of oil washing onto the Gulf beaches. The shallow, depressed beach profile and three major storms resulted in the deposition of oil and oiled water in a relatively wide zone above the mean high water line, where adsorption of hydrocarbons to the quartz grains (Wu *et al.*, 2006) effectively trapped oil. Beach sands have a high capacity for oil adsorption and microbial colonization due to the relatively high specific surface area of the sand. The buildup of the up to 70 cm thick contaminated sand layer between and after the storms prevented further oil deposition on the beach plateau and locked oil in the beach. Similarly, a succession of four storms produced oil contaminated sand layers up to 1 m thick buried as deep as 3 m in sandy beaches after the 2002 Prestige oil spill off the Spanish coast (Bernabeu *et al.*, 2009).

The burial of oil can restrict access to O_2 such that the oiled layers become anoxic, thereby bringing the biodegradation process to a near halt (Prince, 2010). The steady O_2 decrease we observed in oiled Gulf sediment cores incubated in the lab (Figure 3.8 B) suggested that the layers below 20 cm depth would turn anoxic within 3-4 months if O_2 would be supplied exclusively by diffusion across the sediment surface. O_2 profiles measured in the oil-contaminated beach in September revealed reduced O_2 concentrations in layers with increased oil concentrations (Figure 3.3 A) but O_2 depletion was not observed. Tidal pumping prevented O_2 depletion around the oil layers in Pensacola Beach sands and supported aerobic degradation of the buried oil (Figure 3.10). Although the heavily oiled sediment layers reduced the sediment permeability k about 2-fold (k_{oiled} = 3.1 $\times$ 10^{-11} m^2, 1SD = 9.7 $\times$ 10^{-13} m^2), the well-sorted beach sand remained highly permeable to air. Through the perpetual tidal air circulation through the sediment and ensuing mixing of inflowing and pore air, tidal pumping could lessen O_2 and CO_2 gradients developing around buried oil, thus maintaining conditions for rapid aerobic hydrocarbon degradation. In the laboratory tide simulator experiments, the exclusion of tidal pumping increased the calculated half life of the buried oil 30-fold from 58 to 1733 days, emphasizing the role of tidal pumping for microbial oil degradation. In previous studies, tidal pumping was found to transport critical O_2 to rooting plants (Jiao and Li, 2004) and sea turtle nests (Suss *et al.*, 2012) in beach ecosystems. The effect of tidal pumping on O_2 distribution is supported by model calculations that show O_2 increases in beach sand after water drained from the pores at ebb tide (Geng *et al.,* 2015). Tidal pumping also could enhance moisture in the oiled sand layers, thereby supporting microbial activities during phases with little rain as in September/October 2010 (Figure 3.3 D). A water film of a few nanometers corresponding

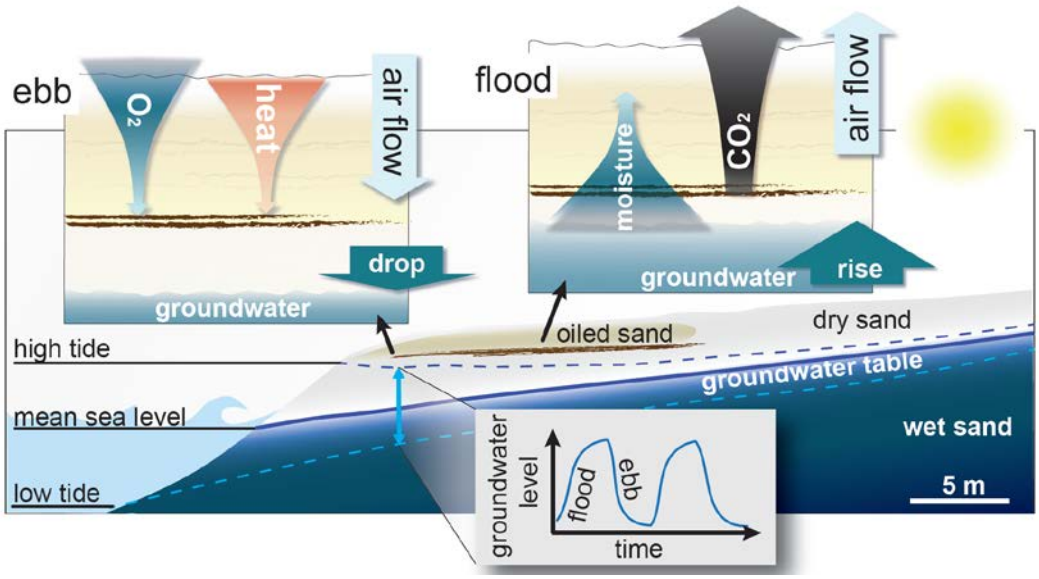

Figure 3.10 The effect of tidal pumping on gas, heat and moisture transport in the oil-contaminated Gulf beach. The dropping groundwater table during ebb tide drew warm O_2-saturated air into the sediment thereby supporting aerobic oil degradation in the beach. During the flood, the rising groundwater table pumped moist air from the previously water-saturated sand layer upward, which supported the water film on particles that is critical for microbial growth. The rising water table also pumped air, reduced in O_2 and enriched in CO_2 by the sedimentary aerobic decomposition, out of the beach. Thick dark brown lines in main figure and inserts: heavily-oil layers in the beach sand. Light brown areas in main figure and inserts: lightly-oiled beach sand. Solid blue line: groundwater table. Dashed light-blue line: groundwater table at low tide. Dashed dark-blue line: groundwater table at high tide. Left insert: Transport processes during falling tide. Middle insert: Changes in the height of the groundwater table over time. Right insert: Transport processes during rising tide.

to a moisture of ~ 1% in the beach sand is prerequisite for microbial growth in sediments (Rivkina *et al.*, 2000; Or *et al.*, 2007). Beach exhalation carried moist air from the deep sand layers, left wet by the dropping groundwater table during ebb, upward into the drier sand layers, supporting moisture levels >2% except in the uppermost 10 cm of the beach. Nevertheless, the tidal pumping could not transport dissolved substances to the oil, thus, the supply of major nutrients may have limited the oil degradation. An elevated abundance of nitrogen fixation genes in the oiled PB sands (Rodriguez-R *et al.*, 2015) indicates that

the micoorganisms had mechanisms to compensate for potential nitrogen limitation.

Natural seeps release 2 to 9 × 10^4 m^3 y^{-1} oil (Kvenvolden and Cooper, 2003; MacDonald *et al.*, 2015) to the Gulf, and oil-degrading bacteria are ubiquitous in Gulf ecosystems (Smith, 1952; Atlas and Hazen, 2011; King *et al.*, 2015; Rodriguez-R *et al.*, 2015; Joye *et al.*, 2016). In oil mousse collected near the DWH location as well as in mousse washing onto the Mississippi coast, Alpha and Gammaproteobacteria dominated, with the oil-degrading genera *Marinobacter, Alcanivorax, Pseudomonas, Alteromonas* being the most abundant genera (Redmond and Valentine, 2012; Liu and Liu, 2013), i.e. the same genera that were central for the degradation of the buried oil at Pensacola Beach. A survey conducted prior to the DWH spill found that petroleum hydrocarbons were present in 67 % of the sediment samples collected at 63 sites along the coast from Texas to Florida (Lisle and Stellick, 2011). Pre-adaptation of the sedimentary microbial community (Leahy and Colwell, 1990) can enable a rapid induction of hydrocarbon-degrading enzymes upon contact with oil (Valentine *et al.*, 2012; Hazen *et al.*, 2016).

Bacteria in Pensacola Beach sands were 2 orders of magnitude more abundant in the presence of oil contamination (Figure 3.6 A) and RNA-based analyses (Kostka *et al.*, 2011) support the conclusion that the majority of bacteria in these oiled sands were active. Early responding microbial populations included a number of bacterial groups (*Alcanivorax, Marinobacter, Muricauda, Oceanicaulis*) known to metabolize aliphatic compounds, which were present in highest abundance in PB sands from July to September. These results are corroborated by findings at other Gulf beaches after contamination by DWH oil: at Elmer's Island/LA, microbial cell counts rose by two orders of magnitude with members of the *Alpha- and Gammaproteobacteria* dominating in the polluted sand *(Lamendella et*

al., 2014). Newton (2013) reported that *Alcanivorax*, *Alteromonas*, *Marinobacter*, *Winogradskyella*, and *Zeaxanthinibacter* exhibited the largest relative abundance increases in oiled surface sands collected from beaches along Mississippi, Alabama, and Florida coasts between June and November 2010.

Upon depletion of the highly-degradable low molecular weight n-alkanes and aromatic hydrocarbons in PB sands, members of the orders *Chromatiales* (Gammaproteobacteria) and *Hyphomonas* (Alphaproteobacteria) became more abundant from end of July to October 2010. *Chromatiales* were also reported from beach sands polluted by the Prestige oil spill (Jiménez *et al.*, 2007). These bacteria are among the predominant microbial groups in natural asphalt pits (Kim and Crowley, 2007) suggesting their ability to benefit from highly weathered hydrocarbons. *Chromatiales* thus may use products of the initial degradation phase in the beach.

The average half-life of the GC-amenable oil components in the Pensacola beach sand ranged from 53 to 69 days, with shorter half lives in the sand layers, where oil was concentrated (25 d for aliphatics, 22 d for aromatics). This agrees with half-lives of 27 d and 33 d for hopane-normalized alkane and aromatic concentrations reported for oil-contaminated Delaware beach surface sands (Venosa *et al.*, 1997), and 69 d (alkanes) and 87 d (aromatics) determined in DWH-SRBs collected at Louisiana's Fourchon Beach and Elmer's Island (Elango *et al.*, 2014). A comprehensive compilation of published decay rates for crude oil components (Howard *et al.*, 2005), lists half-lives of less than 25 d for n-alkanes up to carbon number C21, 100 to 175 d for C22 to C30, and 276 to 383 d for n-alkanes greater than C30. The half-lives on PAHs with 3 to 4 rings fell in the same range (38-378). The average half-lives we measured thus were in the more rapid range of those

listed by Howard et al. (2005), which we attribute to the relatively high content of saturated hydrocarbons in the light DWH crude oil, the warm temperatures in the Gulf, and the tidal pumping.

By end of June 2010, the decomposition process had more than doubled the number of hydrocarbon components in the buried oil, mostly through the production of thousands of oxygenated compounds absent in the source oil (Ruddy *et al.*, 2014). The degradation of these compounds and less degradable resins and asphaltenes can occur through co-metabolism or co-oxidation (Hazen, 2010; Nzila, 2013). Highly degradable alkanes and aromatics, preserved in the anoxic core of larger buried oil-sand-aggregates, may have been a source for such growth substrates. This is supported by a temporary increase in the relative abundance of some early responder microbial groups (e.g. *Alcanivorax*) shortly after ODC's sifting process destroyed such aggregates and mixed degradable and recalcitrant oil components. Similarly, ODC's mixing of fresh detrital material from the beach surface (e.g. algae) into the re-deposited sand may have promoted the buried oil degradation (Mortazavi *et al.*, 2013; Horel *et al.*, 2014).

After ODC, the decreasing buried oil concentrations did not support the large microbial blooms that were observed prior to the cleaning, and the abundance peaks of oil degrading bacteria disappeared by November 2010. In June 2011, the resurgence of the chemo*autotrophic* archaeon *Nitrosopumilus*, which is highly sensitive to the toxic effects of oil (Urakawa *et al.*, 2012), reflected the decrease of petroleum hydrocarbon concentrations to background levels. The recovered Pensacola Beach microbial community differed from the pre-spill community, which may be related to long-term effects of the oil disturbance or changes in other environmental factors (Rodriguez-R *et al.*, 2015).

3.6 Conclusions

Our results suggest that the sand beach at Pensacola functioned as an effective biocatalytical oil filter at the land-ocean interface. The tidal pumping of O_2 into and CO_2 out of the beach bears similarities to breathing, enhancing the efficiency of gas exchange and ensuing metabolic processes in the sand. After the pollution of Pensacola Beach, initial cleaning operations removed oil from the beach surface, but a ~70 cm thick layer of oil contaminated sand remained that contained about 2/3 of the oil washed onto the shore. The biocatalytical activity of the beach removed the majority of the small oil particles adhering to the sand grains within the first four months after oil came to shore, and Operation Deep Clean eliminated most of the remaining larger oil-sand aggregates. Although deeply buried, sand-oil aggregates with anoxic cores can persist in beaches for decades, the combination of beach morphodynamics producing sand level changes of > 70 cm within 3 months and the biocatalytical activity of the sand provide powerful natural mechanisms to the Gulf beaches to recover from oil contamination.

3.7 Acknowledgements

This research was made possible in part by grants from The Gulf of Mexico Research Initiative as part of the DEEP-C and C-IMAGE II consortia as well as through RFP V funding. This research was also supported by the National Science Foundation (OCE-1044939 and OCE-1057417), the Florida Institute of Oceanography (FIO 4710-1101-00-1), and the Northern Gulf Institute (NG1 191001-306811-03). Data reported in this paper are tabulated in the Supplementary Materials and are publicly available through the Gulf of Mexico Research Initiative Information & Data Cooperative (GRIIDC) at

https://data.gulfresearchinitiative.org and archived at the National Center for Biotechnology Information (NCBI) under BioProject ID PRJNA294056.

CHAPTER 4. DEFINING THE SEAFLOOR MICROBIOME OF THE GULF OF MEXICO AND ITS RESPONSE TO PERTURBATION

4.1 Abstract

The microbial ecology of oligotrophic deep ocean sediments is understudied relative to their shallow counterparts, and this lack of understanding hampers our ability to predict responses to current and future perturbations. The Gulf of Mexico has experienced two of the largest accidental marine oil spills, i.e., the 1979 Ixtoc-1 blowout in the Southern Gulf of Mexico (GoM) and the 2010 Deepwater Horizon (DWH) explosion in the Northern GoM. In the case of the DWH spill, 2-15% of the oil released was transported to the seafloor where it was subject to degradation and transformation by sedimentary microorganisms. However, prior to the DWH disaster, the microorganisms present in the oligotrophic Gulf of Mexico deep seafloor were virtually unknown. Thus, focusing on the Gulf seafloor, the objectives of this research were to (1) characterize deep ocean sedimentary microbial communities to establish baseline conditions over large spatial scales, (2) map the biogeographical patterns in microbial community structure, (3) generate a biogeography model of microbial community structure that can predict the abundance and distribution of dominant microbial populations, and (4) determine if impacted regions had returned to baseline conditions. Microbial communities were characterized via next generation sequencing of SSU rRNA gene sequences for 29 sites across multiple years in the Gulf of Mexico, represented by >700 samples. The distribution of seafloor microbial communities is broadly consistent across the entire region in terms of the OTUs detected

and their relative abundances. The seafloor microbiome was well approximated by the overlying water depth and depth within the sediment column, which together explained 38 % of our observed variation, regardless of geographic sampling region. Biogeographical distributions were used to generate a depth-stratified predictive model for over 4000 dominant OTUs that relies on easy-to-obtain geospatial variables (water depth, sediment depth, latitude, and longitude). Microbial community structure is linked to oxygen penetration depth and sediment geochemical regime, which are likely controlled through carbon delivery. Our results further demonstrate that sediments impacted by the DWH spill had returned to near baseline conditions after two years. The distributions of key microbial populations can now be calculated and constrained while deviations from these predictions may be evaluated to pinpoint impacted sites, and more importantly, in future response efforts or long-term stability studies.

4.2 Introduction

The deep ocean floor at greater than 1000 m water depth covers approximately 50% of the Earth's surface. The seafloor of the deep ocean is comprised predominately of muddy sediments, and solute transport rates in these sediments are dominated by diffusion, while larger particles are transported through burial (Burdige, 2006). The biogeochemistry regimes of deep ocean sediments are largely governed by the quality and quantity of deposited organic matter, and nearly all organic matter introduced into these sediments originated in the photic zone via photosynthesis or through riverine inputs (Jørgensen and Boetius, 2007; Arndt *et al.*, 2013). Furthermore, in deep ocean environments, the majority of organic matter is decomposed while traveling through the water column prior to reaching the seafloor (Canfield et al. 2006). Therefore, oligotrophic sediments typically have very

low organic carbon contents and <20% is recognizable as one of the main biomolecular classes (Canfield et al. 2006; Teske 2013).

In contrast to the complexity and patchiness of the sedimentary carbon content, the oligotropic deep ocean is characterized by consistent physiochemical gradients (temperature, pressure, salinity, pH) that are often noted as the primary variables in controlling bacterial diversities in other environments (Lozupone and Knight, 2007; Bienhold *et al.*, 2012). In part, this temporal and spatial stability is thought to contribute to the higher diversity and lower variation in community structure observed in deep marine sediments compared to their coastal and pelagic counterparts (Jørgensen and Boetius, 2007; Zinger *et al.*, 2011; Bienhold *et al.*, 2016). Additionally, bacterial communities sampled from deep benthic marine sediments across the globe have thus far demonstrated few cosmopolitan groups with most populations geographically limited to one sample or one ocean region (Bienhold *et al.*, 2016). However, apparent cosmopolitan populations detected from relatively sparse datasets generally consist of the most dominant groups detected, namely the JTB255 clade (Gammaproteobacteria, Xanthomonadales) and the OM1 clade (Actinobacteria, Acidimicrobiales) (Bienhold *et al.*, 2016). The main environmental variables identified driving community composition are the total organic carbon content, water depth, geographic distance, and overlying ecosystem productivity (Wei *et al.*, 2010; Zinger *et al.*, 2011; Bienhold *et al.*, 2016).

While deep marine sediments are thought to be relatively stable, they are not impervious to ecological disturbances including phytoplankton and marine snow deposition (Billett *et al.*, 1983), whale-falls (Smith and Baco, 2003), biogenic burial (Kukert and Smith, 1992), and sediment transport (Aller, 1989). In macrofaunal

communities, these processes along with slow recovery rates contribute to a high level of diversity and patchy composition (Kukert and Smith, 1992; Ebbe *et al.*, 2010). Much less is known about how benthic microbial communities respond to disturbances.

One glaring example of such a disturbance is the Deepwater Horizon oil spill (DWH), which represents the largest accidental marine oil spill in history, released an estimated 4.1 – 4.9 million barrels of crude oil and a third as much natural gas at approximately 1500 m water depth (Lubchenco *et al.*, 2010; Joye *et al.*, 2011). Although the amounts and chemical composition of DWH oil remaining in the environment remain uncertain, the largest reservoir is thought to be primarily in deep ocean sediments with a considerable, but unknown, amount deposited near coastal sediments or onshore (King *et al.*, 2014). Approximately 12% of the 2 million barrels entrained in the deep ocean was transported to a 3200 km^2 region of the seafloor (Valentine *et al.*, 2014; Joye, 2015). The fate of this oil will largely be determined by microbial metabolisms in these environments and by burial.

A substantial challenge in determining the impacts of this oil being deposited into deep ocean sediments is the nearly complete lack of studies on Gulf of Mexico deep sea benthic microbial communities performed prior to DWH. Due to interest in the Gulf for petroleum exploration, previous studies focused almost entirely on deep subsurface sediments with the shallowest samples collected at ~4 meters below the seafloor, or on sediments impacted by natural hydrocarbon seeps (Nunoura *et al.*, 2009; Orcutt *et al.*, 2010; Biddle *et al.*, 2011). Due to this limitation in the knowledge of surficial microbial communities, the majority of studies on deep ocean sediments associated with the DWH event used samples that were collected outside of impacted areas as controls (Kimes *et*

al., 2013; Liu and Liu, 2013; Mason *et al.*, 2014; Yang *et al.*, 2016). Sediments were primarily impacted as deep water oil intrusion layers impinged on the seafloor and by a large sedimentation event of marine oil-derived snow (Passow, Ziervogel, Asper, and a Diercks, 2012; Hollander *et al.*, 2013; Valentine *et al.*, 2014; Brooks *et al.*, 2015; Romero *et al.*, 2015). While the datasets on benthic microbes are limited to relatively few samples, results indicate that microbial communities responded quickly to oil perturbation and shifts in community composition as well as total metabolic potential were observed (Kimes *et al.*, 2013; Mason *et al.*, 2014; Yang *et al.*, 2016). While there are conflicting reports and few samples (< 10), sedimentary microbial communities may have returned to baseline conditions within one year following the spill (Liu and Liu, 2013; Yang *et al.*, 2016).

With some similarities to the Deepwater Horizon oil spill, the Ixtoc-I well blowout that began in 1979, released approximately 3.5 million barrels of crude oil, and represents the second largest accidental marine oil spill in history (Jernelöv and Lindén, 1981). Similar to the petroleum hydrocarbons released during the DWH disaster, Ixtoc-I crude oil was saturated with gaseous hydrocarbons and had a similar chemical composition. While the Ixtoc-I blowout occurred in shallow water (52 m water depth), subsurface plumes also appear to have formed in some regions owning to temperature and salinity density stratifications. Also similar to the DWH blowout, oil appears to have been transported to the seafloor through marine oil-derived snow and approximately 25% of the total oil released during Ixtoc is thought to have remained in seafloor sediments (Jernelöv and Lindén, 1981). Unfortunately, the long-term fate of this Ixtoc-I oil is not well understood (Schrope, 2010), and due to technical limitations at the time, little is

known about the *in situ* microbial community response (R M Atlas, 1981).

Here, we present the largest benthic marine microbial community study conducted to date, and by far the most extensive in the Gulf of Mexico. We focus on two regions in the Gulf of Mexico that were both impacted by massive marine oil spills. Over 700 samples were analyzed representing 29 distinct sites, across up to four years, and we generated >120 million SSU rRNA gene sequences, including both archaeal and bacterial members. Our objectives were to (1) characterize un-impacted sedimentary microbial communities to establish a baseline, (2) map the biogeographical patterns in microbial community structure across the Gulf of Mexico, (3) using this map, generate a Gulf of Mexico biogeography model of microbial community structure that can predict the abundance of dominant microbial populations, and (4) determine if impacted regions had returned to baseline conditions. For the first time on a region-wide scale, we determine the environmental parameters structuring microbial communities, including the stratification of microbial communities according to sediment depth and across oxygen gradients. In addition, we address the temporal stability of microbial communities across the region.

4.3 Material and Methods

4.3.1 Sediment Sample Collection

Samples were collected during five research cruises from 2012 to 2015 across the Northern and Southern Gulf of Mexico (see Table C.1, Figure 4.1). Sediment samples were collected using a MC-800 multicorer capable of collecting up to eight, 10-cm diameter by 70 cm long cores per deployment. Cores were sectioned at either sub-

centimeter (2 mm sections) or 1 cm resolution using a calibrated threaded rod attached to a core clamp stand with a tight fitting plunger (see Table C.1 for the full sample list)

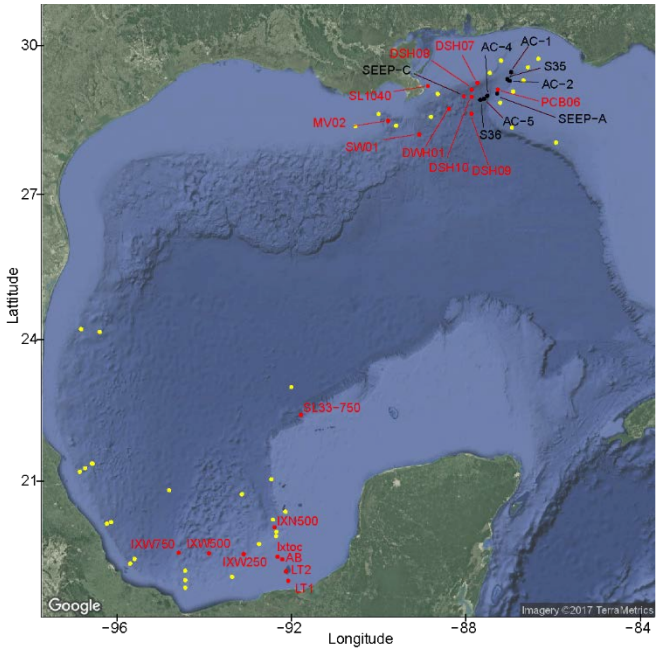

Figure 4.1 Map of the Gulf of Mexico. All yellow points are sites that were profiled for oxygen concentrations, while sites with black points are those that only have microbial community data. Sites in red are represented by both oxygen and microbial community data. All sites sampled for microbial data are labeled with the site name, which can be seen in Table S1.

(Schwing *et al.*, 2016). Sectioned sediments were frozen immediately in a portable -80 °C freezer onboard the vessel and transported back to the laboratory for DNA extraction.

In the Northern Gulf of Mexico (GoM), we collected sediment samples across approximately 100,000 square kilometers, primarily focusing on the Desoto Canyon feature and in close proximity to the Deepwater Horizon well-head (Table C.1, Figure 4.1). Sampling sites ranged from 56 m (SL1040) near the Mississippi River Delta to 2293 m (DSH09) southeast of the DWH wellhead, spanning three years (2012 – 2014) and four sampling time points (Table C.1). In the Southern Gulf of Mexico, sampling sites spanned

approximately 40,000 square kilometers ranging from 16-1470 m, primarily focusing on the Ixtoc-I well blowout site and the western transect (Figure 4.1) (Soto *et al.*, 2014). Cores from the southern GoM were all collected from one cruise in 2015. For each region, sediment core profiles extend to at least 10 cm depth below the seafloor, with a subset including sections up to 20 cm of the sediment column. Our experimental design incorporated multiple levels of replication to address variation due to sampling effort, as well as spatial and temporal heterogeneity. These include: (1) technical replicates with duplicate DNA extractions performed and separate libraries generated on the same depth section, (2) multicore cast replicates where triplicate cores from the same cast were analyzed separately representing variation across approximately $1m^2$ of the seafloor, (3) replicates at the site level where triplicate casts were deployed at the same site and cores from cast was analyzed separately, and (4) temporal replicates where the same site was sampled up to 4 times in 3 years (Figure C.1).

4.3.2 Oxygen Profiles

Oxygen concentration profiles were determined using a Presens Microx4 needle-microoptode (Presens, Regensburg, Germany) along with a CHPT micromanipulator (Composite High Pressure Technologies, Lewes, Delaware). Immediately after the cores were retrieved from the multicorer, a core was mounted on the extruder for stabilization and oxygen was profiled at mm-scales until the sensor measured 0 umol/L oxygen concentration. This was typically accomplished in < 15 minutes, although deeper sites required longer profiling times. Between sites, the optode was calibrated following the manufacturer's protocol using sodium sulfite for the 0% solution and bubbling with air for the 100% solution. The depth of oxygen penetration was imported into Ocean Data View

v4.6.3 (Schlitzer, 2012) and predictive surfaces were generated using DIVA gridding with automatic scale lengths and with a signal to noise ratio of 50.

4.3.3 DNA Extraction, SSU rRNA Gene Sequencing and Processing

Sediment was sub-sectioned using a flame sterilized drillbit and total genomic DNA extractions performed on approximately 0.25 g using a MoBio Powersoil DNA extraction kit following the manufacturer's protocol. Samples collected in 2012 and 2013 were extracted using the MoBio Powersoil Highthroughput extraction kit, while those from 2014 and 2015 were extracted using the single-prep kit. The V4 region of the SSU rRNA was amplified using the commonly used 515F/806R primer set that targets both Archaeal and Bacterial domains and sequenced on an Illumina MiSeq with 2x250 v2 chemistry (Caporaso et al., 2012; Green et al., 2015, see Supplementary Information). All paired-end reads were merged using PEAR v0.9.6 with default parameters (Zhang *et al.*, 2013) and assembled reads were quality filtered in QIIME using a minimum phred score of 30 (Q=30) (J. Caporaso *et al.*, 2010). Mothur was used to remove sequences less than 250bp or greater than 255bp (Schloss *et al.*, 2009). D*e novo* based chimera detection followed by reference based chimera detection against the SILVA gold database was performed with vsearch v1.9.6 (Rognes *et al.*, 2016). The remaining high quality sequences were dereplicated using vsearch v1.9.6 and operational taxonomic units (OTUs) were picked using Swarm v2.1.8 with default parameters (Mahé *et al.*, 2014; Rognes *et al.*, 2016). Overall patterns were similar as determined with uclust_reference and de novo based methods, but these would not complete on the full sample set (data not shown, a brief discussion is available here: http://waoverholt.github.io/testing_otu_picking/).

Singletons and OTUs present in less than 10 samples were removed, producing approximately 300,000 OTUs using 47 million reads (75% of initial raw reads). Samples with less than 5000 sequence counts were removed from further analysis. Taxonomic affiliations for each OTU were determined using the SILVA v123 database formatted for use with QIIME (J. G. Caporaso, Kuczynski, *et al.*, 2010; Quast *et al.*, 2012). Representative sequences were aligned using the PyNAST implementation in QIIME with the SILVA alignment and a phylogenetic tree for determining phylogenetic diversity metrics was generated with fasttree v2.1.3 (J. Caporaso *et al.*, 2010; J. G. Caporaso, Bittinger, *et al.*, 2010; Price *et al.*, 2010). All raw sequences have been uploaded to NCBI under Bioproject PRJNA414249.

4.3.4 OTU Analysis

OTU counts were normalized using the metagenomeSeq package in R, scaling by 1000 and without a log-transform (Paulson *et al.*, 2013). Trends were confirmed with rarefaction to 5000 sequences per sample (data not shown). Beta diversity was determined using Bray Curtis dissimilarity implemented in the R package 'vegan' (Oksanen *et al.*, 2007; R Core Team, 2014), while weighted and unweighted Unifrac distances were calculated using the implementation found in the R package 'phyloseq' (McMurdie and Holmes, 2013). Patterns were consistent and Bray Curtis dissimilarities are shown. Nonmetric multidimensional scaling (NMDS) ordination was generated using the R package 'vegan' without transformation and patterns were indistinguishable to those observed using Principal Coordinates Analysis (PCoA) also generated with 'vegan' (Oksanen *et al.*, 2007; R Core Team, 2014). Patterns in Bray Curtis dissimilarities were tested using multiple linear regressions in R (R Core Team, 2014). The most significant

regression used the formula (dissimilarity ~ sediment depth difference * water depth difference * geographic distance * Sampling Year). Linear regression models were compared using Analysis of Variance (ANOVA), and the percent each variable contributed to the patterns observed was determined with ANOVA (Table C.2, Table C.3). While all interaction terms were significant, only those that contributed >1% variance were retrained and the model was reconstructed after dropping those terms to reduce its complexity (dissimilarity ~ sediment depth difference + water depth difference + geographic distance + sampling year + sed:water). All plots generated use the ggplot2 package in R (Wickham, 2009; R Core Team, 2014).

4.3.5 Meta-Analysis: Incorporating Impacted Surficial Sediments

Sequences generated by Mason and colleagues targeted the same region of the 16S rRNA gene, although sequence lengths were substantially shorter (on average 100 bp after Q30 trimming) (Mason *et al.*, 2014). These sequences were incorporated into this study by using our previously identified OTUs as reference sequences and using the QIIME script 'parallel_pick_otus_uclust_ref.py'. Without chimera checking (as the references were already cleared) we matched 75% of all Mason 16S sequences (20 million reads) to one of our OTUs at 3% sequence difference or less. Since the Mason et al., 2014 study used only surficial sediments (top 1 cm), we restricted our comparison samples to include only depths in the same interval.

4.3.6 Constructing a Gulf-Wide Model for Microbial Community Composition

A model for microbial community composition across the Gulf of Mexico was constructed using random forest regression implemented in the R package 'randomForest'

at the OTU level (Liaw and Wiener, 2002). Random Forest regression is an ensemble machine learning method where multiple individual decision trees are constructed and ultimately averaged to minimize over-fitting and improve prediction accuracy. Individual decision trees are generated from a subset of the response variable (OTU abundance) and each fork or node in the tree is guided by predictor variables (again a randomized subset) to maximize differences in the branches. Random Forest is robust to outliers, does not assume specific distributions (nonparametric), and tests/trains the model by subsampling the response variable at each step and testing the decision node with the remaining data (Wei *et al.*, 2010).

Water depth, sediment depth, latitude, and longitude were chosen as predictor variables and were used as proxies for sediment carbon input, oxygen concentrations, geological regime shifts from E-W and N-S as well as riverine inputs. Latitude, longitude, and water depths were extracted from the NGDC Coastal Relief model (Divins and Metzger, 2008). The Random Forest regression model for each response variable was constructed with 500 trees, a minimum of 5 terminal nodes per tree, and randomly subsampling 1/3 of the response variable (OTU normalized counts) for each node of each tree. Only response variables of which >50% of the variance could be explained by the regression forest were retained. The effectiveness of the model was evaluated by randomizing the predictor variables 1000 times and comparing the root mean squared errors of the constructed models with the random model using a Z-test. All the code and raw data that was generated for this study can be found at GRIIDC (https://data.gulfresearchinitiative.org) and can be accessed at (doi: 10.7266/N70G3HN3).

4.4 Results and Discussion

4.4.1 Environmental parameters structuring benthic microbial distributions across the Gulf of Mexico

In the Northern Gulf of Mexico (GoM), we collected sediment samples across approximately 100,000 square kilometers, and in the Southern Gulf of Mexico samples span approximately 40,000 square kilometers. Sampling sites ranged from 16 to 2300 m water depth, focusing on regions adjacent to the Deepwater Horizon (DWH) and Ixtoc I blowouts. As part of this study, we address technical and temporal variation at different spatial resolutions (Figure C.1). Technical and cast level (1 m^2 bottom area) replicates showed similar Bray-Curtis dissimilarity values (mean = 0.23, sd= ± 0.05; 0.25 ± 0.05, respectively) and site level replicates (10-100 m^2) were less similar (0.34 ± 0.09). Sampling temporally (across 3 years), lower similarity (0.54 ± 0.12) was observed, although this value may be inflated due to a small change in DNA extraction technique between 2013 and 2014 sampling years. All sites sampled at greater than 500 m water depth for the entire study show a mean dissimilarity of 0.61 ± 0.15 in comparison to a mean dissimilarity of 0.51 ± 0.13 for sites sampled at less than 100 m. However, the shallow sites were primarily sampled from the SGoM during the same year (Figure 4.2 C). We note that our data suggest these communities to be more similar than other studies, likely since we are sampling the same relatively small ocean basin and our analyses employ a more restrictive OTU abundance filtering, although our ranges overlap with observations by Zinger et al. (2011) conducted over larger spatial scales in multiple oceans.

Overall, the distribution of microbial populations with sediment depth across these geographically distant regions of the Gulf were remarkably consistent, and were structured primarily based on overlying water depth along sediment core depth (Figure 4.2 A, B). Our

sampling design focused primarily on shallow sites (<100 m) and deep sites (>1000 m), and thus the down core sediment progressions seen in Figure 4.2 A are structured into two

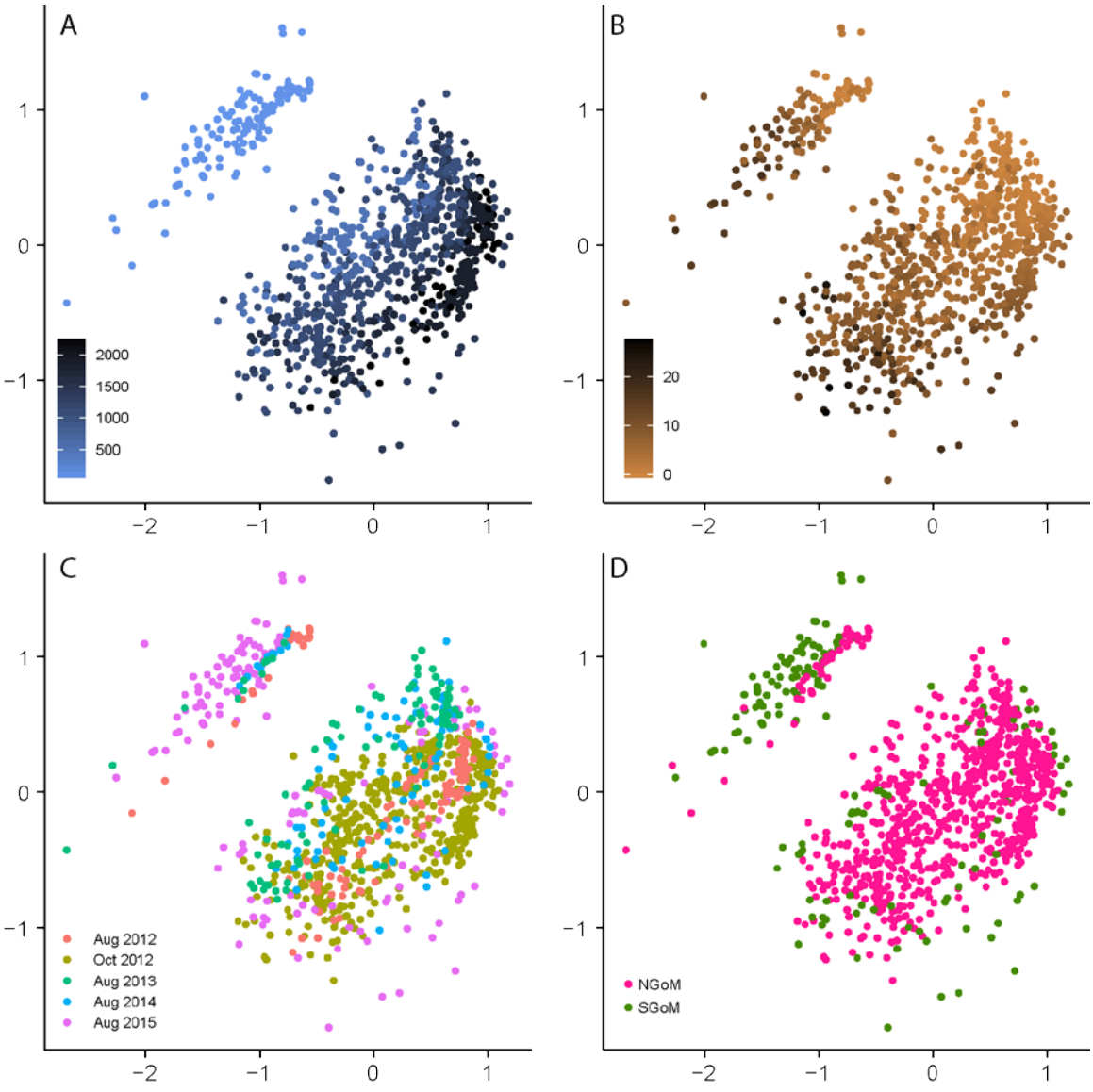

Figure 4.2 Large-scale patterns in microbial biogeography. All plots are generated from the same NMDS ordination of Bray-Curtis dissimilarity. The stress for each plot is 0.152. (A) Samples are colored based on increasing water depth. The shallow water samples (< 100m) clearly separate from the deeper water samples (> 400m). Note the intermediate water depths were not sampled. (B) Samples are colored darker with increasing sediment depths. Although there are a few outliers, there is a clear and consistent downcore progression from the "top-right" of the NMDS plot towards the bottom left in every core sampled. (C) Samples are colored based on collection date. (D) Cores were collected from the Southern Gulf of Mexico (colored in green) and the Northern Gulf of Mexico (colored in pink)

main clusters primarily along the Y-axis. However, a continuous gradient with increasing water depth is expected, and indeed such a gradient is observed at the sites >1000m water depth. Performing a multiple linear regression analysis and partitioning the variance resulted in water depth explaining 22.1% of the total variation ($F = 1.29e5$, $p < 2e\text{-}16$, Table C.2).

The effect of sediment depth is primarily observed along the x-axis with surficial sediment samples clustering in the upper right of Figure 4.2 proceeding down core towards the bottom left, consistent with other studies (Figure 4.2 B) (Teske, 2013). Sediment depth explained 14.2% of the total microbial community variation ($F = 8.3e4$, $p < 2e\text{-}16$), and together with water depth, these variables could explain 36% of our observed variance (74% of our total explained variance, Table C.2). In contrast, geographic distance was of limited effectiveness in distinguishing microbial community compositions, explaining just 6% of the variance ($F = 3.6e4$, $p < 2e\text{-}16$). If we change this to a discrete variable (NGoM vs SGoM), it instead explains 4% of the variance ($F = 3.2e4$, $p < 2e\text{-}16$) and this is visualized in Figure 4.2 C. We note that we have fewer core profiles from the southern GoM, all collected during 2015. Similarly, we found the sampling time point explained 5% of the variance ($F = 2.9e4$, $p < 2e\text{-}16$) and differences were not visible in Figure 4.2 D. Due to a slight change in DNA extraction technique, the change in microbial communities with time may be partially or solely a technical issue. In total, water depth, sediment depth, geographic distance, sampling time point and their interactions explained 52% of the observed variation. Simplifying this model by removing interaction variables that contributed little to the percent variance explained (see methods), 49% of the observed variance can be explained (Table C.2).

This study represents the largest marine benthic biogeography study to date based on sample size and sequencing effort by a significant margin. In addition, this sampling effort was focused on a relatively small ocean region in comparison to similar studies, which provides both greater spatial resolution, while the focus on distinct regions in the Gulf of Mexico allowed for better generalization across the basin. One of the better studied regional ocean basins, with respect to biogeographic patterns in microbial community structure is the Arctic ocean (Bienhold *et al.*, 2012; Jacob *et al.*, 2013). Jacob et al. (2013) used spatial variables similar to this study consisting of latitude, longitude, geographic distance, and water depth at the Arctic Long-Term Ecological Research (LTER) site to constrain microbial community variation in 13 surficial sediment samples collected along two transects. Using redundancy analysis, Jacob et al. (2013) found that bacterial community structure significantly varied with water depth and longitude (7% and 3% of the variance, respectively), while geographic distance was not significant (Jacob *et al*., 2013). Somewhat surprisingly, a proxy for phytodetrius input (CPE) explained less variation than water depth, although this was potentially due to the low sampling effort. Also in the Arctic, Bienhold et al. (2012) linked microbial community structure and diversity to energy availability in benthic sediments using pyrosequencing on 10 samples and fingerprinting methods on 42 samples. Contrasting with the results from this study, the authors linked changes in community composition primarily with geographic distance (10% of the variation), followed by sediment pigment concentrations (5%). Sediment depth and water depth had low explanatory power, although again, this may have been due in part to a much smaller sample set (Bienhold *et al.*, 2012). In the southern Atlantic Ocean, a study by Schauer et al. (2010) examined biogeographic patterns in deep marine surficial

sediments across 3 basins (Cape, Angola, and Guinea) generating three SSU rRNA clone libraries and analyzing another 51 samples using a fingerprinting method. Their results showed that microbial communities were significantly different between the basins examined and that within a basin there was a spatial effect. In another regional study of surficial benthic microbial communities, the authors sampled 24 surficial sediments in two geographically distinct regions in a 5500 km transect in the Southern Ocean off the coast of Western Antarctica (Learman *et al.*, 2016). This study consisted of SSU rRNA gene amplicons generated from the same primers used in this study and found that microbial community composition was linked to the bioavailability of carbon and nutrient availability. However, this finding was confounded by large physiochemical differences between the distinct regions, that had unique community compositions (Learman *et al.*, 2016).

On a global scale, water depth appears to have less explanatory power than observed in this study, while geographic distance tends to have more power (Zinger *et al.*, 2011; Bienhold *et al.*, 2016; Danovaro *et al.*, 2016). The reduced power of water depth on a global scale is well documented, poorly understood, and is unlikely to be related to a breakdown in the correlation between water depth and the quality and quantity of carbon inputs (Danovaro et al., 2016 and the refs within). In a global study, Zinger *et al.* constrained 22 % of the benthic microbial community variation and found that geographic distance best explained surficial microbial community variation at 6 %, similar in explanatory power to the results in this study (Zinger et al., 2011). These authors also found that coastal benthic microbial communities varied more than their deep ocean counterparts, which is the opposite of what was observed in this study (Figure C.1). This could be due

to several reasons including our shallow samples were mostly retrieved from the same year, and sampled more extensively in one geographic region. In a following, global-scale study focusing exclusively on deep marine benthic microbial communities (>1000m depths), (Bienhold *et al.*, 2016) observed that microbial communities were increasingly distinct with increasing geographic distance, and this distance-decay relationship was even greater when one considers water flow paths instead of straight lines between sites. Total organic carbon explained the most variation in microbial community structure (10%) followed by geographic distance (4%), although the sample set consisted of 1-6 samples per ocean region (Bienhold *et al.*, 2016). Using non-sequence based techniques, Danovaro et al. (2016) found that the absolute abundances of bacteria, total archaea, Marine Group I Archaea, and Marine Group II Archaea did not significantly vary within the same ocean basin, however, there were differences between ocean basins. Danovaro et al. (2016) also demonstrated that archaeal and bacterial abundances were partially controlled by the same factors, namely biopolymeric carbon concentrations, and bacterial abundances were primarily influenced by carbon inputs while archaeal abundances were primarily influenced by bottom water temperature.

This study greatly contributes to our knowledge of the environmental parameters structuring the seafloor microbiome. Furthermore, this is the first study to examine large scale biogeographic patterns within a sediment core-profile in the deep ocean. Future global studies are encouraged to explore constraining the variation in microbial communities using a basin-based nested approach to improve the statistical models. However, sufficient samples from the region need to be collected in order to explore basin-wide biogeographic patterns. Here we demonstrate within the Gulf of Mexico water depth

explains a relatively high percent of total variation compared to similar studies even though we do not focus solely on surficial sediments. This result is likely due to close coupling with organic matter inputs in the region (discussed below).

4.4.2 Sedimentary oxygen concentrations throughout the Gulf of Mexico

Sedimentary oxygen profiles were determined for 42 sites across the northern and southern regions of the Gulf of Mexico using a micro-optode and micromanipulator at millimeter resolution. Oxygen profiles were obtained at the majority of sites where cores were sectioned for microbial community composition analysis, as well as over a substantially larger area (Figure 4.1, Table C.1). Typical core profiles are found in Figure 4.4 (B, D), while the interpolated maximum oxygen penetration depths across the study area are shown in Figure 4.3 A. At shallow, neritic sites, oxygen was depleted within the first millimeter, while oxygen penetration depths extended to 16 cm at the deepest sites (~ 3700 m). As anticipated, oxygen penetration increased nearly linearly with increasing water depths (Figure 4.3 B, Wenzhöfer and Glud, 2002). This likely results from a greater amount of phytodetritus reaching the seafloor in shallower environments as well as increases in primary productivity closer to the coast (Honjo *et al.*, 2008; Glud *et al.*, 2013). On the shelf, elevated chlorophyll α and β concentrations and depleted major nutrients are indicative of higher primary production (Moss *et al.*, 2016). The oxic-anoxic interface was closer to the sediment surface in the northern Gulf in comparison to the southern Gulf at

similar water depths, likely due to a lower sedimentary carbon deposition regulated by riverine inputs (Figure 4.3 C). The northern Gulf of Mexico is greatly influenced by the Mississippi River, the fifth largest river by volume in the world and the primary source

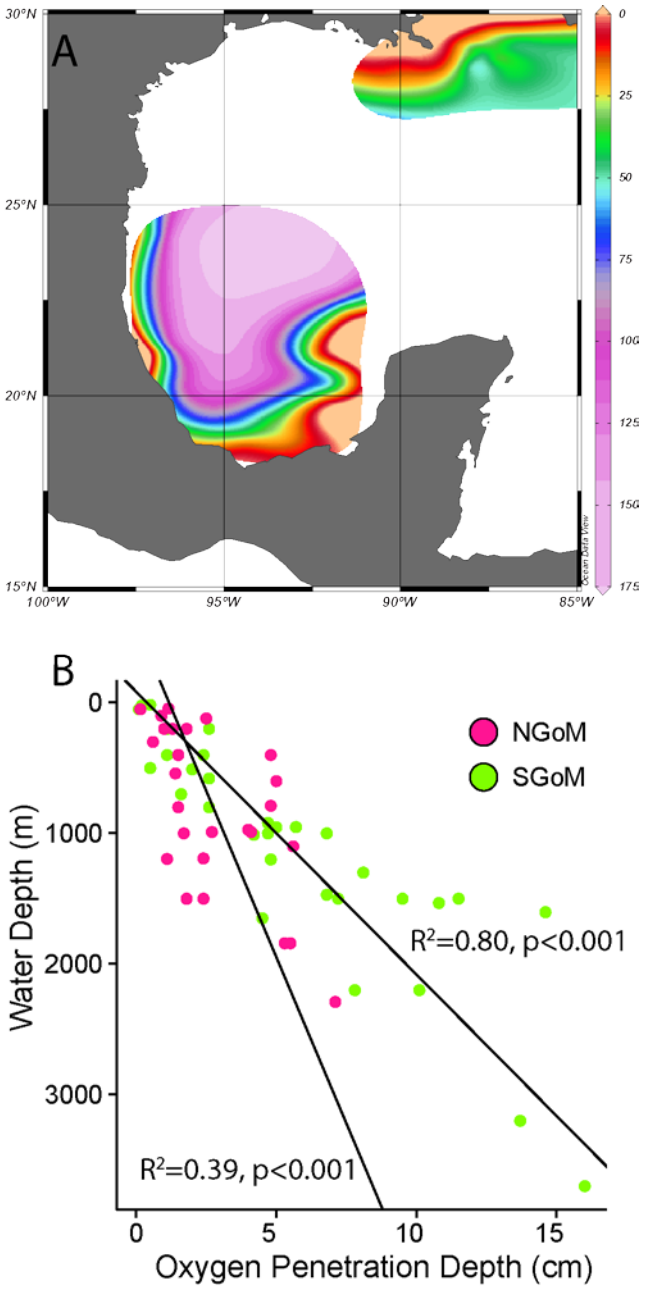

Figure 4.3 Oyxgen profiles collected throughout the Gulf of Mexico. (A) Interpolated plot showing predicted oxygen penetration depths across our study site. (B) Oxygen penetration plotted against water column depth.

(~90%) of both sediment and freshwater to the entire Gulf (Dunn, 1996; Goñi *et al.*, 1997; Meybeck and Ragu, 2012). This region also has one of the largest and best studied anthropogenically induced "dead zones" in the world, directly related to the high nutrient loadings linked to large phytoplankton blooms and massive deposition events to the NGoM (Turner *et al.*, 2008; Bianchi *et al.*, 2010). Furthermore, in late 2010 following the Deepwater Horizon oil spill, a massive offshore (>300m – 1500m sites) sedimentation event was observed where oily marine snow was deposited at 4-5 fold higher rates than typically observed (Passow, Ziervogel, Asper, and a Diercks, 2012; Brooks *et al.*, 2015). Relative to the northern Gulf of Mexico, the southern Gulf of Mexico generally receives lower riverine inputs (~10% of the northern Gulf input) (Meybeck and Ragu, 2012). However, our southern Gulf samples were collected in close proximity to the second largest riverine system in the Gulf of Mexico, the Grijalva-Usumacinta system as well as the smaller Coatzacoalcos and Papaloapan systems (Day *et al.*, 1982; Soto *et al.*, 2014).

4.4.3 Inter-basin microbial biogeography

Significant differences in microbial community composition ($p < 2e\text{-}16$, var. explained = 4%) were observed between the northern and southern Gulf of Mexico, although these differences were small relative to the impacts of overlying water column depth and depth within the sediments (Figure 4.2). These modest differences can potentially be attributed to differences in oxygen penetration depths (Figure 4.3). When comparing the microbial community composition of sediments from similar water depths

in each region, community composition in the northern Gulf of Mexico more closely resembled shallower sites in the southern Gulf of Mexico (Figure 4.4). This effect became more apparent when selecting sediments collected from 1000-1300 m water depths (Figure

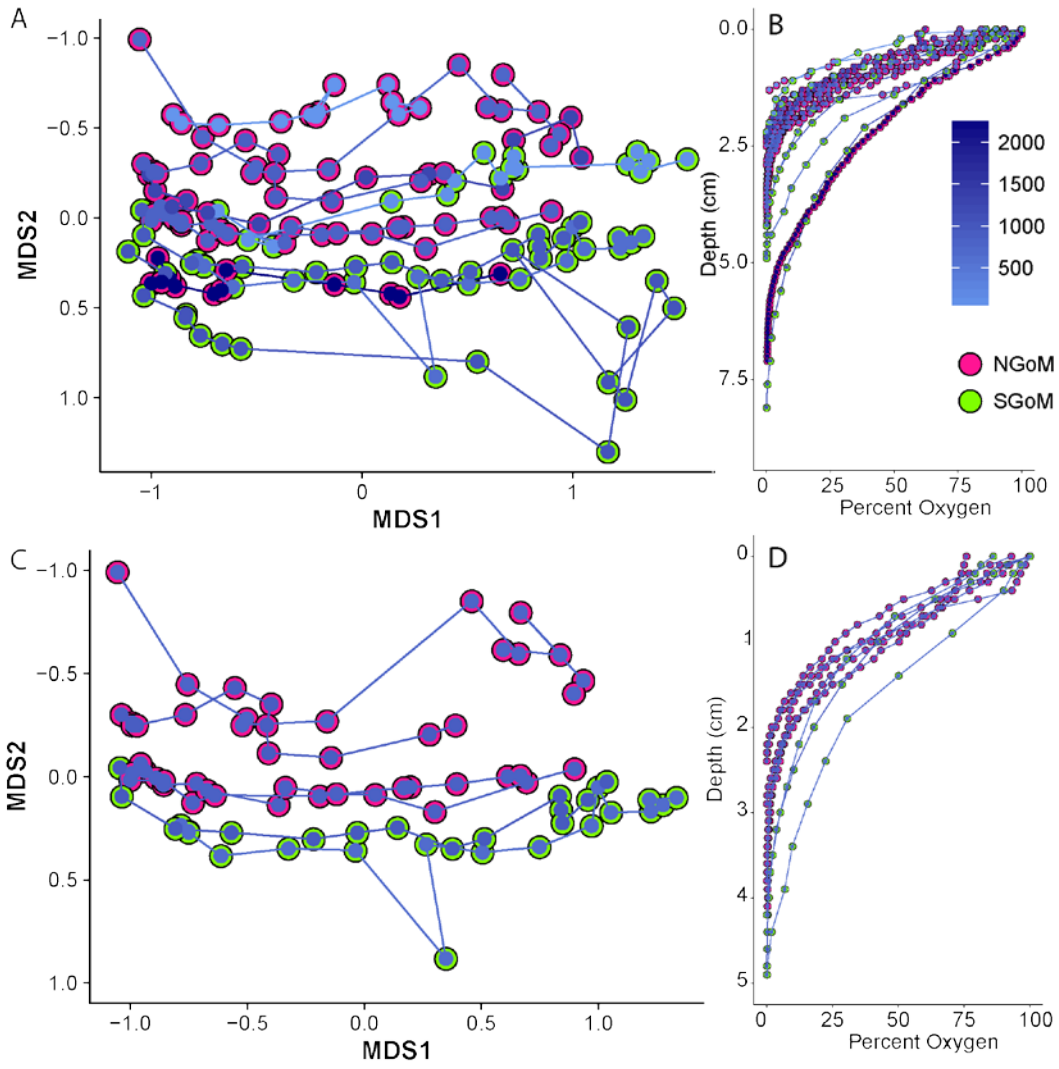

Figure 4.4 Subtle differences in community progression between the Northern and Southern Gulf of Mexico. The SGoM sites sampled have deeper depths of oxygen penetration and correspond to a community composition more similar to shallower sites in the NGoM. (A) NMDS of Bray-Curtis dissimilarity values for cores collected in 2014 (NGoM, pink) or 2015 (SGoM, green) from 500m – 2300m water depths. Down core progression is indicated by the connecting lines from surficial sediments on the left towards deeper samples on the right. (B) Corresponding oxygen profiles to all cores presented in A. (C, D) Same as plots A & B except only displaying sites collected between 1000-1300m.

4.4 C). Both southern Gulf microbial community core profiles cluster below (in the direction of increasing water depth profiles) similar northern Gulf profiles. This is clearly reflected in the deeper depths of oxygen penetration in the southern Gulf of Mexico and the maintenance of higher oxygen concentrations through the core profile (Figure 4.4 D). The microbial community profile from the deepest site (DSH09, 2293 m) from the northern Gulf of Mexico, with the deepest oxygen penetration depths, was similar to microbial communities obtained from 1300 m in the southern Gulf of Mexico (Figure 4.4 A, B). Overall, these data are consistent with greater organic matter deposition in the northern Gulf of Mexico due to the greater carbon and nutrient contributions of the Mississippi River relative to the Grijalva- Usumacinta system (Dunn, 1996). It was remarkable how similar the sedimentary microbial communities in these geographically distinct regions with such different quantities of riverine inputs were, following a simple water depth adjustment.

4.4.4 The core seafloor microbiome across the Gulf of Mexico

Shifts in community composition with changes in water depth and sediment depth were apparent at the class level. In the deep Gulf of Mexico (>1000 m), surficial sediments (0-1 cm) were dominated by *Gammaproteobacteria* (25.6% ± 4.0, n = 126) followed by Marine Group I *Thaumarchaeota* (21.0% ± 0.08), *Deltaproteobacteria* (13.1% ± 3.4), and *Alphaproteobacteria* (10.2% ± 3.1) (Figure 4.5). The second most abundant class we detected, the MG-I *Thaumarchaeota*, were missed in previous studies due to recent advances in sequencing technology and primer design (Zinger *et al.*, 2011; Bienhold *et al.*, 2016). Commonly detected, but at low relative abundances in surficial sediments, were the classes *Gemmatimonadetes* (2.6% ± 0.63), *Phycisphaerae* (2.6% ± 0.84), *Acidobacteria* (2.0% ± 3.9), and *Planctomycetacia* (2.1% ± 1.5). Microbial communities were strongly

stratified with sediment depth. Progressing downcore, class level shifts were apparent with decreasing *Gammaproteobacteria* (11.3% ± 5.3 at 8-10 cm), *Thaumarchaeota* (4.5% ± 3.7), and *Alphaproteobacteria* (6.6% ± 3.5) relative abundances and corresponding increases in *Deltaproteobacteria* (20.1% ± 5.5), *Planctomycetacia* (7.2% ± 3.7), and *Phycisphaerae* (10.1% ± 6.1) groups (Figure 4.5).

In general, the same progression in class level distributions occurred in each core profile. However, the inflection points in these class distributions shifted down the sediment column with increasing water depth (Figures 4.2, 4.5). This was most clearly observed by comparing the relative abundance of the aerobic Marine Group I (*Thaumarchaeota*) in sites DSH08 (1110 m), DSH10 (1500 m) and DSH09 (2293 m) (Figure 4.5). In addition, the transition between MG-I *Thaumarchaeota* and *Phycisphaerae* typically coincided with the oxygen gradient and the oxic-anoxic interface, which increased in sediment column with increasing water depth. This oxic-anoxic transition zone also coincided with highest relative abundances of *Planctomycetacia*.

In deep ocean oligotrophic sediment studies conducted across the globe, *Gammaproteobacteria* and *Deltaproteobacteria* also dominate surficial communities (Schauer *et al.*, 2010; Zinger *et al.*, 2011; Bienhold *et al.*, 2012, 2016; Learman *et al.*, 2016; Yang *et al.*, 2016). Following these two classes, *Alphaproteobacteria*, *Actinobacteria*, *Planctomycetacia*, and *Acidobacteria* are often dominant and well represented. Less abundant groups include *Flavobacteria*, *Betaproteobacteria*, *Gemmatimonadetes*, and *Chloroflexi*. The majority of studies have focused on bacterial groups, however, when universal primers are used, Marine Group I *Thaumarchaea* are shown to be very abundant

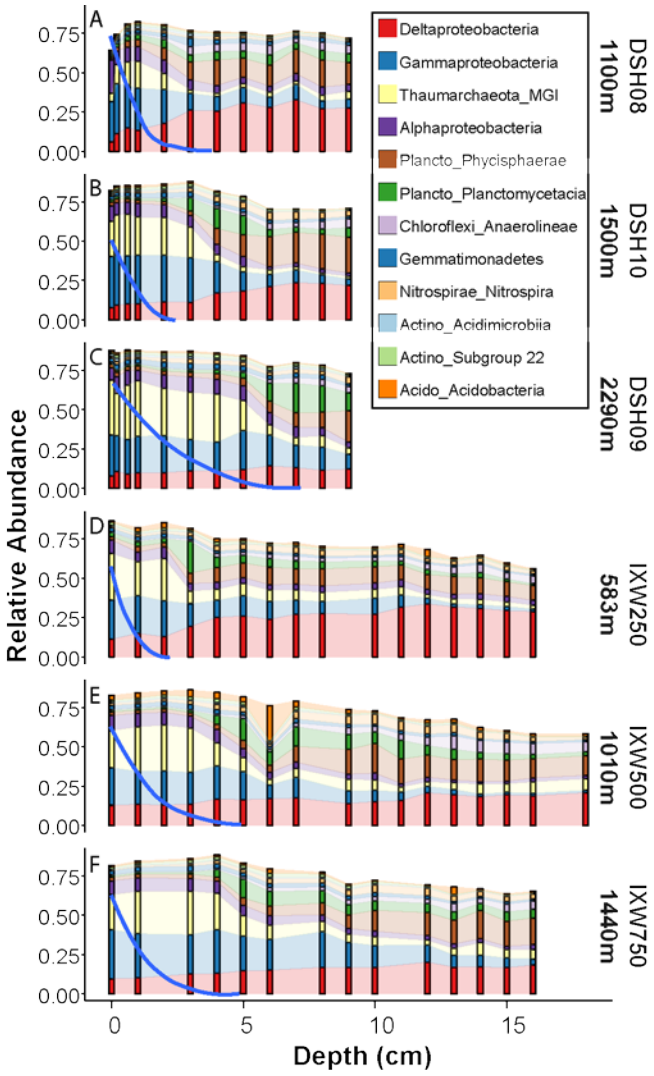

Figure 4.5 Core profiles from representative deep water sites. We show class level stacked-barplots of the 12 most abundant classes detected. (A-C) Representative profiles from the Northern Gulf of Mexico from the DSH core transect going offshore towards increasing water depth. (D-F) Representative profiles from the Southern Gulf of Mexico along a westward transect from the Ixtoc wellhead, also organized from shallowest to deepest site in the transect. In all plots, blue lines represent the percent oxygen concentration relative to the initial overlying water oxygen concentration.

(Learman *et al.*, 2016). Although previous work in the Gulf of Mexico did not incorporate Archaea, our results are corroborated by clone libraries of bacterial communities constructed from surficial sediments that were sampled prior to oil impacts which showed similar dominant classes (Yang *et al.*, 2016). We observed much lower relative abundances

of *Bacteriodetes* and *Betaproteobacteria* across all the surficial sediments, potentially due to the different primers used or related to the sampling size differences between these studies.

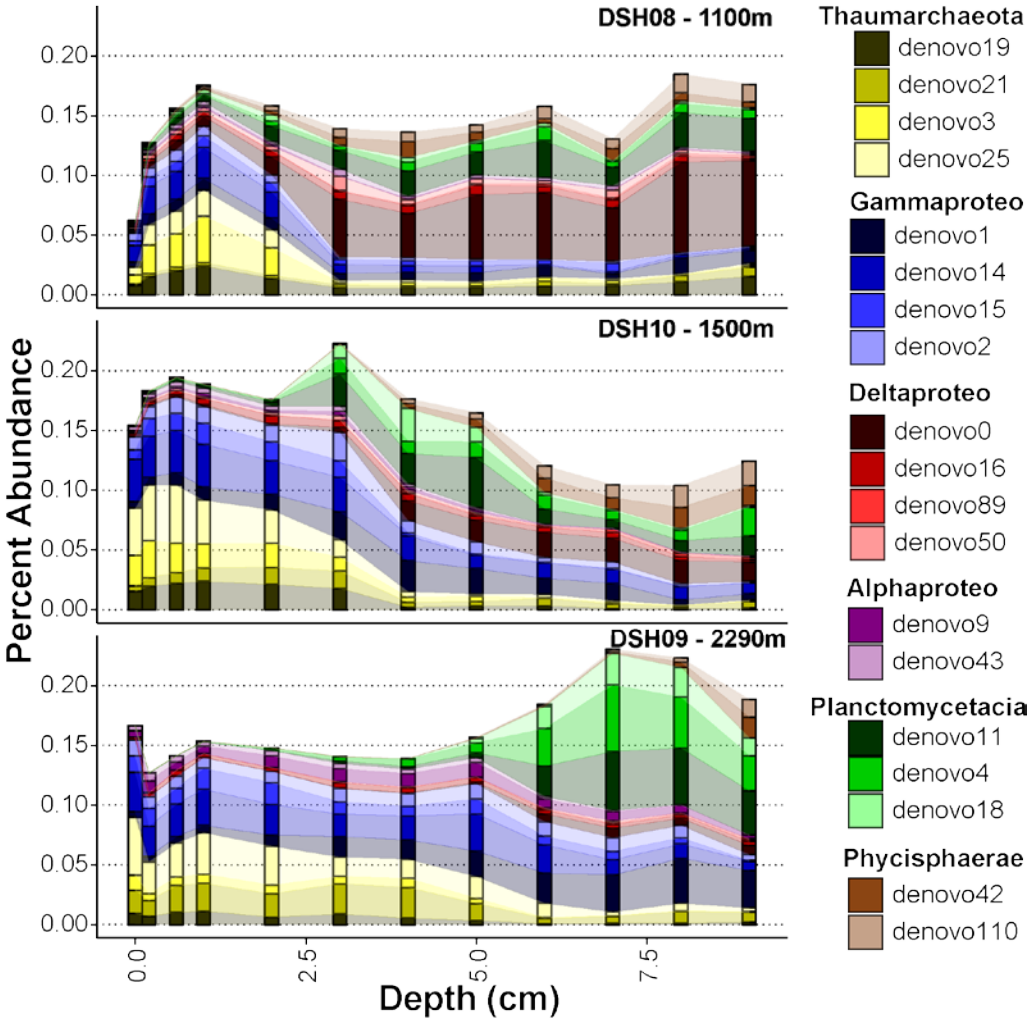

Figure 4.6 Core profiles representing deep water sites in the Northern Gulf of Mexico showing population (OTU) level distributions with increasing sediment and water depths. Core profiles are taken from the DSH transect and are arranged in order of increasing water depth. See Figure S3 for similar trends within the Southern Gulf of Mexico.

4.4.5 Microbial population specific distributions across the Gulf of Mexico

These biogeographic patterns were evident at higher taxonomic resolution, and the most abundant and representative OTU for 6 dominant classes were selected for further study (Figures 6, C.2, C.3, C.6-10). An overview for the distributions of dominant OTU across the Gulf of Mexico are presented here while the specifics are available in the Supplementary Information. The four most abundant Marine Group I OTU (Thaumarchaeota) were all phylogenetically related to *Nitrosopumilus maritimus* (3 OTU >97% sequence identity and 1 OTU at 93% identity). Specific OTU abundances were related to the overlying water depth, showing population level niche differences. Niche differences for these four abundant *Nitrosopumilus*-like populations were not driven by depth within the sediment column as was found by Durbin and Teske (2010).

Marine Group I *Thaumarchaeota* are well known members of oxic and suboxic sediments (Gillan and Danis, 2007; Durbin and Teske, 2010, 2011, 2012; Pester *et al.*, 2011; Danovaro *et al.*, 2016; Learman *et al.*, 2016). All characterized isolates similar to these 4 OTU are aerobic autotrophs capable of oxidizing ammonia at very low concentrations. Increases in their relative abundances have been shown to be concurrent with decreases in the quality and quantity of organic carbon within sediments (Learman *et al.*, 2016). It has also been shown that in deep, low energy pelagic environments a large portion of *Nitrosopumilus*-like populations were capable of using urea as a carbon and ammonia source to fuel autotrophic nitrification (Alonso-Saez *et al.*, 2012). Conversely, in a global survey of bacterial and archaeal abundances in surficial oxygenated deep sea sediments, MG-I *Thaumarchaeal* absolute abundances were primarily related to bottom water temperatures and not to quality and quantity of carbon sources (Danovaro *et al.*,

2016). In the Gulf of Mexico, however, there were high relative abundances of these groups at both shallow, warm water, sites as well as deep permanently cold sites and there was not clear evidence that this group as a whole was driven by water temperature instead of quality and quantity of carbon in the distribution of dominant OTUs.

Unlike the *Thaumarchaea*, the dominant *Gammaproteobacteria* detected in the deep GoM sediments were distinct from those in the shallower sediments. While there were still water depth and sediment depth dependent shifts in these top 4 *Gammaproteobacterial* OTU, there was a greater distinction between shallow and deep-water sites than was observed for the MG-I. Three of the dominant OTU belonged to the JTB255 marine benthic group, currently within the *Xanthomonadales*. The JTB225 marine benthic group was previously shown to be abundant and cosmopolitan at the seafloor, and was previously detected in abundance in Gulf of Mexico surficial sediments (Zinger *et al.*, 2011; Bienhold *et al.*, 2016; Yang *et al.*, 2016). A recent genomic study suggested this group is affiliated with the *Woeseiaceae* family and members within this group are metabolically diverse, capable of aerobic or anaerobic respiration as well as chemolithoautotrophy using reduced sulfur-compounds or hydrogen (Du *et al.*, 2016; Mußmann *et al.*, 2017). These three populations show clear niche partitioning likely related to electron acceptor differences (Figure 4.6, C.7).

Similar to the *Gammaproteobacteria*, little overlap was observed between *Deltaproteobacterial* OTU associated with the shallower sites and those in the deeper sites (Figure 4.6, C.8). In deep ocean sediments, most of the sequences affiliated with *Deltaproteobacteria*, belong to denovo0. This was the most abundant OTU detected in our dataset, and its relative abundance increased with increasing sediment depth. All dominant

Deltaproteobacteria OTU reach maximum abundances below the oxic-anoxic interface and are affiliated with poorly characterized groups.

All dominant OTU affiliated with the *Planctomycetacia* were closely related to *Candidatus Scalindua* spp (99-100%). These dominant OTU are likely anaerobic ammonium oxidizing bacteria (anammox), which are chemoautotrophic, ubiquitously found in anoxic systems, and couple the oxidation of ammonium with nitrite as the electron acceptor (Penton *et al.*, 2006; Oshiki *et al.*, 2016). Members from this genus tend to be psychrophilic, and are inhibited by low sulfide concentrations (4-100 μM), which potentially explains their depth limits in our study, although it may also be due to ammonium or nitrite availability (Oshiki *et al.*, 2016). The *Planctomycetes* were nearly absent in the shallowest sites, and absent in surficial sediments, in agreement with previous studies that indicate ca. *Scalindua* is more abundant in oligotrophic systems (Canion *et al.*, 2014; Learman *et al.*, 2016). All dominant *Planctomycetes* OTU tended to reach a maximal relative abundance at mid-sediment depths below the oxic-anoxic interface with an overlapping distribution to the *Nitrosopumulis*-like OTUs (Figures 4.6, C.3, C.9). Ammonium oxidizing archaea may provide a nitrite source *Scalindua*, and the mostly exclusive zonation patterns observed may limit direct competition for ammonium (Lipsewers *et al.*, 2014).

While speculative, there was evidence of inorganic nitrogen species being important electron acceptors and donors in deep Gulf of Mexico sediments, particularly for fueling autotrophic metabolisms. In addition to the putative *Nitrosopumilus-like* aerobic ammonium oxidizers and *Scalindua-like* anaerobic ammonium oxidizers, we observed putative bacterial ammonium oxidizers (*Nitrosococcus-like*, and an unclassified

Nitrosomonadaceae OTU) that were not present in shallow sediments and increase in relative abundance with increasing water depth (Figure C.11). While the uncharacterized *Nitrosomonadaceae* OTU (denovo23) co-occured with *Nitrosopumilus*-like OTU, the *Nitrosococcus*-like OTU populations increased in relative abundance below the *Nitrosopumilus-like* populations. Abundant putative nitrite oxidizers affiliated with *Nitrospira* and *Nitropina* groups were detected that were also only present in deep water sediments below the aerobic-anaerobic transition zone, similar to the *Scalindua*-like population distributions.

4.4.6 Construction of a predictive microbial community composition model throughout the Gulf of Mexico

After visualizing the consistent biogeographic patterns portrayed in Figure 4.2, it was recognized that a regression-based model may be able to estimate the relative abundances of microbial groups across these regions. We employed the machine learning method, random forest regression, that has previously been successful in population distribution models, although this method is not well utilized in marine microbiology scenarios (Cutler *et al.*, 2007; Oppel and Huettmann, 2010; Smith *et al.*, 2010; Wei *et al.*, 2010; Bradter *et al.*, 2013). As stated in the methods section, the model was constructed using the variables water depth, sediment depth, latitude, and longitude as proxies for carbon input, redox state, and geographic variations due to riverine inputs and differing geochronology across the Gulf of Mexico (Brooks *et al.*, 2015).

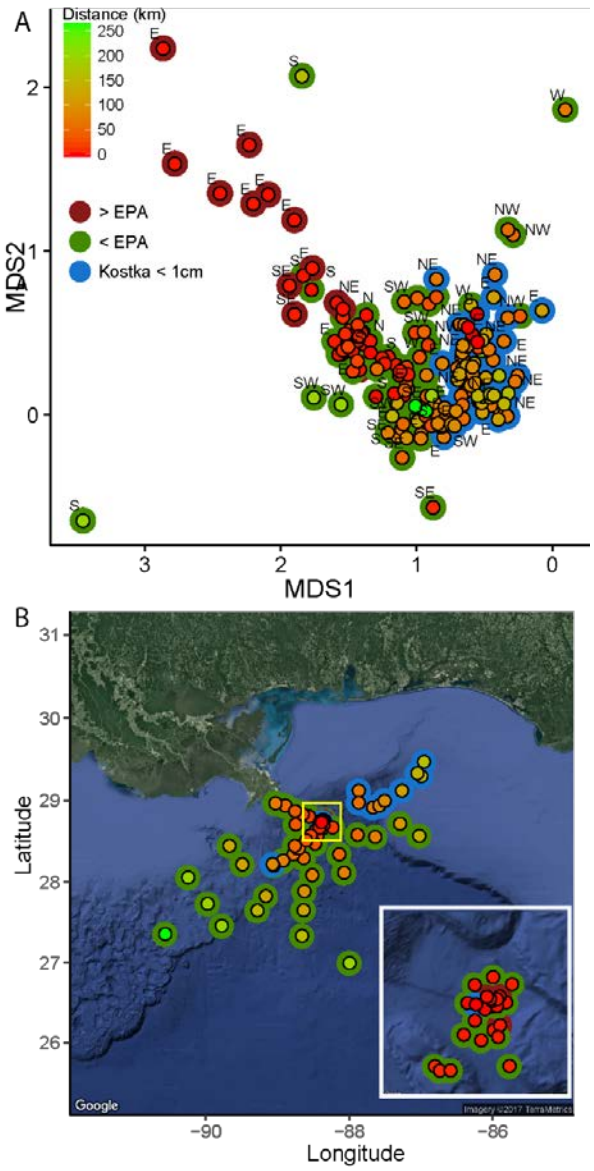

Figure 4.7 Meta-study revealing localized impact and subsequent recovery. Data generated by Mason et al., 2014 from surficial samples (red, green) was re-analyzed with surficial samples from this study (blue). (A) NMDS of Bray-Curtis dissimilarity values. Samples outlined in red from Mason et al., exceeded EPA benchmarks while samples outlined in green were below EPA benchmarks. The fill color for each point represents distance from well head, going from red to green with increasing distance. (B) Geographic map plotting each sampling location, same color scheme used as in (A). The inset is a magnification of the wellhead region, the blue samples were collected directly over the wellhead and represents cores collected in Aug 2012 and Aug 2013 at multiple depths < 1 cmbsf.

This analysis was run for every abundantly detected OTU (9588 OTU). All OTU with greater than 50% variance explained by the full model were retained (4129 OTU, 43% of the abundant OTU). Overall, and as expected, the models fit the observed data well (R^2 = 0.88). The residuals were weakly correlated with OTU abundance as the model tends to underestimate the very abundant OTU. The model was further tested by calculating the root mean squared error (RMSE) compared to 1000 bootstrapped randomly permuted RMSE and was found to be highly significant ($p < 2e^{-16}$, Z-test).

To verify the utility of the model, model predictions were compared with observed counts for the dominant OTU (Figure C.4, C.5-S9). However, it is anticipated that the model can be used as a tool to assess future impacted sediments that may be poorly characterized. In order to test this, we hindcasted the microbial community composition at previously impacted sediments by determining how far the observed microbial community deviated from the model's prediction. This was accomplished by calculating the total root mean squared error (RMSE) for each sample, including the Mason et al. (2014) surficial sample set (Figure 4.7). The most impacted sites had higher RMSE values than the below EPA limits sites, although both were skewed to the right of the model predictions for our data (Figure C.10). One possible explanation for the higher RMSE values from control sites may be due to different DNA extraction techniques which are known to produce different microbial community profiles (Carrigg *et al.*, 2007). Therefore, while controlling for experimental based variation, this model can still be effective at determining impacts.

4.4.7 Impacts of the DWH and internal testing of the predictive model

The earliest samples included in this study were collected in August 2012, over two years after the Deepwater Horizon well blowout. No evidence of a large oil spill signature was detected in sediments sampled from areas known to be impacted by sedimentary oil deposition related to the DWH blowout (Chanton *et al.*, 2012; Valentine *et al.*, 2014; Romero *et al.*, 2015, 2017). At the broad biogeographic scale visualized in Figure 4.2, the lack of an "oil-impacted cluster" indicated that any potential impact on community composition was small relative to the strong environmental gradients influenced primarily by water depth and sediment depth. To compare our data explicitly with sediments that were shown to be strongly impacted by oil, a meta-analysis based approach was employed. We observe that all surficial sediment samples from this study, including those collected close to the DWH wellhead, clustered adjacent to samples classified as below EPA limits and were distinct from those classified as most impacted by oiling (Mason *et al.*, 2014) (Figure 4.7). Furthermore, the similarities between the below EPA limit samples and our dataset indicated a temporally stable and Gulf-wide conserved microbial community relative to a strong pulse disturbance. Finally, previously impacted sediments that were collected and analyzed during this study did not deviate from model predictions, unlike those collected in 2010 (Figure C.10).

These results are corroborated by a previous study that detailed a microbial community succession event in oil impacted surficial sediments immediately following the oiled marine snow sedimentation event, through the generation of full length SSU rRNA gene clone libraries (Yang *et al.*, 2016). The authors suggested that by November 2010 the microbial community composition once again resembled pre-impacted surficial microbial communities (Yang *et al.*, 2016). Our first samples were collected in August

2012 and much of our dataset comes from 2013 and 2014 for the NGoM, years following a potential return to baseline condition. We also do not observe a disturbance signature in cores collected at the Ixtoc-I wellhead or within the PEMEX (Mexican state-owned petroleum company) restricted area that has extensive oil extraction pressures. The lack of an Ixtoc-I signature in the microbial community is expected concerning the resilience observed in the sedimentary communities in the northern Gulf of Mexico, and the lack of a PEMEX oil signature indicates we did not sample sediments that were recently exposed to oil.

4.5 Conclusions

The primary objectives of this study were to define the core microbiome across the Gulf of Mexico seafloor, characterize biogeographic patterns in microbial populations in Gulf sediments, and use these results to constrain the impacts of petroleum hydrocarbons from the Deepwater Horizon oil spill to sedimentary microbial communities. Using the largest marine sediment microbial community composition dataset generated to date, we show that the distribution of microbial communities is broadly consistent across the entire region in terms of the populations (OTU) detected and their relative abundances. We further demonstrate that the distribution of seafloor microbial communities is well approximated by the overlying water depth and depth within the sediment column, which together explain 38% of our observed variation, regardless of geographic sampling region. The small differences between the regions are potentially related to the amount of organic carbon reaching the seafloor, with the southern Gulf showing greater depths of oxygen penetration as well as microbial communities that had greater similarity to deeper counterparts in the northern Gulf. Microbial community composition across the Gulf

revealed similar taxonomic groups as observed in other marine sediment biogeography studies across the globe and is dominated primarily by groups that are poorly characterized with unknown ecological functions within the sediment.

The lack of a strongly perturbed community in our dataset, along with the incorporation of previous studies demonstrating an oil related perturbation signal, suggests that impacted sediment communities had returned or are returning to baseline conditions. Finally, the biogeographical distributions of seafloor microbial populations were used to generate a predictive model for over 4000 dominant populations that relies on easy-to-obtain geospatial variables. With this model, it is possible to predict community compositions across the Gulf of Mexico, and use deviations from such a prediction as a tool to assess future impacted sediments that may be poorly characterized along with natural ecosystems that are conspicuously different from oligotrophic ecosystems such as cold seeps.

4.6 Acknowledgements

This work was made possible in part by a grant from The Gulf of Mexico Research Initiative to the C-IMAGE II consortium and in part by a National Science Foundation Graduate Research Fellowship (WAO) under grant no. 2013172310. The authors would like to thank the ship crews on the R/V Weatherbird III and the R/V Justo Sierra that made the sample collection possible. Data are publicly available through the Gulf of Mexico Research Initiative Information and Data Cooperative (GRIIDC) at https://data.gulfresearchinitiative.org (doi: 10.7266/N70G3HN3). Any opinions, findings,

and conclusions or recommendations expressed in this material are those of the authors and do not necessarily reflect the views of the National Science Foundation.

CHAPTER 5. WEATHERED CRUDE OIL ALTERS BIOGEOCHEMICAL CYCLES AND MICROBIAL POPULATIONS IN PERMEABLE SUBTIDAL SEDIMENTS

5.1 Abstract

An estimated 22,000 tons of weathered crude oil from the Deepwater Horizon blowout contaminated Gulf coast beaches in 2010 and deposited an unknown amount into nearshore environments, which so far have received little attention. In this study, we employed advective-flow chambers that simulate *in-situ* pressure gradients found in saturated subtidal coastal sediments to test the underlying ecological principles governing the microbial response to an oil disturbance. Specific objectives were to (1) determine oil-induced disruptions to carbon and nitrogen biogeochemical cycling processes, (2) quantify potential rates of oil degradation and transformation attributable to microbial biodegradation independent of transport, (3) determine acute impacts of weathered crude oil to sensitive microbial populations, and (4) examine the controls on biodegradation activity. Incubations were conducted over a 3.5-month period and oxygen consumption rates as well as nutrient concentrations were monitored. At regular intervals, oil chemistry, viable cell counts, microbial metabolisms, and specific metabolic rates were determined. Results indicate sustained and increasing rates of respiration in oiled chambers two times higher than observed in controls. Ammonium, nitrite, and nitrate concentrations remained depleted in oiled chambers, while in the controls, ammonium was rapidly released into the overlying water, followed by a transient increase in nitrite, and finally a large increase of nitrate. The dynamics of dissolved nitrogen species were corroborated by a high potential

for nitrification observed in the control chambers and not in the oiled chambers. In contrast, nitrogen fixation and denitrification potentials were enhanced in oiled treatments in comparison to the controls. Furthermore, a similar succession in microbial populations as observed in the field was recapitulated in the mesocosms. Overall, the results will contribute to a comprehensive prediction on the fate, impacts, and microbial community response to buried oil in sandy subtidal coastal sediments under a "no hydrocarbon transport" regime.

5.2 Introduction

An estimated 26 % of the 4.9 million barrels of crude oil released from the Deepwater Horizon oil spill was transported to the shoreline or deposited in offshore sediments (Lubchenco *et al.*, 2010). The suspended oil that reached the sea surface was depleted of gaseous n-alkanes (C1-C5) and monoaromatic hydrocarbons (BTEX) primarily due to aquatic dissolution (Reddy *et al.*, 2012). Once at the sea surface, this oil was further weathered by photooxidiation, evaporation, and dissolution leading to a large reduction in C9-C16 alkanes and 2-ring aromatics (naphthalene, acenaphthene, fluorene) (Liu *et al.*, 2012). Model estimates indicate that 11 % of the oil that reached the surface was transported to and contaminated 2113 km of Gulf of Mexico shorelines with roughly 22,000 tons of oil (Michel *et al.*, 2013; Nixon *et al.*, 2016). All told, 965 km of sandy beaches were exposed to lightly weathered crude oil, where it mixed with particles in the surf zone and was either deposited onshore, above the tide mark, or was transported and buried in subtidal zones (Warnock *et al.*, 2015; Nixon *et al.*, 2016).

A growing body of knowledge surrounds the fate of oil that was deposited in the supratidal zone and impacts of this oil on beach ecosystems. The rate of biodegradation for

total petroleum hydrocarbons as well as for specific compounds was unexpectedly high in Gulf Coast sands, with half-lives of aliphatic compounds ranging from 25-69 days and from 22-87 days for aromatic compounds (Elango *et al.*, 2014; Snyder *et al.*, 2014; Huettel *et al.*, 2018). These high rates are in part attributed to tidal pumping maintaining fully aerobic conditions throughout the contaminated beach layers stimulating microbial biodegradation (Huettel *et al.*, 2018). Microbial activity is thought to mediate an increase in oxyhydrocarbon concentrations with time (Aeppli *et al.*, 2012; Ruddy *et al.*, 2014) and explain the chemical changes in PAH profiles observed with time (Liu *et al.*, 2012; Elango *et al.*, 2014; Huettel *et al.*, 2018). In further support of biodegradation, there is a well-documented increase in the absolute and relative abundance of oil-degrading microbial populations, metabolic functions associated with oil degradation pathways, and their expression levels in these impacted beaches (Newton *et al.*, 2013; Kappell *et al.*, 2014; Lamendella *et al.*, 2014; Rodriguez-R *et al.*, 2015). The responding oil-degrading populations were potentially limited by nutrient availability, moisture content, or elevated salinity levels (Elango *et al.*, 2014; Rodriguez-R *et al.*, 2015; Huettel *et al.*, 2018).

In addition to oil deposited above the intertidal zone, a substantial and mostly unconstrained portion was transported back to the intertidal or subtidal zone. The most recognizable and concentrated deposits formed large submerged oil mats (SOMs) or smaller surface residual balls (SRBs) (Operational Science Advisory Team, 2013; Warnock *et al.*, 2015). After 2 years of intense clean-up efforts, over 20 % of coastline segments remained contaminated due to re-oiling events from these submerged oil sources, reflecting both the large amount of buried offshore oil and the high level of mobility and fragility of these deposits (Operational Science Advisory Team, 2013; Hayworth *et al.*,

2015; Warnock *et al.*, 2015). Compared to these concentrated oil-deposits, less heavily contaminated sediments are more mobile, harder to detect, and likely impact a larger area surrounding SOMs. The potential consequences of such subtidal and intertidal oil deposits to ecosystem function are largely unknown and have far reaching implications (Huettel *et al.*, 2014; Warnock *et al.*, 2015).

Due to challenges in studying diffuse oil contamination in permeable sediments of subtidal zones, almost no research has been conducted on its fate, or implications for ecosystem function. Here we present a mescosm-based study that focuses on shallow subtidal sandy sediments contaminated with weathered crude oil. Objectives of the study were to (1) determine oil-induced disruptions to carbon and nitrogen biogeochemical cycling processes, (2) quantify potential rates of oil degradation and transformation attributable to microbial biodegradation independent of transport, (3) determine acute impacts of weathered crude oil to sensitive microbial populations, and (4) examine the controls on biodegradation activity.

5.3 Material and Methods

5.3.1 Sample collection, mesocosm preparation, and mesocosm Operation

All sand used for this experiment was collected from Pensacola Municipal Beach, Pensacola, Florida (30°19’32.08 N, 87°10’30.55 W) on March 20th, 2016. The sand was collected approximately 200 m offshore in 2 m water depth and transported back to the laboratory on the same day. All sand was pre-incubated under fully saturated conditions in a sterilized cooler for three weeks to reduce replicate variation due to labile carbon concentrations. The sand was mixed daily to prevent anoxia.

The experiment was carried out in 6 identical flow advection chambers as previously described (Huettel and Gust, 1992; Khalili *et al.*, 1997; Cook *et al.*, 2007; Evrard *et al.*, 2012). Each chamber has an internal height of 30 cm with a 19 cm inner diameter, and sand was added to a total height of 5 cm. Each chamber was stirred with a 15 cm diameter disk at 40 rpm set 10 cm above the sand surface, generating a pressure gradient of 2.5 Pa between the circumference of the chamber and the center, or approximately 0.26 Pa cm^{-1}, which is similar to what has been observed for calm days at the sampled water depth at the site (Gihring *et al.*, 2010). The chambers were connected serially and all controlled by the same stirrer motor and control unit, ensuring similar pressure gradients occurred in each.

Three of the chambers were amended with 5 g of weathered crude oil collected during the Deepwater Horizon response efforts (OFS-2010719-Juniper-001, WF), consistent with the observed concentration of oil at Pensacola Beach (Kostka *et al.*, 2011). The total oil mass was mixed with 500 g of clean sand, added to the chamber, and capped with 500 g of clean sand to bind the crude oil to the sand matrix, creating tar layers similar to what was observed at the study site. The remaining three chambers were used as un-amended controls. The total mass of sand added to the oil treatment was 2458 ± 168 g, and to the controls 2434 ± 294 g of sand was added. Instant ocean sea salt (Spectrum Brands, Blacksburg, Virginia, USA) was mixed with DI water to 36 ppt, identical to the measured salinity when the sand was collected, and added to each chamber with care to prevent bubble formation. The chambers were sealed with gas tight lids to prevent atmospheric gas exchange. All six chambers were incubated in a 250 L water bath and the temperature of each chamber varied from 18 – 21.6 °C (mean = 19.8, standard deviation = 0.8). The

experiment began on April 12th, 2016 and ran for 112 days (3 months, 13 days) until August 2nd, 2016. This timeframe corresponds to twice the total petroleum hydrocarbon (TPH) half-life calculated at this site (Huettel *et al.*, 2018).

Oxygen concentrations were monitored through ports in the lid of each chamber using a Presens Microx4 needle-microoptode (Presens, Regensburg, Germany). The needle optode was calibrated following the manufacturer's protocol using sodium sulfite for the 0 % saturation and bubbling with air for the 100 % saturation, and the calibration was checked weekly using fresh solutions. When one of the chambers reached approximately 50 % oxygen saturation, all the chambers were re-oxygenated using airstones through ports in the lids to prevent anoxia in the overlying water. Initially, 5 ml of water was collected daily from each chamber for inorganic nutrient profiling that became weekly as the experiment progressed. The sample was filtered with a 0.2 µm syringe filter and stored frozen. The water was replaced with oxygenated artificial seawater at 36 ppt following each sampling to prevent any headspace from forming.

Sediments from the chambers were extracted five times throughout the course of the experiment to monitor changes to the microbial community and the oil chemistry. To measure the immediate impacts of oil to the microbial community, sediment was collected after one hour, one day, and one week of operation. To better elucidate long-term impacts as well as community adaptation to the oil treatment, one-month and 3.5-month timepoints were collected. In order to collect the sediment, the stirring unit was disconnected, the chamber lids and the stirring disks were removed. Triplicate sub-cores were collected randomly throughout the sediment column (representing ~35 cm^3 of sand), homogenized, and flash frozen in liquid nitrogen followed by storage at -80 °C for DNA-based analyses.

Triplicate sub-cores were also collected separately for hydrocarbon analysis in certified pre-baked glass jars from VWR (Part No: 89093-980, Protocol A, level PC) and stored frozen. An additional 5 cm^3 was collected for cultivation-dependent enumeration that was conducted immediately following sample collection.

5.3.2 Oxygen Consumption Rates

Oxygen concentrations were measured every 4-6 hours for the first week followed by daily measurements for the remainder of the experiment. Oxygen consumption rates were calculated for each period between re-oxygenating the overlying water using linear regression in R (R Core Team, 2014). The oxygen concentration profiles for the full experiment are shown in Figure D.1. Oxygen saturation was estimated using previously established functions and constants (Lysiak-Pastuszak and Krysell, 2004).

5.3.3 Inorganic Nutrient Analyses

Nitrite and nitrate concentrations from the overlying water were determined using the method outlined by (Garcia-Robledo *et al.*, 2014). Ammonium concentrations were quantified using the indophenol blue method outlined by (Strickland and Parsons, 1972), and soluble reactive phosphate concentrations were determined using the method outlined by (Murphy and Riley, 1962). Spectrophotometry was conducted on a SpectraMax M2 microplate reader (Molecular Devices Corporation, Sunnyvale, California, USA). For each nutrient measurement, samples were run in triplicate (9 samples per chamber per timepoint), and duplicate standard curves were generated for each set of analyses.

5.3.4 Enumeration of Cultivatable Heterotrophic Microorganisms

Cultivatable microbial populations were enumerated by counting colony-forming-units (CFU) on petri plates. Triplicate 10-fold serial dilutions were performed for each chamber using approximately 0.5 g of sand into 4.5 ml of Zobell Marine Broth 2216 (HiMedia, Kelton, Pennsylvania, USA). Each dilution was spread onto triplicate Zobell agar plates (9 plates per chamber per dilution) and CFUs were counted after two weeks of growth at room temperature.

5.3.5 Nitrogen Transformation Rate Potential Measurements

Following the completion of the 3.5-month experiment, sand from each chamber was collected to determine rate potentials for nitrogen-transforming metabolic processes. Nitrification rate potentials were estimated using the allylthiourea inhibition assay (Hall, 1984). Triplicate assays were performed for each chamber with and without the inhibitor. Each replicate assay was performed in a 125 ml Erlenmeyer flask with 50 ml of artificial seawater amended with 10 mM sodium chlorate, 500 µM ammonium sulfate, and control flasks were amended with 20 mg L^{-1} of allylthiourea. Approximately 5 g of wet sand was added to each flask. All samples were shaken at 140 rpm and 25 °C, and samples were collected, filter sterilized, and frozen every 4 hours for 24 hours. At the end of the assay, all samples were analyzed for nitrite concentrations using the method described above. Nitrification potential was determined by comparing the nitrite produced relative to the allylthiourea controls.

Nitrogen-fixation rate potentials were determined using the acetylene reduction assay (Capone, 1993). For each chamber, 5 g of sediment was added to a 12 ml serum vial with 5 ml of filter sterilized, artificial seawater at 36 ppt. Serum vials were sealed with blue bromobutyl stoppers with a 1% acetylene headspace under oxic (atmospheric) conditions.

In parallel, controls included samples without acetylene as well as autoclaved-killed samples. Samples were incubated for 3 weeks in the dark at room temperature. A GC-FID (Greenhouse Gas Monitoring GC, SRI Instruments, Torrance, California, USA) equipped with dual 2 m HayeSep-D columns was used to quantify ethylene production. Samples were measured for ethylene production daily until production was linear. Controls not amended with acetylene did not produce ethylene, as well as the killed controls.

Denitrification rate potentials were determined using the acetylene inhibition assay conducted in sealed 60 ml serum vials consisting of 5 g of sand, 20 ml of sterilize artificial seawater, 20 mM potassium nitrate, and 3 ml of acetylene (Sørensen, 1978). In parallel, controls consisted of autoclaved killed and no-acetylene added treatments. Prior to the addition of acetylene, the headspace was flushed with 100 % N_2 gas. Headspace was sampled over the course of 6 hours and analyzed on the same GC as described above except using the ECD detector to quantify N_2O production.

5.3.6 Nucleic Acid Extraction and Library Preparations

Total genomic DNA was extracted from 0.25 g of sand in triplicate from each chamber at each major sediment sampling point with a MoBIO PowerSoil DNA Extraction kit following the manufacturers protocol (Table D.1). For the 16S SSU rRNA gene amplicon libraries, the triplicate extracts were amplified using the Earth Microbiome Project primers (515F / 806R) with a Fluidigm Access Array kit common sequence to allow secondary indexing, as has previously been described (Caporaso et al., 2012; Overholt et al., 2018). The triplicate PCR products for each sample were pooled in equimolar amounts, and the resultant mix was indexed. Multiplexed samples were pooled at equimolar ratios and paired-end sequenced (2x250 bp) on an Illumina MiSeq (Green *et al.*, 2015).

5.3.7 SSU rRNA Gene Amplicon Analyses

The SSU rRNA amplicon data was analyzed as previously described (Overholt et al., 2018). In brief, paired-end reads were merged using PEAR v0.9.6 (Zhang *et al.*, 2013) and assembled reads were quality filtered in QIIME using a minimum phred score of 30 (J. Caporaso *et al.*, 2010). Sequences screened to include only those with 250-255 bp with Mothur (Schloss *et al.*, 2009). D*e novo* based chimera detection followed by reference based chimera detection against the SILVA gold database was performed with vsearch v1.9.6 (Rognes *et al.*, 2016). The remaining high-quality sequences were dereplicated using vsearch v1.9.6 and operational taxonomic units (OTUs) were picked using Swarm v2.1.8 with default parameters (Mahé *et al.*, 2014; Rognes *et al.*, 2016). Singletons and OTUs present in less than 2 samples were removed. Samples with less than 5000 sequence counts were removed from further analysis. Taxonomic affiliations for each OTU were determined using the SILVA v123 database formatted for use with QIIME (J. G. Caporaso, Kuczynski, *et al.*, 2010; Quast *et al.*, 2012).

5.3.8 Hydrocarbon Analyses

Extraction and analysis of hydrocarbon compounds was performed according to a modified version of EPA method 3510C with accompanying QA/QC protocols. Oil and control treatments were extracted for quantification of total petroleum hydrocarbons (TPHs) as well as the specific hydrocarbon compound classes, aliphatics (*n*-alkanes C_{12}-C_{40}, and isoprenoids pristine and phytane) and polycyclic aromatic hydrocarbons (PAHs). Extracts were concentrated under a gentle stream of nitrogen using a TurboVap and reconstituted in hexane (100%) for chromatographic analysis. TPHs in the samples was

quantified using GC-FID. A one mL of EPH Surrogate Spiking Solution (ISM-581X, Lot CL-1009, Ultra, Kingstown, RI, USA) containing *o*-terphenyl and 1-chlorooctadecane was added directly to the separatory funnel before extraction. TPH concentrations were corrected for extraction efficiency based on recovery of the EPH spiking solution and mass of oil added.

Samples (25 ml) were transferred to 250 ml separatory funnels, and 15 ml of dichloromethane was added. Sample glassware containers were rinsed with an additional 15 mL of dichloromethane to collect all residual oil. Separatory funnels were shaken for 2 minutes, and the organic layer was collected in a 60-ml vial. The extraction step was repeated 3x, and 2-4 g of anhydrous sodium sulfate was added to the resulting organic extracts. All solvents used were at the highest purity available and without further purification. All glassware used was previously combusted at 450°C for 4 hours, and rinsed with dichloromethane prior to extraction. An extraction blank was included with each set of samples (10-12 samples) to ensure no contamination from chemicals, glassware and/or laboratory equipment.

Aliphatics and aromatics were quantified in a gas chromatograph/mass spectrometric detector (GC/MS) in full scan mode (*m/z* 50-550). Splitless injections of 1μL of the sample were conducted, and a RXi®5sil column (30 m x 0.25 mm x 0.25 μm) was used. Quantitative analysis of aliphatics and PAHs were conducted using the IS method. Samples were spiked before extraction with perdeuterated *n*-alkane (d_{50}-Tetracosane, Ultra Scientific) and PAHs (Deuterated PAH Mixture: d_{10}-acenaphthene, d_{10}-phenanthrene, d_{10}-fluoranthene, d_{12}-benz(a)anthracene, d_{12}-benzo(a)pyrene, d_{14}-dibenz(ah)anthracene, d_{14}-benzo(ai)perylene; Ultra Scientific). For *n*-alkanes analysis, GC oven temperature was

programmed as 80°C held for 0.5 min, then increased to 320°C at a rate of 10°C min^{-1} and held for 5.5 min. Injector temperature was set to 280°C. Identification and quantification of *n*-alkanes (nC_{12}-nC_{40}) and isoprenoids pristine (Pr) and phytane (Phy) were conducted by comparing with a reference standard (Fuel Oil Degradation mixture, Ultra Scientific; C8-C40 Alkane Certification Standard; Supelco) and the spike standard (d_{50}-Tetracosane). For PAHs, a GC oven temperature was programmed as 60°C held for 8 min, then increased to 290°C at a rate of 6°C/min and held for 4 min, then increased to 340°C at a rate of 14°C/min, and held at the upper temperature for 5 min. The temperature of the MS detector was 250°C. Concentrations of PAHs were calculated using response factors by comparison with a known standard mixture (16-unsubstituited EPA Priority Pollutants and selected congeners: Ultrascientific US-106N PAH mix, NIST 1491a) and the spike standard. When no commercial reference standard was available, compounds were quantitated using the response factor for an isomer. Therefore, the concentrations determined for many of the alkylated PAHs were semiquantitative. Recoveries were generally within QA/QC criteria of 70-120%.

5.4 RESULTS

5.4.1 Oxygen consumption throughout the experimental time course

Following a three-week pre-incubation, three chambers were amended with oil and the remaining three were left as controls. The chambers ran continuously for 3.5 months and were re-oxygenated every 3 days on average. The oiled chambers always showed higher rates of oxygen consumption than was observed in the control chambers, although initially the rates were similar (Figure 5.1). In the oiled chambers, the rate of oxygen consumption

linearly increased for 55 days before leveling off at 1.9 ± 0.22 µmol L^{-1} hr^{-1}, equivalent to a benthic flux of 11.26 ± 1.30 mmol m^{-2} d^{-1} (mean ± standard deviation). The average benthic flux of oxygen for the oiled chambers across the full-time course was 10.67 ± 1.30 mmol m^{-2} d^{-1} (1.8 ± 0.22 µmol L^{-1} hr^{-1}). The control chambers also exhibited continuous oxygen consumption rates approximately half of that observed in the oiled chambers, at 1.0 ± 0.15 µmol L^{-1} hr^{-1}, or a flux of 5.93 ± 0.89 mmol m^{-2} d^{-1} (Table 5.1). In contrast to observations in the oiled chambers, the oxygen consumption rates significantly decreased in the controls (linear regression, $R^2 = 0.17$, $p < 0.01$), however, the change in rate of -2.4×10^{-8} is unlikely to be biologically relevant over the course of the experiment.

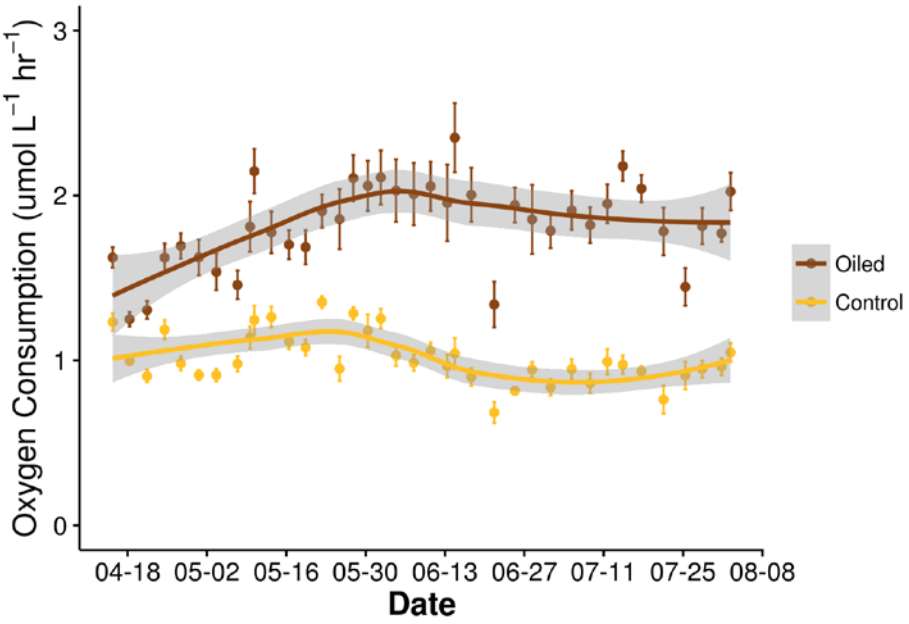

Figure 5.1 Oxygen consumption rates in mesocosm treatments over the 3.5-month time course. Rates are derived from linear regressions of changes in oxygen concentration with time between aeration events. Error bars indicate standard error of the mean.

5.4.2 Impacts to inorganic nutrient fluxes attributed to weathered oil

In the oiled chambers, soluble reactive phosphate concentrations were below our detection limit (0.5 µM) for most of the incubation period, with the exception of samples

collected after 6, 78, and 106 days that respectively reached 0.58 ± 0.09, 0.53 ± 0.04, and 0.56 ± 0.11 µM (Figure 5.2 A). The control chambers exhibited two spikes in phosphate levels within the first month that exceeded the detection limit, after 9 days (0.57 ± 0.28 µM) and again after 26 days (1.04 ± 0.37 µM), followed by a continuous and linear increase in phosphate concentrations beginning on day 44 until reaching a maximum of 8.6 ± 0.16 µM on day 106 (Table 5.1).

Table 5.1 The dynamics of inorganic nutrients in the overlying water of mesocosms as determined by production rates and areal fluxes. The top section presents rates calculated from linear changes in measured water column concentrations. The bottom section presents related process rate potentials determined at the end of the experiment.

Solute Rates	Treatment	Rate (umol L^{-1} d^{-1})	Chamber Rate (umol d^{-1})	Benthic Flux (mmol m^{-2} d^{-1})
oxygen	Oil	43.2 ± 5.28	302.4 ± 37.0	10.67 ± 1.30
	Control	24.0 ± 3.6	168 ± 25.2	5.93 ± 0.89
Ammonium	Oil	-	-	-
	Control	0.92 ± 0.10	6.44 ± 0.70	0.228 ± 0.0247
Nitrite	Oil	-	-	-
	Control	0.23 ± 0.05	1.61 ± 0.35	0.0568 ± 0.0124
Nitrate	Oil	-	-	-
	Control	1.27 ± 0.04	8.89 ± 0.28	0.314 ± 0.00988
Phosphate	Oil	-	-	-
	Control	0.10 ± 0.02	0.70 ± 0.14	0.0247 ± 0.00494
Process Rates	**Treatment**	**(nmol g^{-1} d^{-1})**	**(umol d^{-1})**	**(mmol m^{-2} d^{-1})**
Nitrification	Oil	-	-	-
	Control	59.48 ± 2.285	144.77 ± 18.4	5.11 ± 0.65
Denitrification	Oil	6.64 ± 1.40	16.32 ± 3.62	0.576 ± 0.128
	Control	0.709 ± 0.237	1.726 ± 0.613	0.0609 ± 0.0216
Nitrogen Fixation	Oil aerobic	0.0230 ± 0.0116	0.0564 ± 0.0287	0.00199 ± 0.00101
	Oil anaerobic	0.100 ± 0.0129	0.246 ± 0.0356	0.00867 ± 0.00126
	Control	-	-	-

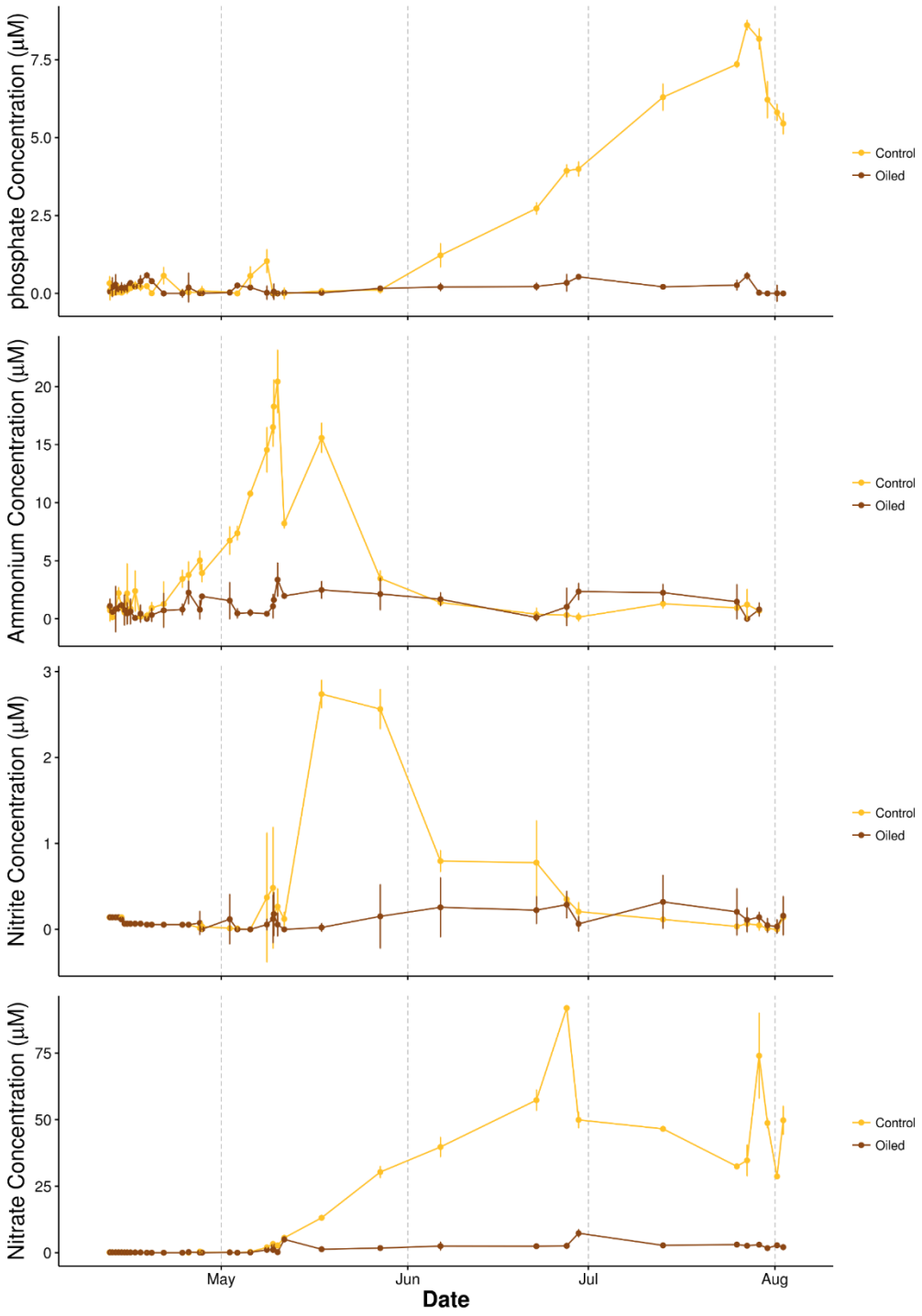

Figure 5.2 Major inorganic nutrient concentrations determined with incubation time in the overlying water column of mesocosms.

This was followed by a decrease in phosphate to 5.4 ± 0.34 µM on the final sampling day. From day 44 to day 106, the phosphate flux into the water column was 0.10 ± 0.02 umol L^{-1} d^{-1} (linear regression, $R^2 = 0.81$, $p < 0.0001$).

Ammonium concentrations in the oiled chambers remained at detectable, but low concentrations throughout the experiment (Figure 5.2 B). Concentrations averaged 1.12 ± 0.82 µM, and measurements were consistently above our detection limit of 1 µM after the second week (1.41 ± 0.88 µM). The concentrations did not linearly change with time ($R^2 = 0.008$, $p > 0.25$). In the control chambers, ammonium concentrations remained low (below 1 µM) for 8 days followed by a rapid increase in fluxes to the overlying water at a average rate of 0.92 ± 0.10 umol L^{-1} d^{-1} for 20 days ($R^2 = 0.89$, $p < 0.00001$) until a maximum of 20.43 ± 2.7 µM was reached (Table 5.1). Ammonium was then rapidly consumed or removed from the water column to below detection levels by day 71 at an exponential rate (decay constant = 0.087 d^{-1} ± 0.01, $R^2 = 0.92$, $p < 0.002$; the linear regression had an $R^2 = 0.56$, $p > 0.05$), where it remained below detection for the remainder of the experiment and below the concentrations observed in the oiled treatments.

Nitrite concentrations remained below 0.31 µM in the oiled chambers for the duration of the experiment (Figure 5.2 C). Average concentrations remained below detection in the oiled chambers for 44 days, then slightly increased and remained at an average of 0.17 ± 0.09 µM (linear regression, $p > 0.05$). In the control chambers, nitrite remained below detection for 26 days, before rapidly increasing to 2.7 ± 0.16 µM on the 35^{th} day at a rate of 0.23 ± 0.05 µM per day ($R^2 = 0.75$, $p < 0.01$). Nitrite then decreased back to below detection levels by day 92 at an exponential rate (decay constant = 0.057, $R^2 = 0.90$, $p < 0.00001$).

Nitrate levels in the oiled chambers were below detection for the first 26 days of incubation (< 0.2 µM) then rose to an average of 2.53 ± 1.57 µM for the remainder of the experiment (Figure 5.2 D; linear regression, $R^2 = 0.006$, $p > 0.3$). There were two sampling timepoints that showed > 5 µM nitrate, day 29 and day 78, with the maximum observed on day 78 of 7.32 ± 1.41 µM. Similar to observations in the oil treatment, nitrate concentrations in the control chambers remained below detection until day 23, before rapidly and linearly increasing at 1.27 ± 0.04 µM d^{-1} ($R^2 = 0.99$, $p < 0.000001$) until 57.3 ± 3.96 µM on day 71. Two sharp outliers were detected in which nitrate concentrations exceeded 75 µM, but excluding those, nitrate remained relatively constant at 43.52 ± 10.19 µM ($R^2 = 0.29$, $p > 0.1$).

5.4.3 Impacts of weathered oil to biogeochemical rate measurements

At the end of the experiment, potential rates of nitrogen transforming processes were determined to support the inorganic nitrogen species fluxes that were observed in the overlying water. Potential rates of ammonium oxidation were used as a proxy for total nitrification. Only the control chambers showed evidence of ammonium oxidation, with a rate of 59.48 ± 2.285 nmol nitrite produced g^{-1} d^{-1} (Figure D.2). This would equate to a total sedimentary production rate of 144.77 ± 18.4 µmol nitrite produced d^{-1}, and a benthic flux of 5.15 ± 0.65 mmol nitrite m^{-2} d^{-1} into the overlying water (Table 5.1). Samples from the oil-amended treatment and the allylthiourea controls shared overlapping 95 % confidence intervals, no nitrite production with time (linear regressions, p values > 0.3), and mean nitrite concentrations at the last time point were not different from zero (student's T test, p values > 0.1).

Potential denitrification rates were detected in both control and oil chambers (Figure 5.3, Table 5.1). In the oiled sands, the mean denitrification rate was 6.64 ± 1.40 nmol N g^{-1} d^{-1}, equivalent to a maximum potential of 16.32 ± 3.62 µmol nitrate respired per day for the total sediment column, and a flux of 0.576 ± 0.128 mmol m^{-2} d^{-1}. An order of magnitude lower denitrification rates of 0.709 ± 0.237 nmol g^{-1} d^{-1} were observed in the control chambers (Table 5.1). All killed controls and controls without acetylene did not produce nitrous oxide (p values > 0.4). Similarly, potential nitrogen fixation rates were detected in the oiled chambers only and not in the control chambers or the non-acetylene containing controls. Approximately four times higher nitrogen fixation rates were determined under anaerobic conditions in comparison to aerobic conditions 0.0230 ± 0.0116 nmol g^{-1} d^{-1} compared to 0.100 ± 0.0129 nmol g^{-1} d^{-1}, respectively (Table 5.1).

5.4.4 Evidence of biodegradation in amended weathered oil

Samples were collected for GC-based oil analysis prior to the start, after one month and at the end of the experiment (3.5 months). Oil extracts were fractionated and n-alkanes (C12 – C37) along with the branched alkanes pristine and phytane were analyzed separately from aromatic hydrocarbons. Of the initial 5 g of crude oil added to each chamber, approximately 4.5 ± 0.35% (mean ± sd) was GC-amenable (225.41 ± 17.5 mg extrapolated from the T0 total petroleum hydrocarbon (TPH) concentration). A single replicate sampled from the oiled chambers at the end of the incubation showed an extremely high concentration of total aromatic hydrocarbons in comparison to initial values, and this replicate was removed from the analysis.

Initially, saturated hydrocarbons (n-alkanes + branched alkanes) comprised 86.9 ± 1.2% of the extractable hydrocarbons which dropped to 74.5 ± 1.03% by the end of the experiment, indicating that aliphatic compounds were preferentially degraded or transformed during the time course. In the oiled chambers, total alkanes are degraded or transformed with an exponential decay constant of 0.017 ± 0.0042 d^{-1} which translates to a summed alkane half-life of 40.7 ± 10.0 days (R^2 = 0.66, $p < 0.005$). Of the original concentration of extractable alkanes measured, 81.9 ± 15.2% remained after one month, and 23.5 ± 25.4% remained by the end of the experiment (Figure 5.3 C). Two of the three replicates showed very similar trends with 5564 ± 228 ng total alkanes per g dry sand remaining at the end of the experiment (8.86 ± 0.42% of the original measured concentration) while the third had a 6-fold higher concentration of 35,485 ng g^{-1} (52.9% of the initial) at the end of the experiment.

Since weathered crude oil was employed in this study, the total aliphatic profile was mostly composed of compounds with more than 16 carbons, of which the n-alkane C19 was the most abundant (Figure 5.3 B). Concentrations of n-alkanes ranging from C20 to C34 were remarkably similar initially. Exponential decay models were applied to all compound measured, those with p values less than 0.05 were retained, and the half-life was derived (Figure 5.3 A). N-alkanes from C18 to C33 had half-lives ranging from 25 to 42 days (mean = 34 d). C35 and C36 n-alkanes had the slowest decay rates, with half-lives of

65 ± 20 and 69 ± 28 respectively, while the largest n-alkane we measured, C37, did not significantly decrease with time.

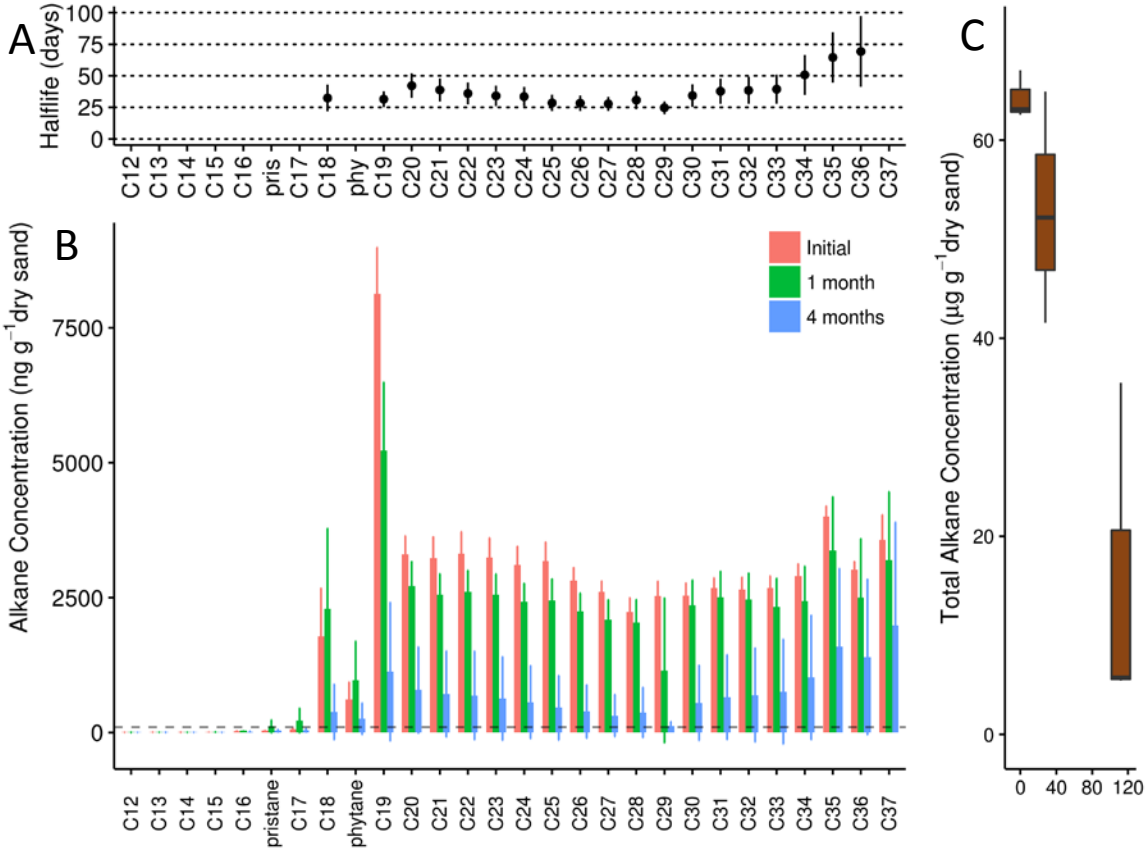

Figure 5.3 (A) Degradation of aliphatic compounds with incubation time expressed as half-life calculated from first order kinetics. Only compounds with significant regressions are included. Error bars represent the standard error of the mean. (B) Measured concentration for each aliphatic compound class. (C) Box plot for the summed concentration of aliphatic compounds determined for each timepoint.

Changes in total aromatic hydrocarbon concentrations were also well approximated by first order decay kinetics with an estimated decay rate for PAHs of 0.0051 ± 0.0011 d^{-1}, representing a half-life of 137 ± 31 days. By the end of the first month, 76.3 ± 15.6% of the total PAHs remained in the oiled chambers, and at the end of the experiment 54.9 ± 6.62% remained. In general, the PAH profile from the initial weathered oil was dominated by alkylated homologues of parent PAHs. The most concentrated groups belonged to

phenanthrene and anthracene parent compounds (3-ringed PAHs) with 2-4 alkyl-side chains, followed by benz[α]anthracene-chrysene (4-ringed PAHs) homologues with 1-4 alkyl-side groups, then alkylated fluoranthenes and pyrenes (3-4 ringed), and finally alkylated benzopyrenes and perylenes (4-5 constituent rings) (Figure 5.4 B). Smaller PAHs including naphthalene, acenaphthylene, acenaphthene, and fluorene were slightly above background concentrations further indicating the weathered state of the oil used (Figure D.7).

In general, all concentrated PAHs exhibited signs of degradation or transformation except the largest 4-5 ringed PAHs (Figure 5.4 A). The alkylated phenanthrenes and anthracenes had a mean half-life of 125 ± 21.8 days, excluding groups with a single alkyl group which did not significantly decrease ($p > 0.5$, $R^2 = 0.23$). The alkylated fluoranthrenes-pyrenes had a mean half-life of 163.0 ± 24.9 days, and the alkylated benz[α]anthracene-chrysene compounds had a mean half-life of 216.7 ± 38.0 days. As expected, the parent compounds tended to have shorter half-lives (quicker degradation rates) than their alkylated homologs to varying degrees, for example (benz[α]anthracene = 103.0 ± 28; chrysene = 194 ± 67; fluoranthene = 111 ± 39; Figure 5.4 B).

The control chambers were also analyzed for hydrocarbon content as a proxy for background concentrations. Compared to the weathered oil, the aliphatic constituents in control chambers were composed of shorter n-alkanes, with the most abundant compounds C18, C19, and phytane (Figure D.6). All n-alkanes with more than 21 carbons as well as those with less than 16 carbons were below detection initially. The total alkane concentration present in the control chambers was approximately 3 orders of magnitude lower than was observed in the oiled chambers initially with 91.3 ± 24.6 ng g^{-1} dry weight,

compared to 64.3 ± 2.45 µg g^{-1}. Interestingly, none of the abundant alkanes in the control

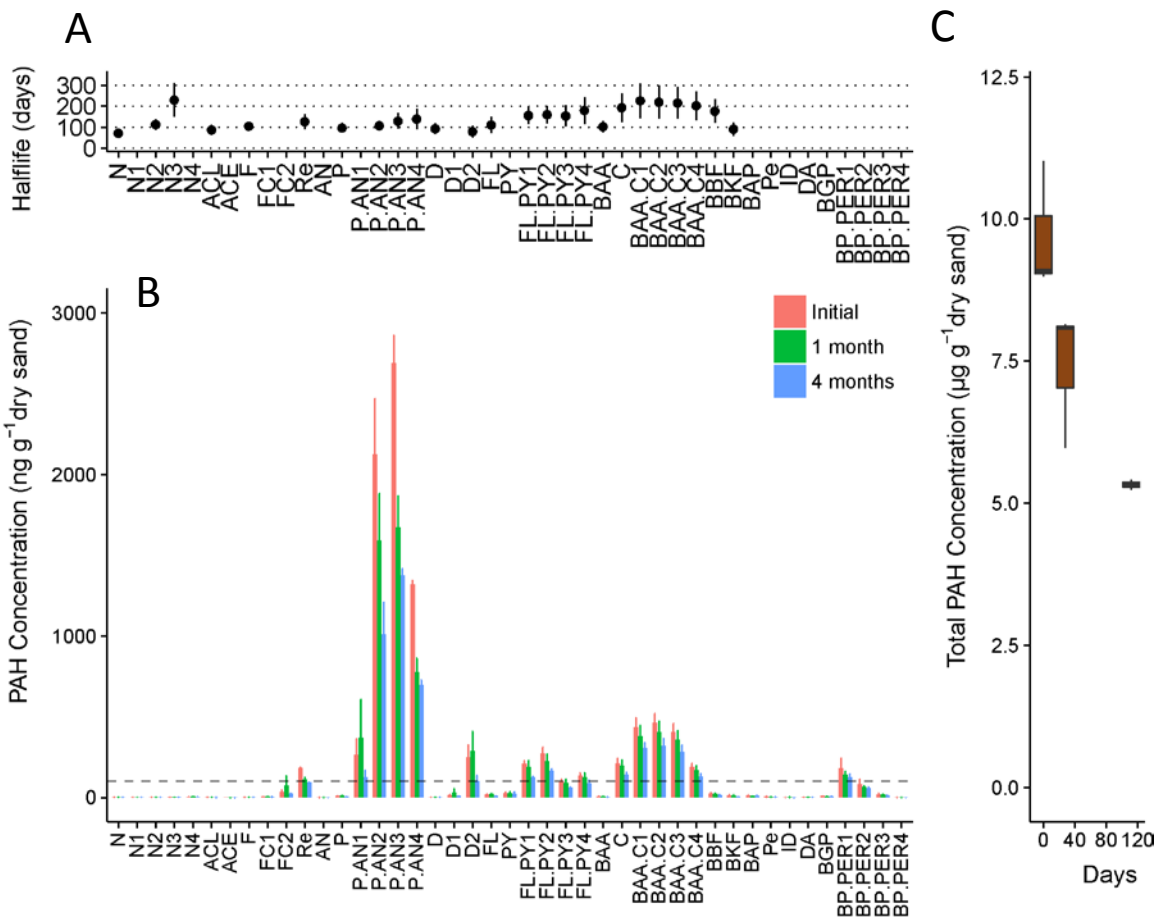

Figure 5.4 (A) Degradation of aromatic compounds with incubation time expressed as half-life determined from first order kinetics. Only compounds with significant regressions are included. Error bars represent the standard error of the mean. (B) Measured concentration for each aromatic compound. (C) Box plot for the summed concentration of aromatic compounds measured at each timepoint. One replicate from the final timepoint was removed as an outlier. Target PAHs are: Naphthalene (N) and alkylated homologues (N_{C1-C4}), Acenaphthylene (ACL), Acenaphthene (ACE), Fluorene (F), Retene (Re), Phenanthrene (P), Anthracene (AN), and their alkylated homologues (P/AN_{C1-C4}), Dibenzothiophene (D) and alkylated homologues (D_{C1-C2}), Fluoranthene (FL), Pyrene (PY), and their alkylated homologues (FL/PY_{C1-C4}), Benz[a]anthracene (BAA), Chrysene (C), and their alkylated homologues (BAA/C_{C1-C4}), Benzo[b]fluoranthene (BBF), Benzo[k]fluoranthene (BKF), Benzo[a]pyrene (BAP), Perylene (Pe), Indeno[1,2,3-cd]pyrene (ID), Dibenz[a,h]anthracene (DA), and alkylated homologues (BP/PER_{C1-C4}), and Benzo[ghi]perylene (BGP).

chambers significantly decreased with time. Within the aromatic fraction, the control sands contained alkylated fluorenes, phenanthrene, and alkylated homologs of phenanthrene and anthracene. The most concentrated aromatic class were the single-alkylated phenanthrenes and anthracenes (Figure D.7). While not significant, these compounds appeared to increase within the first month. The total aromatic concentration within the control chambers was 2 orders of magnitude lower than the oiled chambers at the start of the experiment (77.1 ± 17.5 ng g^{-1}, 9.70 µg ± 1.15 ng g^{-1}). Finally, unlike the weathered oil added where 87% of the extractable hydrocarbons were aliphatic compounds, the aliphatic fraction of the control sands was 54 ± 18%.

5.4.5 Response of the microbial community to buried oil and incubation within the chambers

In all chambers, colony forming units (CFUs) of cultivatable aerobic marine heterotrophic microorganisms increased with time (ANOVA with Welch's correction for unequal variances, $F = 94.4$, $p < 2 \times 10^{-16}$) and showed increased variation within the treatment over time (Figure D.5). Posthoc pairwise T-tests with Bonferroni correction indicated that the one-week and one-month sampling timepoints for both oiled and control chambers did not have significantly different CFUs from the initial sampling, likely due to the high variance observed from the initial timepoint. However, after one-week and one-month, the mean CFUs observed for the oiled chambers were significantly higher ($p < 0.001$) than the control chambers (Figure D.4). At the end of the experiment, the trend switched and the control chambers had significantly higher counts than the oiled chambers at 7.3×10^5 ± 10% and 5.2×10^5 ± 20%, respectively (mean ± 95% confidence intervals; $p < 0.000001$). Using linear regression models, CFUs increased in the oiled chambers at a

rate of 4.08 x 10^4 ± 400 CFUs d^{-1} ($p < 1 \times 10^{-15}$) and in the control chambers at a rate of 6.6 x 10^4 ± 260 d^{-1} ($p < 1 \times 10^{-16}$).

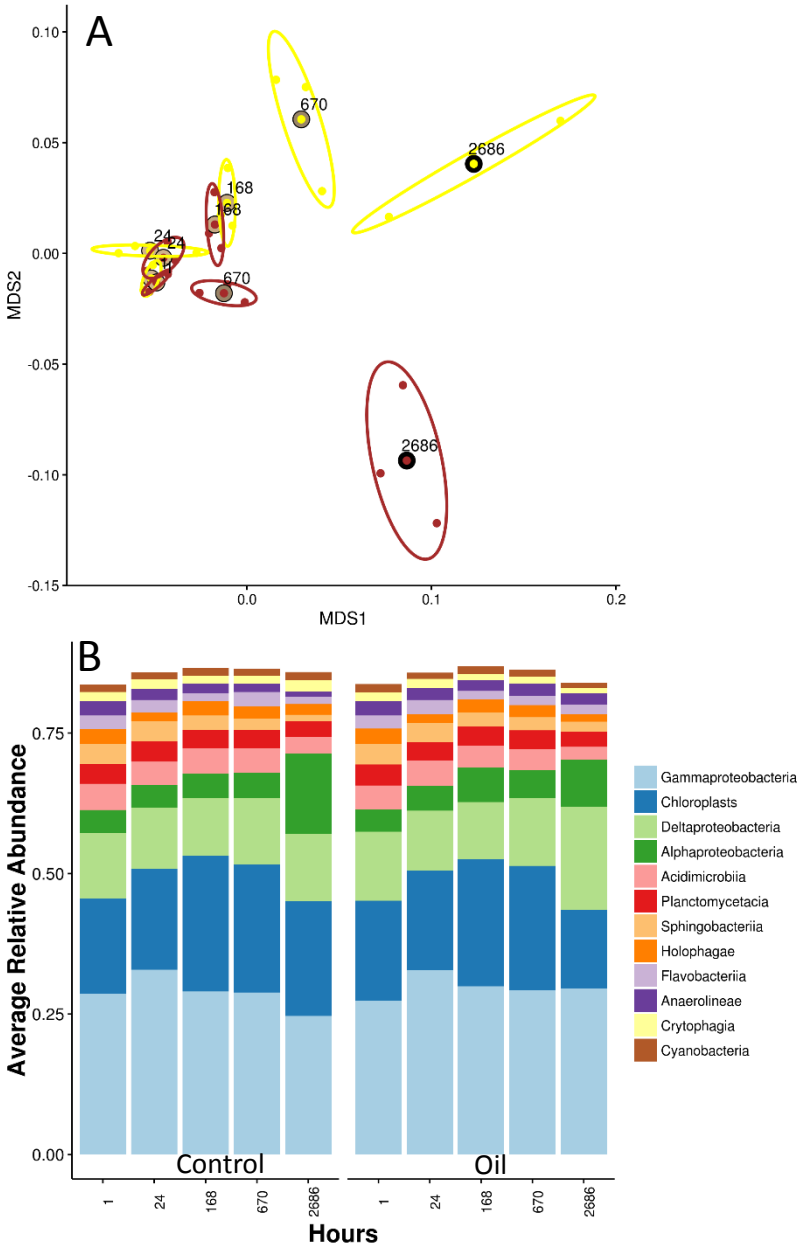

Figure 5.5 (A) Beta diversity of microbial communities visualized by non-metric multidimensional scaling generated from normalized SSU rRNA gene counts under a variance stabilizing transformation. Stress is 0.10. (B) The dominant microbial classes detected throughout the experiment.

The microbial community composition of each chamber was elucidated and populations tracked with time using SSU rRNA gene amplicons. Microbial community composition was remarkably consistent over time in all chambers (Figure 5.5 A), with no significant effects observed for oil treatment, time point, or the interaction of the two (permanova, $p > 0.05$). However, the power of the nonparametric test was low due to the small group sizes (3 chambers), and a relatively large effect size (33% of the variation) could be explained. The dominant classes detected in all chambers at all timepoints were Gammaproteobacteria, Deltaproteobacteria, Alphaproteobacteria, Acidimicrobiia, Planctomycetacia, and Sphingobacteriia (Figure 5.5 B).

Nonetheless, several genera were differentially abundant based on sampling timepoint and treatment. The most abundant putative oil-degrading taxa detected belonged to the genera *Alteromonas*, *Pseudoalteromonas*, *Marinobacter*, *Alcanivorax*, *Hyphomonas*, *Oleiphilus*, and *Labrenzia* (Figure 5.6 A). Interestingly many of these groups, to varying degrees, showed an increase in relative abundance in both the control and oil chambers. In particular, populations affiliated with *Alteromonas* and *Pseudoalteromonas* both rapidly increased in relative abundance within the first day in both treatments and then declined in relative abundance in parallel through the end of the experiment to below detection levels. *Marinobacter* and *Alcanivorax* spp. also greatly increased in relative abundance in the first day, and showed the highest relative abundance after 1 week. *Marinobacter* populations rapidly decreased through the first month, while *Alcanivorax* remained close to the same relative abundance through the end of the experiment. Conversely, *Hyphomonas*, *Labrenzia*, and *Oleiphilus* spp. were highest in

relative abundance at the end of the experiment in the oil chambers, with most of the increase observed after the one-month timepoint.

Putative ammonium oxidizing populations affiliated with *Nitrosococcus* remained abundant throughout the time course, under both treatments, although an increase in relative abundance with time was observed in the control chambers (Figure 5.6 B). Populations of the putative archaeal ammonium oxidizer, *Nitrosopumilus*, were only abundant at the end of the experiment in the control chambers. Two putative nitrite oxidizing groups, *Nitrospira* spp. and *Nitrosomonas* spp. showed similar trends as *Nitrosopumilus* with a large increase in relative abundance occurring between the 1 month and 3.5-month time points in the control chambers only.

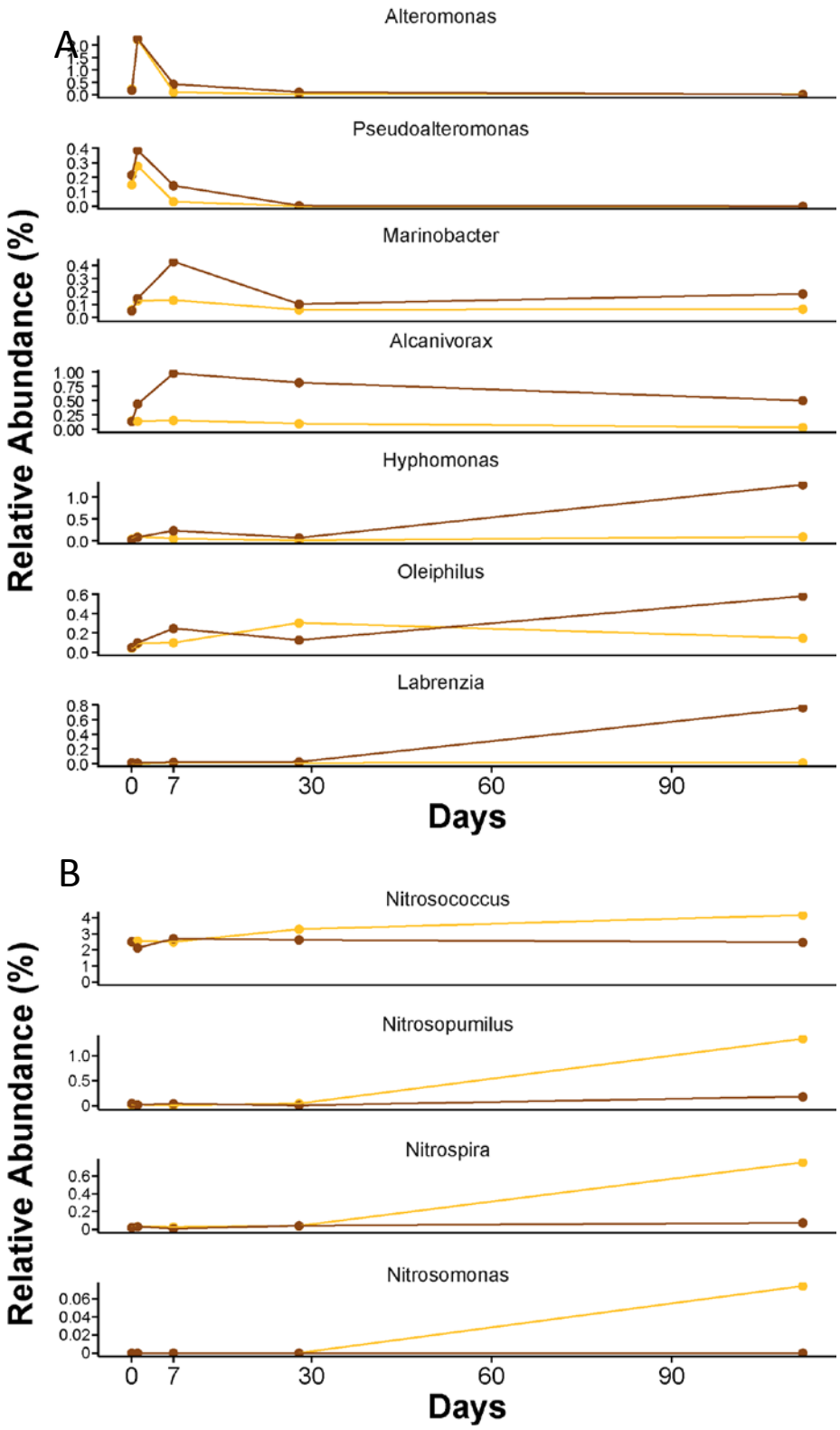

Figure 5.6 Distributions of putative (A) hydrocarbon-degrading and (B) nitrifying prokaryotes.

5.5 Discussion

A substantial but unknown portion of weathered crude oil from the Deepwater Horizon disaster that reached sandy shorelines along the Gulf of Mexico was trapped in intertidal and subtidal zones where it remains difficult to detect, study, and remove (Operational Science Advisory Team, 2013; Warnock *et al.*, 2015). The most recognizable deposits are classified into three main types: submerged oil mats (SOMs), tar patties, and surface residual balls (SRBs) (Operational Science Advisory Team, 2013). In addition, more diffuse oil particles generated through the mechanical shearing and break-up of larger deposits are likely widespread and continuously generated. The impact and fate of these oil deposits is not understood and has not been addressed.

The rates of decay for the majority of sequestered oil compounds will be ultimately determined by microbial degradation activity, which is in turn controlled by oxygen and nutrient levels (Prince, 2010). In unsaturated supratidal sandy sediments of Florida beaches contaminated by DWH oil, oxygen was not depleted due to high airflow rates driven by tidal pumping, and evidence indicates that biodegradation activity was limited by nutrient concentrations (Huettel *et al.*, 2018). In contrast, oxygen concentrations in permeable subtidal sediments, which are saturated with seawater, are controlled by the advective exchange of overlying water with sedimentary pore-water (Huettel *et al.*, 2014). Exchange rates, or advective-flow rates, are driven by pressure gradients generated from bottom topology, current flow, surface gravity wave action, and macrofaunal activity (Huettel and Gust, 1992; Huettel and Rusch, 2000; Huettel *et al.*, 2014). In addition to oxygen, advective-flow transports nutrients and particulate organic matter into sediments, while removing metabolic wastes and reduced electron acceptors. Advective transport stimulates

sediment metabolisms and biogeochemical cycles, causing increased rates of organic matter mineralization (Huettel *et al.*, 2014).

Buried oil deposits in sufficiently high concentrations can shutdown critical advective-flow transport processes by reducing sediment permeability, potentially explaining the low rate of degradation observed in re-exposed SRBs (Yin, John, *et al.*, 2015). However, the permeability observed at Pensacola Beach in the most heavily oiled layers remained sufficient for solute transport to be dominated by advection in surficial sediments (Huettel *et al.*, 2014, 2018). Under such conditions, ecosystem function may be strongly impacted due to altered nutrient availability and poisoning of sensitive microbial populations. In this study, the amended oil concentrations of 1% (wt/wt) were chosen based upon field observations of DWH oil concentrations in supratidal sands at Pensacola Beach, FL, and considered to be representative of oiled-sediments that were transported and buried offshore (Kostka *et al.*, 2011; Huettel *et al.*, 2018). Oil concentrations in this mesocosm study are lower than observed in resuspended intact SRBs (Mulabagal *et al.*, 2013; Yin, John, *et al.*, 2015), and enable advection-dominated chemical exchange through the generated oil layer. Thus, changes in nutrient availability, oxygen demand, and impacts to microbial populations are considered in the context of active, advective transport.

5.5.1 Oxygen consumption linked to oil biodegradation in the oiled chambers

In this study, oil-contaminated subtidal sands showed twice the oxygen consumption rates as was observed in the control sands. This oxygen consumption is likely fueled by both aerobic respiration coupled to organic matter decomposition as well as oxidation of reduced compounds (such as reduced metals, reduced sulfur, or ammonium and nitrite) generated by anaerobic metabolism (Sørensen *et al.*, 1979). However,

differences in oxygen consumption between treatments can be used as a conservative estimate of total oxygen requirements for oil remineralization, as the homogenized sands can be assumed to exhibit a similar organic matter content. Furthermore, this estimate can be considered conservative as additional bioavailable organic carbon generated by autotrophic microbial processes in control chambers, such as nitrification, would increase rather than limit oxygen demands.

The observed 1 μmol L^{-1} hr^{-1} difference in oxygen consumption attributable to the oiling effect is equivalent to 168 μmol O_2 d^{-1} consumed in the sediment column. If this oxygen was only used for initial hydrocarbon activation (by mono- or dioxygenases), then total hydrocarbons would be activated (and thus removed from the GC-based quantification analysis) at an equivalent rate of 168 μmol d^{-1} (Widdel and Musat, 2010).

Oxygen demand can be generally compared to hydrocarbon degradation rates, with the following assumptions: 1) oxygen is used to activate n-alkanes, which represented 87% of the initial GC-amenable fraction, 2) the total n-alkane profile is represented by the weighted mean molecular mass observed at the beginning of the experiment, 383 g mol^{-1} (C27), 3) the 33 mg loss in extractable n-alkanes that occurred during the first month of incubation is approximate to a loss of 86 μmol of alkanes, and concurrently 4540 μmol O_2 was consumed by the sediment column due to oil amendment. Taken together, approximately 2 % of the measured difference in oxygen consumption between the oiled and control chambers can be attributed to the first step in alkane degradation (Rojo, 2009). This is not unexpected as the measured total aliphatics represented < 5% of the total mass of weathered oil added, and most of the oil transformation products generated *in situ* at

Pensacola Beach were identified as oxygenated aromatic hydrocarbons, primarily attributed to their alkyl-side chains (Ruddy *et al.*, 2014)

Focusing on the GC-amenable fractions quantified during this study, the average half-life for all measured aliphatic compounds was 41 days. This is slightly shorter, but within the range of previous observations (53 – 69 days) from intertidal and supratidal sands from the region (Elango *et al.*, 2014; Snyder *et al.*, 2014; Huettel *et al.*, 2018). Similar to results presented in Huettel et al. (2018), these rates greatly exceed published, predicted hydrocarbon biodegradation rates from a compilation of studies (Howard *et al.*, 2005). For example, for C22-C30 n-alkanes, we observed a half-life < 50 days while predicted half-lives ranged from 100-175 days (Howard *et al.*, 2005). For n-alkanes > C30, we calculated half-lives < 100 days as compared to 276-383 days for C31-C34 (Howard *et al.*, 2005). In contrast, longer half times for PAH degradation (137 days) were estimated in this study as compared to predictions (67-87 days) (Elango *et al.*, 2014; Snyder *et al.*, 2014; Huettel *et al.*, 2018). Our observed rates of 100-150 days were slower than expected for 3-ring PAHs (38-44 days) and within the expected range for 4-ring PAHs, at 140-250 days compared to a predicted 141 – 378 days (Howard *et al.*, 2005).

5.5.2 Oil alters nitrogen cycling processes in benthic permeable sediments

Ammonium concentrations in the oiled chambers remained above detection for the duration of this experiment, with the exception of days 7-14. This suggests that the remineralization of *in situ* organic matter generated sufficient nitrogen to supply requirements for microbial growth. Rather, it appears that phosphate was limiting microbial growth in the chambers, with phosphate consumed by heterotrophic microbial populations

as quickly as it was produced. However, the periodic detection of phosphate concentrations in the overlying water throughout the course of the experiment, as well as the faster than predicted rates of n-alkane and 4-ring PAH transformations suggest that phosphate was continuously generated. The periodic pulses in detected phosphate concentrations on days 78 and 106 also suggest that phosphate concentrations do not explain the increase in oxygen consumption until day 55. Results presented here conflict with those of from intertidal mesocosms studied in (Mortazavi *et al.,* 2013), in which oil-only amendments were not nitrogen or phosphorus limited. This is surprising as the authors used un-weathered crude oil at a higher concentration than employed here, but can potentially be explained by higher *in situ* organic matter concentrations in Dauphin Island, AL sands (Mortazavi *et al.*, 2013).

Nitrite and nitrate levels in the oiled sands remained low or undetectable for the duration of the experiment, suggesting that nitrification rates were low or coupled denitrification-nitrification was sufficient to maintain the low levels (Lehmann *et al.*, 2004; Gihring *et al.*, 2010; Horak *et al.*, 2013). However, the nitrification rate potential measurements indicate that nitrification rates were low relative to the control sediments and nitrifying microbial populations were either inhibited or present at low abundances. The results further suggest that denitrification rates were also low in oiled sediments due to the low availability of nitrate, as they did show a high potential for denitrification.

5.5.3 Microbial community response to weathered oil amendments

In contrast to field observations in beach sands impacted by the DWH spill, microbial community composition remained remarkably consistent throughout the entire

3.5 month mesocosm experiment (Kostka *et al.*, 2011; Newton *et al.*, 2013; Kappell *et al.*, 2014; Lamendella *et al.*, 2014; Rodriguez-R *et al.*, 2015; Huettel *et al.*, 2018). After applying strong transformations to the normalized gene counts, non-metric multidimensional scaling plots do show different trajectories in community composition in each treatment with time. This indicates that relatively rare populations were responding to the treatment effect, while most members did not significantly shift (Anders and Huber, 2010). We postulate that the closed nature of the flux chambers impedes dispersal, preventing dormant or inactive cells from being removed or new populations from entering. It has previously been shown that intertidal microbial populations are readily mobilized through pore-water fluxes, and the feature is important for beach microbial community dynamics (Boehm *et al.*, 2014).

However, upon examining shifts in specific microbial populations putatively associated with hydrocarbon degradation we observe that very similar taxonomic groups positively responded to the oil amendments as seen in intertidal and supratidal sands. *Marinobacter* spp. and *Alcanivorax* spp. responded rapidly to the oil treatment, increasing in relative abundance 5-10 times higher than initial levels or compared to the controls chambers sediments over the same time period. Multiple studies have implicated either or both these groups as the primary responders to permeable sediment oiling (Kostka *et al.*, 2011; Newton *et al.*, 2013; Lamendella *et al.*, 2014). *Marinobacter* populations tend to have a more diverse metabolic repertoire including aerobic or anaerobic growth, capacity to use a broad range of hydrocarbon classes, and tended to be more abundant in intertidal sands than supratidal sands (Kostka *et al.*, 2011; Singer *et al.*, 2011; Newton *et al.*, 2013; Lamendella *et al.*, 2014). *Alcanivorax* populations are generally adapted for growth on

aliphatic compounds and are often detected as first responders to oil in across the globe surficial marine waters or beaches (Yakimov *et al.*, 2007; Sabirova *et al.*, 2008; Vila *et al.*, 2010; Naether *et al.*, 2013). While *Alcanivorax* relative abundances remain high throughout the remainder of the experiment, we were surprised to see a decrease in *Marinobacter* relative abundances following the first week, as the broad substrate ranges typically allow *Marinobacter* to persist in the environment. In our system, this decrease in *Marinobacter* may be due to direct competition with other late stage hydrocarbon degrading populations thought to primarily utilize the aromatic fraction, including the Aphaproteobacterial groups *Hyphomonas* and *Labrenzia* (Kostka *et al.*, 2011; Overholt *et al.*, 2013; Joye *et al.*, 2016). Of interest, *Alteromonas*, *Pseudoalteromonas*, and to a lesser extent, *Oleiphilus* increased in relative abundance in both the control and oiled treatments. While all are putatively associated with oil degradation, these groups may have been remineralizing *in situ* organic matter (Head *et al.*, 2006; Joye *et al.*, 2016).

5.5.4 Oxygen consumption and nutrient fluxes within the control sediments

The rate of oxygen consumption observed in the control chambers corresponds to the low end of the range determined in previous studies that employed advective flow chambers in situ in Gulf coast permeable sediments (Gihring *et al.*, 2010; Chipman *et al.*, 2016). The lower rates we observe compared to *in situ* rate measurements is attributable to the three week pre-incubation period that will have removed almost all labile dissolved organic matter, as well as a substantial portion of semi-labile DOM (Hansell *et al.*, 2012).

Assuming that measured rates of nitrite and nitrate production that we observe in the control sands (0.23 and 1.27 μmol L^{-1} d^{-1}) are due to nitrification, these rates equate to

approximately 1-5% of the measured oxygen consumption. The potential for nitrification, the likely source generating these fluxes, is approximately 20-fold higher than measured production. This disparity is likely due to several factors including ammonium limitation in the chambers, denitrification consuming the produced nitrite and nitrate, as well as inorganic nutrient assimilation. We do not expect denitrification to greatly contribute to this observed disparity due to the low potential observed in these control sediments. In addition, the maintenance of high oxygen concentrations and advective flow are expected to be sufficient to fully flush the sediment column with oxygenated overlying water (Khalili *et al.*, 1997).

Due to the patterns in inorganic nutrient fluxes we observe, the microbial communities in the control chambers also appear to be phosphate limited at least initially. Rapid mineralization of organic matter generated a net flux of ammonium into the overlying water column starting after the first week, however, phosphate did not begin accumulating until day 44. The two peaks at day 9 and day 26 in the phosphate profile suggest that phosphate was being produced simultaneously with ammonium as expected, but was consumed at an equal rate. If we relate the organic matter mineralization to the flux in nitrate and phosphate, we observe a N:P flux ratio of 12.7±2:1, close to the predicted ratio observed in particulate natural organic matter (Hopkinson Jr and Vallino, 2005).

In support of the evidence for high rates of nitrification occurring in the control chambers, as well as the strong potential for nitrification observed at the end of the experiment, putative nitrifying microbial groups increase in relative abundance with time in the control chambers. The bacterial ammonium oxidizer, *Nitrosococcus* is among the most abundant genera detected in the chambers in both treatments. *Nitrosococcus* species

exhibit the largest cell sizes among all ammonium oxidizing bacteria and tend to be the most resistant to inhibitory compounds and hydrocarbons in general (Campbell *et al.*, 2011; Urakawa *et al.*, 2012; Sipos and Urakawa, 2016). However, *Nitrosococcus* groups are obligate chemolithoauthotrophic ammonium oxidizers and the lack of nitrification potential in the oiled sands suggest they are dormant or have low nitrification activities here. This is further supported by the static relative abundances across all timepoints in the oiled sediments. Conversely, *Nitrosopumilus* populations are known to be among the most sensitive groups to hydrocarbon contamination (Urakawa *et al.*, 2012). These putative archaeal ammonium oxidizers are undetectable in the oiled chambers throughout the time course. They also appear sensitive to ecosystem disturbances and were not present in the sands at the initial timepoint. However, by the end of the experiment, populations associated with *Nitrosopumilus* represented 1 % of the total community. In field observations, the abundance of *Nitrosopumilus* SSU rRNA genes was strongly negatively correlated with hydrocarbon contamination and their resurgence is thought to be associated with a recovery of the beach ecosystem (Rodriguez-R *et al.*, 2015; Huettel *et al.*, 2018).

Populations associated with the second step of nitrification, nitrite oxidation, exhibited similar patterns to *Nitrosopumilus*. Both *Nitrospira* spp. and *Nitrosomonas* spp. exhibited a large increase in relative abundance occurring between the 1 month and 3.5-month time points in the control chambers from less than 0.01% of the initial community. The increase in relative abundance starting on day 27 in these two groups parallels the decrease in nitrite concentrations that begins on day 35, and the increase in nitrate concentrations that begins on day 26. In the oiled chambers, these putative nitrite-oxidizing groups remain at very low levels throughout the timecourse, supporting our conclusions

that coupled nitrification-denitritification is disrupted following sediment oiling (Urakawa et al., In Submission).

5.6 Conclusions

The addition of relatively low levels (1% wt/wt) of weathered crude oil used in this study as compared to those found in submerged oil mats and patties (5-10% wt/wt) is sufficient to disrupt natural coastal biogeochemical cycles, particularly pathways within the nitrogen cycle. At these concentrations, advection remains as the primary mechanism of solute and particulate transport into the sedimentary matrix, and the full sediment column does not go anoxic. However, nitrification is impeded by either inhibition or competitive exclusion of the microbial populations responsible which alters the fluxes of these nutrients between the sediment-water interface. We also report rapid rates of n-alkane degradation within the estimates previously reported at Gulf coast beaches, and approximately 75 % of the measured aliphatic compounds were transformed or degraded. Rates of 3+ ring aromatic degradation was slower than observed in coastal beaches, although still sufficient to degrade or transform 50 % of the initial PAH concentrations. The addition of weathered crude oil doubled the rate of benthic oxygen flux, and of the oxygen consumed, we estimate that a minimum of 2 % is linked to n-alkane transformation. Furthermore, results indicate that aerobic respiration coupled to hydrocarbon degradation was limited by phosphate and not inorganic nitrogen. In contrast to field studies, the lack of dispersal of microbial populations in mesocosms appeared to greatly limit overall shifts in microbial community composition; however, the dominant putative oil-degrading populations were similar to those observed in the field across Gulf coast beaches. Overall,

this study addresses our lack of knowledge towards the fate and consequences of subtidal oil deposits across the northern Gulf of Mexico.

CHAPTER 6. FINAL CONCLUSIONS

The Deepwater Horizon (DWH) oil spill in the Gulf of Mexico represents the largest accidental marine oil spill in history, the first large spill that occurred in the deepsea, and is unique in the unparalleled volumes of chemical dispersant that were applied during emergency response efforts. Subsequent to the DWH disaster, intense research efforts seek to understand the consequences of oil contamination to Gulf ecosystems as well as to improve mitigation strategies and emergency response efforts for future oil spills. The work presented in this dissertation addresses knowledge gaps associated with the environmental controls of the structure and function of benthic microbial communities across the Gulf as well as their response to major pertubations such as oil contamination. Specifically, the overall goal was to advance our understanding of the fate and consequences of deposited DWH crude oil to benthic ecosystems and the *in situ* microbial community. Objectives were to: (1) determine the impacts of chemical dispersant on individual oil-degrading microbial populations and the consequences to oil ecotoxicity, (2) interrogate the natural or baseline state of benthic microbial communities and construct a model to predict their distribution throughout oligotrophic sediments, and (3) quantify the environmental controls of biodegradation and impacts to microbially-mediated ecosystem services, specifically nitrogen cycling, in sandy coastal ecosystems.

Chemical dispersants represent a primary emergency response strategy that aims to minimize coastal impacts, decrease oil-associated toxicity by dilution, and stimulate biodegradation by increasing the surface area to volume ratio of oil droplets, thereby alleviating nutrient stresses. Over seven million liters of chemical dispersants were applied

at depth or on surface oil slicks during the DWH spill. The second chapter of this dissertation investigates the fundamental assumption that dispersant application increases rates of biodegradation using pure cultures of hydrocarbon-degrading bacteria isolated from beach sands which were impacted by the DWH discharge. The results presented here contribute to the growing understanding that chemical dispersants can have unintended consequences for the microbially-mediated biodegradation of petroleum hydrocarbons. Microbial populations were shown to have disparate responses in growth rate and biodegradation efficiency to dispersed oil or crude oil. These differences in physiological response have the potential to directly impact the ecotoxicity of dissolved or dispersed oil constituents as well as intermediate degradation products.

Of the DWH oil that was transported to coast, a large portion was deposited above the intertidal zone and sequestered in heavily-contaminated sand layers. An additional unconstrained portion of the oil that initially came ashore was transported back offshore, remains buried, and may be mobilized under certain circumstances. While biodegradation of these two forms of buried oil deposits will largely be controlled by oxygen and nutrient concentrations, reactive-transport conditions differ and will impact the persistence of contamination. In chapter 3, tidally-driven mechanisms that determine the fate of oil buried in coastal sands as well as the response of microbial communities to oil contamination were interrogated. The abundance, composition, and succession of sand microbial communities closely paralleled changes in the evolution of petroleum hydrocarbon (PHC) chemistry in a 2-year time series at Pensacola Beach. Microbial community structure and abundance as well as PHC content were shown to return to near baseline within one year after the initial oiling event. Rapid rates of PHC degradation were observed that could be attributed to

tidal pumping that transported oxygen into the buried oil layers while removing carbon dioxide. While soluble nutrients are not transported by tidal pumping, higher than anticipated rates of hydrocarbon degradation suggest that these oiled sands were not strongly nutrient limited, potentially due to microbial community adaptation.

The rationale of the second theme of this dissertation asserts that in order to assess the impacts of perturbations to ecosystems, the baseline or unimpacted state must be understood. Prior to the DWH disaster, the indigenous microbial communities and their distribution on the oligotrophic Gulf of Mexico deep seafloor were virtually unknown. Therefore, in order to characterize the baseline condition for deep ocean sedimentary microbial communities at the ocean-basin-wide scale, the study reported in chapter 4 of this dissertation generated the largest dataset ever compiled for the composition of seafloor microbial communities. Microbial community distribution was mapped across gradients in environmental parameters including sedimentary oxygen content, water depth, sediment depth, latitude, and longitude in the Gulf of Mexico. Based on these well resolved microbial distributions, a predictive model was developed using a machine learning approach (random forest regression). The sole inputs to the model were environmental parameters that could be derived from freely available maps. The applicability of the model was verified by using previously published datasets on Gulf microbial communities acutely impacted by the DWH oil spill. Model results showed that highly contaminated sites deviate strongly from the model predictions, while unimpacted samples are consistent with our predictions of baseline microbial community composition as the seafloor. By determining deviations from predicted baseline, the model can be used as a tool to assess risk for future impacted sediments that may be poorly characterized. One major finding

from this chapter shows that impacted sediments returned to stable baseline conditions within 2 years of the oiling event. In addition, and separate from oil spill remediation work, this model can be applied to determine, and quantify, regions in the Gulf of Mexico that are conspicuously different from oligotrophic ecosystems, such as cold seeps.

In the final chapter, the controls of oil biodegradation and impacts of oil contamination on microbial community structure/ function relationships were investigated in saturated subtidal sediments through a long-term mesocosm experiment that employed advective flow chambers to reproduce near *in situ* conditions in permeable sands. Similar to field observations in the supratidal zone (chapter 3), rapid rates of oil degradation were observed, indicating that nutrient limitation did not substantially impede the activity of hydrocarbon-degrading microbial populations. The most significant findings from the mesocosm study demonstrate the occurrence of large-scale disruptions to the marine nitrogen cycle in subtidal sands in response to oil contamination through the inhibition of nitrification. This disruption can be linked to the microbial populations that mediate nitrification along with other nitrogen cycling processes. These results can be directly incorporated into predictive models to forecast ecosystem health and recovery for future oil spills as well as hindcast the fate of remaining DWH oil.

One recurrent theme throughout this dissertation is the resiliency of sedimentary microbial communities to ecological disturbance. Oil contamination represents a particularly strong disturbance, both as an energy dense carbon source for heterotrophic microbial communities as well as the inherent toxicity of certain constituents such as polycyclic aromatic hydrocarbons (PAHs). These properties apply strong positive selection pressures towards microbial groups capable of degrading hydrocarbons along with strong

negative pressures towards sensitive groups. Nonetheless, results presented throughout this dissertation demonstrate that benthic microbial communities, from the shoreline to the deep ocean across the Gulf of Mexico, have recovered from the DWH discharge within 1-2 years. In deep fine-grained oligotrophic sediments within 5 km of the wellhead, benthic microbial communities returned to the predicted baseline state by 2012, and remained consistent with the communities of unimpacted regions during subsequent sampling events (chapter 4). Along the coast, oil-degrading populations and absolute abundances decreased to background levels observed in pre-spill or control samples, concurrent with a rebound in sensitive populations with the potential to carry out chemolithoautotrophic nitrification (chapter 3). Interestingly, the resiliency of microbial communities in coastal ecosystems was strongly linked to the removal of petroleum hydrocarbons to background levels, while in the deep ocean, recovery occurred despite the persistence of contaminants. One plausible explanation is the mechanism of oil delivery to the seafloor, where a large region of the deep ocean benthic environment was blanketed in oiled-marine snow, which diluted out the petroleum hydrocarbon content. This dilution effect may have been exacerbated by the return of bioturbation mediated by meio- and megafauna observed over a similar time period at some sites.

The research presented herein contributes to a predictive understanding of the environmental and ecological controls that regulate microbial biodegradation as well as the response of benthic microbial communities to oil contamination from the deep ocean to coastal sands. From modeling and data products, rates of benthic ecosystem recovery may be predicted and future response strategies improved. Finally, this work highlights knowledge gaps that remain to be addressed in future studies regarding microbial

transformation products, the interplay between anaerobic and aerobic metabolisms in heavily oiled offshore deposits, and the metabolic pathways in unimpacted deep benthic environments.

6.1 Recommendations for Future Directions

The results presented in chapter three demonstrate that rates of hydrocarbon degradation under fully aerobic conditions are driven by tidal pumping in sands of the supratidal zone. In addition, supratidal beach sands undergo limited solute transport rates that rely on large storm surge events or run-off from the land surface. In chapter five, hydrocarbon degradation rates were quantified in subtidal sands at low to intermediate oiling levels that did not substantially impede advective flow rates. Amendments to mesocosms were chosen to replicate oil levels observed in the field at Pensacola Beach as well as to link lab studies with field observations of dominant microbial response pathways. Submerged oil mats (SOMs) resulting from transport and sheering processes acting upon more concentrated oil deposits are likely to be exposed to similar subtidal conditions as those represented in the mesocosm experiments. However, these SOMs can reach tens of centimeters thick and hundreds of square meters in surface area, with an expected oil content of 10-20 %. In such large oil aggregations, advective pore-water exchange is likely to be completely blocked, preventing oxygen and solute exchange. The fate of oil in SOM remains virtually unstudied and will depend upon the interplay between anaerobic metabolisms within the SOM and aerobic metabolism along the surface or outer edge. The experimental approach outlined in chapter 5 could be applied to provide a predictive understanding of the fate of SOM in subtidal sands.

If possible, this experiment should be accompanied by research investigating the break-up and transportation dynamics of buried SOM deposits. Field evidence indicates that violent storm events fracture large portions of the SOM, generating smaller tar patties or surface residual balls (SRBs) that are highly mobile. However, the weathering and integrity of SOMs under a variety of forces is not well understood. While it may be possible to study these dynamics in the field, numerous challenges must be overcome, notwithstanding actually finding SOMs. Instead, well-designed laboratory experiments in similar advective flow chambers with varying pressure gradients may be used, or in larger laboratory flumes where different flow rates can simulate physical weathering forces. With an understanding of the rate of oil degradation within the SOM, and the rate of degradation of SOM fragments, as well as an understanding of the physical weathering of SOM, the fate of subtidal oil deposits will be better constrained.

Although the succession of microbial populations in subtidal mesocosms was correlated with oil chemistry over time as in the field, smaller changes in community composition were observed in comparison to field observations. This disconnect between the field and mesocosm results could be explained by the closed nature of the mesocosm experiments which prevents fresh microbial transport from overlying seawater as well as the removal of dormant or dead cells from the sediments. While the exchange of particulate organic matter into permeable subtidal sediments is well constrained, the ramifications of such transport on microbial community assembly processes are not understood. By employing the flow advection chambers and exchanging the overlying water with fresh or unfiltered seawater, the role of dispersal and transport on microbial communities could be elucidated and linked to the fate of buried oil.

Finally, the metabolic potential of dominant benthic microbial populations in the oligotrophic deepsea could be linked with their known and predicted biogeographical distributions. By using only previously generated metagenomes, the applicability and insights of the model generated here could be greatly expanded to further interrogate the consequences of large scale oil-disturbances in the Gulf of Mexico. Moreover, the dominant seafloor microbial populations elucidated here for the Gulf are globally distributed and globally abundant. Therefore, determination of their metabolic potential would be directly applicable to > 60% of the entire surface area of the planet. The generation of a relatively small number of additional metagenomes from key locations could expand this dataset to encompass the metabolic repertoire of populations located at different niches within the stratified sediment column instead of only focusing on surficial sediments. The relevance of such a study is challenging to predict, but it has the potential for greatly improving our knowledge and functioning of global biogeochemical cycles.

APPENDIX A. SUPPLEMENTAL INFORMATION FOR CHAPTER 2

A.1 Detailed Hydrocarbon Analysis Methodology

Extraction and analysis of hydrocarbon compounds was performed according to a modified version of EPA method 3510C with accompanying QA/QC protocols. Bacterial and control treatments were extracted for quantification of total petroleum hydrocarbons (TPHs) as well as the specific hydrocarbon compound classes aliphatics (*n*-alkanes C_{12}-C_{40}, and isoprenoids pristine and phytane) and polycyclic aromatic hydrocarbons (PAHs). Samples (25 ml) were transferred to 250 ml separatory funnels, and 15 ml of dichloromethane was added. Sample glassware containers were rinsed with an additional 15 mL of dichloromethane to collect all residual oil. Separatory funnels were shaken for 2 minutes, and the organic layer was collected in a 60-ml vial. The extraction step was repeated 3x, and 2-4 g of anhydrous sodium sulfate was added to the resulting organic extracts. Hydrocarbon fractions were separated using solid-phase extraction (SPE) with silica/cyanopropyl glass columns (SiO2/C3-CN, 1 g/0.5 g, 6 mL) made at the University of South Florida. Fractions were collected by sequentially eluting the extracts with hexane (100%) to collect aliphatic hydrocarbons, and hexane/dichloromethylene mixture (3:1, v:v) to collect aromatic hydrocarbons. Both fractions were concentrated and spiked with d14-terphenyl. All solvents used were at the highest purity available. All solvents used were at the highest purity available and without further purification. All glassware used was previously combusted at 450°C for 4 hours, and rinsed with dichloromethane prior to extraction. An extraction blank was included with each set of samples (10-12 samples) to

ensure no contamination from chemicals, glassware and/or laboratory equipment. Extracts were stored in glass amber vials at 4 °C until GC analysis.

Aliphatics and aromatics were quantified in a gas chromatograph/mass spectrometric detector (GC/MS) in full scan mode (*m/z* 50-550). Splitless injections of 1μL of the sample were conducted, and a RXi®5sil column (30 m x 0.25 mm x 0.25 μm) was used. Quantitative analysis of aliphatics and PAHs were conducted using the IS (internal standard) method. Samples were spiked before extraction with perdeuterated *n*-alkane (d_{50}-Tetracosane, Ultra Scientific) and PAHs (Deuterated PAH Mixture: d_{10}-acenaphthene, d_{10}-phenanthrene, d_{10}-fluoranthene, d_{12}-benz(a)anthracene, d_{12}-benzo(a)pyrene, d_{14}-dibenz(ah)anthracene, d_{14}-benzo(ai)perylene; Ultra Scientific). For *n*-alkanes analysis, GC oven temperature was programmed as 80°C held for 0.5 min, then increased to 320°C at a rate of 10°C min^{-1} and held for 5.5 min. Injector temperature was set to 280°C. Identification and quantification of *n*-alkanes (nC_{12}-nC_{40}) and isoprenoids pristine (Pr) and phytane (Phy) were conducted by comparing with a reference standard (Fuel Oil Degradation mixture, Ultra Scientific; C8-C40 Alkane Certification Standard; Supelco) and the spike standard (d_{50}-Tetracosane). Recoveries were high within QA/QC criteria of 90-120%. Concentrations are expressed as volume sample (L) concentrations. For PAHs, a GC oven temperature was programmed as 60°C held for 8 min, then increased to 290°C at a rate of 6°C/min and held for 4 min, then increased to 340°C at a rate of 14°C/min, and held at the upper temperature for 5 min. The temperature of the MS detector was 250°C. Concentrations of PAHs were calculated using response factors by comparison with a known standard mixture (16-unsubstituited EPA Priority Pollutants and selected congeners: Ultrascientific US-106N PAH mix, NIST 1491a) and the spike standard. When

no commercial reference standard was available, compounds were quantitated using the response factor for an isomer. Therefore, the concentrations determined for many of the alkylated PAHs were semiquantitative. Recoveries were generally within QA/QC criteria of 70-120%. Aromatic compounds are expressed as volume sample (L) concentrations.

A.2 Outlier in Acinetobacter Oil Degradation

There was an outlier in the dispersed oil treatments inoculated with *Acinetobacter* which produced a higher total peak area than any of the control treatments, after correction for extraction efficiency and total mass of oil added to each replicate. In the main text this outlier was removed (n=2), and the results are displayed in Figure 2.2 B. If we include this outlier (n=3), no significant degradation was observed in the *Acinetobacter*-treated dispersed oil treatments relative to the un-inoculated control ($t = -1.08$, $p = 0.38$, Figure A.3).

Table A.1 Welch's t-test results comparing the mean total protein concentration at the final timepoint for each treatment listed compared to the respective un-inoculated controls (n=3 in all cases).

Treatment		Mean (µg/ml)	t	p-value
Alcanivorax				
	Crude Oil	563.8	17.17	0.004
	Dispersed Oil	618.1	9.4	0.011
	COREXIT	58.3	4.05	0.015
Acinetobacter				
	Crude Oil	1988	36.8	0.0007
	Dispersed Oil	1310	7.79	0.016
	COREXIT	183.2	20.99	0.002

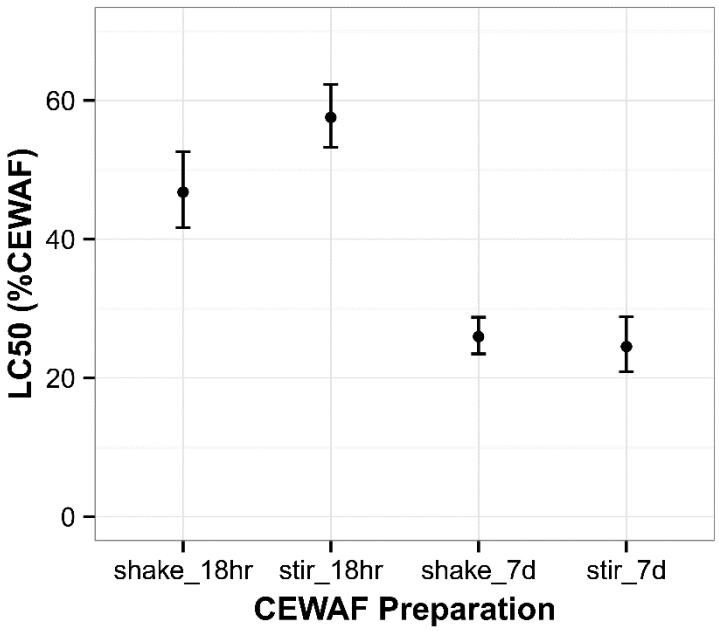

Figure 29 Comparing toxicity results from our modified method for generating WAF compared to Singer et al. (Mar Pollut Bull 40:1007-1016, 2000). Results only include toxicity of the CEWAFs since WAFs were not toxic to Brachionus plicatilis.

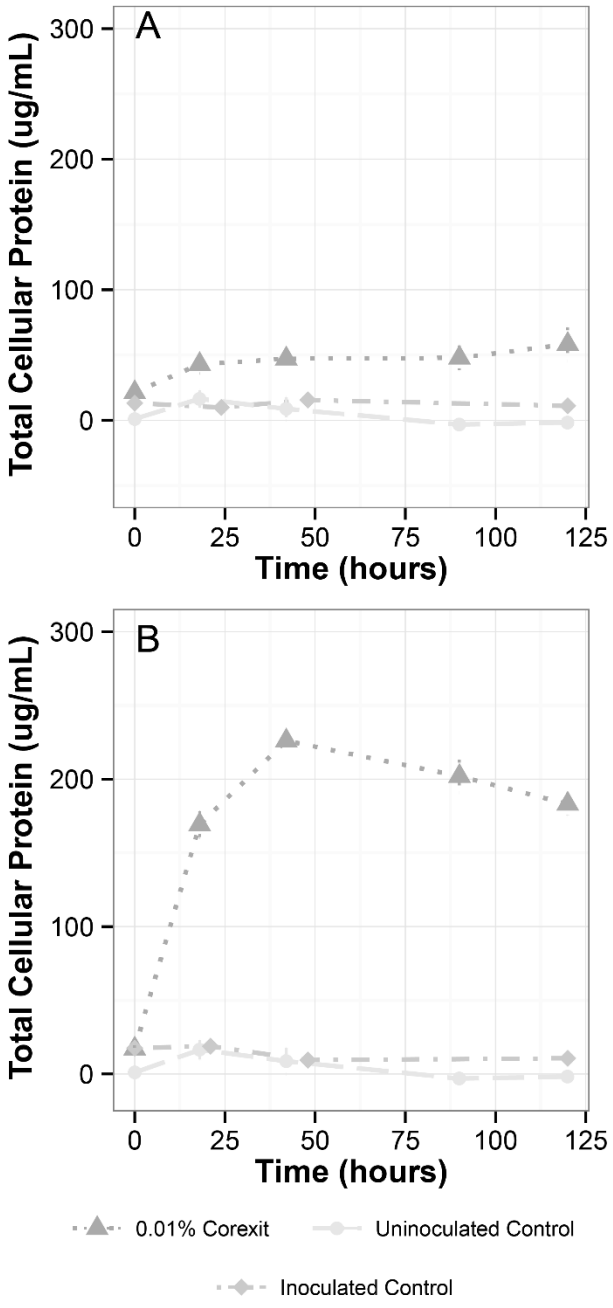

Figure 25 Modified version of Figure 2.1 demonstrating growth of (A) Alcanivorax and (B) Acinetobacter on COREXIT alone.

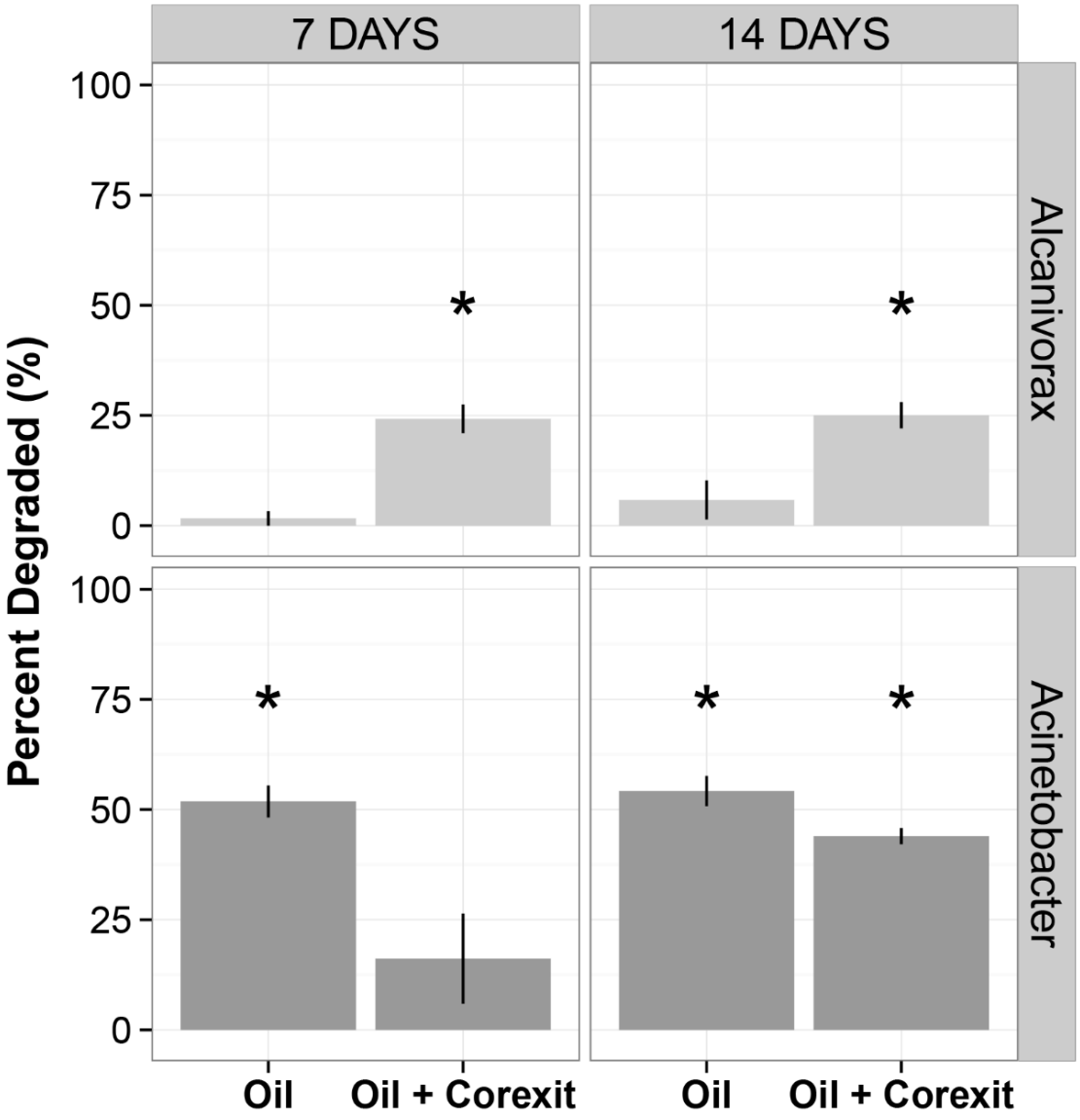

Figure 31 Biodegradation potential of Alcanivorax and Acinetobacter assessed after extending incubation times to 14 days.

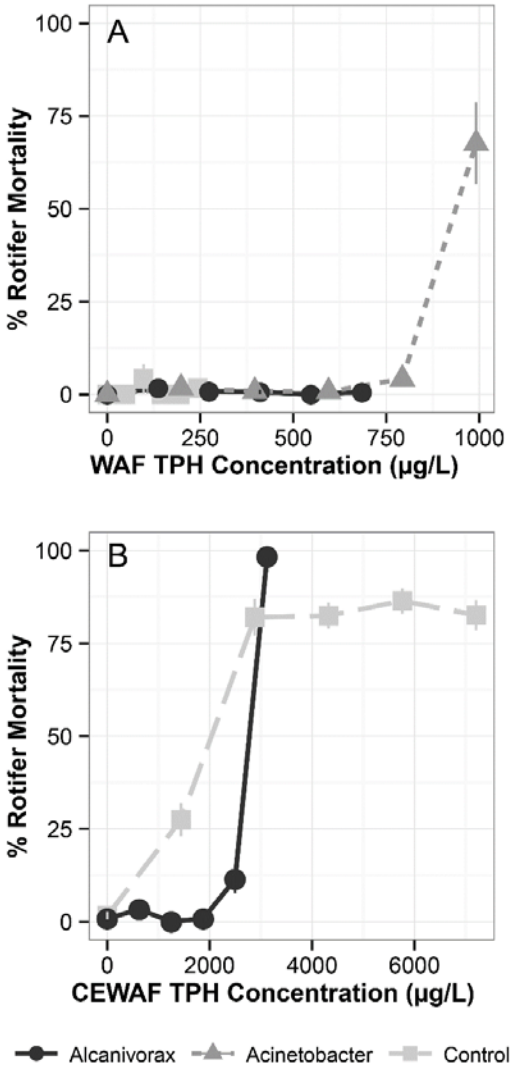

Figure 32 Ecotoxicity of bacterial treated crude oil and dispered crude oil normalized to TPH concentrations using GC/MS values. *Acinetobacter* treated dispersed oil samples were excluded from this figure due to extraction difficulties in separating EPS from hydrocarbons. All toxicity measurements were determined using the marine rotifer *Brachionus plicatilis*. (A) Toxicity associated with 0.5% (v/v) Macondo surrogate crude oil. (B) Toxicity associated with 1:50 COREXIT 9500A dispersed Macondo crude oil.

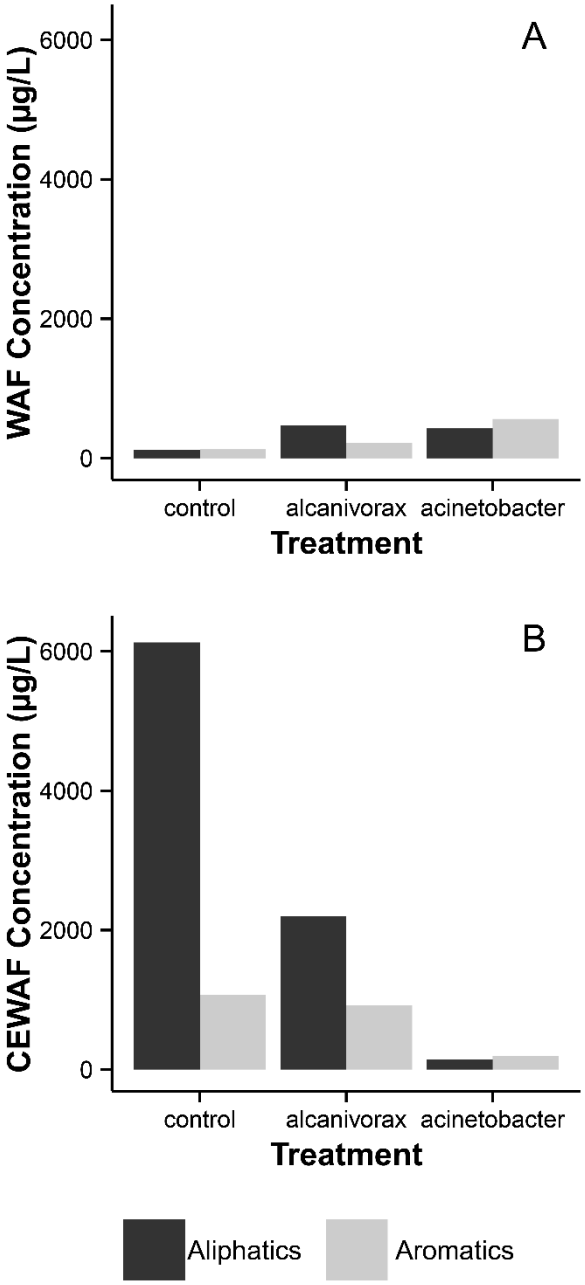

Figure 33 Total aliphatic and aromatic hydrocarbon concentrations in the (A) WAF (crude oil) or (B) CEWAF (dispersed crude oil).

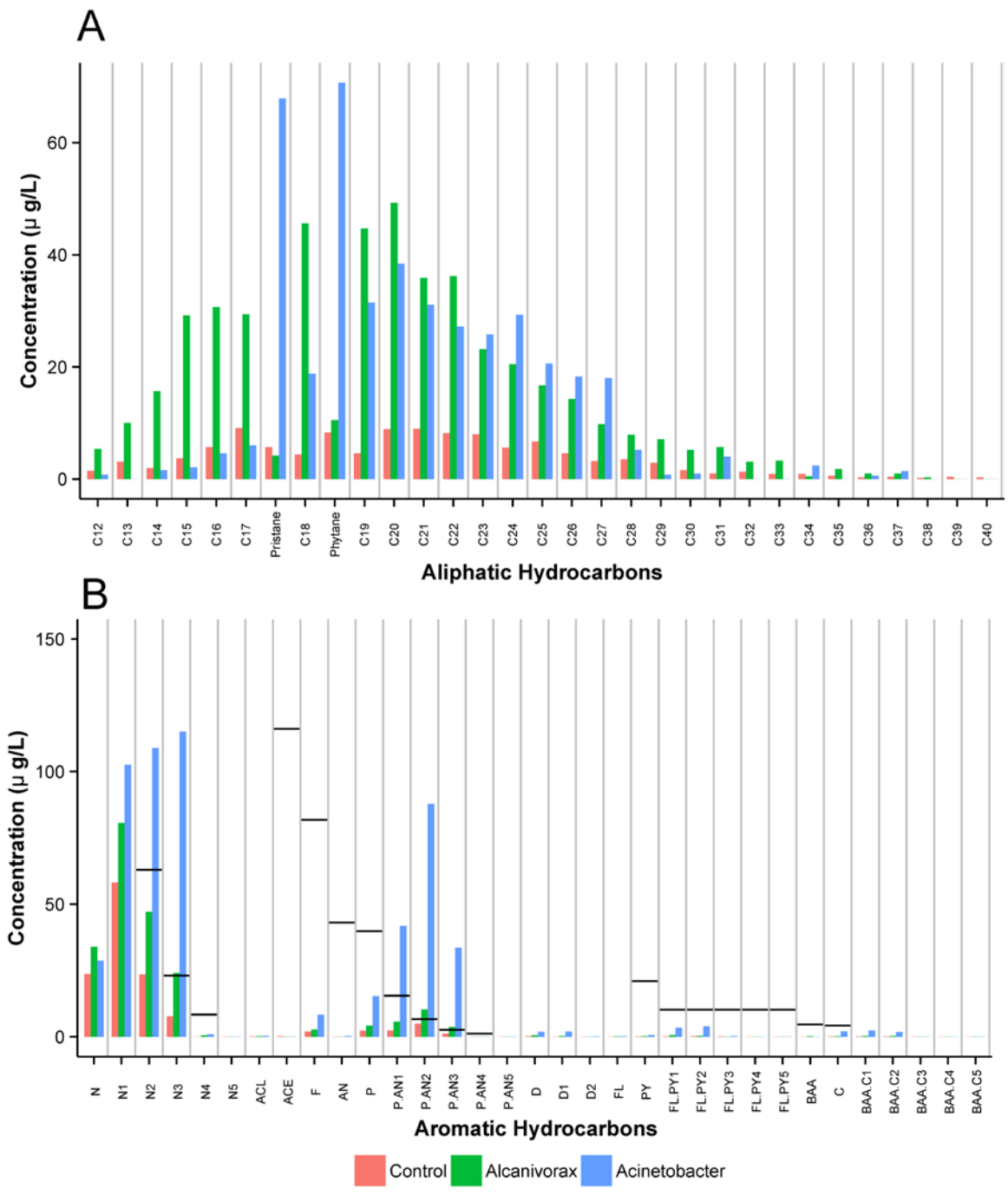
A
Concentration (µ g/L)
0
20
40
60
C12
C13
C14
C15
C16
C17
Pristane
C18
Phytane
C19
C20
C21
C22
C23
C24
C25
C26
C27
C28
C29
C30
C31
C32
C33
C34
C35
C36
C37
C38
C39
C40
Aliphatic Hydrocarbons
B
Concentration (µ g/L)
0
50
100
150
N
N1
N2
N3
N4
N5
ACL
ACE
F
AN
P
P.AN1
P.AN2
P.AN3
P.AN4
P.AN5
D
D1
D2
FL
PY
FL.PY1
FL.PY2
FL.PY3
FL.PY4
FL.PY5
BAA
C
BAA.C1
BAA.C2
BAA.C3
BAA.C4
BAA.C5
Aromatic Hydrocarbons
Control
Alcanivorax
Acinetobacter

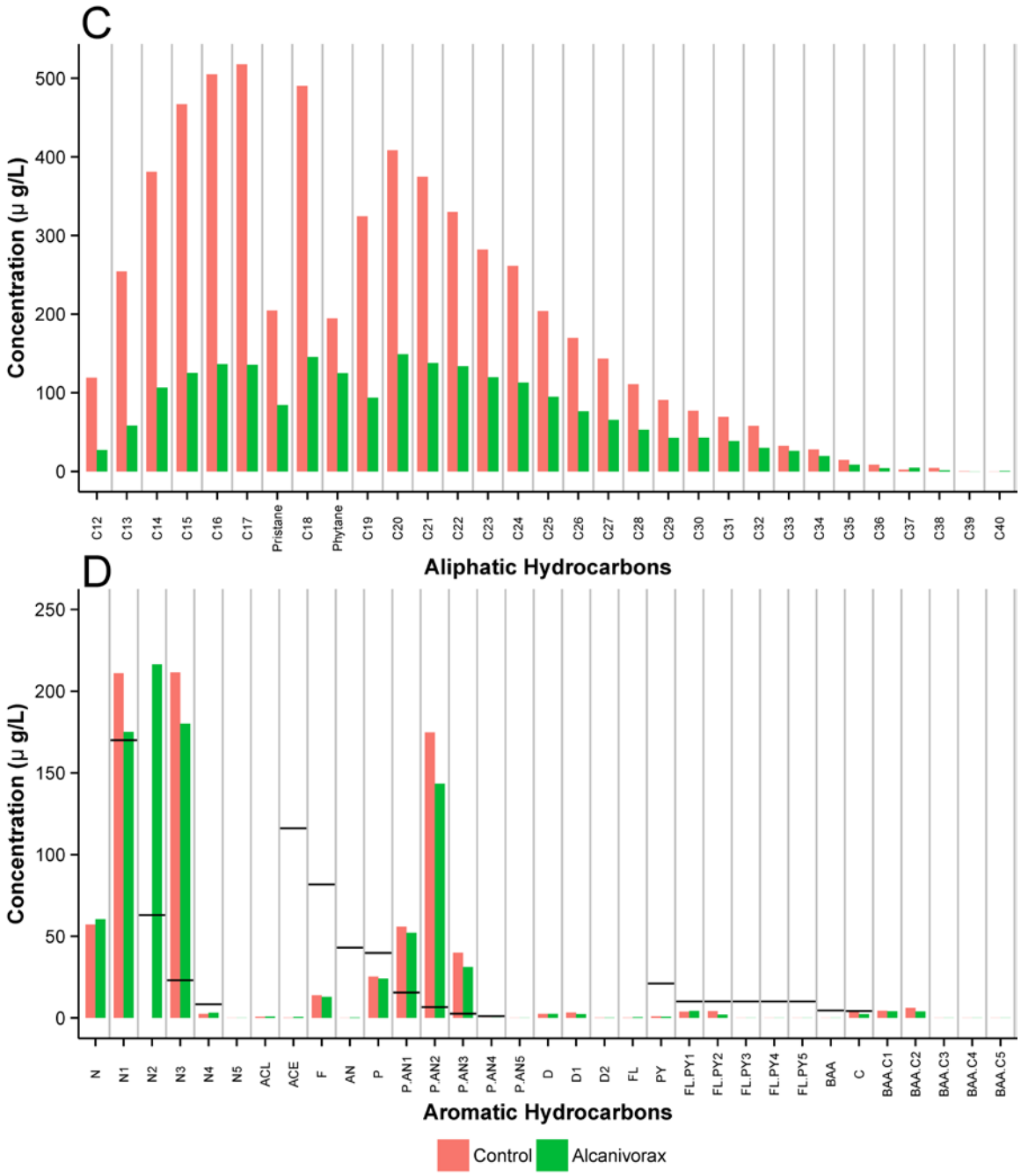

Figure 34 Expanded Figure 2.4: Detailed analysis of aliphatic (A, C) and aromatic (B, D) hydrocarbons present in the water accommodated fraction from the crude oil treatment (A, B) or the chemically enhanced water accommodated fraction from the dispersed oil treatment (C, D). Controls are indicated by red bars, *Alcanivorax* treated samples by green bars, and *Acinetobacter* treated samples by blue bars. *Acinetobacter* treated dispersed oil samples were excluded from this figure due to extraction difficulties in separating EPS from hydrocarbons. EPA acute potency divisor values for aromatic hydrocarbons are indicated on plots B, D by black bars.

APPENDIX B. SUPPLEMENTAL INFORMATION FOR CHAPTER 3

Table B.1 Concentrations of aliphatic and aromatic petroleum hydrocarbons and total petroleum hydrocarbons (TPH) measured in the beach sand layers at Pensacola Beach during the sampling period from 6/30/2010 to 6/16/2011.

Date	Sediment Depth (cm)	Aliphatic hydrocarbons (mg kg^{-1})	Aromatic hydrocarbons (mg kg^{-1})	TPH (mg kg^{-1})
6/30/10	5	14.64	12.55	27.19
	10	11.20	23.71	34.92
	15	156.35	12.71	169.06
	20	58.52	24.73	83.24
	25	137.88	12.68	150.56
	30	6.55	6.02	12.57
	35	0.88	0.50	1.00
6/30/10	5	14.64	12.55	27.19
	10	11.20	23.71	34.92
	15	156.35	12.71	169.06
	20	58.52	24.73	83.24
	25	137.88	12.68	150.56
	30	6.55	6.02	12.57
	35	0.88	0.50	1.00
6/30/10	5	1.79	8.71	10.50
	10	8.57	24.73	33.30
	15	1464.53	284.86	1749.39
	20	21.14	10.55	31.68
	25	1.95	10.56	12.50
	30	1.37	9.57	10.94
7/25/10	5	5.84	39.75	45.59
	10	3.90	22.22	26.12
	15	3.28	17.71	20.98
	20	2.17	21.65	23.82
	25	6.10	35.72	41.83
	30	3.44	49.67	53.11
	35	3.82	31.22	35.04
	40	5.50	18.83	24.34
	45	10.40	42.96	53.37
7/25/10	5	2.38	35.58	37.96
	10	5.65	26.72	32.37
	15	2.32	20.70	23.02
	20	19.31	31.42	50.73
	25	4.12	24.69	28.82
	30	5.78	54.48	60.26

Table B.1 continued

	35	6.25	27.34	33.58
	40	39.37	41.31	80.68
	45	101.60	48.67	150.27
	50	3.93	21.51	25.43
7/25/10	5	3.14	31.92	35.06
	10	3.80	21.72	25.53
	15	5.61	23.97	29.57
	20	5.00	15.85	20.86
	25	3.62	46.40	50.01
	30	2.85	14.82	17.67
	35	6.68	16.68	23.36
	40	4.84	32.66	37.50
	45	12.46	25.88	38.34
9/1/10	5	5.04	9.62	14.66
	10	5.00	15.91	20.90
	15	5.16	14.66	19.82
	20	6.63	22.16	28.78
	25	9.37	10.73	20.10
	30	8.20	2.84	11.03
	35	7.09	10.83	17.92
	40	6.65	8.40	15.05
	45	5.63	40.03	45.66
	50	5.23	21.03	26.26
	55	5.20	23.73	28.93
	60	5.52	20.06	25.58
	65	19.07	33.40	52.47
	70	5.89	6.33	12.22
9/1/10	5	6.21	32.88	39.09
	10	3.09	4.43	7.51
	15	1.78	3.75	5.53
	20	3.99	7.68	11.67
	25	4.33	2.17	6.50
	30	4.08	27.23	31.32
	35	4.48	20.52	25.01
	40	40.61	12.13	52.74
	45	16.75	10.92	27.67
	50	10.74	10.85	21.58
	55	4.82	3.37	8.19
	60	5.65	19.77	25.43
	65	4.72	15.62	20.33
	70	7.82	17.43	25.25
	75	8.55	9.92	18.46
9/1/10	5	7.91	9.87	17.78
	10	3.53	8.09	11.62
	15	3.52	7.51	11.03

Table B1. Continued

	20	6.90	2.93	9.82
	25	3.30	4.02	7.32
	30	2.85	2.80	5.65
	35	10.81	5.55	16.36
	40	4.34	8.55	12.88
	45	10.77	5.86	16.62
	50	4.64	9.51	14.15
	55	5.11	6.45	11.56
	60	4.82	5.18	10.00
	65	7.46	7.09	14.54
	70	6.66	5.64	12.30
10/20/1				
0	5	1.52	0.50	2.02
	10	0.99	0.74	1.74
	15	2.44	6.85	9.29
	20	1.19	0.18	1.37
	25	2.61	1.59	4.20
	30	2.58	1.22	3.80
	35	1.32	3.39	4.71
	40	1.03	1.45	2.48
	45	0.73	0.66	1.39
	50	0.88	1.76	2.64
10/20/1				
0	5	2.04	0.66	2.69
	10	1.98	4.76	6.74
	15	1.70	5.20	6.89
	20	1.87	2.60	4.47
	25	1.00	2.09	3.09
	30	27.58	6.73	34.31
	35	2.33	1.97	4.30
	40	1.48	0.93	2.41
	45	4.19	2.81	7.00
10/20/1				
0	5	0.85	7.92	8.77
	10	0.90	1.38	2.28
	15	1.68	8.18	9.86
	20	1.58	14.78	16.36
	25	0.93	5.91	6.84
	30	0.92	12.69	13.61
	35	1.24	10.66	11.90
	40	1.28	12.41	13.68
	45	1.87	16.23	18.10
	50	1.82	5.65	7.48
	55	1.39	1.12	2.51
	60	0.80	0.53	1.33

Table B.1 continued

	65	0.67	1.39	2.05
12/2/10	5	0.49	16.77	17.27
	10	0.41	12.56	12.97
	15	0.32	8.21	8.53
	20	0.40	9.98	10.38
	25	0.30	10.50	10.80
	30	0.56	23.79	24.35
	35	0.50	20.66	21.16
	40	0.25	25.82	26.07
	45	0.46	15.77	16.23
	50	0.38	13.24	13.62
	55	0.31	10.74	11.05
12/2/10	5	2.40	0.72	3.12
	10	2.55	2.43	4.98
	15	0.31	3.75	4.07
	20	0.23	2.66	2.89
	25	0.13	4.15	4.29
	30	0.31	8.01	8.32
	35	0.78	2.27	3.06
	40	0.26	2.14	2.40
	45	0.22	6.53	6.75
	50	0.22	1.38	1.60
	55	0.27	0.51	0.78
	60	0.22	1.15	1.37
	65	0.75	8.27	9.02
12/2/10	5	0.88	23.79	24.67
	10	0.71	3.24	3.95
	15	1.05	12.46	13.52
	20	1.81	15.58	17.39
	25	0.95	12.80	13.75
	30	0.63	17.36	17.99
	35	1.12	31.35	32.47
	40	0.83	23.71	24.54
	45	0.60	13.77	14.37
	50	0.63	26.70	27.33
1/19/11	5	0.69	7.82	8.51
	10	1.77	9.99	11.77
	15	1.45	8.86	10.31
	20	1.55	10.06	11.61
	25	1.36	8.98	10.34
	30	1.42	10.43	11.85
	35	1.62	9.95	11.58
	40	0.87	8.83	9.70
	45	1.00	7.92	8.92
	50	0.70	7.66	8.37

Table B.1 continued

1/19/11	5	0.57	0.43	1.00
	10	0.41	1.00	1.41
	15	0.48	0.48	0.96
	20	0.78	1.25	2.02
	25	0.88	1.10	1.98
	30	0.81	1.87	2.68
	35	0.75	0.39	1.15
	40	1.04	9.18	10.22
	45	0.68	1.12	1.81
1/19/11	5	0.20	0.34	0.54
	10	0.22	1.34	1.57
	15	0.54	0.83	1.37
	20	0.26	0.32	0.58
	25	0.14	0.64	0.79
	30	0.56	0.83	1.39
	35	0.43	0.86	1.29
	40	0.44	0.94	1.38
	45	0.41	0.42	0.84
	50	0.48	0.70	1.17
	55	0.20	0.39	0.59
3/2/11	5	0.69	0.20	0.89
	10	0.39	0.43	0.81
	15	0.28	0.19	0.47
	20	0.32	0.26	0.58
	25	0.53	0.23	0.76
	30	0.50	0.45	0.95
	35	0.71	0.39	1.10
	40	0.28	0.24	0.52
	45	0.56	0.48	1.04
	50	11.78	1.09	12.87
	55	0.91	1.65	2.56
	60	1.25	1.77	3.02
3/2/11	5	0.31	1.11	1.42
	10	1.78	0.30	2.08
	15	0.32	0.62	0.93
	20	0.34	0.34	0.68
	25	0.29	4.96	5.25
	30	0.44	0.39	0.83
	35	0.46	2.34	2.80
	40	0.30	0.92	1.23
	45	0.43	1.57	2.00
3/2/11	5	0.70	0.28	0.98
	10	1.17	1.33	2.49
	15	1.18	0.13	1.31
	20	1.05	0.88	1.93

Table B.1 continued

	25	7.46	0.90	8.36
	30	0.92	0.76	1.68
	35	1.20	0.20	1.41
	40	1.09	0.63	1.72
	45	0.98	1.05	2.03
	50	1.91	0.31	2.22
	55	2.46	0.55	3.01
4/21/11	5	0.56	0.29	0.85
	10	0.11	0.24	0.35
	15	0.13	0.17	0.30
	20	2.70	41.31	44.02
	25	0.56	0.63	1.19
	30	0.18	0.02	0.21
	35	0.17	0.65	0.82
	40	0.31	0.71	1.02
	45	0.44	0.38	0.82
	50	0.60	0.31	0.91
	55	8.24	1.37	9.61
	60	1.25	11.08	12.33
	65	0.52	0.43	0.95
4/21/11	5	0.16	0.32	0.47
	10	0.24	0.68	0.92
	15	0.18	0.12	0.29
	20	0.29	0.17	0.46
	25	0.16	0.41	0.57
	30	0.30	0.07	0.37
	35	0.34	0.45	0.79
	40	0.47	0.52	1.00
	45	0.21	0.15	0.36
	50	0.25	0.17	0.42
	55	0.03	1.91	1.94
	60	0.22	0.12	0.34
	65	4.59	0.70	5.30
	70	0.54	0.69	1.22
4/21/11	5	0.43	0.33	0.76
	10	0.41	0.35	0.76
	15	0.38	0.21	0.58
	20	0.76	0.30	1.07
	25	0.36	0.26	0.61
	30	0.57	0.32	0.89
	35	0.29	0.26	0.55
	40	0.30	0.26	0.55
	45	0.44	0.43	0.87
	50	3.54	2.02	5.56
	55	0.18	0.02	0.19

Table B.1 continued

	60	0.15	0.19	0.34
6/16/11	5	1.66	0.79	2.45
	10	1.60	18.48	20.08
	15	1.30	5.36	6.67
	20	0.58	15.89	16.47
	25	0.97	0.29	1.26
	30	0.96	1.94	2.89
	35	0.20	0.62	0.83
	40	0.24	1.88	2.12
	45	0.15	1.43	1.58
	50	0.18	0.69	0.88
	55	0.21	0.59	0.81
	60	0.16	0.48	0.64
6/16/11	5	2.20	1.21	3.40
	10	0.25	0.55	0.80
	15	0.39	7.58	7.97
	20	0.56	0.60	1.16
	25	6.80	1.41	8.22
	30	0.60	0.91	1.52
	35	0.29	0.33	0.61
	40	1.16	1.98	3.14
	45	0.42	0.56	0.98
	50	0.52	0.69	1.22
	55	0.55	0.82	1.38
	60	0.52	0.44	0.96
6/16/11	5	0.30	1.14	1.44
	10	0.17	1.05	1.22
	15	0.22	2.07	2.29
	20	0.20	0.69	0.89
	25	0.17	1.50	1.67
	30	0.20	1.51	1.71
	35	0.27	0.73	1.00
	40	0.28	0.81	1.09
	45	0.23	0.26	0.49
	50	0.19	0.48	0.67
	55	0.27	0.98	1.25
	60	0.30	0.77	1.07
	65	0.28	0.35	0.63

Table B.2 Decay rate coefficients and their standard errors calculated for aliphatics (Ali), aromatics (Aro) and total petroleum hydrocarbons (TPH) in the contaminated Pencacola Beach sands. Upper table depicts coefficients for the period 30 June 2010 to 20 October 2010. Lower table depicts coefficients calculated for the period 2 December 2010 to 16 June 2011.

Pre-cleaning

Sediment depth interval		Ali		Aro		TPH	
Upper limit (cm)	Lower limit (cm)	Coef. (d^{-1})	SE (d^{-1})	Coef. (d^{-1})	SE (d^{-1})	Coef. (d^{-1})	SE (d^{-1})
0	5	0.013	0.004	0.024	0.007	0.019	0.003
5	10	0.015	0.004	0.023	0.005	0.020	0.004
10	15	0.027	0.007	0.016	0.008	0.023	0.008
15	20	0.019	0.004	0.022	0.016	0.020	0.011
20	25	0.019	0.010	0.019	0.005	0.021	0.009
25	30	0.008	0.003	0.018	0.009	0.011	0.005
30	35	0.007	0.001	0.020	0.006	0.018	0.004
35	40	0.025	0.013	0.028	0.017	0.027	0.015
40	45	0.024	0.012	0.021	0.015	0.022	0.014
45	50	0.028	0.013	0.031	0.029	0.031	0.024
	Max	0.028		0.031		0.031	
	Min	0.007		0.016		0.011	
	AV	0.019		0.022		0.021	
	SD	0.008		0.005		0.005	

Post-cleaning

Sediment depth interval		Ali		Aro		TPH	
Upper limit (cm)	Lower limit (cm)	Coef. (d^{-1})	SE (d^{-1})	Coef. (d^{-1})	SE (d^{-1})	Coef. (d^{-1})	SE (d^{-1})
0	5	0.008	0.009	0.011	0.008	0.011	0.001
5	10	0.009	0.004	0.015	0.015	0.015	0.012
10	15	0.006	0.004	0.022	0.012	0.018	0.010
15	20	0.002	0.005	0.021	0.016	0.016	0.013
20	25	0.003	0.003	0.014	0.005	0.011	0.002
25	30	0.002	0.003	0.016	0.005	0.012	0.003
30	35	0.007	0.001	0.015	0.006	0.014	0.006
35	40	0.005	0.003	0.015	0.001	0.013	0.003
40	45	0.005	0.004	0.017	0.003	0.014	0.004
45	50	0.000	0.004	0.012	0.008	0.010	0.008
	Max	0.009		0.022		0.018	
	Min	0.000		0.011		0.010	
	AV	0.005		0.016		0.013	
	SD	0.003		0.003		0.002	

APPENDIX C. SUPPLEMENTAL INFORMATINO FOR CHAPTER 4

C.1 Methods

SSU rRNA Gene Sequencing

All samples from 2012-2013 were generated by the Michigan State University sequencing facility. Raw DNA extracts were transferred frozen and were amplified with barcoded 515F/806R primers according the Earth Microbiome Project standard protocol (Caporaso et al., 2012; http://www.earthmicrobiome.org/emp-standard-protocols/16s/). A total of 5 MiSeq 2x250 bp runs were performed and demultiplexed sequences were transferred to Georgia Institute of Technology. Samples collected from 2014-2015 were processed in house using the same primer set targeting the V4 region, however, we employed the Fluidigm Access Array kit to barcode the samples post-PCR amplification. Multiplexed samples were pooled at equimolar ratios and paired-end sequenced (2x250 bp) on an Illumina MiSeq following the protocol outlined in by Green and colleagues (Green *et al.*, 2015). In brief, the 515F/806R primer set was modified with linker sequences at the 5' ends of each primer and the V4 SSU rRNA gene region was amplified. A second stage PCR was performed using a primer set that contains the Illumina sequencing adapters along with sample-specific barcodes (multiplexing stage). At this stage, sample amplicons were pooled at an equimolar ratio and were ready for sequencing.

C.2 Results

Populations Specific Niche Differences

MG-I Archaea

Using the full dataset, the most abundant MG-I OTU (denovo3, 93% identity to *N. maritimus*) dominated sites sampled at approximately 1000 m water depth (Figures 6, Figure S6), while denovo25 (98% to *N. maritimus*) was abundant in the deepest sites. Conversely, denovo19 and denovo21 (97%, 99% to *N. maritimus* respectively) were most abundant at the shallowest sites. However, all four were abundant in surficial sediments across the entire Gulf and did not have a strong differential response to sediment column depth as was found by Durbin and Teske (2010). Instead of oxygen concentrations dictating the niches of these specific OTU (e.g. specific adaptation to low oxygen concentrations), it may be organic matter quantity and quality that structure the niches, as has been shown in surficial sediments in Antarctica (Learman *et al.*, 2016). While water depth best explains these patterns, which governs organic matter inputs in the Gulf, there were latitudinal and longitudinal differences in the dominant MG-I OTU (Figures S2, S6). However, these smaller shifts due to spatial variation were also likely driven by organic matter quality and quantity, which vary based on proximity to the Mississippi river delta across the Gulf (Goñi et al., 1997).

Gammaproteobacteria

Our most abundant Gammaproteobacteria OTU (denovo1) was 96% similar to the only isolated strain, *Woeseia oceani*, and showed maximum relative abundances just below the

oxic-anoxic interface and in deeper water sites, similar to members of the Planctomycetacia group (Figure 6, Figure S7). *Woeseia*-like population may be respiring nitrate or nitrite coupled with chemoorganoheterotrophy (Dyksma *et al.*, 2016; Mußmann *et al.*, 2017). Unlike denovo1, the remaining dominant Gammaproteobacterial OTU were most abundant in surficial, aerobic sediments of the deep ocean, although their abundances also increased with increasing water depth (Figure 6, S3, S7). Denovo14 and denovo15 were both assigned to the JTB255/*Woeseiaceae* group (95% and 98% similarity to denovo1 respectively). The second most abundant OTU, denovo2, was divergent from the JTB255 group and showed 93% sequence identity to denovo1. The closest BLAST hit was to the isolated strain *Thioprofundum hispidum*, at 94% sequence identity. It was < 95% sequence identity to denovo14 and denovo15, although they exhibit similar distribution patterns. While the phylogenetic identity of denovo2 was less certain, *T. hispidum* was characterized as a chemolithoautotrophic sulfur-oxidizing strain within the Chromatiales order (Mori *et al.*, 2011). With the observed distribution patterns, these 3 OTU (denovo14, 15, 2) were likely utilizing oxygen as a terminal electron acceptor either for chemolithoautotrophic processes observed within *Thioprofundum spp.* coupled with sulfur oxidation or as aerobic chemoorganotrophs as observed in the JTB255/*Woeseiaceae* group (Mori *et al.*, 2011; Mußmann *et al.*, 2017).

Deltaproteobacteria

Similar to the Gammaproteobacteria, little overlap was observed between Deltaproteobacterial OTU associated with the shallower sites and those in the deeper sites. In deep ocean sediments, most of the sequences affiliated with Deltaproteobacteria, belong to denovo0. This was the most abundant OTU detected in our dataset, and its relative

abundance increased with increasing sediment depth. Interestingly, maximum relative abundance of denovo0 was found at intermediate water column depths (1000 – 1200 m) (Figure 6, S8). Although not closely affiliated to any cultivated strain, denovo0 was most similar to *Syntrophobacter fumaroxidans* at 91% and assigned to the *Syntrophobacteraceae* family by SILVA. The family consists of strictly anaerobic fermentative or sulfate respiring members that are broadly distributed (Kuever, 2014). The other dominant deep ocean sediment Deltaproteobacterial OTU, denovo16 (<90% similarity to denvo0), showed similar a distribution to denovo0, and did not decrease with increasing water depth. Denovo16 showed 91% sequence similarity to *Deferrisoma camini*, a thermophilic strictly anaerobic iron-reducing bacterium, within the uncharacterized and uncultivated NB1-J group. In the shallow sites, denovo89 and denovo50 were very abundant throughout the sediment column (Figure S8). Denovo50 shares 96% identity to *Desulfatiglans aniline*, and was more abundant in the shallow SGoM than the shallow NGoM, and was not abundant at deeper sites. Of note, denovo89 was closely affiliated (98% identity) with the deep ocean OTU denovo0, and thus also likely represents a poorly characterized population within the *Syntrophobacteraceae* family.

Planctomycetacia

All dominant OTU affiliated with the Planctomycetacia were closely related to *Candidatus Scalindua* spp (99-100%). These dominant OTU are likely anaerobic ammonium oxidizing bacteria (anammox), which are chemoautotrophic, ubiquitously found in anoxic systems, and couple the oxidation of ammonium with nitrite as the electron acceptor (Penton *et al.*, 2006; Oshiki *et al.*, 2016). Members from this genus tend to be psychrophilic, and are inhibited by low sulfide concentrations (4-100 µM), which potentially explains their depth

limits in our study, although it may also be due to ammonium or nitrite availability (Oshiki *et al.*, 2016). The Planctomycetes were nearly absent in the shallowest sites, and absent in surficial sediments, in agreement with previous studies that indicate ca. *Scalindua* is more abundant in oligotrophic systems (Canion *et al.*, 2014; Learman *et al.*, 2016). All dominant Planctomycetes OTU tended to reach a maximal relative abundance at mid-sediment depths below the oxic-anoxic interface with an overlapping distribution to the *Nitrosopumulis*-like OTUs (Figures 6, S3, S9). Ammonium oxidizing archaea may provide a nitrite source *Scalindua*, and the mostly exclusive zonation patterns observed may limit direct competition for ammonium (Lipsewers *et al.*, 2014). In some sites, a clear "bubble" in abundance surrounded this zone, while in other sites they persist through the top 10-20 cm (Figures 6, S3, S9). Denovo4 tended to be more abundant with increasing water depth, while denovo11 had higher relative abundances in the 600-1200 m water depth range. Denovo18 was co-localized with denovo4 although this population tended to be deeper in the sediment profile (Figure 6). Previous studies focusing on surficial sediments typically found low Planctomycetacia abundances (Schauer *et al.*, 2010; Bienhold *et al.*, 2016; Learman *et al.*, 2016) while studies that included a larger depth range, or core profiles found higher abundances with depth than at the surface (Zinger *et al.*, 2011; Canion *et al.*, 2014).

Phycisphaerae

The dominant Phycisphaerae OTU were only abundant in the deep ocean and different OTU were present in the shallower sites (Figures 5, S10). All increased in relative abundance with increasing sediment depth and were only present below the aerobic to anaerobic transition zone. These OTU were more relatively abundant in the NGoM than

the SGoM although the same OTUs were detected in both regions (Figures 6, S3, S10). The more abundant OTU, denovo42, was affiliated with an uncharacterized family, MSBL9, in SILVA taxonomy with no closely related named strains (< 80% sequence identity) although closest BLAST hits were from anaerobic marine sediments with a 100% 16S clone sequence from Gulf of Mexico sediments (Reed *et al.*, 2006). Denovo110 was also affiliated with and uncharacterized family, MLA10 with close BLAST hits from clone sequences generated from anoxic marine sediments.

Table C.1 List of all sites used in this study.

Sampling Site	Water Depth (m)	Latitude	Longitude	Number of Unique Samplings	Number of Years	16S Sequences	Oxygen Profile
Abkatum	50	19.314270	-92.208000	1	1	Y	Y
AC-1	490	29.474500	-86.958700	1	1	Y	Y
AC-2	845	29.297600	-86.996800	1	1	Y	Y
AC-4	1732	29.000300	-87.507400	1	1	Y	Y
AC-5	1850	28.940100	-87.582400	1	1	Y	Y
DSH07	400	29.255817	-87.732383	1	1	Y	Y
DSH08	1100	29.122783	-87.867733	1	1	Y	Y
DSH08	1100	29.122783	-87.867733	3	3	Y	Y
DSH09	2290	28.636500	-87.868500	2	2	Y	Y
DSH10	1500	28.979050	-87.891617	4	4	Y	Y
DWH01	1500	28.736669	-88.387161	2	2	Y	Y
IWX250	583	19.430680	-93.094970	1	1	Y	Y
IXN500	1200	20.014000	-92.389000	1	1	Y	Y
IXTOC	60	19.370080	-92.317180	2	1	Y	Y
IXW500	1010	19.443000	-93.889000	1	1	Y	Y
IXW750	1470	19.458000	-94.587000	1	1	Y	Y
LT1	16	18.808000	-92.057000	1	1	Y	Y
LT2	21	19.061000	-92.127000	1	1	Y	Y
MV02	541	28.494167	-89.779367	2	2	Y	Y
PCB06	990	29.122700	-87.266217	3	3	Y	Y
PCB06	990	29.122700	-87.266217	1	1	Y	Y
S35	670	29.333600	-87.050200	1	1	Y	Y

Table C.1 continued

S36	1841	28.916400	-87.669100	1	1	Y	Y
SE02	972	28.359167	-86.944267	1	1	Y	Y
SEEP-A	1110	29.043000	-87.282400	1	1	Y	No
SEEP-C	1116	28.990000	-88.045500	1	1	Y	No
SL1040	50	29.196050	-88.868833	3	3	Y	Y
SL33-750	1300	22.415000	-91.785000	1	1	Y	Y
SW01	1192	28.220867	-89.069500	4	4	Y	Y
SL26A250	500	21.199	-96.851	1	1	No	Y
SL26A750	1500	21.37	-96.559	1	1	No	Y
IXNW1600	3200	20.804	-94.803	1	1	No	Y
23-92	3700	23	-92	1	1	No	Y
SL33-200	400	22.333	-91.7	1	1	No	Y
SL31A-1000	2200	20.718	-93.137	1	1	No	Y
IXN1000	2200	20.345	-92.137	1	1	No	Y
IXN750	1650	20.172	-92.423	1	1	No	Y
IXN250	800	19.912	-92.342	1	1	No	Y
IXN100	400	19.817	-92.349	1	1	No	Y
SL31-100	200	21.038	-92.46	1	1	No	Y
Ixtoc 1	50	19.366	-92.313	1	1	No	Y
Abkatun	50	19.913	-92.206	1	1	No	Y
LT3	50	19.36	-92.28	1	1	No	Y
IXNW350	700	19.645	-92.741	1	1	No	Y
IXW250	580	19.429	-93.094	1	1	No	Y
SL30A-100	200	18.936	-93.36	1	1	No	Y
SL30-500	920	19.071	-94.433	1	1	No	Y
SL30-250	510	18.866	-94.433	1	1	No	Y
SL30-100	200	18.7	-94.433	1	1	No	Y
SL28-750	1500	19.324	-95.594	1	1	No	Y
SL28-500	1000	19.224	-95.696	1	1	No	Y
SL27-750	1500	20.12	-96.133	1	1	No	Y
SL27-500	1000	20.085	-96.233	1	1	No	Y
SL26-750	1533	21.37648	-96.57455	1	1	No	Y
SL26-500	953	21.27383	-96.72933	1	1	No	Y
SL25-750	1603	24.15995	-96.39425	1	1	No	Y
SL25-500	952	24.21741	-96.82131	1	1	No	Y
PCB06	990	29.1227	-87.26622	1	1	No	Y
PCB03	100	29.73833	-86.33833	1	1	No	Y
SL7150	200	29.56833	-86.57833	1	1	No	Y
MC04	400	29.30575	-86.67637	1	1	No	Y
DSH08	1100	29.12278	-87.86773	1	1	No	Y

Table C.1 continued

DSH07	400	29.25582	-87.73238	1	1	No	Y
SL1040	50	29.19605	-88.86883	1	1	No	Y
DWH01	1500	28.73667	-88.38716	1	1	No	Y
HC01	45	28.38413	-90.53097	1	1	No	Y
MV02	541	28.49417	-89.77937	1	1	No	Y
SW01	1192	28.22087	-89.0695	1	1	No	Y
SW03	1196	28.57558	-88.80043	1	1	No	Y
SE02	972	28.35917	-86.94427	1	1	No	Y
DSH09	2290	28.6365	-87.8685	1	1	No	Y
S36	1841	28.9164	-87.6691	1	1	No	Y
NT800	789	28.056	-85.93351	1	1	No	Y
MC06	600	29.08355	-86.91452	1	1	No	Y
SL8100	200	29.70167	-87.19167	1	1	No	Y
SL1460	120	29.45648	-87.45088	1	1	No	Y
DSH10	1500	28.97905	-87.89162	1	1	No	Y
PCB09	1000	28.85912	-87.21468	1	1	No	Y
SL11150	300	29.03785	-88.64423	1	1	No	Y
MV03	800	28.39825	-89.59938	1	1	No	Y
SL16150	200	28.63537	-90.0015	1	1	No	Y

Table C.2 Analysis of variance table for multiple linear regressions used in this study.

	Df	Sum Sq	Mean Sq	F value	Pr(>F)	Percent Variance Explained
water_dif	1	1475.448	1.48E+03	129176.4	0	22.09
sed_dif	1	951.5594	9.52E+02	83309.6	0	14.25
geo_dist	1	405.9833	4.06E+02	35544.09	0	6.08
same_date	1	328.1475	3.28E+02	28729.52	0	4.91
water_dif:sed_dif	1	101.5731	1.02E+02	8892.788	0	1.52
Residuals	299145	3416.824	1.14E-02	NA	NA	51.15

Full best fit model

	Df	Sum Sq	Mean Sq	F value	Pr(>F)	Percent Variance Explained
water_dif	1	1475.45	1.48E+03	136850.79	0.0E+00	22.09
sed_dif	1	951.56	9.52E+02	88259.06	0.0E+00	14.25
geo_dist	1	405.98	4.06E+02	37655.77	0.0E+00	6.08
same_date	1	328.15	3.28E+02	30436.35	0.0E+00	4.91
water_dif:sed_dif	1	101.57	1.02E+02	9421.11	0.0E+00	1.52
water_dif:geo_dist	1	0.83	8.26E-01	76.60	2.1E-18	0.01
sed_dif:geo_dist	1	16.57	1.66E+01	1536.90	0.0E+00	0.25
water_dif:same_date	1	55.50	5.55E+01	5147.61	0.0E+00	0.83
sed_dif:same_date	1	6.67	6.67E+00	618.97	1.7E-136	0.10
geo_dist:same_date	1	93.49	9.35E+01	8671.52	0.0E+00	1.40
water_dif:sed_dif:geo_dist	1	3.11	3.11E+00	288.75	1.0E-64	0.05
water_dif:sed_dif:same_date	1	1.31	1.31E+00	121.58	2.9E-28	0.02
water_dif:geo_dist:same_date	1	5.82	5.82E+00	540.25	2.1E-119	0.09
sed_dif:geo_dist:same_date	1	2.55	2.55E+00	236.91	1.9E-53	0.04
water_dif:sed_dif:geo_dist:same_date	1	5.86	5.86E+00	543.22	4.8E-120	0.09
Residuals	299135	3225.105	1.08E-02	NA	NA	48.28

Table C.3 Sequential analysis of variance of multiple linear regression models. Model 5 represents the model that explains the most variance, while model 6 is the simplified model using only terms that explain >1% of the variance. Water = water depth, sed = sediment depth, distance = geographic distance between sites, environment = binary factor representing N of S Gulf of Mexico, date = factor for sampling date (5 sampling timepoints).

	Res.Df	RSS	Df	Sum of Sq	F	Pr(>F)
1. water	299149	5204.1				
2. water * sed	299147	4150.5	2	1053.58	48860.7	< 2.2e-16
3. water * sed * distance	299143	3726	4	424.51	9843.6	< 2.2e-16
4. water * sed * environment	299143	3786.5	0	-60.5		
5. water * sed * distance * date	299135	3225.1	8	561.39	6508.7	< 2.2e-16
6. water + sed + distance + date + water:sed	299145	3416.8	-10	-191.72	1778.2	< 2.2e-16

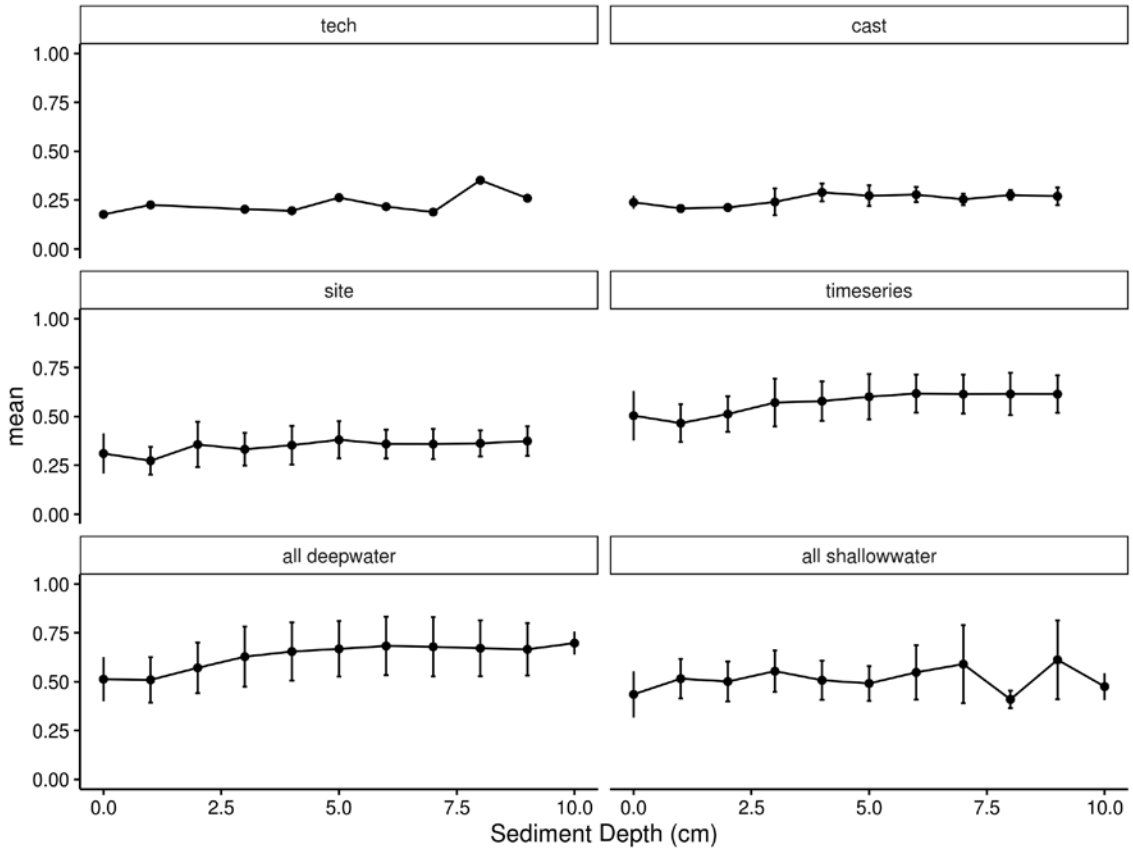

Figure 30 Changes in microbial community similarity at different levels of replication. Pairwise Bray-Curtis similarities were calculated for every sample, and samples were binned into 1 cm depth increments to enable cross study comparisons. Average replicate level dissimilarity value is shown in the top right of each plot with the standard deviation. Error bars represent standard deviation about the mean for each sediment depth bin. (A) The same core (AC-5) depth sections were independently extracted and sequenced in duplicate. (B) For three sites, within 1 multicorer cast, triplicate cores were extruded and depth sections were extracted and sequenced. This represents variation within 1m2 of the seafloor. (C) For 10 sites, triplicate multicore deployments were performed, 1 core from each deployment was extruded, and DNA extractions and sequencing was performed on the sections. This represents community variation of tens to hundreds of square meters on the seafloor. (D) Seven sites were sampled over multiple cruises. (E) All sites sampled at water depths > 800m, representing the deep Gulf of Mexico. (F) All sites sampled at water depths less than 100m, representing the shallow Gulf of Mexico.

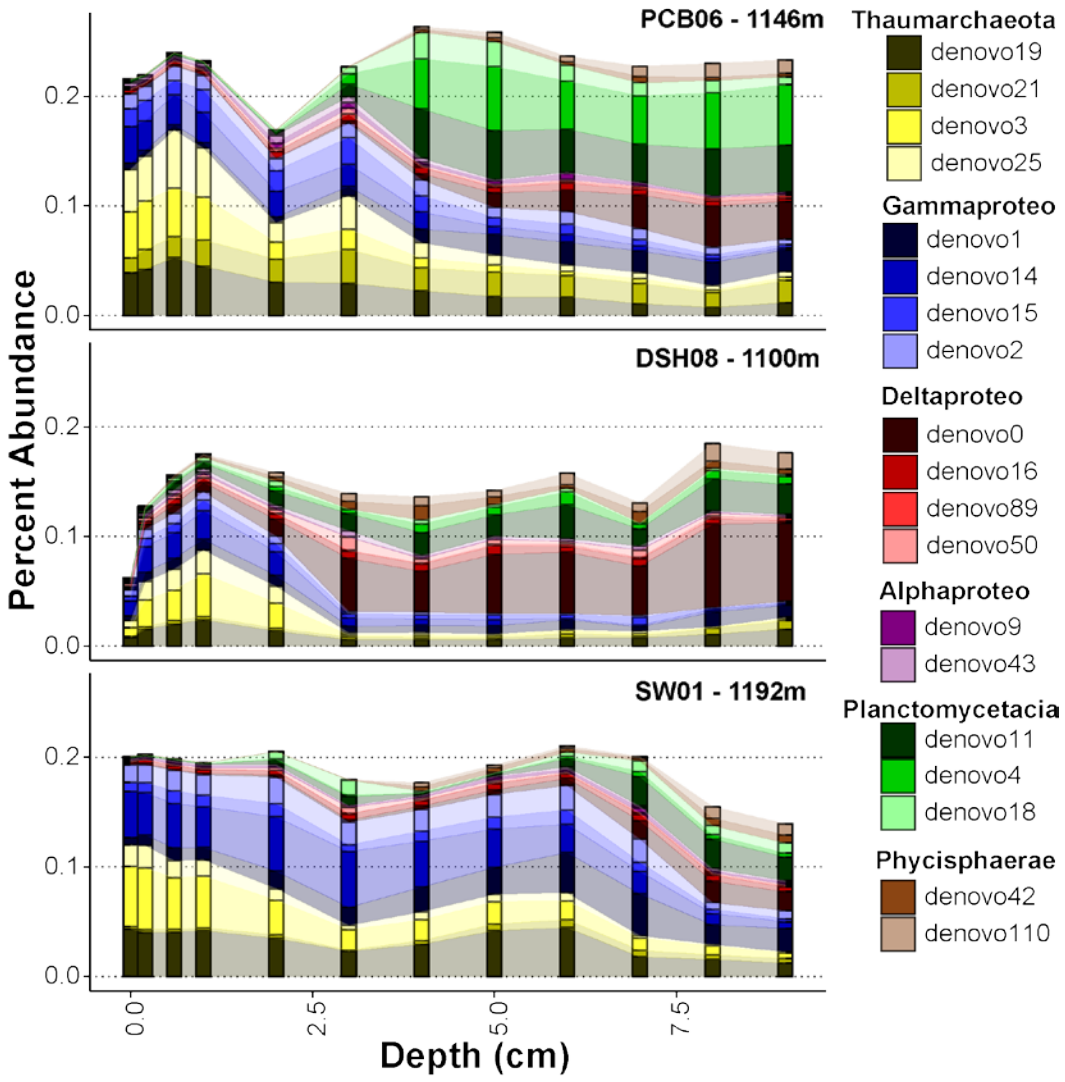

Figure 31 Core profiles representing an East to West transect sampled at approximately 1100m water depth in the Northern Gulf of Mexico showing population (OTU) level distributions. Core profiles are arranged from the eastern most site to the western most site.

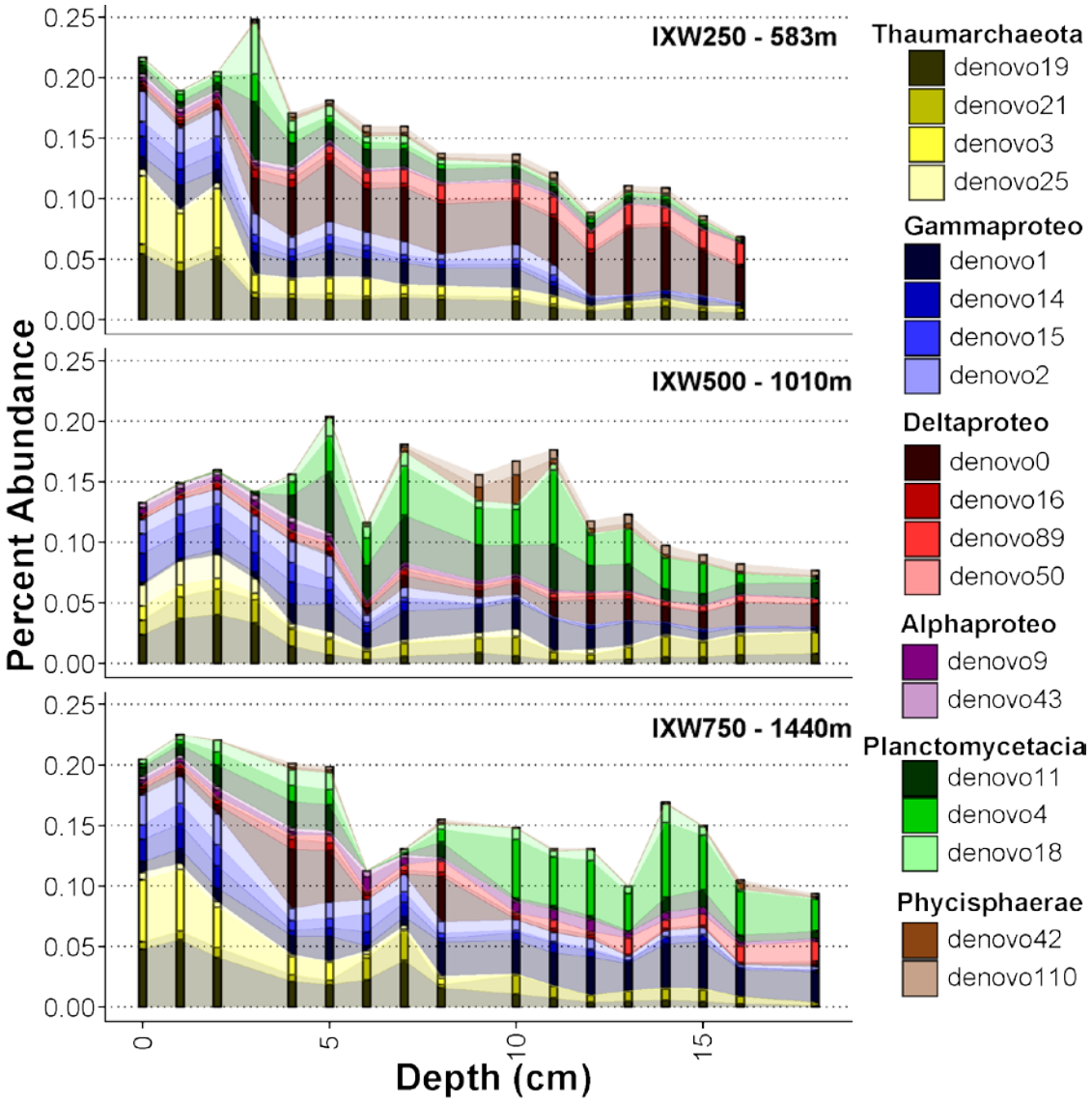

Figure 32 Core profiles representing a depth transect in the Southern Gulf of Mexico showing population (OTU) level distributions. Core profiles are arranged with increasing water depth.

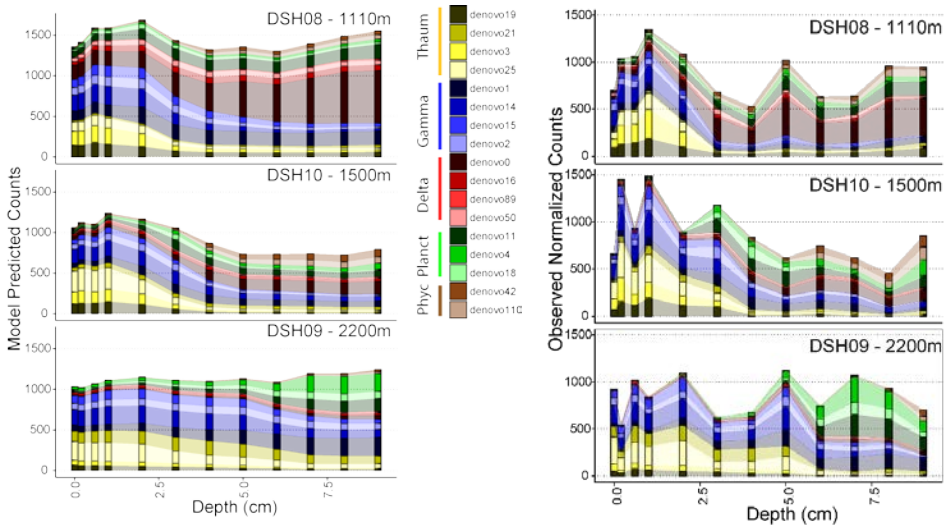

Figure 38 A comparison of the model predictions for these abundant OTU relative to the observed values shown in Figure 7.

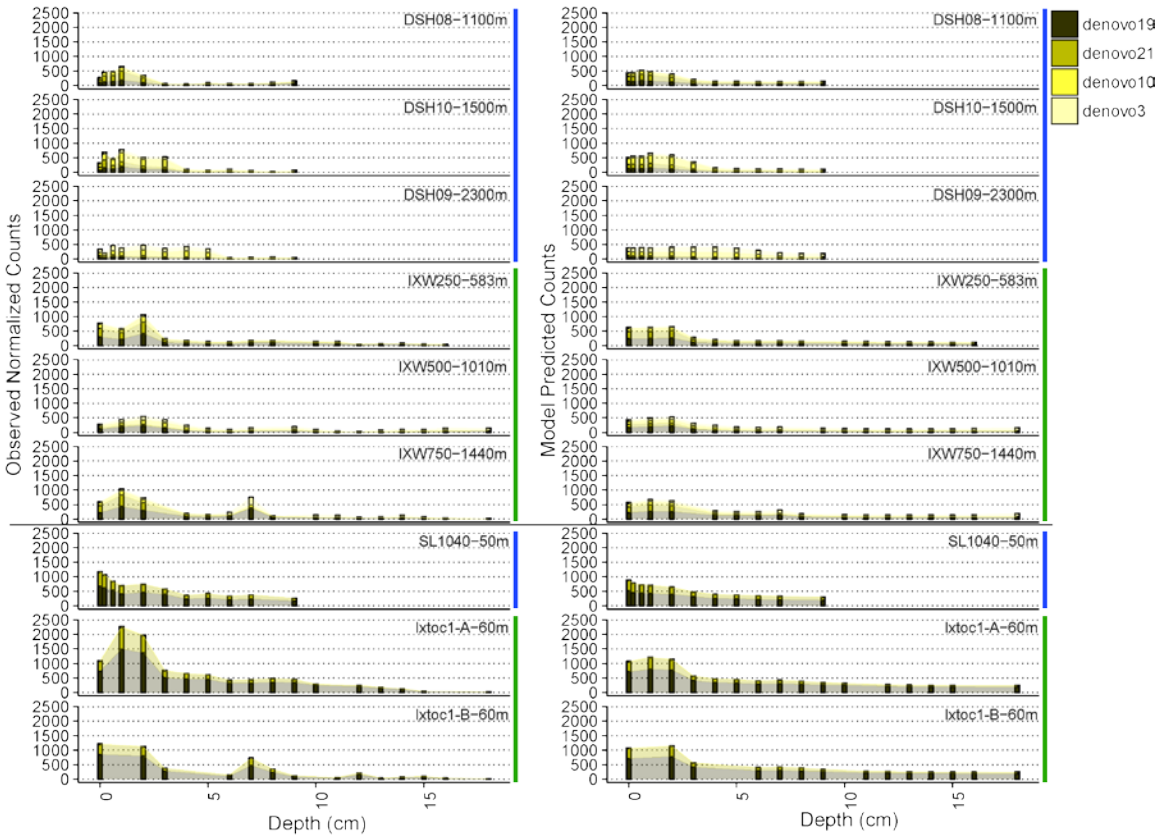

Figure 34 Biogeography of the dominant Thaumarchaeota OTU. The left side of the figure shows the observed counts for each of the OTU, while the right side shows the corresponding model predictions. Above the horizontal black line are deep water sites, while those below are shallow water sites. Blue horizontal bars to the right of the figures indicate samples collected in the northern Gulf of Mexico, while green horizontal bars indicate those from the southern Gulf of Mexico.

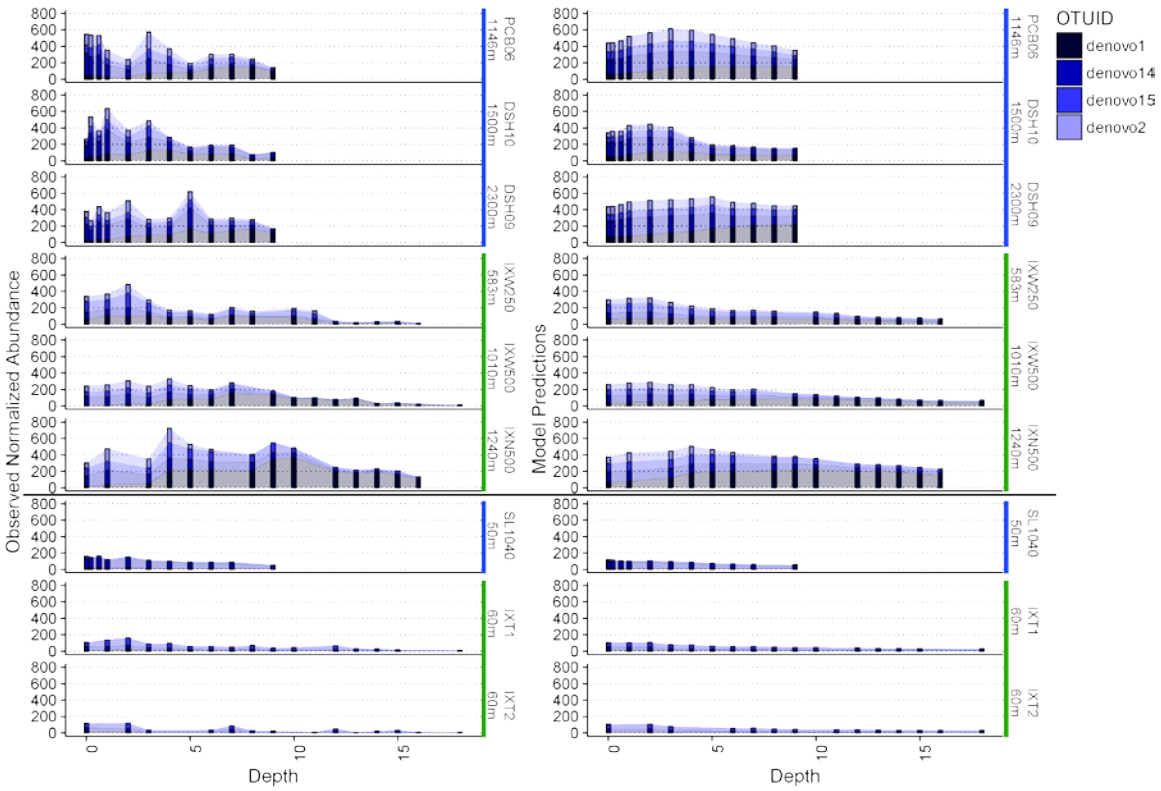

Figure 35 Biogeography of the dominant Gammaproteobacteria OTU. The left side of the figure shows the observed counts for each of the OTU, while the right side shows the corresponding model predictions. Above the horizontal black line are deep water sites, while those below are shallow water sites. Blue horizontal bars to the right of the figures indicate samples collected in the northern Gulf of Mexico, while green horizontal bars indicates those from the southern Gulf of Mexico.

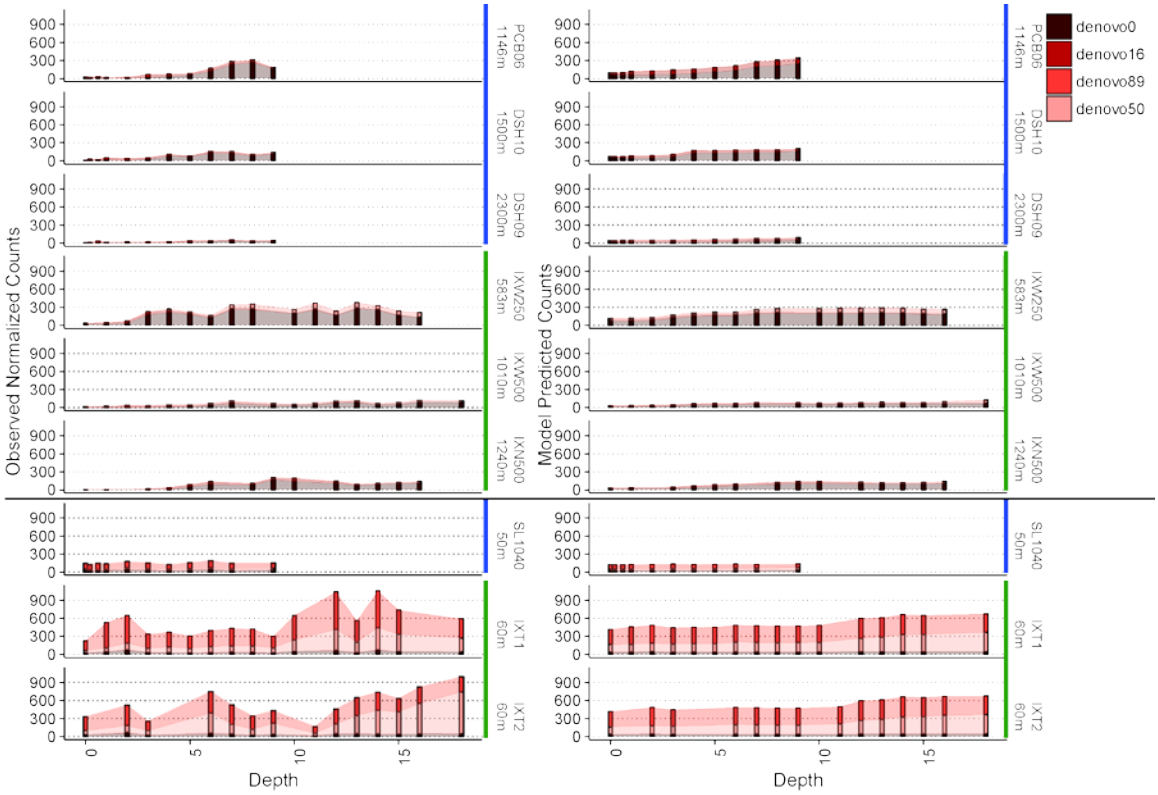

Figure 36 Biogeography of the dominant Deltaproteobacteria OTU. The left side of the figure shows the observed counts for each of the OTU, while the right side shows the corresponding model predictions. Above the horizontal black line are deep water sites, while those below are shallow water sites. Blue horizontal bars to the right of the figures indicate samples collected in the northern Gulf of Mexico, while green horizontal bars indicate those from the southern Gulf of Mexico.

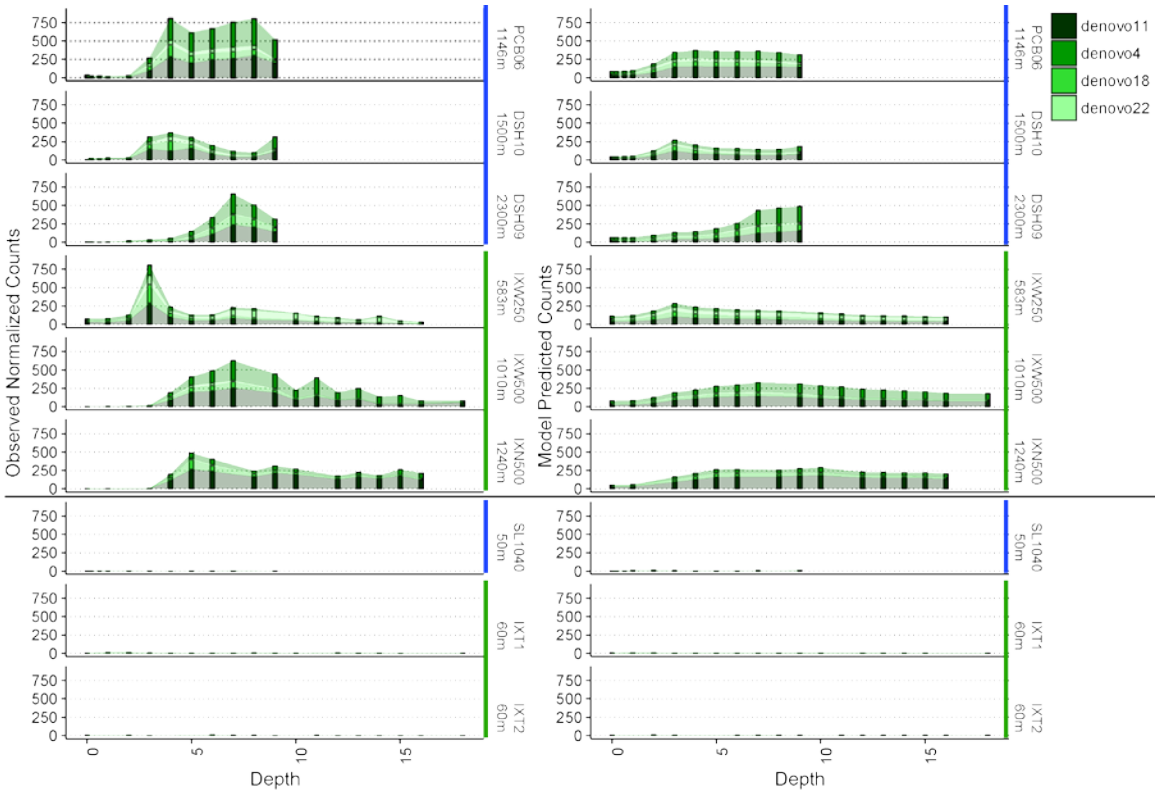

Figure 37 Biogeography of the dominant Planctomycetes OTU. The left side of the figure shows the observed counts for each of the OTU, while the right side shows the corresponding model predictions. Above the horizontal black line are deep water sites, while those below are shallow water sites. Blue horizontal bars to the right of the figures indicate samples collected in the northern Gulf of Mexico, while green horizontal bars indicate those from the southern Gulf of Mexico.

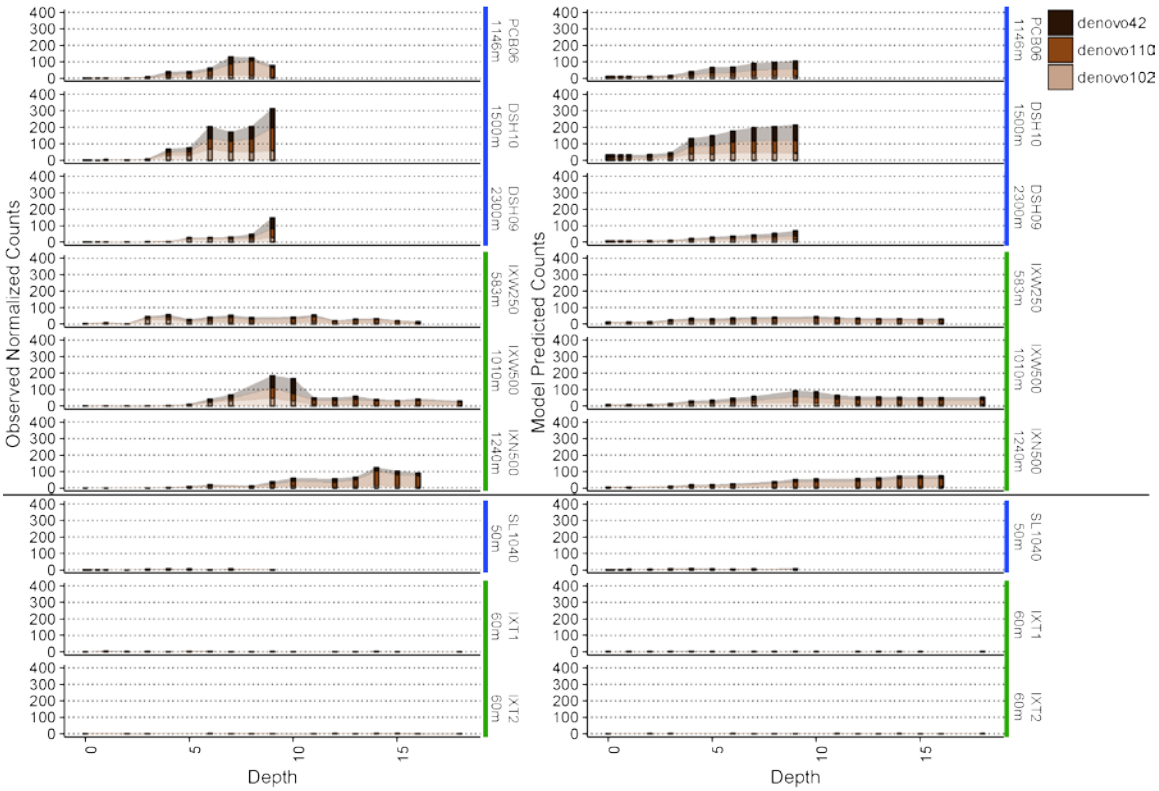

Figure 38 Biogeography of the dominant Phycisphaerae OTU. The left side of the figure shows the observed counts for each of the OTU, while the right side shows the corresponding model predictions. Above the horizontal black line are deep water sites, while those below are shallow water sites. Blue horizontal bars to the right of the figures indicate samples collected in the northern Gulf of Mexico, while green horizontal bars indicate those from the southern Gulf of Mexico.

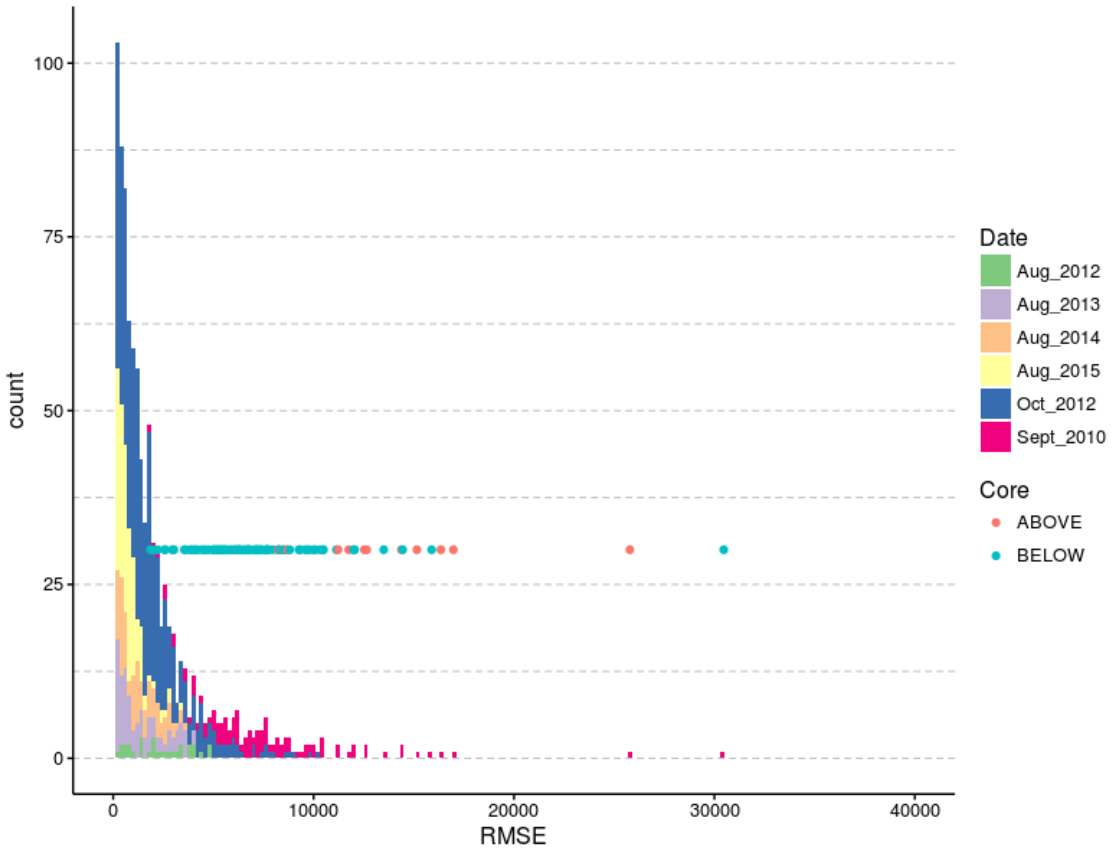

Figure 39 Distribution of how well the predicted counts match observed counts for each sample in the dataset. Total root mean square error was calculated for each sample and plotted as a histogram. Samples are colored based on the year sampled. The samples collected in 2010 were imported from Mason et al., 2014 and a red dot indicates oil impacted samples that had contamination above EPA level requirements while a blue dot represents those that were below EPA level requirements. In general, the model was more accurate for samples collected during our study likely in part due to different DNA extraction techniques. Overall, the model was more accurate for un-impacted samples from the Mason study than the oil contaminated ones, although there is a lot of spread.

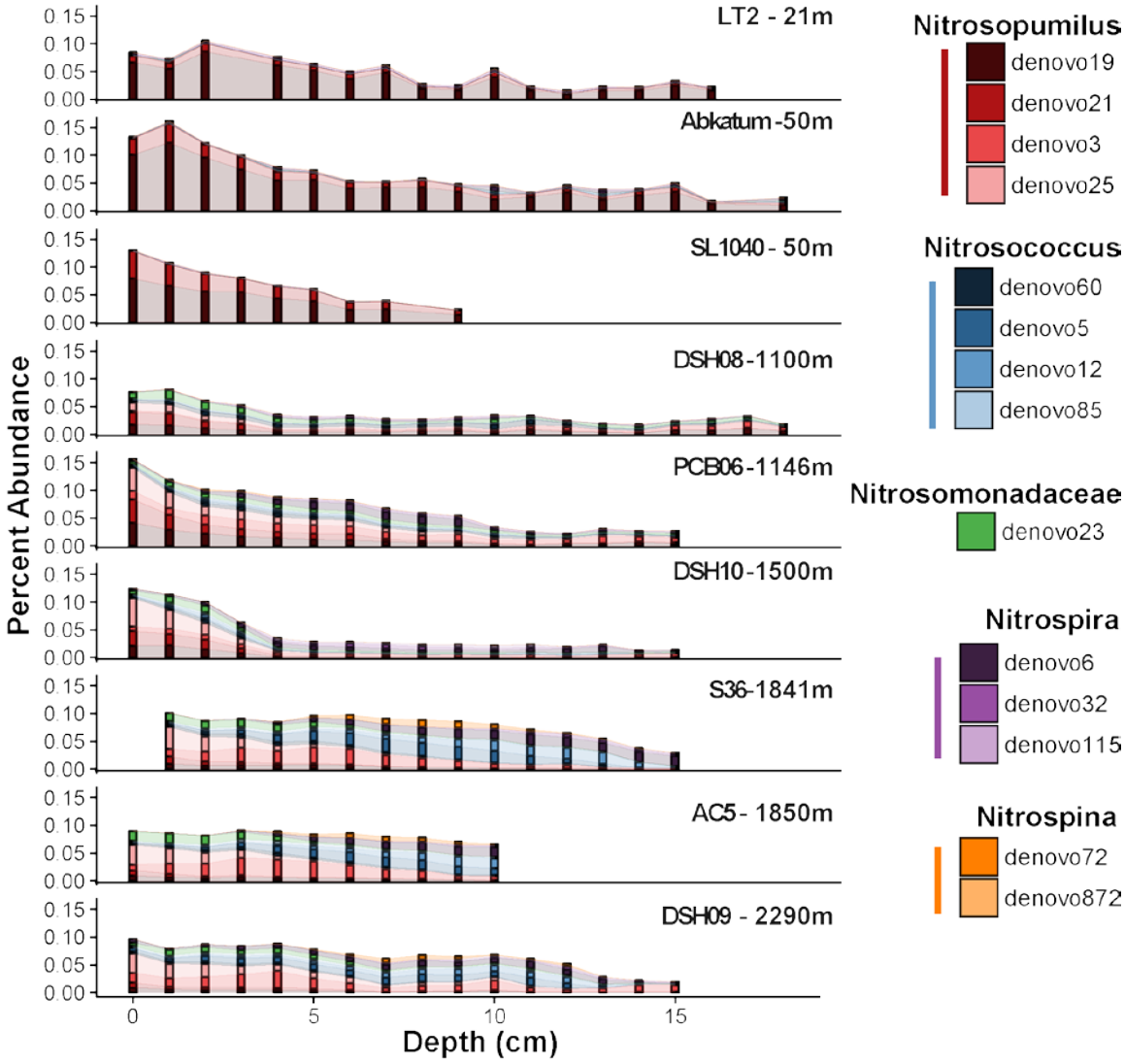

Figure 40 Biogeographic patterns in putative nitrifying populations throughout the Gulf of Mexico. All core profiles are organized from the shallowest site at the top to the deepest site at the bottom. Nitrosopumilus, Nitrosococcus, and the Nitrosomonadaceae family are considered as putative ammonium oxidizers, while Nitrospira and Nitrospina are considered here as putative nitrite oxidizers.

APPENDIX D. SUPPLEMENTAL INFORMATION FOR CHAPTER 5

Table 2 Description of samples used for 16S rRNA gene analysis.

Timepoint-ID	Treatment	Chamber	POSIXct_time	Hours	Group
T0	Control	T0	4/12/2016 10:35	0	Control.0
T1	Control	1	4/12/2016 12:01	1	Control.1
T1	Control	2	4/12/2016 12:01	1	Control.1
T1	Control	3	4/12/2016 12:01	1	Control.1
T1	Oil	1	4/12/2016 12:01	1	Oil.1
T1	Oil	2	4/12/2016 12:01	1	Oil.1
T1	Oil	3	4/12/2016 12:01	1	Oil.1
T6	Control	1	4/13/2016 10:35	24	Control.24
T6	Control	2	4/13/2016 10:35	24	Control.24
T6	Control	3	4/13/2016 10:35	24	Control.24
T6	Oil	1	4/13/2016 10:35	24	Oil.24
T6	Oil	2	4/13/2016 10:35	24	Oil.24
T6	Oil	3	4/13/2016 10:35	24	Oil.24
T29	Control	1	4/19/2016 10:35	168	Control.168
T29	Control	2	4/19/2016 10:35	168	Control.168
T29	Control	3	4/19/2016 10:35	168	Control.168
T29	Oil	1	4/19/2016 10:35	168	Oil.168
T29	Oil	2	4/19/2016 10:35	168	Oil.168
T29	Oil	3	4/19/2016 10:35	168	Oil.168
T74	Control	1	5/10/2016 8:36	670	Control.670
T74	Control	2	5/10/2016 8:36	670	Control.670
T74	Control	3	5/10/2016 8:36	670	Control.670
T74	Oil	1	5/10/2016 8:36	670	Oil.670
T74	Oil	2	5/10/2016 8:36	670	Oil.670
T74	Oil	3	5/10/2016 8:36	670	Oil.670
T74	Oil	1	5/10/2016 8:36	670	Oil.670
T222	Control	2	8/2/2016 9:00	2686	Control.2686
T222	Control	3	8/2/2016 9:00	2686	Control.2686
T222	Control	1	8/2/2016 9:00	2686	Control.2686
T222	Oil	1	8/2/2016 9:00	2686	Oil.2686
T222	Oil	2	8/2/2016 9:00	2686	Oil.2686
T222	Oil	3	8/2/2016 9:00	2686	Oil.2686
T222	Oil	3	8/2/2016 9:00	2686	Oil.2686
T222	Oil	1	8/2/2016 9:00	2686	Oil.2686
T222	Oil	2	8/2/2016 9:00	2686	Oil.2686

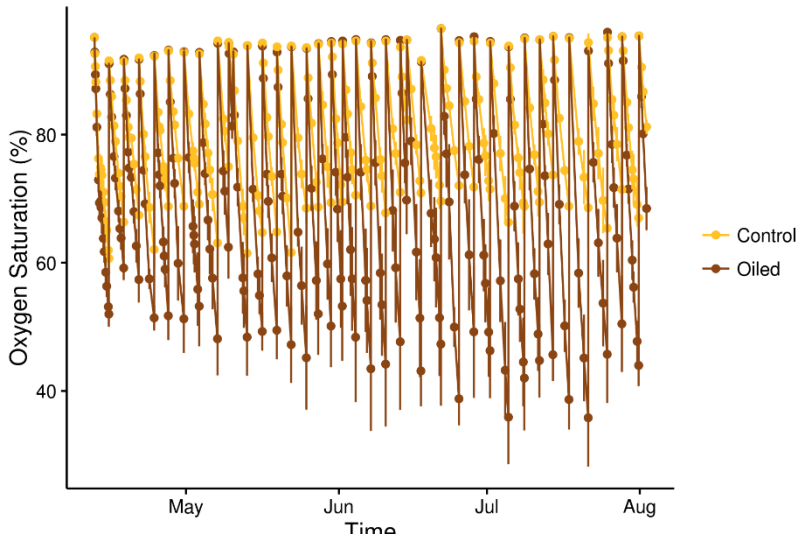

Figure 46 Oxygen concentrations throughout the full experiment. Each local maximum represents an aeration event.

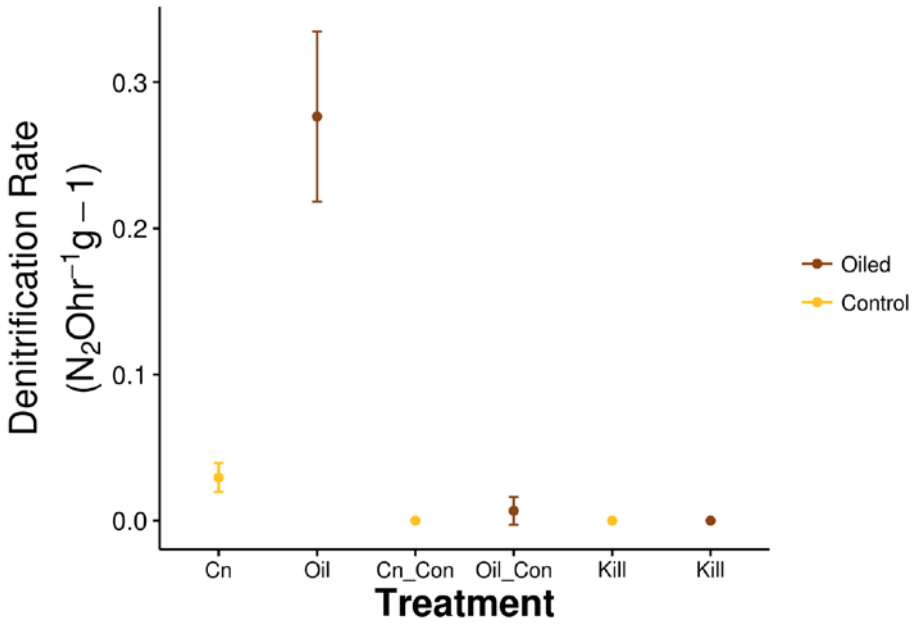

Figure 47 Potential denitrification rate determined from sands at collected at the end of the experiment. Killed sands were autoclaved twice, while control treatments were not amended with acetylene.

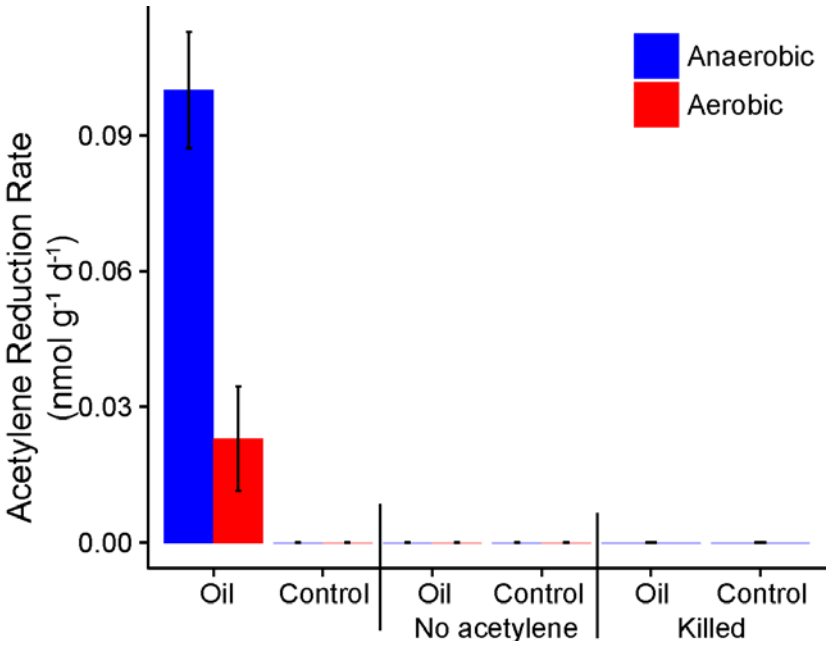

Figure 48 Acetylene reduction assay to determine nitrogen fixation rates from sands collected at the end of the experiment.

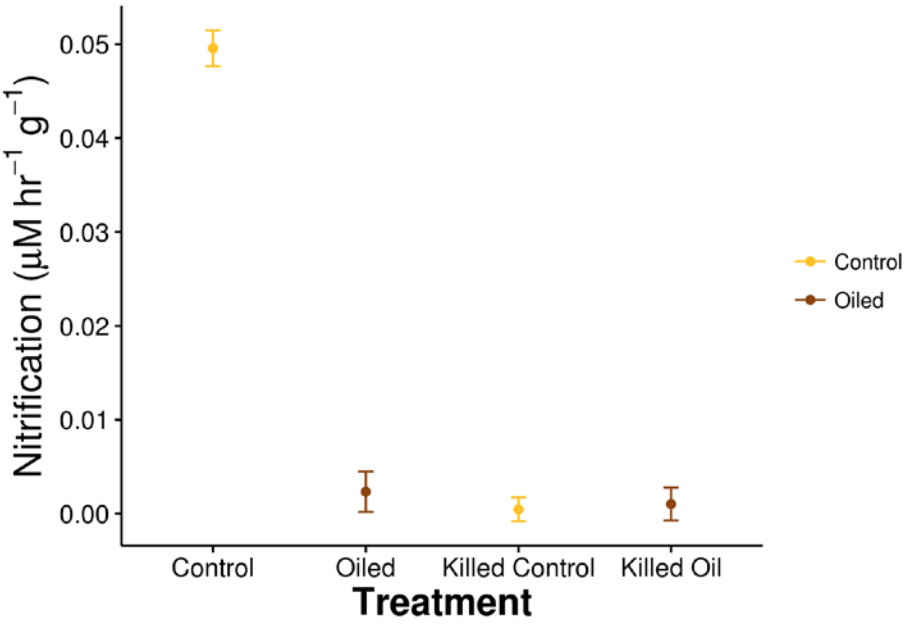

Figure 49 Potential denitrification rates determined from sands at collected at the end of the experiment. Killed sands were autoclaved twice.

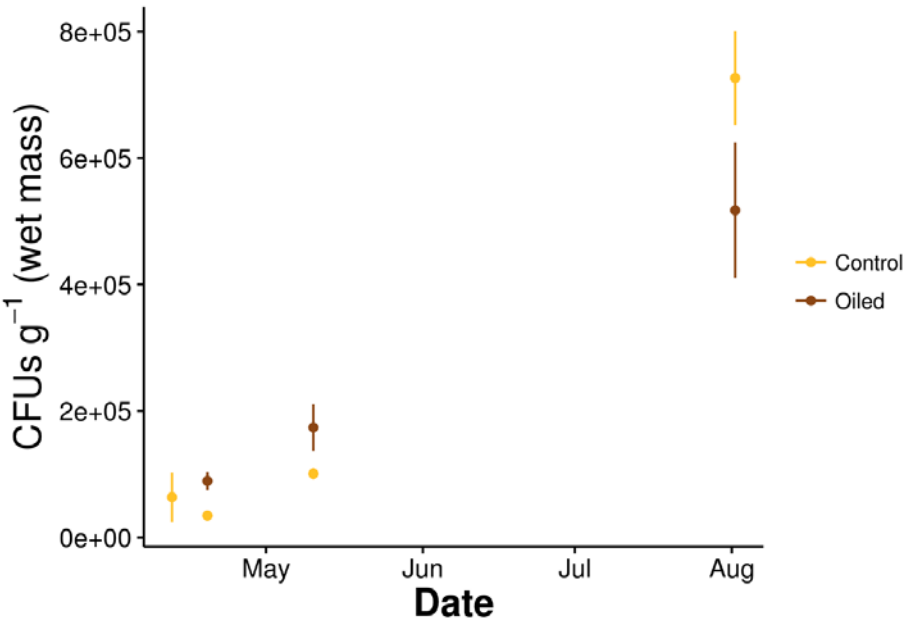

Figure 50 Cultivatable counts of marine heterotrophic microbes.

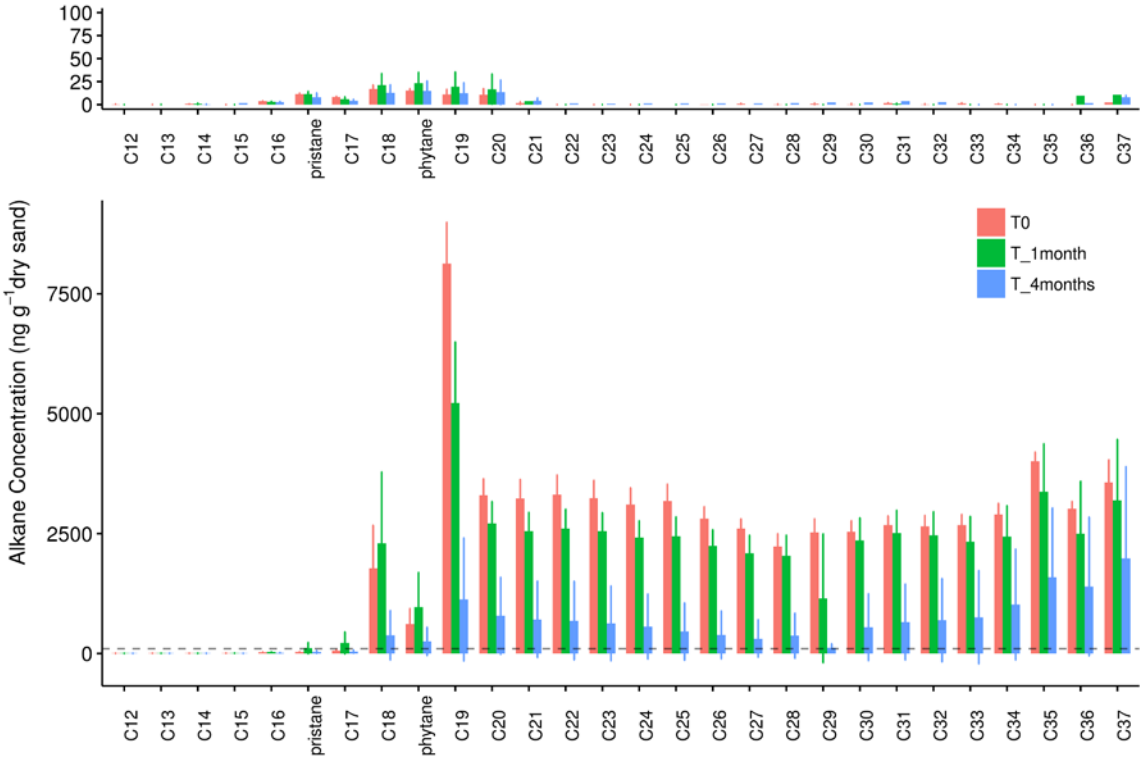

Figure 51 Measured aliphatic concentrations for (A) control sediments and (B) oiled sediments from each major sampling point.

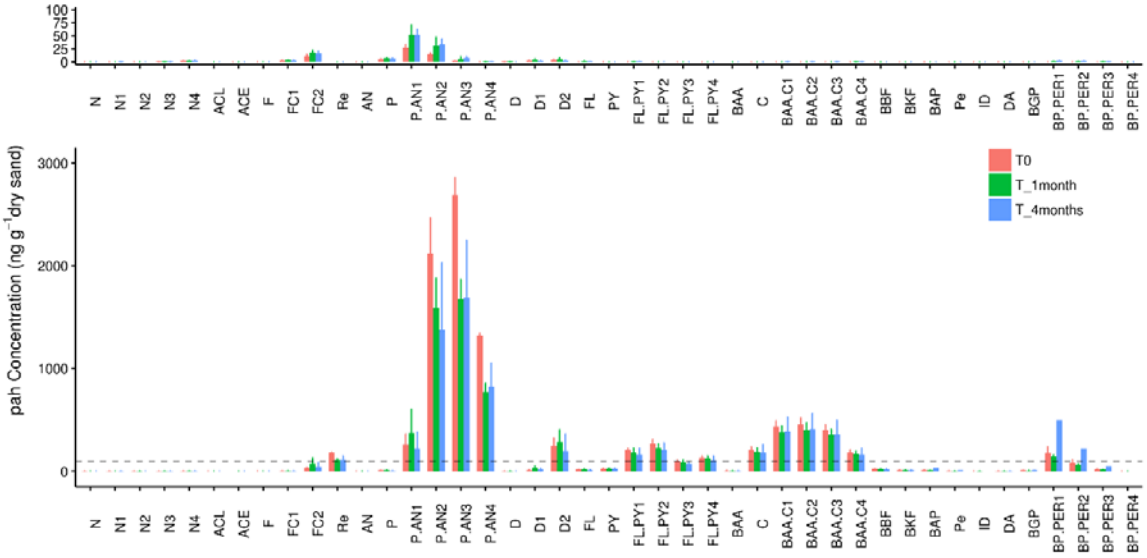

Figure 52 Measured aromatic concentrations for (A) control sediments and (B) oiled sediments from each major sampling point. Target PAHs are: Naphthalene (N) and alkylated homologues (N_{C1-C4}), Acenaphthylene (ACL), Acenaphthene (ACE), Fluorene (F), Retene (Re), Phenanthrene (P), Anthracene (AN), and their alkylated homologues (P/AN_{C1-C4}), Dibenzothiophene (D) and alkylated homologues (D_{C1-C2}), Fluoranthene (FL), Pyrene (PY), and their alkylated homologues (FL/PY_{C1-C4}), Benz[a]anthracene (BAA), Chrysene (C), and their alkylated homologues (BAA/C_{C1-C4}), Benzo[b]fluoranthene (BBF), Benzo[k]fluoranthene (BKF), Benzo[a]pyrene (BAP), Perylene (Pe), Indeno[1,2,3-cd]pyrene (ID), Dibenz[a,h]anthracene (DA), and alkylated homologues (BP/PER_{C1-C4}), and Benzo[ghi]perylene (BGP).

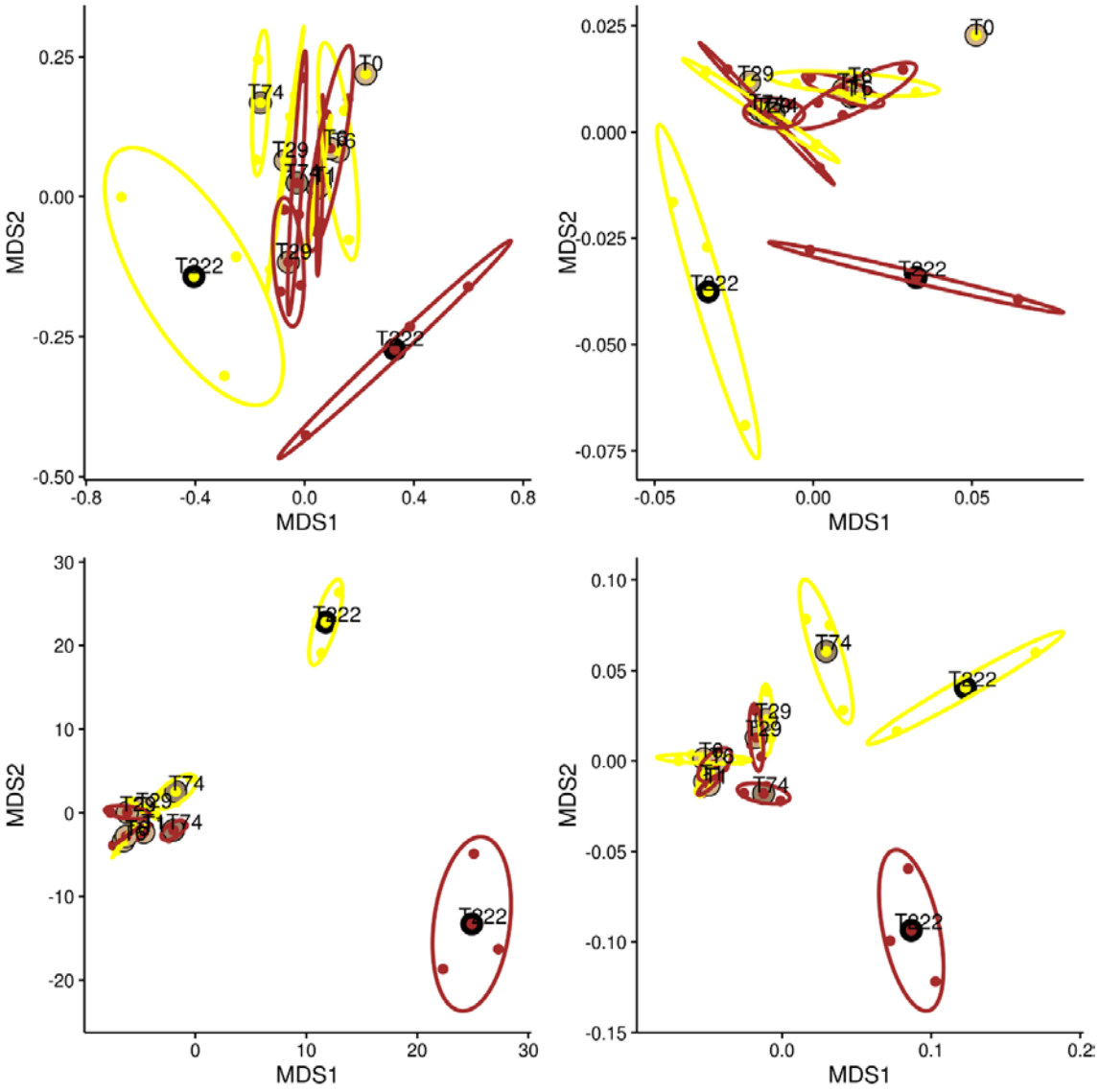

Figure 53 Non-metric multidimensional scaling plots generated from normalized 16S rRNA gene counts under different transformations. (A) Un-transformed data with bray-curtis dissimilarity. (B) Un-transformed data with weighted-unifrac distances. (C) Regularized log transformed data with Euclidean distances. (D) Variance stabilizing transformation with Euclidean distances.

APPENDIX E. BIOINFORMATIC APPROACHES AND DELIVERABLES

- **Bioinformatics Analysis Pipeline Development:** 16s amplicon sequence analysis toolkit
    - ***Problem:*** no efficient, scalable toolkit existed for the analysis of thousands of samples in the Gulf of Mexico Seafloor Microbiome (GMSM) dataset
    - ***Solution:*** development, validation, and application of a standalone, automated 16s amplicon sequence analysis pipeline: the ***snakemake_16S_pipeline*** (www.github.com/waoverholt)
    - ***Software:*** Python, Linux Bash Utilities, PEAR, QIIME, mothur, VSEARCH, SWARM, Python Modules: biom_format, numpy, scipy, snakemake, pyyaml
    - ***Validation:*** compared beta-diversity measures and dominant OTU abundances to community standard protocols using randomly subsampled data
    - ***Application:*** applied in parallel (see next section) to the GMSM dataset for the characterization of the benthic and seafloor microbial communities

- **High Performance Computing (HPC) and Parallelization:** parallel deployment on PACE
    - ***Problem:*** serial computing environment was not sufficient to analyze the GMSM dataset at scale
    - ***Solution:*** developed a massively parallelized implementation of my ***snakemake_16S_pipeline*** for deployment in the PACE HPC environment
    - ***Software:*** Python, Snakemake, QSUB, Linux Bash Utilities
    - ***Validation:*** compared runtime and analysis results to the parallelized implementation of QIIME
    - ***Application:*** allowed for the complete analysis of the GMSM dataset in 18 hours (compared to QIIME, which was never able to complete on PACE)

- **Integrative Data Analysis:** joint 16s sequence and environmental parameter analysis
    - ***Problem:*** characterization of the GMSM entailed integrative analysis of disparate data types: 16s amplicon sequence data together with numerous environmental, spatial, and temporal parameters
    - ***Solution:*** integrated multiple linear regression with sequential ANOVA for simultaneous multivariate constraint analysis of 16s sequence data
    - ***Software:*** R stats-package, R vegan

- ***Application:*** applied to the results of GMSM 16s data analysis results to partition the microbial community structure across the Gulf of Mexico

- **Machine Learning for Biogeography:** spatial population distribution modelling
  - ***Problem:*** need a tool to impute microbial community structure for areas not sampled (*i.e.* the problem of missing data) in order to maximize impact of the work – prediction, forecasting, and hindcasting
  - ***Solution:*** used Random Forest regression models in order to develop a tool that predicts microbial community composition based on geospatial parameters
  - ***Software:*** R stats-package, R MASS, R RandomForest, R geosphere, R raster, R dismo, R maptools, R rgdal, R rgeos, R ggmap, R plyr, R doParallel, R doSNOW, R rgl, R rasterVis,
  - ***Application:*** applied to the results of the GMSM 16s OTU results and geospatial data in order to derive a predictive model for microbial community composition

Validation: compared predicted to observed OTU results using permutation of geospatial variables to show that model accurately predicts community composition

Table E.1 Collection of Programs used throughout this dissertation

Software	URL	Function
PEAR[1]	https://sco.h-its.org/exelixis/web/software/pear/	Merge mate pairs
VSEARCH[2]	https://github.com/torognes/vsearch	QA/QC, dereplicate, denovo & reference chimera search,
MOTHUR[3]	https://www.mothur.org/	Trim 16S primers and length based sized filtering
SWARM[4]	https://github.com/torognes/swarm	OTU picking
UCLUST[5]	https://drive5.com/usearch/manual/uclust_algo.html	Reference based OTU picking
QIIME[6]	http://qiime.org/	Merge OTU maps
RDP[7]	https://rdp.cme.msu.edu/classifier	Classify representative OTU sequences
SILVA[8]	https://www.arb-silva.de/	Sequence database for taxonomic classification
R_stats[9]	https://stat.ethz.ch/R-manual/R-devel/library/stats/html/00Index.html	Various statistical tests and regressions
R_vegan[10]	https://cran.r-project.org/web/packages/vegan/index.html	Computing alpha and beta diversity indices
R_DESeq2[11]	https://bioconductor.org/packages/release/bioc/html/DESeq2.html	Normalize libraries, determine differentially abundant OTU
R_metagenomeSeq[12]	https://bioconductor.org/packages/release/bioc/html/metagenomeSeq.html	Normalize libraries, determine differentially abundant OTU
R_randomForest[13]	https://cran.r-project.org/web/packages/randomForest/	Generate regression models for OTU distributions
R_tsk[14]	https://rdrr.io/rforge/tsk/	Calculate LC50 values for rotifer ecotoxicity assay
R_phyloseq[15]	https://joey711.github.io/phyloseq/	Generate UniFrac Distance for microbial community analysis
R_ggplot2[16]	https://cran.r-project.org/web/packages/ggplot2/index.html	Generate figures
R_grid[17]	https://stat.ethz.ch/R-manual/R-devel/library/grid/html/grid-package.html	Generate figures
R_gridExtra[18]	https://cran.r-project.org/web/packages/gridExtra/index.html	Generate figures
R_MASS[19]	https://cran.r-project.org/web/packages/MASS/index.html	Collection of statistical functions
R_geosphere[20]	https://cran.r-project.org/web/packages/geosphere/geosphere.pdf	Calculate distances between geospatial points
R_raster[21]	https://cran.r-project.org/web/packages/raster/index.html	Reading, writing, manipulating, analyzing, and modeling spatial data
R_dismo[22]	https://cran.r-project.org/web/packages/dismo/index.html	Functions for species distribution modeling
R_maptools[23]	https://cran.r-project.org/web/packages/maptools/index.html	Manipulating and reading geographic data
R_rgdal[24]	https://cran.r-project.org/web/packages/rgdal/index.html	Provides bindings to the 'Geospatial' Data Abstraction Library
R_geos[25]	https://cran.r-project.org/web/packages/rgeos/index.html	Interface to Geometry Engine - Open Source ('GEOS')

Table E.1 continued

R_ggmap[26]	https://cran.r-project.org/web/packages/ggmap/index.html	Visualize spatial data and models on top of static maps
R_plyr[27]	https://cran.r-project.org/web/packages/plyr/index.html	Data operations and transformations
R_doParallel[28]	https://cran.r-project.org/web/packages/doParallel/index.html	Parallel adaptor package
R_doSNOW[29]	https://cran.r-project.org/web/packages/doSNOW/index.html	Parallel adaptor for SNOW package
R_rgl[30]	https://cran.r-project.org/web/packages/rgl/index.html	3D visualization of gridded data
R_rasterVIS[31]	https://cran.r-project.org/web/packages/rasterVis/index.html	Visualization and interaction with raster data

1. Zhang, J., Kobert, K., Flouri, T., and Stamatakis, A. (2013) PEAR: a fast and accurate Illumina Paired-End reAd mergeR. Bioinformatics 1–7.
2. Rognes, T., Flouri, T., Nichols, B., Quince, C., and Mahe, F. (2016) VSEARCH : a versatile open source tool for metagenomics (# 13057). PeerJ Preprints 1–30.
3. Schloss, P.D., Westcott, S.L., Ryabin, T., Hall, J.R., Hartmann, M., Hollister, E.B., et al. (2009) Introducing mothur: Open-source, platform-independent, community-supported software for describing and comparing microbial communities. Applied and Environmental Microbiology 75: 7537–7541.
4. Mahé, F., Rognes, T., Quince, C., de Vargas, C., and Dunthorn, M. (2014) Swarm: robust and fast clustering method for amplicon-based studies. PeerJ 2: e593.
5. Edgar, R.C. (2010) Search and clustering orders of magnitude faster than BLAST. Bioinformatics (Oxford, England) 26: 2460–1.
6. Caporaso, J., Kuczynski, J., and Stombaugh, J. (2010) QIIME allows analysis of high-throughput community sequencing data. Nature Methods 7: 335–336.
7. Wang, Q., Garrity, G.M., Tiedje, J.M., and Cole, J.R. (2007) Naïve Bayesian Classifier for Rapid Assignment of rRNA Sequences into the New Bacterial Taxonomy. Applied and Environmental Microbiology 73: 5261–5267.
8. Quast, C., Pruesse, E., Yilmaz, P., Gerken, J., Schweer, T., Yarza, P., et al. (2012) The SILVA ribosomal RNA gene database project: improved data processing and web-based tools. Nucleic Acids Research 41: D590–D596.
9. R Core Team (2014) R: A Language and Environment for Statistical Computing.
10. Oksanen, J., Blanchet, F.G., Kindt, R., Legendre, P., Minchin, P.R., O'Hara, R.B., et al. (2007) The Vegan Package. Community Ecology Package 10: 631–637.
11. Love, M.I., Huber, W., and Anders, S. (2014) Moderated estimation of fold change and dispersion for RNA-Seq data with DESeq2. bioRxiv.
12. Paulson, J.N., Stine, O.C., Bravo, H.C., and Pop, M. (2013) Differential abundance analysis for microbial marker-gene surveys. Nature methods 10: 1200–2.
13. Liaw, A. and Wiener, M. (2002) Classification and Regression by randomForest. R News 2: 18–22.
14. Stone, B.R. (2012) tsk: Trimmed Spearman-Karber Method.
15. McMurdie, P.J. and Holmes, S. (2013) phyloseq: an R package for reproducible interactive analysis and graphics of microbiome census data. PloS one 8: e61217.
16. Wickham, H. (2009) ggplot2: elegant graphics for data analysis Springer New York.
17. Murrell, P. (2005) R Graphics. Chapman & Hall/CRC Press.
18. Auguie, B. (2016) gridExtra: Miscellaneous Functions for" Grid" Graphics. R package version 2.2. 1
19. Venables, W. N. & Ripley, B. D. (2002) Modern Applied Statistics with S. Fourth Edition. Springer, New York. ISBN 0-387-95457-0
20. C.F.F. Karney, 2013. Algorithms for geodesics, J. Geodesy 87: 43-55. https://dx.doi.org/10. 1007/s00190-012-0578-z

21. Hijmans, R. J., & van Etten, J. (2014) raster: Geographic data analysis and modeling. R package version, 2(8).
22. Hijmans, R. J., Phillips, S., Leathwick, J., & Elith, J. (2013) dismo: Species distribution modeling. R package version 0.9–3
23. Bivand, R., & Lewin-Koh, N. (2013) maptools: Tools for reading and handling spatial objects. R package version 0.8, 23
24. Keitt, T. H., Bivand, R., Pebesma, E., & Rowlingson, B. (2011) rgdal: bindings for the Geospatial Data Abstraction Library. R package version 0.7-1
25. Bivand, R., & Rundel, C. (2014) rgeos: Interface to Geometry Engine–Open Source (GEOS). R Package Version 0.3–6. Comprehensive R Archive Network, Vienna, Austria.
26. Kahle, D., & Wickham, H. (2013) ggmap: Spatial Visualization with ggplot2. R Journal, 5(1).
27. Hadley Wickham. (2011) The Split-Apply-Combine Strategy for Data Analysis. Journal of Statistical Software, 40(1), 1-29
28. Analytics, R., & Weston, S. (2014). doParallel: Foreach parallel adaptor for the parallel package. R package version, 1(8)
29. Analytics, R., & Weston, S. (2014). doSNOW: Foreach parallel adaptor for the snow package. R Package version, 1, 12.
30. Adler, D., Murdoch, D., Nenadic, O., & Urbanek, S. (2007). rgl: 3D visualization device system (OpenGL). R package version 0.75
31. Hijmans, R. J., & van Etten, J. (2014). raster: Geographic data analysis and modeling. R package version, 2(8).

REFERENCES

(Firm), B. (2010) Deepwater Horizon Accident Investigation Report BP.

Abbasian, F., Lockington, R., Megharaj, M., and Naidu, R. (2015) A Review on the Genetics of Aliphatic and Aromatic Hydrocarbon Degradation. *Appl. Biochem. Biotechnol.* 224–250.

Abraham, W.R., Meyer, H., and Yakimov, M. (1998) Novel glycine containing glucolipids from the alkane using bacterium Alcanivorax borkumensis. *Biochim. Biophys. Acta - Lipids Lipid Metab.* **1393**: 57–62.

Aeppli, C., Carmichael, C. a, Nelson, R.K., Lemkau, K.L., Graham, W.M., Redmond, M.C., et al. (2012) Oil weathering after the Deepwater Horizon disaster led to the formation of oxygenated residues. *Environ. Sci. Technol.* **46**: 8799–807.

Agarry, S.E., Aremu, M.O., and Aworanti, O.A. (2013) Kinetic modelling and half-life study on enhanced soil bioremediation of bonny light crude oil amended with crop and animal-derived organic wastes. *J. Pet. Environ. Biotechnol.* **4**: 137–147.

Allen, T. (2010) National Incident Commander's Report, MC252 Deepwater Horizon'. *Washington, DC*.

Aller, J.Y. (1989) Quantifying sediment disturbance by bottom currents and its effect on benthic communities in a deep-sea western boundary zone. *Deep Sea Res. Part A, Oceanogr. Res. Pap.* **36**: 901–934.

Alonso-Saez, L., Waller, a. S., Mende, D.R., Bakker, K., Farnelid, H., Yager, P.L., et al. (2012) Role for urea in nitrification by polar marine Archaea. *Proc. Natl. Acad. Sci.* **109**: 17989–17994.

Anders, S. and Huber, W. (2010) Differential expression analysis for sequence count data. *Genome Biol.* **11**: R106.

Anderson, J. a, Kuhl, A.J., and Anderson, a N. (2014) Toxicity of oil and dispersed oil on juvenile mud crabs, Rhithropanopeus harrisii. *Bull. Environ. Contam. Toxicol.* **92**: 375–380.

Arndt, S., Jørgensen, B.B., LaRowe, D.E., Middelburg, J.J., Pancost, R.D., and Regnier, P. (2013) Quantifying the degradation of organic matter in marine sediments: A review and synthesis. *Earth-Science Rev.* **123**: 53–86.

Atlas, R.M. (1975) Effects of temperature and crude oil composition on petroleum biodegradation. *Appl. Microbiol.* **30**: 396–403.

Atlas, R.M. (1981) Fate of oil from two major oil spills: Role of microbial degradation in removing oil from the Amoco Cadiz and IXTOC I spills. *Environ. Int.* **5**: 33–38.

Atlas, R.M. (1981) Microbial degradation of petroleum hydrocarbons: an environmental perspective. *Microbiol. Rev.* **45**: 180.

Atlas, R.M. and Hazen, T.C. (2011) Oil biodegradation and bioremediation: a tale of the two worst spills in U.S. history. *Environ. Sci. Techol.* **45**: 6709–15.

Atlas, R.M., Stoeckel, D.M., Faith, S.A., Minard-Smith, A., Thorn, J.R., and Benotti, M.J. (2015) Oil Biodegradation and Oil-Degrading Microbial Populations in Marsh Sediments Impacted by Oil from the Deepwater Horizon Well Blowout. *Environ. Sci. Technol.* **49**: 8356–8366.

Austin, R.N. and Groves, J.T. (2011) Alkane-oxidizing metalloenzymes in the carbon cycle. *Metallomics* **3**: 775–87.

Baelum, J., Borglin, S., Chakraborty, R., Fortney, J.L., Lamendella, R., Mason, O.U., et al. (2012) Deep-sea bacteria enriched by oil and dispersant from the Deepwater Horizon spill. *Environ. Microbiol.* **14**: 2405–16.

Bagby, S.C., Reddy, C.M., Aeppli, C., Fisher, G.B., and Valentine, D.L. (2016) Persistence and biodegradation of oil at the ocean floor following *Deepwater Horizon*. *Proc. Natl. Acad. Sci.* 201610110.

Bagi, A., Pampanin, D.M., Brakstad, O.G., and Kommedal, R. (2013) Estimation of hydrocarbon biodegradation rates in marine environments: A critical review of the Q 10 approach. *Mar. Environ. Res.* **89**: 83–90.

Bagi, A., Pampanin, D.M., Lanzén, A., Bilstad, T., and Kommedal, R. (2014) Naphthalene biodegradation in temperate and arctic marine microcosms. *Biodegradation* **25**: 111–125.

Ballou, T.G., Hess, S.C., Dodge, R.E., Knap, a H., and Sleeter, T.D. (1989) Effects of untreated and chemically-dispersed oil on tropical marine communities: a long-term field experiment. *1989 Oil Spill Conf.* 447–454.

Banat, I.M., Franzetti, A., Gandolfi, I., Bestetti, G., Martinotti, M.G., Fracchia, L., et al. (2010) Microbial biosurfactants production, applications and future potential. *Appl. Microbiol. Biotechnol.* **87**: 427–444.

Barkay, T., Navon-Venezia, S., Ron, E.Z., and Rosenberg, E. (1999) Enhancement of solubilization and biodegradation of polyaromatic hydrocarbons by the bioemulsifier alasan. *Appl. Environ. Microbiol.* **65**: 2697–2702.

van Beilen, J.B. and Funhoff, E.G. (2007) Alkane hydroxylases involved in microbial alkane degradation. *Appl. Microbiol. Biotechnol.* **74**: 13–21.

Bejarano, A.C. and Michel, J. (2010) Large-scale risk assessment of polycyclic aromatic hydrocarbons in shoreline sediments from Saudi Arabia: environmental legacy after twelve years of the Gulf war oil spill. *Environ. Pollut.* **158**: 1561–1569.

Bernabeu, A.M., Rey, D., Rubio, B., Vilas, F., Domínguez, C., Bayona, J.M., and Albaigés, J. (2009) Assessment of cleanup needs of oiled sandy beaches: lessons from the Prestige oil spill. *Environ. Sci. Technol.* **43**: 2470–2475.

Bertrand, E.M., Keddis, R., Groves, J.T., Vetriani, C., and Austin, R.N. (2013) Identity and mechanisms of alkane-oxidizing metalloenzymes from deep-sea hydrothermal vents. *Front. Microbiol.* **4**: 109.

Bianchi, T.S., DiMarco, S.F., Cowan, J.H., Hetland, R.D., Chapman, P., Day, J.W., and Allison, M.A. (2010) The science of hypoxia in the Northern Gulf of Mexico: a review. *Sci. Total Environ.* **408**: 1471–1484.

Biddle, J.F., White, J.R., Teske, A.P., and House, C.H. (2011) Metagenomics of the subsurface Brazos-Trinity Basin (IODP site 1320): comparison with other sediment and pyrosequenced metagenomes. *ISME J.* **5**: 1038–47.

Bienhold, C., Boetius, A., and Ramette, A. (2012) The energy–diversity relationship of complex bacterial communities in Arctic deep-sea sediments. *ISME J.* **6**: 724–732.

Bienhold, C., Zinger, L., Boetius, A., and Ramette, A. (2016) Diversity and biogeography

of bathyal and abyssal seafloor bacteria. *PLoS One* **11**: 1–20.

Bik, H.M., Halanych, K.M., Sharma, J., and Thomas, W.K. (2012) Dramatic shifts in benthic microbial eukaryote communities following the Deepwater Horizon oil spill. *PLoS One* **7**: e38550.

Billett, D.S.M., Lampitt, R.S., Rice, A.L., and Mantoura, R.F.C. (1983) Seasonal sedimentation of phytoplankton to the deep-sea benthos. *Nature* **302**: 520–522.

Boehm, A.B., Yamahara, K.M., and Sassoubre, L.M. (2014) Diversity and transport of microorganisms in intertidal sands of the California coast. *Appl. Environ. Microbiol.* **80**: 3943–3951.

Bookstaver, M., Bose, A., and Tripathi, A. (2015) Interaction of *Alcanivorax borkumensis* with a Surfactant Decorated Oil–Water Interface. *Langmuir* **31**: 5875–5881.

Boonmak, C., Takahashi, Y., and Morikawa, M. (2014) Cloning and expression of three ladA-type alkane monooxygenase genes from an extremely thermophilic alkane-degrading bacterium Geobacillus thermoleovorans B23. *Extremophiles* **18**: 515–523.

Borovik, A.S. (2011) Role of metal-oxo complexes in the cleavage of C-H bonds. *Chem. Soc. Rev.* **40**: 1870–1874.

Boufadel, M.C., Abdollahi-Nasab, A., Geng, X., Galt, J., and Torlapati, J. (2014) Simulation of the landfall of the deepwater horizon oil on the shorelines of the Gulf of Mexico. *Environ. Sci. Technol.* **48**: 9496–9505.

Boufadel, M.C., Sharifi, Y., Van Aken, B., Wrenn, B.A., and Lee, K. (2010) Nutrient and oxygen concentrations within the sediments of an Alaskan beach polluted with the Exxon Valdez oil spill. *Environ. Sci. Technol.* **44**: 7418–7424.

Bradter, U., Kunin, W.E., Altringham, J.D., Thom, T.J., and Benton, T.G. (2013) Identifying appropriate spatial scales of predictors in species distribution models with the random forest algorithm. *Methods Ecol. Evol.* **4**: 167–174.

Brakstad, O.G., Throne-Holst, M., Netzer, R., Stoeckel, D.M., and Atlas, R.M. (2015) Microbial communities related to biodegradation of dispersed Macondo oil at low seawater temperature with Norwegian coastal seawater. *Microb. Biotechnol.* **8**: 989–998.

Brooks, G.R., Larson, R.A., Schwing, P.T., Romero, I., Moore, C., Reichart, G.J., et al. (2015) Sedimentation pulse in the NE Gulf of Mexico following the 2010 DWH blowout. *PLoS One* **10**: 1–24.

Burdige, D.J. (2006) Geochemistry of marine sediments Princeton University Press.

Cameotra, S.S. and Singh, P. (2009) Synthesis of rhamnolipid biosurfactant and mode of hexadecane uptake by Pseudomonas species. *Microb. Cell Fact.* **8**: 16.

Camilli, R., Reddy, C.M., Yoerger, D.R., Van Mooy, B. a S., Jakuba, M. V, Kinsey, J.C., et al. (2010) Tracking hydrocarbon plume transport and biodegradation at Deepwater Horizon. *Science* **330**: 201–204.

Campbell, M.A., Chain, P.S.G., Dang, H., El Sheikh, A.F., Norton, J.M., Ward, N.L., et al. (2011) Nitrosococcus watsonii sp. nov., a new species of marine obligate ammonia-oxidizing bacteria that is not omnipresent in the world's oceans: calls to validate the names "Nitrosococcus halophilus" and "Nitrosomonas mobilis." *FEMS Microbiol. Ecol.* **76**: 39–48.

Campo, P., Venosa, A.D., and Suidan, M.T. (2013) Biodegradability of Corexit 9500 and dispersed South Louisiana crude oil at 5 and 25 °C. *Environ. Sci. Technol.* **47**: 1960–1967.

Canion, A., Overholt, W.A., Kostka, J.E., Huettel, M., Lavik, G., and Kuypers, M.M.M. (2014) Temperature response of denitrification and anaerobic ammonium oxidation rates and microbial community structure in Arctic fjord sediments. *Environ. Microbiol.* **16**: 3331–3344.

Capone, D.G. (1993) Determination of nitrogenase activity in aquatic samples using the acetylene reduction procedure. In, Kemp,P.F., Cole,J.J., Sherr,B.F., and Sherr,E.B. (eds), *Handbook of methods in aquatic microbial ecology*. CRC press, pp. 621–631.

Caporaso, J., Kuczynski, J., and Stombaugh, J. (2010) QIIME allows analysis of high-throughput community sequencing data. *Nat. Methods* **7**: 335–336.

Caporaso, J.G., Bittinger, K., Bushman, F.D., DeSantis, T.Z., Andersen, G.L., and Knight, R. (2010) PyNAST: a flexible tool for aligning sequences to a template alignment. *Bioinformatics* **26**: 266–7.

Caporaso, J.G., Kuczynski, J., Stombaugh, J., Bittinger, K., Bushman, F.D., Costello, E.K., et al. (2010) QIIME allows analysis of high-throughput community sequencing data. *Nat. Methods* **7**: 335–336.

Caporaso, J.G., Lauber, C.L., Walters, W. a, Berg-Lyons, D., Huntley, J., Fierer, N., et al. (2012) Ultra-high-throughput microbial community analysis on the Illumina HiSeq and MiSeq platforms. *ISME J.* **6**: 1621–4.

Carrigg, C., Rice, O., Kavanagh, S., Collins, G., and O'Flaherty, V. (2007) DNA extraction method affects microbial community profiles from soils and sediment. *Appl. Microbiol. Biotechnol.* **77**: 955–964.

Di Cello, F., Pepi, M., Baldi, F., and Fani, R. (1997) Molecular characterization of an n-alkane-degrading bacterial community and identification of a new species, Acinetobacter venetianus. *Res. Microbiol.* **148**: 237–249.

Chakraborty, R., Borglin, S.E., Dubinsky, E.A., Andersen, G.L., and Hazen, T.C. (2012) Microbial Response to the MC-252 Oil and Corexit 9500 in the Gulf of Mexico. *Front Microbiol* **3**: 357.

Chanton, J.P., Cherrier, J., Wilson, R.M., Sarkodee-Adoo, J., Bosman, S., Mickle, A., and Graham, W.M. (2012) Radiocarbon evidence that carbon from the Deepwater Horizon spill entered the planktonic food web of the Gulf of Mexico. *Environ. Res. Lett.* **7**: 45303.

Chapman, H., Purnell, K., Law, R.J., and Kirby, M.F. (2007) The use of chemical dispersants to combat oil spills at sea: A review of practice and research needs in Europe. *Mar. Pollut. Bull.* **54**: 827–838.

Charbonnier, C., Anschutz, P., Poirier, D., Bujan, S., and Lecroart, P. (2013) Aerobic respiration in a high-energy sandy beach. *Mar. Chem.* **155**: 10–21.

Chipman, L., Berg, P., and Huettel, M. (2016) Benthic Oxygen Fluxes Measured by Eddy Covariance in Permeable Gulf of Mexico Shallow-Water Sands. *Aquat. Geochemistry* **22**: 529–554.

Cook, P.L.M., Wenzhöfer, F., Glud, R.N., Janssen, F., and Huettel, M. (2007) Benthic solute exchange and carbon mineralization in two shallow subtidal sandy sediments: Effect of advective pore-water exchange. *Limnol. Oceanogr.* **52**: 1943–1963.

Culpepper, M. a and Rosenzweig, A.C. (2012) Architecture and active site of particulate methane monooxygenase. *Crit. Rev. Biochem. Mol. Biol.* **47**: 483–92.

Cutler, D.R., Edwards, T.C., Beard, K.H., Cutler, A., Hess, K.T., Gibson, J., and Lawler, J.J. (2007) Random forests for classification in ecology. *Ecology* **88**: 2783–2792.

Dahms, H.U., Hagiwara, A., and Lee, J.S. (2011) Ecotoxicology, ecophysiology, and mechanistic studies with rotifers. *Aquat. Toxicol.* **101**: 1–12.

Daly, K.L., Passow, U., Chanton, J., and Hollander, D. (2016) Assessing the impacts of oil-associated marine snow formation and sedimentation during and after the Deepwater Horizon oil spill. *Anthropocene* **13**: 18–33.

Dalyander, P.S., Long, J.W., Plant, N.G., and Thompson, D.M. (2014) Assessing mobility and redistribution patterns of sand and oil agglomerates in the surf zone. *Mar. Pollut. Bull.* **80**: 200–209.

Danovaro, R., Molari, M., Corinaldesi, C., and Dell'Anno, A. (2016) Macroecological drivers of archaea and bacteria in benthic deep-sea ecosystems. *Sci. Adv.* **2**: 1–12.

Day, J.W., Day, R.H., Barreiro, M.T., Ley-Lou, F., and Madden, C.J. (1982) Primary production in the Laguna de Terminos, a tropical estuary in the southern Gulf of Mexico. *Oceanol. Acta, Spec. issue*.

Dickey, R. and Huettel, M. (2016) Seafood and beach safety in the aftermath of the Deepwater Horizon oil spill. *Oceanography* **29**: 196–203.

Divins, D.L. and Metzger, D. (2008) NGDC coastal relief model. *Natl. Geophys. Data Center, Natl. Ocean. Atmos. Adm. US Dep. Commer. www. ngdc. noaa. gov/mgg/(last accessed December 2007)*.

Du, Z.J., Wang, Z.J., Zhao, J.X., and Chen, G.J. (2016) Woeseia oceani gen. Nov., sp. nov., a chemoheterotrophic member of the order Chromatiales, and proposal of Woeseiaceae fam. nov. *Int. J. Syst. Evol. Microbiol.* **66**: 107–112.

Dunn, D.E. (1996) Trends in nutrient inflows to the Gulf of Mexico from streams draining the conterminous United States, 1972-93.

Durbin, A.M. and Teske, A. (2012) Archaea in organic-lean and organic-rich marine subsurface sediments: an environmental gradient reflected in distinct phylogenetic lineages. *Front. Microbiol.* **3**: 168.

Durbin, A.M. and Teske, A. (2011) Microbial diversity and stratification of South Pacific abyssal marine sediments. *Environ. Microbiol.* **13**: 3219–34.

Durbin, A.M. and Teske, A. (2010) Sediment-associated microdiversity within the Marine Group I Crenarchaeota. *Environ. Microbiol. Rep.* **2**: 693–703.

Dyksma, S., Bischof, K., Fuchs, B.M., Hoffmann, K., Meier, D., Meyerdierks, A., et al. (2016) Ubiquitous Gammaproteobacteria dominate dark carbon fixation in coastal sediments. *ISME J.* **10**: 1–15.

Ebbe, B., Billett, D.S.M., Brandt, A., Ellingsen, K., Glover, A., Keller, S., et al. (2010) Diversity of abyssal marine life. *Life World's Ocean. Divers. Distrib. Abundance, Ed. by McIntyre, A* 139–160.

Edwards, B.R., Reddy, C.M., Camilli, R., Carmichael, C. a, Longnecker, K., and Van Mooy, B. a S. (2011) Rapid microbial respiration of oil from the Deepwater Horizon spill in offshore surface waters of the Gulf of Mexico. *Environ. Res. Lett.* **6**: 35301.

Elango, V., Urbano, M., Lemelle, K.R., and Pardue, J.H. (2014) Biodegradation of MC252 oil in oil:sand aggregates in a coastal headland beach environment. *Front. Microbiol.* **5**: 1–11.

Engel, A.S. and Gupta, A.A. (2014) Regime shift in sandy beach microbial communities following Deepwater Horizon oil spill remediation efforts. *PLoS One* **9**: e102934.

EPA (2015) Correction of Deepwater Horizon Acute Screening Benchmarks for Aquatic Life.

Evrard, V., Huettel, M., Cook, P.L.M., Soetaert, K., Heip, C.H.R., and Middelburg, J.J. (2012) Importance of phytodetritus and microphyto benthos for heterotrophs in a shallow subtidal sandy sediment. *Mar. Ecol. Prog. Ser.* **455**: 13–31.

F. Widdel (2010) Handbook of Hydrocarbon and Lipid Microbiology. In, Timmis,K.N. (ed), *Handbook of Hydrocarbon and Lipid Microbiology.*, pp. 3788–3797.

Federal Region VI Regional Response Team (2001) FOSC DISPERSANT PRE-APPROVAL GUIDELINES and CHECKLIST.

Feng, L., Wang, W., Cheng, J., Ren, Y., Zhao, G., Gao, C., et al. (2007) Genome and proteome of long-chain alkane degrading Geobacillus thermodenitrificans NG80-2 isolated from a deep-subsurface oil reservoir. *Proc. Natl. Acad. Sci. U. S. A.* **104**: 5602–7.

Fernández-Álvarez, P., Vila, J., Garrido-Fernández, J.M., Grifoll, M., and Lema, J.M. (2006) Trials of bioremediation on a beach affected by the heavy oil spill of the Prestige. *J. Hazard. Mater.* **137**: 1523–1531.

Foght, J. (2008) Anaerobic biodegradation of aromatic hydrocarbons: pathways and prospects. *J. Mol. Microbiol. Biotechnol.* **15**: 93–120.

Foght, J.M., Gutnick, D.L., and Westlake, D.W.S. (1989) Effect of emulsam on biodegradation of crude oil in pure and mixed cultures. *Appl. Environ. Microbiol.* **55**: 36–42.

Froland, W.A., Andersson, K.K., Lee, S., Liu, Y., and Lipscombs, D. (1992) Methane Monooxygenase Component B and Reductase Alter the Regioselectivity of the Hydroxylase Component-catalyzed Reactions. *J. Biol. Chem.* **267**: 17588–17597.

Fuchs, G., Boll, M., and Heider, J. (2011) Microbial degradation of aromatic compounds - from one strategy to four. *Nat. Rev. Microbiol.* **9**: 803–16.

Fuller, C., Bonner, J., and Page, C. (2004) Comparative toxicity of oil, dispersant, and oil plus dispersant to several marine species. *Environ. …* **23**: 2941–2949.

Gao, Y., Yu, X.Z., Wu, S.C., Cheung, K.C., Tam, N.F.Y., Qian, P.Y., and Wong, M.H. (2006) Interactions of rice (Oryza sativa L.) and PAH-degrading bacteria (Acinetobacter sp.) on enhanced dissipation of spiked phenanthrene and pyrene in waterlogged soil. *Sci. Total Environ.* **372**: 1–11.

Garcia-Pineda, O., MacDonald, I., Hu, C., Svejkovsky, J., Hess, M., Dukhovskoy, D., and Morey, S.L. (2013) Detection of floating oil anomalies from the Deepwater Horizon oil spill with synthetic aperture radar. *Oceanography* **26**: 124–137.

Garcia-Robledo, E., Corzo, A., and Papaspyrou, S. (2014) A fast and direct

spectrophotometric method for the sequential determination of nitrate and nitrite at low concentrations in small volumes. *Mar. Chem.* **162**: 30–36.

Gardiner, W.W., Word, J.Q., Word, J.D., Perkins, R. a., Mcfarlin, K.M., Hester, B.W., et al. (2013) The acute toxicity of chemically and physically dispersed crude oil to key arctic species under arctic conditions during the open water season. *Environ. Toxicol. Chem.* **32**: 2284–2300.

Geng, X., Boufadel, M.C., Lee, K., Abrams, S., and Suidan, M. (2015) Biodegradation of subsurface oil in a tidally influenced sand beach: Impact of hydraulics and interaction with pore water chemistry. *Water Resour. Res.* **51**: 3193–3218.

George-Ares, a and Clark, J.R. (2000) Aquatic toxicity of two Corexit dispersants. *Chemosphere* **40**: 897–906.

Gihring, T.M., Canion, A., Riggs, A., Huettel, M., and Kostka, J.E. (2010) Denitrification in shallow, sublittoral Gulf of Mexico permeable sediments. *Limnol. Oceanogr.* **55**: 43–54.

Gillan, D.C. and Danis, B. (2007) The archaebacterial communities in Antarctic bathypelagic sediments. *Deep Sea Res. Part II Top. Stud. Oceanogr.* **54**: 1682–1690.

Gittel, A., Donhauser, J., Røy, H., Girguis, P.R., Jørgensen, B.B., and Kjeldsen, K.U. (2015) Ubiquitous Presence and Novel Diversity of Anaerobic Alkane Degraders in Cold Marine Sediments. *Front. Microbiol.* **6**: 1–15.

Glud, R.N., Wenzhöfer, F., Middelboe, M., Oguri, K., Turnewitsch, R., Canfield, D.E., and Kitazato, H. (2013) High rates of microbial carbon turnover in sediments in the deepest oceanic trench on Earth. *Nat. Geosci.* **6**: 284–288.

Goñi, M.A., Ruttenberg, K.C., and Eglinton, T.I. (1997) Sources and contribution of terrigenous organic carbon to surface sediments in the Gulf of mexico. *Lett. To Nat.* **389**: 275–279.

Goodbody-Gringley, G., Wetzel, D.L., Gillon, D., Pulster, E., Miller, A., and Ritchie, K.B. (2013) Toxicity of Deepwater Horizon Source Oil and the Chemical Dispersant, Corexit?? 9500, to Coral Larvae. *PLoS One* **8**: 1–10.

Green, S.J., Venkatramanan, R., and Naqib, A. (2015) Deconstructing the polymerase

chain reaction: Understanding and correcting bias associated with primer degeneracies and primer-template mismatches. *PLoS One* **10**: 1–21.

Gros, J., Reddy, C.M., Aeppli, C., Nelson, R.K., Carmichael, C. a, and Arey, J.S. (2014) Resolving Biodegradation Patterns of Persistent Saturated Hydrocarbons in Weathered Oil Samples from the Deepwater Horizon Disaster. *Environ. Sci. Technol.* **48**: 1628–1637.

Grundmann, O., Behrends, A., Rabus, R., Amann, J., Halder, T., Heider, J., and Widdel, F. (2008) Genes encoding the candidate enzyme for anaerobic activation of n-alkanes in the denitrifying bacterium, strain HxN1. *Environ. Microbiol.* **10**: 376–385.

Hall, G.H. (1984) Measurement of nitrification rates in lake sediments: comparison of the nitrification inhibitors nitrapyrin and allylthiourea. *Microb. Ecol.* **10**: 25–36.

Hamdan, L. and Fulmer, P. (2011) Effects of COREXIT® EC9500A on bacteria from a beach oiled by the Deepwater Horizon spill. *Aquat. Microb. Ecol.* **63**: 101–109.

Hansell, D.A., Carlson, C.A., and Schlitzer, R. (2012) Net removal of major marine dissolved organic carbon fractions in the subsurface ocean. *Global Biogeochem. Cycles* **26**: 1–9.

Harwood, C.S., Burchhardt, G., Herrmann, H., and Fuchs, G. (1998) Anaerobic metabolism of aromatic compounds via the benzoyl-CoA pathway. *FEMS Microbiol. Rev.* **22**: 439–458.

Harwood, C.S. and Parales, R.E. (1996) the B -Ketoadipate Pathway and the Biology of Self-Identity.

Hayworth, J.S. and Clement, T.P. (2012) Provenance of Corexit-related chemical constituents found in nearshore and inland Gulf Coast waters. *Mar. Pollut. Bull.* **64**: 2005–14.

Hayworth, J.S., Clement, T.P., John, G.F., and Yin, F. (2015) Fate of Deepwater Horizon oil in Alabama's beach system: Understanding physical evolution processes based on observational data. *Mar. Pollut. Bull.* **90**: 95–105.

Hayworth, J.S., Clement, T.P., and Valentine, J.F. (2011) Deepwater Horizon oil spill impacts on Alabama beaches. *Hydrol. Earth Syst. Sci.* **15**: 3639–3649.

Hazen, T.C. (2010) Cometabolic bioremediation. In, *Handbook of Hydrocarbon and Lipid Microbiology*. Springer, pp. 2505–2514.

Hazen, T.C., Dubinsky, E. a, DeSantis, T.Z., Andersen, G.L., Piceno, Y.M., Singh, N., et al. (2010) Deep-sea oil plume enriches indigenous oil-degrading bacteria. *Science* **330**: 204–8.

Hazen, T.C. and Prince, R.C. (2015) Marine Oil Biodegradation. *Environ. Sci. Technol.* **50**: 2121–2129.

Hazen, T.C., Prince, R.C., and Mahmoudi, N. (2016) Marine oil biodegradation.

Head, I.M., Jones, D.M., and Röling, W.F.M. (2006) Marine microorganisms make a meal of oil. *Nat. Rev. Microbiol.* **4**: 173–82.

Heiss, J.W. and Michael, H.A. (2014) Saltwater-freshwater mixing dynamics in a sandy beach aquifer over tidal, spring-neap, and seasonal cycles. *Water Resour. Res.* **50**: 6747–6766.

Hemmer, M.J., Barron, M.G., and Greene, R.M. (2011) Comparative toxicity of eight oil dispersants, Louisiana sweet crude oil (LSC), and chemically dispersed LSC to two aquatic test species. *Environ. Toxicol. Chem.* **30**: 2244–52.

Hernández-López, E.L., Perezgasga, L., Huerta-Saquero, A., Mouriño-Pérez, R., and Vazquez-Duhalt, R. (2016) Biotransformation of petroleum asphaltenes and high molecular weight polycyclic aromatic hydrocarbons by Neosartorya fischeri. *Environ. Sci. Pollut. Res.*

Hollander, D., Brooks, G., Larson, R., Romero, I., and Schwing, P. (2013) Testing the mechanisms of sedimentary oil deposition in the deep-sea. In, *Proceedings of the Gulf of Mexico Oil Spill & Ecosystem Sciences Conference*. New Orleans, LA.

Honjo, S., Manganini, S.J., Krishfield, R.A., and Francois, R. (2008) Particulate organic carbon fluxes to the ocean interior and factors controlling the biological pump: A synthesis of global sediment trap programs since 1983. *Prog. Oceanogr.* **76**: 217–285.

Hopkinson Jr, C. and Vallino, J. (2005) Efficient expert of carbon to the deep ocean through dissolved organic matter. *Nature* **433**: 142–145.

Horak, R.E.A., Whitney, H., Shull, D.H., Mordy, C.W., and Devol, A.H. (2013) The role of sediments on the Bering Sea shelf N cycle: insights from measurements of benthic denitrification and benthic DIN fluxes. *Deep Sea Res. Part II Top. Stud. Oceanogr.* **94**: 95–105.

Horel, A., Bernard, R.J., and Mortazavi, B. (2014) Impact of crude oil exposure on nitrogen cycling in a previously impacted Juncus roemerianus salt marsh in the northern Gulf of Mexico. *Environ. Sci. Pollut. Res.* **21**: 6982–6993.

Howard, P., Meylan, W., Aronson, D., Stiteler, W., Tunkel, J., Comber, M., and Parkerton, T.F. (2005) A new biodegradation prediction model specific to petroleum hydrocarbons. *Environ. Toxicol. Chem.* **24**: 1847–1860.

Huettel, M., Berg, P., and Kostka, J.E. (2014) Benthic exchange and biogeochemical cycling in permeable sediments. *Ann. Rev. Mar. Sci.* **6**: 23–51.

Huettel, M. and Gust, G. (1992) Solute release mechanisms from confined sediment cores in stirred benthic chambers and flume flows. *Mar. Ecol. Prog. Ser.* **82**: 187–197.

Huettel, M., Overholt, W.A., Kostka, J.E., Hagan, C., Kaba, J., Wells, W.B., and Dudley, S. (2018) Degradation of Deepwater Horizon oil buried in a Florida beach influenced by tidal pumping. *Mar. Pollut. Bull.* **126**: 488–500.

Huettel, M. and Rusch, A. (2000) Transport and degradation of phytoplankton in permeable sediment. *Limnol. Oceanogr.* **45**: 534–549.

Jacob, M., Soltwedel, T., Boetius, A., and Ramette, A. (2013) Biogeography of Deep-Sea Benthic Bacteria at Regional Scale (LTER HAUSGARTEN, Fram Strait, Arctic). *PLoS One* **8**: e72779.

Jernelöv, A. and Lindén, O. (1981) Ixtoc I: a case study of the world's largest oil spill. *Ambio* 299–306.

Jiao, J.J. and Li, H. (2004) Breathing of coastal vadose zone induced by sea level fluctuations. *Geophys. Res. Lett.* **31**:.

Jiménez, N., Viñas, M., Bayona, J.M., Albaiges, J., and Solanas, A.M. (2007) The Prestige oil spill: bacterial community dynamics during a field biostimulation assay. *Appl. Microbiol. Biotechnol.* **77**: 935–945.

Jørgensen, B.B. and Boetius, A. (2007) Feast and famine — microbial life in the deep-sea bed. *Nat. Rev. Microbiol.* **5**: 770–781.

Joye, S., Kleindienst, S., Gilbert, J., Handley, K., Weisenhorn, P., Overholt, W., and Kostka, J. (2016) Responses of Microbial Communities to Hydrocarbon Exposures. *Oceanography* **29**: 136–149.

Joye, S.B. (2015) Deepwater Horizon, 5 years on. *Science (80-.).* **349**: 592–593.

Joye, S.B., MacDonald, I.R., Leifer, I., and Asper, V. (2011) Magnitude and oxidation potential of hydrocarbon gases released from the BP oil well blowout. *Nat. Geosci.* **4**: 160–164.

Kang, Y.-S., Jung, J., Jeon, C., and Park, W. (2011) Acinetobacter oleivorans sp. nov. Is capable of adhering to and growing on diesel-oil. *J. Microbiol.* **49**: 29–34.

Kappell, A.D., Wei, Y., Newton, R.J., Van Nostrand, J.D., Zhou, J., McLellan, S.L., and Hristova, K.R. (2014) The polycyclic aromatic hydrocarbon degradation potential of Gulf of Mexico native coastal microbial communities after the Deepwater Horizon oil spill. *Front. Microbiol.* **5**: 1–13.

Khalili, A., Basu, A.J., and Huettel, M. (1997) A non-Darcy model for recirculating flow through a fluid-sediment interface in a cylindrical container. *Acta Mech.* **123**: 75–87.

Kim, J.-S. and Crowley, D.E. (2007) Microbial diversity in natural asphalts of the Rancho La Brea Tar Pits. *Appl. Environ. Microbiol.* **73**: 4579–4591.

Kimes, N.E., Callaghan, A. V, Aktas, D.F., Smith, W.L., Sunner, J., Golding, B., et al. (2013) Metagenomic analysis and metabolite profiling of deep-sea sediments from the Gulf of Mexico following the Deepwater Horizon oil spill. *Front. Microbiol.* **4**: 50.

Kimes, N.E., Callaghan, A. V, Suflita, J.M., and Morris, P.J. (2014) Microbial transformation of the Deepwater Horizon oil spill – past , present, and future perspectives. *Front. Microbiol.* **5**:.

King, G.M., Kostka, J.E., Hazen, T.C., and Sobecky, P.A. (2015) Microbial responses to the Deepwater Horizon oil spill: from coastal wetlands to the deep sea. *Ann. Rev. Mar. Sci.* **7**: 377–401.

King, G.M.M., Kostka, J.E., Hazen, T.C.C., and Sobecky, P.A.A. (2014) Microbial Responses to the Deepwater Horizon oil spill: From Coastal Wetlands to the Deep Sea. *Ann. Rev. Mar. Sci.*

Kleindienst, S., Paul, J.H., and Joye, S.B. (2015) Using dispersants after oil spills: impacts on the composition and activity of microbial communities. *Nat. Rev. Microbiol.* **13**: 388–396.

Koch, D.J., Chen, M.M., van Beilen, J.B., and Arnold, F.H. (2009) In vivo evolution of butane oxidation by terminal alkane hydroxylases AlkB and CYP153A6. *Appl. Environ. Microbiol.* **75**: 337–44.

Kostka, J.E., Prakash, O., Overholt, W.A., Green, S.J., Freyer, G., Canion, A., et al. (2011) Hydrocarbon-degrading bacteria and the bacterial community response in gulf of Mexico beach sands impacted by the deepwater horizon oil spill. *Appl. Environ. Microbiol.* **77**: 7962–74.

Kuever, J. (2014) The Family Syntrophobacteraceae. In, *The Prokaryotes*. Springer, pp. 289–299.

Kukert, H. and Smith, C.R. (1992) Disturbance, colonization and succession in a deep-sea sediment community: artificial-mound experiments. *Deep Sea Res. Part A, Oceanogr. Res. Pap.* **39**: 1349–1371.

Kvenvolden, K.A. and Cooper, C.K. (2003) Natural seepage of crude oil into the marine environment. *Geo-Marine Lett.* **23**: 140–146.

Ladino-Orjuela, G., Gomes, E., da Silva, R., Salt, C., and Parsons, J.R. (2016) Metabolic Pathways for Degradation of Aromatic Hydrocarbons by Bacteria. In, *Reviews of Environmental Contamination and Toxicology Volume 237*. Springer, pp. 105–121.

Lamendella, R., Strutt, S., Borglin, S., Chakraborty, R., Tas, N., Mason, O.U., et al. (2014) Assessment of the Deepwater Horizon oil spill impact on Gulf coast microbial communities. *Front. Microbiol.* **5**: 130.

Lavania, M., Cheema, S., Sarma, P.M., Mandal, A.K., and Lal, B. (2012) Biodegradation of asphalt by Garciaella petrolearia TERIG02 for viscosity reduction of heavy oil. *Biodegradation* **23**: 15–24.

Leahy, J.G. and Colwell, R.R. (1990) Microbial degradation of hydrocarbons in the environment. *Microbiol. Rev.* **54**: 305–315.

Learman, D.R., Henson, M.W., Thrash, J.C., Temperton, B., Brannock, P.M., Santos, S.R., et al. (2016) Biogeochemical and microbial variation across 5500 km of Antarctic surface sediment implicates organic matter as a driver of benthic community structure. *Front. Microbiol.* **7**: 1–11.

Lee, K., Nedwed, T., Prince, R.C., and Palandro, D. (2013) Lab tests on the biodegradation of chemically dispersed oil should consider the rapid dilution that occurs at sea. *Mar. Pollut. Bull.* **73**: 314–318.

Lehmann, M.F., Sigman, D.M., and Berelson, W.M. (2004) Coupling the 15N/14N and 18O/16O of nitrate as a constraint on benthic nitrogen cycling. *Mar. Chem.* **88**: 1–20.

Lehr, B., Bristol, S., and Possolo, A. (2010) Oil Budget Calculator.

Lessard, R.R. and DeMarco, G. (2000) The significance of oil spill dispersants. *Spill Sci. Technol. Bull.* **6**:.

Li, M., Sanford, L., and Chao, S.-Y. (2005) Effects of time dependence in unstratified tidal boundary layers: results from large eddy simulations. *Estuar. Coast. Shelf Sci.* **62**: 193–204.

Liaw, A. and Wiener, M. (2002) Classification and Regression by randomForest. *R News* **2**: 18–22.

Lipsewers, Y.A., Bale, N.J., Hopmans, E.C., Schouten, S., Sinninghe Damst??, J.S., and Villanueva, L. (2014) Seasonality and depth distribution of the abundance and activity of ammonia oxidizing microorganisms in marine coastal sediments (North Sea). *Front. Microbiol.* **5**: 1–12.

Lisle, J.T. and Stellick, S.H. (2011) A survey of microbial community diversity in marine sediments impacted by petroleum hydrocarbons from the Gulf of Mexico and Atlantic shorelines, Texas to Florida.

Liu, Z. and Liu, J. (2013) Evaluating bacterial community structures in oil collected from the sea surface and sediment in the northern Gulf of Mexico after the Deepwater Horizon oil spill. *Microbiologyopen*.

Liu, Z., Liu, J., Zhu, Q., and Wu, W. (2012) The weathering of oil after the DeepwaterHorizon oil spill: Insights from the chemical composition of the oil from the sea surface, salt marshes and sediments. *Environ. Res. Lett.* **7**:.

Lozupone, C. a and Knight, R. (2007) Global patterns in bacterial diversity. *Proc. Natl. Acad. Sci. U. S. A.* **104**: 11436–11440.

Lu, Z., Deng, Y., Van Nostrand, J.D., He, Z., Voordeckers, J., Zhou, A., et al. (2012) Microbial gene functions enriched in the Deepwater Horizon deep-sea oil plume. *ISME J.* **6**: 451–460.

Lubchenco, J., McNutt, M., Lehr, B., Sogge, M., Miller, M., Hammond, S., and Conner, W. (2010) Deepwater Horizon/BP Oil Budget: What happened to the oil? Silver Spring, MD.

Lubchenco, J., McNutt, M.K., Dreyfus, G., Murawski, S. a, Kennedy, D.M., Anastas, P.T., et al. (2012) Science in support of the Deepwater Horizon response. *Proc. Natl. Acad. Sci. U. S. A.* **109**: 20212–21.

Lysiak-Pastuszak, E. and Krysell, M. (2004) Chemical measurements in the Baltic Sea: Guidelines on quality assurance International Council for the Exploration of the Sea.

MacDonald, I.R., Garcia-Pineda, O., Beet, A., Daneshgar Asl, S., Feng, L., Graettinger, G., et al. (2015) Natural and unnatural oil slicks in the Gulf of Mexico. *J. Geophys. Res. Ocean.* **120**: 8364–8380.

Mahé, F., Rognes, T., Quince, C., de Vargas, C., and Dunthorn, M. (2014) Swarm: robust and fast clustering method for amplicon-based studies. *PeerJ* **2**: e593.

Mahmoudi, N., Porter, T.M., Zimmerman, A.R., Fulthorpe, R.R., Kasozi, G.N., Silliman, B.R., and Slater, G.F. (2013) Rapid degradation of deepwater horizon spilled oil by indigenous microbial communities in louisiana saltmarsh sediments. *Environ. Sci. Technol.* **47**: 13303–13312.

Marin-Spiotta, E., Gruley, K.E., Crawford, J., Atkinson, E.E., Miesel, J.R., Greene, S., et al. (2014) Paradigm shifts in soil organic matter research affect interpretations of aquatic carbon cycling: Transcending disciplinary and ecosystem boundaries. *Biogeochemistry* **117**: 279–297.

Mason, O.U., Hazen, T.C., Borglin, S., Chain, P.S.G., Dubinsky, E. a, Fortney, J.L., et al. (2012) Metagenome, metatranscriptome and single-cell sequencing reveal microbial response to Deepwater Horizon oil spill. *ISME J.* **6**: 1715–27.

Mason, O.U., Scott, N.M., Gonzalez, A., Robbins-Pianka, A., Bælum, J., Kimbrel, J., et al. (2014) Metagenomics reveals sediment microbial community response to Deepwater Horizon oil spill. *ISME J.* 1–12.

McMurdie, P.J. and Holmes, S. (2013) phyloseq: an R package for reproducible interactive analysis and graphics of microbiome census data. *PLoS One* **8**: e61217.

McNutt, M.K., Camilli, R., Crone, T.J., Guthrie, G.D., Hsieh, P. a, Ryerson, T.B., et al. (2012) Review of flow rate estimates of the Deepwater Horizon oil spill. *Proc. Natl. Acad. Sci. U. S. A.* **109**: 20260–7.

Meybeck, M. and Ragu, A. (2012) GEMS-GLORI world river discharge database.

Mezić, I., Loire, S., Fonoberov, V.A., and Hogan, P. (2010) A new mixing diagnostic and Gulf oil spill movement. *Science (80-.).* **330**: 486–489.

Michel, J., Owens, E.H., Zengel, S., Graham, A., Nixon, Z., Allard, T., et al. (2013) Extent and degree of shoreline oiling: Deepwater Horizon oil spill, Gulf of Mexico, USA. *PLoS One* **8**: e65087.

Mohajeri, L., Aziz, H.A., Isa, M.H., and Zahed, M.A. (2010) A statistical experiment design approach for optimizing biodegradation of weathered crude oil in coastal sediments. *Bioresour. Technol.* **101**: 893–900.

Mori, K., Suzuki, K.I., Urabe, T., Sugihara, M., Tanaka, K., Hamada, M., and Hanada, S. (2011) Thioprofundum hispidum sp. nov., an obligately chemolithoautotrophic sulfur-oxidizing gammaproteobacterium isolated from the hydrothermal field on Suiyo Seamount, and proposal of Thioalkalispiraceae fam. nov. in the order Chromatiales. *Int. J. Syst. Evol. Microbiol.* **61**: 2412–2418.

Mortazavi, B., Horel, A., Beazley, M.J., and Sobecky, P. a (2013) Intrinsic rates of petroleum hydrocarbon biodegradation in Gulf of Mexico intertidal sandy sediments and its enhancement by organic substrates. *J. Hazard. Mater.* **244**–**245**: 537–544.

Moss, J.A., McCurry, C., Schwing, P., Jeffrey, W.H., Romero, I.C., Hollander, D.J., and

Snyder, R.A. (2016) Molecular characterization of benthic foraminifera communities from the Northeastern Gulf of Mexico shelf and slope following the Deepwater Horizon event. *Deep. Res. Part I Oceanogr. Res. Pap.* **115**: 1–9.

Mulabagal, V., Yin, F., John, G.F., Hayworth, J.S., and Clement, T.P. (2013) Chemical fingerprinting of petroleum biomarkers in Deepwater Horizon oil spill samples collected from Alabama shoreline. *Mar. Pollut. Bull.* **70**: 147–154.

Mulkins-Phillips, G.J. and Stewart, J.E. (1974) Effect of four dispersants on biodegradation and growth of bacteria on crude oil. *Appl. Microbiol.* **28**: 547–552.

Murphy, J. and Riley, J. (1962) A modified single solution method for the determination of phosphate in natural waters. *Anal. Chim. Acta* **27**: 31–36.

Mußmann, M., Pjevac, P., Krüger, K., and Dyksma, S. (2017) Genomic repertoire of the Woeseiaceae/JTB255, cosmopolitan and abundant core members of microbial communities in marine sediments. *ISME J.* 1–6.

Naether, D.J., Slawtschew, S., Stasik, S., Engel, M., Olzog, M., Wick, L.Y., et al. (2013) Adaptation of the hydrocarbonoclastic bacterium Alcanivorax borkumensis SK2 to alkanes and toxic organic compounds: a physiological and transcriptomic approach. *Appl. Environ. Microbiol.* **79**: 4282–93.

National Research Council (2005) Oil Spill Dispersants: Efficacy and Effects National Academies Press, Washington, DC.

Newton, R.J., Huse, S.M., Morrison, H.G., Peake, C.S., Sogin, M.L., and McLellan, S.L. (2013) Shifts in the microbial community composition of gulf coast beaches following beach oiling. *PLoS One* **8**: e74265.

Ng, K.-Y., Tu, L.-C., Wang, Y.-S., Chan, S.I., and Yu, S.S.-F. (2008) Probing the hydrophobic pocket of the active site in the particulate methane monooxygenase (pMMO) from Methylococcus capsulatus (Bath) by variable stereoselective alkane hydroxylation and olefin epoxidation. *Chembiochem* **9**: 1116–23.

Nixon, Z., Zengel, S., Baker, M., Steinhoff, M., Fricano, G., Rouhani, S., and Michel, J. (2016) Shoreline oiling from the Deepwater Horizon oil spill. *Mar. Pollut. Bull.* **107**: 170–178.

Nunoura, T., Soffientino, B., Blazejak, A., Kakuta, J., Oida, H., Schippers, A., and Takai, K. (2009) Subseafloor microbial communities associated with rapid turbidite deposition in the Gulf of Mexico continental slope (IODP Expedition 308). *FEMS Microbiol. Ecol.* **69**: 410–24.

Nzila, A. (2013) Update on the cometabolism of organic pollutants by bacteria. *Environ. Pollut.* **178**: 474–482.

Oksanen, J., Blanchet, F.G., Kindt, R., Legendre, P., Minchin, P.R., O'Hara, R.B., et al. (2007) The Vegan Package. *Community Ecol. Packag.* **10**: 631–637.

on Oil in the Sea, N.R.C. (US). C. and Fates (2003) Oil in the Sea III: Inputs, Fates and Effects national academies Press.

Operational Science Advisory Team (2013) (OSAT-3) - Investigation of Recurring Residual Oil in Discrete Shoreline Areas in the Eastern Area of Responsibility.

Operational Science Advisory Team (OSAT) (2010) Summary report for sub-sea and subsurface oil and disperstant detection: sampling and monitoring. Available at: https://www.restorethegulf.gov/sites/default/files/documents/pdf/OSAT_Report_FINAL_17DEC.pdf.

Oppel, S. and Huettmann, F. (2010) Using a Random Forest Model and Public Data to Predict the Distribution of Prey for Marine Wildlife Management. In, Cushman,S.A. and Huettmann,F. (eds), *Spatial Complexity, Informatics, and Wildlife Conservation*. Springer Japan, Tokyo, pp. 151–163.

Or, D., Smets, B.F., Wraith, J.M., Dechesne, A., and Friedman, S.P. (2007) Physical constraints affecting bacterial habitats and activity in unsaturated porous media--a review. *Adv. Water Resour.* **30**: 1505–1527.

Orcutt, B.N., Joye, S.B., Kleindienst, S., Knittel, K., Ramette, A., Reitz, A., et al. (2010) Impact of natural oil and higher hydrocarbons on microbial diversity, distribution, and activity in Gulf of Mexico cold-seep sediments. *Deep Sea Res. Part II Top. Stud. Oceanogr.* **57**: 2008–2021.

Ornston, L.N. and Stanier, R.Y. (1966) The Conversion of Catechol and Protocatechuate to β-Ketoadipate by Pseudomonas putida I. BIOCHEMISTRY. *J. Biol. Chem.* **241**: 3776–3786.

Ortmann, A.C. and Lu, Y. (2015) Initial community and environment determine the response of bacterial communities to dispersant and oil contamination. *Mar. Pollut. Bull.* **90**: 106–114.

OSAT (2011) Summary Report for Sub-Sea and Sub-Surface Oil and Dispersant Detection: Ecotoxicity Addendum Prepared for.

Oshiki, M., Satoh, H., and Okabe, S. (2016) Ecology and physiology of anaerobic ammonium oxidizing bacteria. *Environ. Microbiol.* **18**: 2784–2796.

Overholt, W.A., Green, S.J., Marks, K.P., Venkatraman, R., Prakash, O., and Kostka, E. (2013) Draft Genome Sequences for Oil-Degrading Bacterial Strains from Beach Sands Impacted by the Deepwater Horizon Oil Spill. *Genome Announc.* **1**: 1–2.

Page, C.A., Bonner, J.S., Sumner, P.L., McDonald, T.J., Autenrieth, R.L., and Fuller, C.B. (2000) Behavior of a chemically-dispersed oil and a whole oil on a near-shore environment. *Water Res.* **34**: 2507–2516.

Passow, U., Ziervogel, K., Asper, V., and Diercks, A. (2012) Marine snow formation in the aftermath of the Deepwater Horizon oil spill in the Gulf of Mexico. *Environ. Sci. Technol.* 1–11.

Passow, U., Ziervogel, K., Asper, V., and Diercks, a (2012) Marine snow formation in the aftermath of the Deepwater Horizon oil spill in the Gulf of Mexico. *Environ. Res. Lett.* **7**: 35301.

Paulson, J.N., Stine, O.C., Bravo, H.C., and Pop, M. (2013) Differential abundance analysis for microbial marker-gene surveys. *Nat. Methods* **10**: 1200–2.

Pelz, O., Brown, J., Huddleston, M., Rand, G., Gardinali, P., Stubblefield, W., et al. (2011) Selection of a Surrogate MC252 Oil as a Reference Material for Future Aquatic Toxicity Tests and Other Studies.

Penton, C.R., Devol, A.H., and Tiedje, J.M. (2006) Molecular evidence for the broad distribution of anaerobic ammonium-oxidizing bacteria in freshwater and marine sediments. *Appl. Environ. Microbiol.* **72**: 6829–6832.

Pester, M., Schleper, C., and Wagner, M. (2011) The Thaumarchaeota: An emerging view of their phylogeny and ecophysiology. *Curr. Opin. Microbiol.* **14**: 300–306.

Pietroski, J.P., White, J.R., and DeLaune, R.D. (2015) Effects of dispersant used for oil spill remediation on nitrogen cycling in Louisiana coastal salt marsh soil. *Chemosphere* **119**: 562–567.

Price, M.N., Dehal, P.S., and Arkin, A.P. (2010) FastTree 2 – Approximately Maximum-Likelihood Trees for Large Alignments. *PLoS One* **5**: e9490.

Prince, R.C. (2010) Bioremediation of Marine Oil Spills. In, Timmis,K.N. (ed), *Handbook of Hydrocarbon and Lipid Microbiology SE - 194*. Springer, Berlin, pp. 2617–2630.

Prince, R.C. and Butler, J.D. (2014) A protocol for assessing the effectiveness of oil spill dispersants in stimulating the biodegradation of oil. *Environ. Sci. Pollut. Res.* **21**: 9506–9510.

Prince, R.C., Lessard, R.R., and Clark, J.R. (2003) Bioremediation of Marine Oil Spills. *Oil Gas Sci. Technol.* **58**: 463–468.

Prince, R.C., McFarlin, K.M., Butler, J.D., Febbo, E.J., Wang, F.C.Y., and Nedwed, T.J. (2013) The primary biodegradation of dispersed crude oil in the sea. *Chemosphere* **90**: 521–526.

Qiao, N. and Shao, Z. (2010) Isolation and characterization of a novel biosurfactant produced by hydrocarbon-degrading bacterium Alcanivorax dieselolei B-5. *J. Appl. Microbiol.* **108**: 1207–1216.

Quast, C., Pruesse, E., Yilmaz, P., Gerken, J., Schweer, T., Yarza, P., et al. (2012) The SILVA ribosomal RNA gene database project: improved data processing and web-based tools. *Nucleic Acids Res.* **41**: D590–D596.

R Core Team (2014) R: A Language and Environment for Statistical Computing.

Ramseur, J.L. (2010) Deepwater Horizon oil spill: the fate of the oil.

Rather, L.J., Knapp, B., Haehnel, W., and Fuchs, G. (2010) Coenzyme A-dependent aerobic metabolism of benzoate via epoxide formation. *J. Biol. Chem.* **285**: 20615–20624.

Reddy, C.M., Arey, J.S., Seewald, J.S., Sylva, S.P., Lemkau, K.L., Nelson, R.K., et al.

(2012) Composition and fate of gas and oil released to the water column during the Deepwater Horizon oil spill. *Proc. Natl. Acad. Sci. U. S. A.* **109**: 20229–20234.

Reddy, C.M., Eglinton, T.I., Hounshell, A., White, H.K., Xu, L., Gaines, R.B., and Frysinger, G.S. (2002) The West Falmouth oil spill after thirty years: the persistence of petroleum hydrocarbons in marsh sediments. *Environ. Sci. Technol.* **36**: 4754–4760.

Redmond, M.C. and Valentine, D.L. (2012) Natural gas and temperature structured a microbial community response to the Deepwater Horizon oil spill. *Proc. Natl. Acad. Sci.* **109**: 20292–20297.

Reed, A.J., Lutz, R.A., and Vetriani, C. (2006) Vertical distribution and diversity of bacteria and archaea in sulfide and methane-rich cold seep sediments located at the base of the Florida Escarpment. *Extremophiles* **10**: 199–211.

Rico-Martínez, R., Snell, T.W., and Shearer, T.L. (2013) Synergistic toxicity of Macondo crude oil and dispersant Corexit 9500A(®) to the Brachionus plicatilis species complex (Rotifera). *Environ. Pollut.* **173**: 5–10.

Rivers, A.R., Sharma, S., Tringe, S.G., Martin, J., Joye, S.B., and Moran, M.A. (2013) Transcriptional response of bathypelagic marine bacterioplankton to the Deepwater Horizon oil spill. *ISME J.* **7**: 1–15.

Rivkina, E.M., Friedmann, E.I., McKay, C.P., and Gilichinsky, D.A. (2000) Metabolic activity of permafrost bacteria below the freezing point. *Appl. Environ. Microbiol.* **66**: 3230–3233.

Rodriguez-R, L.M., Overholt, W. a, Hagan, C., Huettel, M., Kostka, J.E., and Konstantinidis, K.T. (2015) Microbial community successional patterns in beach sands impacted by the Deepwater Horizon oil spill. *ISME J.* 1–13.

Rognes, T., Flouri, T., Nichols, B., Quince, C., and Mahe, F. (2016) VSEARCH : a versatile open source tool for metagenomics (# 13057). *PeerJ Prepr.* 1–30.

Rojo, F. (2009) Degradation of alkanes by bacteria. *Environ. Microbiol.* **11**: 2477–90.

Romero, I.C., Schwing, P.T., Brooks, G.R., Larson, R.A., Hastings, D.W., Ellis, G., et al. (2015) Hydrocarbons in deep-sea sediments following the 2010 Deepwater Horizon

blowout in the northeast Gulf of Mexico. *PLoS One* **10**: 1–23.

Romero, I.C., Toro-Farmer, G., Diercks, A.R., Schwing, P., Muller-Karger, F., Murawski, S., and Hollander, D.J. (2017) Large-scale deposition of weathered oil in the Gulf of Mexico following a deep-water oil spill. *Environ. Pollut.* **228**: 179–189.

Ron, E.Z. and Rosenberg, E. (2002) Biosurfactants and oil bioremediation. *Curr. Opin. Biotechnol.* **13**: 249–252.

Rosenberg, E. and Ron, E.Z. (2013) Biosurfactants. In, Rosenberg,E., Delong,E.F., Lory,S., Stackebrandt,E., and Thompson,F. (eds), *The Prokaryotes*. Springer-Verlag, Berlin, Heidelberg, pp. 545–577.

Rowland, A.P., Lindley, D.K., Hall, G.H., Rossall, M.J., Wilson, D.R., Benham, D.G., et al. (2000) Effects of beach sand properties, temperature and rainfall on the degradation rates of oil in buried oil/beach sand mixtures. *Environ. Pollut.* **109**: 109–118.

Ruddy, B.M., Huettel, M., Kostka, J.E., Lobodin, V. V, Bythell, B.J., McKenna, A.M., et al. (2014) Targeted petroleomics: analytical investigation of Macondo well oil oxidation products from Pensacola Beach. *Energy & Fuels* **28**: 4043–4050.

Ryerson, T.B., Camilli, R., Kessler, J.D., Kujawinski, E.B., Reddy, C.M., Valentine, D.L., et al. (2012) Chemical data quantify Deepwater Horizon hydrocarbon flow rate and environmental distribution. *Proc. Natl. Acad. Sci. U. S. A.* **109**: 20246–53.

Sabirova, J.S., Chernikova, T.N., Timmis, K.N., and Golyshin, P.N. (2008) Niche-specificity factors of a marine oil-degrading bacterium Alcanivorax borkumensis SK2. *FEMS Microbiol. Lett.* **285**: 89–96.

Santos, I.R., Burnett, W.C., Dittmar, T., Suryaputra, I.G.N.A., and Chanton, J. (2009) Tidal pumping drives nutrient and dissolved organic matter dynamics in a Gulf of Mexico subterranean estuary. *Geochim. Cosmochim. Acta* **73**: 1325–1339.

Schauer, R., Bienhold, C., Ramette, A., and Harder, J. (2010) Bacterial diversity and biogeography in deep-sea surface sediments of the South Atlantic Ocean. *ISME J.* **4**: 159–170.

Schlitzer, R. (2012) Ocean data view.

Schloss, P.D., Westcott, S.L., Ryabin, T., Hall, J.R., Hartmann, M., Hollister, E.B., et al. (2009) Introducing mothur: Open-source, platform-independent, community-supported software for describing and comparing microbial communities. *Appl. Environ. Microbiol.* **75**: 7537–7541.

Schrope, M. (2010) The lost legacy of the last great oil spill.

Schwing, P.T., Romero, I.C., Larson, R.A., O'Malley, B.J., Fridrik, E.E., Goddard, E.A., et al. (2016) Sediment Core Extrusion Method at Millimeter Resolution Using a Calibrated, Threaded-rod. *J. Vis. Exp.*

Seidel, M., Kleindienst, S., Dittmar, T., Joye, S.B., and Medeiros, P.M. (2015) Biodegradation of crude oil and dispersants in deep seawater from the Gulf of Mexico: Insights from ultra-high resolution mass spectrometry. *Deep Sea Res. Part II Top. Stud. Oceanogr.*

Shafir, S., Van Rijn, J., and Rinkevich, B. (2007) Short and long term toxicity of crude oil and oil dispersants to two representative coral species. *Environ. Sci. Technol.* **41**: 5571–5574.

Shi, R. and Yu, K. (2014) Impact of exposure of crude oil and dispersant (COREXIT EC 9500A) on denitrification and organic matter mineralization in a Louisiana salt marsh sediment. *Chemosphere* **108**: 300–305.

Sikkema, J., De Bont, J.A., and Poolman, B. (1995) Mechanisms of membrane toxicity of hydrocarbons. *Microbiol. Rev.* **59**: 201–222.

Simister, R.L., Poutasse, C.M., Thurston, A.M., Reeve, J.L., Baker, M.C., and White, H.K. (2015) Degradation of oil by fungi isolated from Gulf of Mexico beaches. *Mar. Pollut. Bull.* **100**: 327–333.

Singer, E., Webb, E. a, Nelson, W.C., Heidelberg, J.F., Ivanova, N., Pati, A., and Edwards, K.J. (2011) Genomic potential of Marinobacter aquaeolei, a biogeochemical "opportunitroph". *Appl. Environ. Microbiol.* **77**: 2763–71.

Singer, M.M., Aurand, D., Bragin, G.E., Clark, J.R., Coelho, G.M., Sowby, M.L., and Tjeerdema, R.S. (2000) Standardization of the preparation and quantitation of water-accommodated fractions of petroleum for toxicity testing. *Mar. Pollut. Bull.* **40**: 1007–1016.

Sipos, A.J. and Urakawa, H. (2016) Differential responses of nitrifying archaea and bacteria to methylene blue toxicity. *Lett. Appl. Microbiol.* **62**: 199–206.

Smith, A., Sterba-Boatwright, B., and Mott, J. (2010) Novel application of a statistical technique, Random Forests, in a bacterial source tracking study. *Water Res.* **44**: 4067–4076.

Smith, C.R. and Baco, A.R. (2003) Ecology of whale falls at the deep-sea floor. *Oceanogr. Mar. Biol.* **41**: 311–354.

Smith, P. V (1952) The occurrence of hydrocarbons in recent sediments from the Gulf of Mexico. *Science (80-.).* 437–439.

Snell, T.W. and Janssen, C.R. (1995) Rotifers in ecotoxicology: a review. In, *Rotifera VII*. Springer, pp. 231–247.

Snyder, R.A., Vestal, A., Welch, C., Barnes, G., Pelot, R., Ederington-Hagy, M., and Hileman, F. (2014) PAH concentrations in Coquina (Donax spp.) on a sandy beach shoreline impacted by a marine oil spill. *Mar. Pollut. Bull.* **83**: 87–91.

Sørensen, J. (1978) Denitrification rates in a marine sediment as measured by the acetylene inhibition technique. *Appl. Environ. Microbiol.* **36**: 139–143.

Sørensen, J., Jørgensen, B.B., and Revsbech, N.P. (1979) A comparison of oxygen, nitrate, and sulfate respiration in coastal marine sediments. *Microb. Ecol.* **5**: 105–115.

Soto, L.A., Botello, A. V., Licea-DurÃ¡n, S., LizÃ¡rraga-Partida, M.L., and YÃ¡Ã±ez-Arancibia, A. (2014) The environmental legacy of the Ixtoc-I oil spill in Campeche Sound, southwestern Gulf of Mexico. *Front. Mar. Sci.* **1**: 1–9.

Stone, B.R. (2012) tsk: Trimmed Spearman-Karber Method.

Strickland, J.D.H. and Parsons, T.R. (1972) A practical handbook of seawater analysis Fisheries Research Board of Canada.

Suss, J.S., Honarvar, S., Spotila, J.R., and O'Connor, M.P. (2012) Beach characteristics affect the gas exchange environment for sea turtle nests. In, *INTEGRATIVE AND COMPARATIVE BIOLOGY*., pp. E335--E335.

Swannell, R.P.J. and Daniel, F. (1999) Effect of dispersants on oil biodegradation under simulated marine conditions. *Int. Oil Spill Conf.* **1999**: 169–176.

Syed, K., Kattamuri, C., Thompson, T.B., and Yadav, J.S. (2011) Cytochrome b 5 reductase--cytochrome b 5 as an active P450 redox enzyme system in Phanerochaete chrysosporium: Atypical properties and in vivo evidence of electron transfer capability to CYP63A2. *Arch. Biochem. Biophys.* **509**: 26–32.

Teske, A. (2013) Marine deep sediment microbial communities. In, Rosenberg,E., DeLong,E.F., Lory,S., Stackebrandt,E., and Thompson,F. (eds), *The Prokaryotes*. Springer Berlin Heidelberg, Berlin, Heidelberg, pp. 123–133.

Teufel, R., Mascaraque, V., Ismail, W., Voss, M., Perera, J., Eisenreich, W., et al. (2010) Bacterial phenylalanine and phenylacetate catabolic pathway revealed. *Proc. Natl. Acad. Sci.* **107**: 14390–14395.

Throne-Holst, M., Wentzel, A., Ellingsen, T.E., Kotlar, H.-K., and Zotchev, S.B. (2007) Identification of novel genes involved in long-chain n-alkane degradation by Acinetobacter sp. strain DSM 17874. *Appl. Environ. Microbiol.* **73**: 3327–32.

Turner, I.L. and Nielsen, P. (1997) Rapid water table fluctuations within the beach face: Implications for swash zone sediment mobility? *Coast. Eng.* **32**: 45–59.

Turner, R.E., Overton, E.B., Meyer, B.M., Miles, M.S., and Hooper-Bui, L. (2014) Changes in the concentration and relative abundance of alkanes and PAHs from the Deepwater Horizon oiling of coastal marshes. *Mar. Pollut. Bull.* **86**: 291–297.

Turner, R.E., Overton, E.B., Meyer, B.M., Miles, M.S., McClenachan, G., Hooper-Bui, L., et al. (2014) Distribution and recovery trajectory of Macondo (Mississippi Canyon 252) oil in Louisiana coastal wetlands. *Mar. Pollut. Bull.* **87**: 57–67.

Turner, R.E., Rabalais, N.N., and Justic, D. (2008) Gulf of Mexico hypoxia: aleternate states and a legacy. *Environ. Sci. Technol.* **42**: 2323–2327.

U.S. Coast Guard and Agency, U.S.E.P. (2010) Dispersant Monitoring and Assessment Directive for Subsurface Dispersant Application.

Urakawa, H., Garcia, J.C., Barreto, P.D., Molina, G. a, and Barreto, J.C. (2012) A sensitive crude oil bioassay indicates that oil spills potentially induce a change of major

nitrifying prokaryotes from the archaea to the bacteria. *Environ. Pollut.* **164**: 42–45.

Urbano, M., Elango, V., and Pardue, J.H. (2013) Biogeochemical characterization of MC252 oil: sand aggregates on a coastal headland beach. *Mar. Pollut. Bull.* **77**: 183–191.

US Environmental Protection Agency (2014) COREXIT EC9500A.

Valentine, D.L., Fisher, G.B., Bagby, S.C., Nelson, R.K., Reddy, C.M., Sylva, S.P., and Woo, M. a. (2014) Fallout plume of submerged oil from Deepwater Horizon. *Proc. Natl. Acad. Sci.* 1–6.

Valentine, D.L., Kessler, J.D., Redmond, M.C., Mendes, S.D., Heintz, M.B., Farwell, C., et al. (2010) Propane respiration jump-starts microbial response to a deep oil spill. *Science* **330**: 208–11.

Valentine, D.L., Mezić, I., Maćešić, S., Črnjarić-Žic, N., Ivić, S., Hogan, P.J., et al. (2012) Dynamic autoinoculation and the microbial ecology of a deep water hydrocarbon irruption. *Proc. Natl. Acad. Sci. U. S. A.* **109**: 20286–91.

Vaneechoutte, M., Tjernberg, I., Baldi, F., Pepi, M., Fani, R., Sullivan, E.R., et al. (1999) Oil-degrading Acinetobacter strain RAG-1 and strains described as "Acinetobacter venetianus sp. nov." belong to the same genomic species. *Res. Microbiol.* **150**: 69–73.

Varadaraj, R., Robbins, M.L., Bock, J., Pace, S., and Macdonald, D. (1995) Dispersion and Biodegradation of Oil Spills on Water. In, *International Oil Spill Conference.*, pp. 101–106.

Venosa, A.D., Suidan, M.T., King, D., and Wrenn, B.A. (1997) Use of hopane as a conservative biomarker for monitoring the bioremediation effectiveness of crude oil contaminating a sandy beach. *J. Ind. Microbiol. Biotechnol.* **18**: 131–139.

Vila, J., María Nieto, J., Mertens, J., Springael, D., and Grifoll, M. (2010) Microbial community structure of a heavy fuel oil-degrading marine consortium: linking microbial dynamics with polycyclic aromatic hydrocarbon utilization. *FEMS Microbiol. Ecol.* **73**: 349–62.

Vilcáez, J., Li, L., and Hubbard, S.S. (2013) A new model for the biodegradation kinetics

of oil droplets: application to the Deepwater Horizon oil spill in the Gulf of Mexico. *Geochem. Trans.* **14**: 4.

Vyas, T.K. and Dave, B.P. (2007) Effect of crude oil concentrations, temperature and pH on growth and degradation of crude oil by marine bacteria.

Wang, P. and Roberts, T.M. (2013) Distribution of Surficial and Buried Oil Contaminants across Sandy Beaches along NW Florida and Alabama Coasts Following the Deepwater Horizon Oil Spill in 2010. *J. Coast. Res.* **291**: 144–155.

Wang, W. and Shao, Z. (2013) Enzymes and genes involved in aerobic alkane degradation. *Front. Microbiol.* **4**: 116.

Warnock, A.M., Hagen, S.C., and Passeri, D.L. (2015) Marine Tar Residues: a Review. *Water, Air, {&} Soil Pollut.* **226**: 68.

Watkinson, R.J. and Morgan, P. (1990) Physiology of aliphatic hydrocarbon-degrading microorganisms. *Biodegradation* **1**: 79–92.

Wei, C.-L., Rowe, G.T., Escobar-Briones, E., Boetius, A., Soltwedel, T., Caley, M.J., et al. (2010) Global Patterns and Predictions of Seafloor Biomass Using Random Forests. *PLoS One* **5**: e15323.

Wenzhöfer, F. and Glud, R.N. (2002) Benthic carbon mineralization in the Atlantic : a synthesis based on in situ data from the last decade. *Deep. Res. I* **49**: 1255–1279.

Wickham, H. (2009) ggplot2: elegant graphics for data analysis Springer New York.

Widdel, F. and Musat, F. (2010) Energetic and other quantitative aspects of microbial hydrocarbon utilization. In, *Handbook of Hydrocarbon and Lipid Microbiology*. Springer, pp. 729–763.

Widdel, F. and Rabus, R. (2001) Anaerobic biodegradation of saturated and aromatic hydrocarbons. *Curr. Opin. Biotechnol.* **12**: 259–76.

Wilkes, H., Rabus, R., Fischer, T., Armstroff, A., Behrends, A., and Widdel, F. (2002) Anaerobic degradation of n-hexane in a denitrifying bacterium: Further degradation of the initial intermediate (1-methylpentyl)succinate via C-skeleton rearrangement.

Arch. Microbiol. **177**: 235–243.

Wu, J.W., Zheng, X.L., Li, L.L., and Sun, J. (2006) Adsorption of aqueous oil on sands and its studies of effective factors. *Huan jing ke xue= Huanjing kexue* **27**: 2019–2023.

Yakimov, M.M., Golyshin, P.N., Lang, S., Moore, E.R.B., Abraham, W., Lunsdorf, H., and Timmis, K.N. (1998) Alcanivorax borkumensis gen. nov., sp. nov., a new, hydrocarbon-degrading and surfactant-producing marine bacterium. 339–348.

Yakimov, M.M., Timmis, K.N., and Golyshin, P.N. (2007) Obligate oil-degrading marine bacteria. *Curr. Opin. Biotechnol.* **18**: 257–66.

Yang, T., Speare, K., McKay, L., MacGregor, B.J., Joye, S.B., and Teske, A. (2016) Distinct Bacterial Communities in Surficial Seafloor Sediments Following the 2010 Deepwater Horizon Blowout. *Front. Microbiol.* **7**: 1–18.

Yin, F., Hayworth, J.S., and Clement, T.P. (2015) A Tale of Two Recent Spills—Comparison of 2014 Galveston Bay and 2010 Deepwater Horizon Oil Spill Residues. *PLoS One* **10**: e0118098.

Yin, F., John, G.F., Hayworth, J.S., and Clement, T.P. (2015) Long-term monitoring data to describe the fate of polycyclic aromatic hydrocarbons in Deepwater Horizon oil submerged off Alabama's beaches. *Sci. Total Environ.* **508**: 46–56.

Zahed, M.A., Aziz, H.A., Isa, M.H., and Mohajeri, L. (2010) Enhancement biodegradation of n-alkanes from crude oil contaminated seawater.

Zahed, M.A., Aziz, H.A., Isa, M.H., Mohajeri, L., Mohajeri, S., and Kutty, S.R.M. (2011) Kinetic modeling and half life study on bioremediation of crude oil dispersed by Corexit 9500. *J. Hazard. Mater.* **185**: 1027–1031.

Zhang, J., Kobert, K., Flouri, T., and Stamatakis, A. (2013) PEAR: a fast and accurate Illumina Paired-End reAd mergeR. *Bioinformatics* 1–7.

Zinger, L., Amaral-Zettler, L. a, Fuhrman, J. a, Horner-Devine, M.C., Huse, S.M., Welch, D.B.M., et al. (2011) Global patterns of bacterial beta-diversity in seafloor and seawater ecosystems. *PLoS One* **6**: e24570.

Zobell, C.E. (1946) Action of microrganisms on hydrocarbons. *Bacteriol. Rev.* **10**: 1.

Zuijdgeest, A. and Huettel, M. (2012) Dispersants as used in response to the MC252-spill lead to higher mobility of polycyclic aromatic hydrocarbons in oil-contaminated Gulf of Mexico sand. *PLoS One* **7**: e50549.